07919-6001-R000

CR 66596

SCOUT ERROR ANALYSIS PHASE I FINAL REPORT

GPO PRICE	$
CFSTI PRICE(S)	$
Hard copy (HC)	3.00
Microfiche (MF)	.65

ff 653 July 65

FACILITY FORM 602

N66 35396	
(ACCESSION NUMBER)	(THRU)
167	1
(PAGES)	(CODE)
	31
(NASA CR OR TMX OR AD NUMBER)	(CATEGORY)

PREPARED FOR

NATIONAL AERONAUTICS AND SPACE ADMINISTRATION

UNDER CONTRACT NO. NAS 1-6969

TRW SYSTEMS

SCOUT ERROR ANALYSIS PHASE I FINAL REPORT

PREPARED FOR

NATIONAL AERONAUTICS AND SPACE ADMINISTRATION

UNDER CONTRACT NO. NAS 1-6969

TRW SYSTEMS

07919-6001-R000

CR 66596

SCOUT ERROR ANALYSIS PHASE I FINAL REPORT

Distribution of this report is provided in the interest of information exchange. Responsibility for the contents resides in the author or organization that prepared it.

Prepared by: L. B. Cohen
Program Manager

Approved by: P. Steiner, Manager
Guidance and Analysis Dept.

CONTENTS

SUMMARY

This report is presented in partial fulfillment of contract No. NAS1-6969 "Scout Error Analysis Program." The program consisted of the following items:

(1) Investigation of the guidance and control system error sources both as to character and magnitude, referring to field data and post-flight reports where available

(2) Development of a digital simulation incorporating six dimensional dynamics and the modeling of the second and third stage on-off control systems

(3) Incorporation into this simulation of the effects of the 103 error sources which were considered

(4) The generation of both linear and higher order sensitivity coefficients for use in a Monte Carlo Error Analysis Program.

The results of the analyzing a polar mission with 200 n.mi. perigee and 1000 n.mi. apogee produced the following one sigma errors at burnout:

	nominal conditions	mean dispersion	deviation
Velocity	26107 ft/sec	13.24 ft/sec	72.9 ft/sec
Altitude	288 n.mi.	.402 n.mi.	6.5 n.mi.
Inclination	90.0 deg	.0081 deg	.258 deg
Flight Path Angle	-.392 deg	-.032 deg	.263 deg

These results agree quite closely with the observed flight results if the two outlier flights are neglected.

Of the 103 parameters investigated, 29 proved to be of significance and of these non-linear considerations discovered a bias in the velocity vector at burnout of 13 ft/sec, an effect which had been noted in the post flight reconstructions.

INTRODUCTION

This report is presented in fullfillment of Part IV A.3. of contract No. NAS1-6969 entitled "Contract for Error Analysis Study for the Scout Vehicle" and covering all work performed under Paragraph A, Phase I of Part III. Quoting from Part III "Statement of Work:" "Phase I shall be concerned with three (3) specific goals:

(1) Determination of error sources, their magnitudes and statistical distributions

(2) Mathematical and logical incorporation of the error sources into ascent trajectory calculations and into other programs to determine the effects of these error sources on various flight parameters.

(3) Preparation of a detailed plan to derive the vehicle orbital and reentry accuracy capability."

A detailed discussion of the effort expended in achieving each of these tasks and the results which were obtained is contained in the subsequent sections. However a brief description of the scope of the work and the conditions of its performance are presented here.

In the determination of error sources, it was specified that all propulsion system errors would be taken from NASA CR-336 (Reference 1). In addition, the government undertook to supply fourth stage angular separation errors. TRW's responsibility was to investigate all significant effects associated with:

(1) Inertial Reference Package

(2) Control System

(3) Pitch Programer

(4) Aerodynamic Coefficients

(5) Vehicle Alignment and Weight Variations

All of these error sources were then to be incorporated into a Scout Vehicle simulation to determine their effect on the orbital insertion accuracy. This effort was accomplished in two stages; first, the simulation on the TRW N-Stage Program of the Scout Vehicle and Control System; and secondly, the modeling of the effect of each error source on the trajectory.

Each error source was then used to determine the deviation from nominal conditions caused by that error at four points of the trajectory:

(1) Second Stage Ignition Time

(2) Third Stage Ignition Time

(3) Fourth Stage Ignition Time

(4) Fourth Stage Burnout

These deviations, both linear and nonlinear in nature, were collected and then subjected to a Monte Carlo Analysis.

LIST OF SYMBOLS

Aerodynamic Symbols

α	=	Pitch angle of attack
β	=	Yaw angle of attack
C_{A_o}	=	Drag coefficient
C_N	=	Normal force coefficient
		$C_{N\alpha}$, $C_{N\delta q}$
C_Y	=	Side force coefficient
		$C_{Y\beta}$, $C_{Y\delta r}$
C_l	=	Roll moment coefficient
		$C_{\ell\delta p}$, $C_{\ell p}$
C_m	=	Pitch moment coefficient
		C_{Mo}, $C_{m\alpha}$, $C_{m\delta q}$, C_{mq}
C_n	=	Yaw moment coefficient
		$C_{n\beta}$, $C_{n\delta r}$, C_{nr}
δp	=	Roll control deflection
δq	=	Pitch control deflection
δr	=	Yaw control deflection
$\Delta\eta, \Delta\zeta, \Delta\xi$	=	Static margin shifts
$M_\eta, M_\zeta, M\xi$	=	Total aerodynamic moments

Control System Symbols

$\dot{\theta}_{PC}, \dot{\theta}_{VC}, \dot{\theta}_{RC}$	=	Commanded body angular rates in the pitch, yaw and and roll directions
$\dot{\theta}_P, \dot{\theta}_Y, \dot{\theta}_R$	=	Measured body rates in pitch, yaw and roll
K_{PP}, K_{PY}, K_{PR}	=	Proportional gain values
K_{RP}, K_{RY}, K_{RR}	=	Rate gain values
ε	=	Error signal

Guidance System Symbols

W_{IA}, W_{OA}, W_{SA}	=	Vehicle rates along a gyro input, output and spin axes
A_P, A_Y, A_R	=	Accelerations along the vehicle pitch, yaw and roll axes
$\dot{\theta}_{EP}, \dot{\theta}_{EY}, \dot{\theta}_{ER}$	=	Uncompensated gyro drift rates

DISCUSSION OF ERROR SOURCES AND THEIR MAGNITUDES

Since a prime object of this error analysis was to evaluate hardware tolerances, errors induced by vehicle assembly, and flight acceptance specifications, the first step was to assemble all conceivable error sources according to each discipline. This was done in the following order:

1. Identification and listing of error sources.
2. Assignment of a numerical value to each error and determination of its statistical characteristics.
3. Derivation of an error model and determination of the relationship of each error source to the model.
4. Consultation and assistance in interpretation of results.

Under the first item a list of possible error sources was prepared and is presented as Table 1. This table is annotated with the symbol for the error source or combination of error sources which was used in the analysis. Much of the effort required to obtain values for these quantities was expended in an examination of the Scout Standard Procedures for vehicle assembly, checkout and launch and the corresponding data in the logbooks which contained the measurements made in the field prior to launch.

The assignment of numerical values to the various error sources was the most critical part of the analysis. These numbers were discovered in various ways and have varying degrees of reliability. In this study unless there is definite information to the contrary, it is assumed that the distribution is normal, the error corresponds to the standard deviation, and any combination is by the root-sum-square method.

If the results of a sufficient number of actual measurements of a given quantity are available, the standard deviation is obtained by the usual formula:

$$\sigma = \sqrt{\frac{\Sigma\Delta^2}{n-1}}$$

TABLE 1. ERROR SOURCES CONSIDERED

A. Trajectory Factors

- I Motor Parameters
  1. Specific Impulse Variation (ISP1, ISP2, ISP3, ISP4)
  2. Mass Flow Rate (MFR1, MFR2, MFR3, MFR4)
  3. Propellant Weight (PW10, PW20, PW30, PW40)
- II Vehicle Inert Weight (SIW1, SIW2, SIW3, SIW4)
- III Atmospheric and Aerodynamic Factors
  1. Drag Coefficient (CAϕ1, CDϕ2)
  2. Normal Force (CNAL, CNDQ, CNA2, ZET2)
  3. Side Force (CYBA, CYDR)
  4. Roll Moment (CLDP, CLP1)
  5. Pitch Moment (CMϕ1, CMDQ, CMQ1, CMAL)
  6. Yaw Moment (NCBA, NCDR, NCR1)
  7. Static Margin Shifts (LSMY, LSMP, MSMP, MSMR, NSMY, NSMR)
  8. Wind (FWN1)
  9. Density (DRHϕ)
- IV Vehicle Structure
  1. Fin Misalignment (CNDR, CNDQ, CYDQ, CLDR, CLDQ, CMDR, NDCQ)
  2. Jet Vanes (CDV1, CDV2, CDV3, LDA2)
  3. Control Nozzle Misalignment (C2PY, C2YP)

B. Guidance and Control

- I Guidance
  - a. Initial Alignment
    1. Launch elevation (Pitch)
       - 1.1 IRP-Vehicle misalignment THϕP
       - 1.2 Transit reading error
       - 1.3 Adjustment error
    2. Launch azimuth (Roll)
       - 2.1 IRP-Vehicle roll alignment
       - 2.2 Transit reading error
       - 2.3 Adjustment error THϕR
       - 2.4 Azimuth deviation error
       - 2.5 Azimuth ring calibration
       - 2.6 Geodetic Factors

3. Launcher Yaw Adjustment

3.1 IRP-Vehicle misalignment
3.2 Transit reading error
3.3 Adjustment error

(THΦY)

b. Gyro Drift Errors

1. Fixed Torque

1.1 Measurement error
1.2 Compensation error

(DTER, DTEP, DTEY)

2. Mass Unbalance

2.1 MU_{SRA} (KPSA)
2.2 MU_{IA} (KRIA, KYIA)

3. Anisoelasticity

3.1 Steady state component
3.2 Vibration rectification
a) In-Phase
b) Cylindrical torque

(KPAN, KRAN, KYAN)

4. IA-Case misalignment

4.1 OA component
4.2 SA component

5. Dynamic errors

5.1 Spin Modulation
a) In-phase
b) Quadrature
5.2 Anisoinertia (in-phase only)
5.3 Spin-input rectification
a) In-phase
b) Quadrature
5.4 Spin-output rectification
a) In-phase
b) Coning

These effects were eventually neglected as being insignificant

6. Rate gyro error

6.1 Misalignment TYRG, TRRG
6.2 Bias DRBE, DYBE, DPBE

c. Pitch Program

1. Amplitude error
2. Gyro torquer scale factor } DKSG
3. Time error (clock stability, switching time) (TIM1, TIM2, TIM3, ····· TIM7)

II Control System

a. Displacement Gain (I)

1. Pitch (KPP1)
2. Roll (KPR1)
3. Yaw (KPY1)

b. Rate Gain

1. Pitch (KRP1, KRP2, KRP3)
2. Roll (KRR1, KRR2, KRR3)
3. Yaw (KRY1, KRY2, KRY3)

c. Deadband

1. Gain II
   1.1 Pitch (DBP2)
   1.2 Roll (DBR2)
   1.3 Yaw (DBY2)
2. Gain III
   2.1 Pitch (DBP3)
   2.2 Roll (DBR3)
   2.3 Yaw (DBY3)

d. Stage Misalignments

1. Thrust
   1.1 Stage 1 (TMP1, TMY1)
   1.2 Stage 2 (TMP2, TMY2)
   1.3 Stage 3 (TMP3, TMY3)
   1.4 Stage 4 (TMP4, TMY4)

III Miscellaneous

a. Fourth stage tip-off (W4CP, W4CY)

b. Roll offset errors (RΦE2, RΦE3)

If only a small number of readings are available the standard deviation may be approximated by the relation between range (max - min) and standard deviation (σ) (Noel, "Introduction to Mathematical Statistics", Page 241). Thus max-min = 1.128σ if n=2, max-min = 2.059σ if n=4, max-min = 3.078σ if n=10, etc. Where a reading is obtained by estimating the interpolated position of an index between the divisions of a scale and actual results are not available for analysis, the 1σ measurement error may be approximated by assuming that the smallest scale division is equal to 3σ. If the only available information was a specification, a specified tolerance limit was used as a 3σ value. Catalog information was used when no better information was available.

Figure 1 is a block diagram of the Scout subsystem interconnections with the emphasis on the guidance and control system. Since TRW was directed to analyze these errors only, the other subsystem errors were taken directly from the indicated sources and no additional analysis was expended on them.

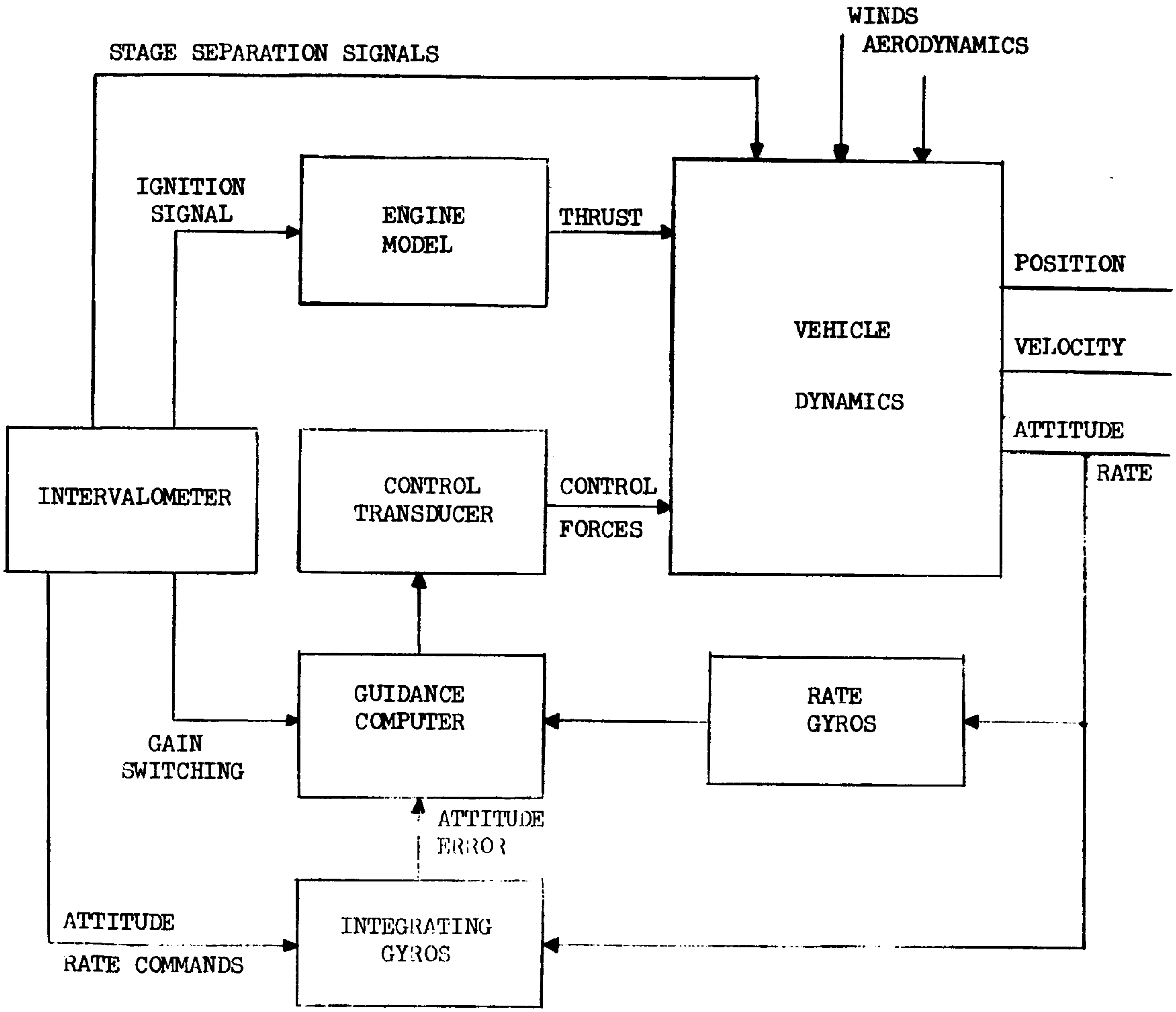

Figure 1. Scout Guidance and Control Block Diagram

The values given for all engine error sources, specifically propellant weight uncertainties (PW10, PW20, PW30, PW40) stage inert weight (SIW1, SIW2, SIW3, SIW4) specific impulse (ISP1, ISP2, ISP3, ISP4) mass flow rate (MFR1, MFR2, MFR3, MFR4) thrust misalignment (in the pitch and yaw direction (TMP1, TMY1, TMP2, TMY2, TMP3, TMY3, TMP4, TMY4) are taken from the PAPS Report (CR336, Reference 1).

The aerodynamic coefficient variation for both first and second stages was communicated in a letter from R. Keynton of Langley Research Center and reflects the uncertainties in wind tunnel data. These coefficients are listed with their conventional aerodynamic symbol in Table 8. The interested reader is referred to Appendix B for the details of the aerodynamic simulation.

The wind velocity is taken from "PMR Reference Atmosphere for Pt. Anguello," (Ref. 15) which is a compilation of wind data at WTR. A representative wind profile incorporating velocity and direction was constructed as a function of altitude and is presented as Table 2. Examination of the data shows that the direction of the wind is relatively constant, always blowing in an easterly direction. In the simulation, the direction was taken as a constant 270 degree heading and the velocity magnitudes were considered to be a 1σ deviation from the nominal no wind condition.

Static margin shifts in each axis (LSMY, LSMP, MSMP, MSMR, NSMY, NSMR) were based on best judgement since no data was available.

Fourth stage coning rates (W4CP, W4CY) was based on data transmitted verbally by D. Eide of Langley Research Center and is the result of actual flight data.

The next series of error sources was derived in most cases from field or flight data and represents the actual flight values.

TABLE 2. REPRESENTATIVE WIND TABLE

ALTITUDE IN FT.	SPEED IN FPS	AZIMUTH IN DEG FROM N
0	16.76 fps	274.58
1640	32.15	279.46
3281	32.81	274.76
4921	37.73	270.00
6562	44.29	270.94
8202	50.20	271.41
9842	54.46	270.57
13123	62.01	268.69
16404	74.15	267.77
19685	84.32	266.97
22966	94.49	265.48
26247	104.66	266.15
29527	118.44	265.57
32808	124.34	267.24
36089	133.86	267.38
39370	127.30	268.51
42651	120.08	268.46
45932	112.53	268.73
49212	101.71	268.98
52493	87.60	269.29
55774	71.20	270.88
59055	54.46	273.16
62336	41.67	275.92
65617	32.48	281.16
68897	27.56	284.32
72178	26.25	286.70
75459	28.54	289.18
78740	31.50	282.99
82021	35.43	272.13
85302	39.37	274.52
88582	42.32	292.49
91863	52.49	270.00
95144	51.09	266.88
98425	65.29	265.43

The guidance system parameters were obtained from a series of logbook measurements on several vehicles. These parameters are proportional gains in each axis (KPP1, KPR1, KPY1) rate gains (KRP1, KRY1, KRR1, KRP2, KRP3, KRY3) dead band errors (DBP2, DBY2, DBP3, DBY3). These values and the number of readings which comprised each of them is presented in the following table:

TABLE 3. CONTROL SYSTEM VARIATIONS

	Pitch Value $\pm$ 1σ	No. of Rdgs.	Roll Value $\pm$ 1σ	No. of Rdgs.	Yaw Value $\pm$ 1σ	No. of Rdgs.
Proportional Gain (I) volts/deg	2.84±.07	50	69.4±2.12 (MV)	20	6.01±.14	10
Rate Gain volts/deg/sec	1.14±.05	4	28.1±.71 (MV)	6	2.38±.05	4
Deadband (Gain II) deg 5/22/65	1.628±.021	7	2.867±.050	5	1.590±.018	7
repeat 6-9-65	1.628±.021	6				
Deadband (Gain III) deg 5/22/65	.457±.007	7	.843±.014	12	.460±.008	8
repeat 6/9/65	.461±.007	8				

It was decided by Langley Scout Office personnel that the dead band errors would be raised to .1 of nominal for use in this analysis in order to accentuate any effects due to this error source. At the same time an additional source representing a roll offset angle in second and third stage (ROE2, ROE3) of magnitude .25 degrees (1σ) was postulated as a way of generating dispersions due to roll axis dead zone error.

Gyroscope drift and mass unbalance errors were also gathered from logbook data. This data was incorporated into error sources DTER, DTEP, DTEY, KRIA, KPSA and KYIA. The method used is to rotate the gyro package to twelve different orientations in order to isolate the uncompensated drift and the mass unbalance effects for each gyro. The torquer drift compensation setting is not altered from its factory setting so that the drift measured in the field is not compensated but the resultant must be within a specified tolerance of 5 deg/hr drift and 3.5 deg/hr/g mass unbalance.

The measured values taken from the logbook for vehicle S154 gave the following values:

TABLE 4. GYROSCOPE ERROR MAGNITUDES

		Pitch	Yaw	Roll
Mass Unbal	(IA)	$.27 \times 10^{-7}$	1.03×10^{-7}	1.03×10^{-7}
rad/sec/ft/sec^2	(SA)	1.08×10^{-7}	2.5×10^{-7}	$.20 \times 10^{-7}$
Drift (rad/sec)		$.125 \times 10^{-5}$	$.2 \times 10^{-5}$	$.328 \times 10^{-5}$

Rate gyro data on biases and misalignments (DRBE, DYBE, DPBE, TRRG and TYRG) and position gyro anisoelastic effects (KPAN, KVAN, KRAN) were taken from catalog data supplied by Minneapolis Honeywell (Ref. 7).

As an introduction to initial alignment a few preliminary remarks will outline the difference between optical instruments. A theodolite measures angular displacement by turning the instrument telescope and reading the angle on a graduated scale using optical magnification. In an autocollimator the line of sight is rotated without moving the telescope by moving an optical wedge in the light path. Readout is by optical measurement of the motion of the wedge. A surveyor's transit is a theodolite which is capable of being plunged. A jig transit measures linear displacement by translating the line of sight parallel to itself by means of motion of a parallel optical plate. In all cases the optical readout device is called an optical micrometer although in the jig transit it is calibrated in units of linear displacement and in the other instruments it is calibrated in angular units. The theodolite, autocollimator, and surveyor's transit are basically accurate in the measurement of angle. Their use to measure linear displacement would depend on the distances involved and the accuracy of such measurement would degrade rapidly with distance. The jig transit is basically accurate in the measurement of linear displacement and its use to indirectly measure angle is accordingly inaccurate.

In missile guidance it is customary to perform alignment using a mirror mounted in the guidance package, a window in the vehicle shell, and one of the angle measuring instruments. In the Scout Vehicle, however, angular displacements in verticality or azimuth appear as (approximately) linear displacements of painted bench marks on the outer casing of the 3rd stage motor and the D transition section. The jig transit is therefore the appropriate instrument for alignment in this case.

The length of the Antares motor (and, therefore, the spacing between upper and lower bench marks) is approximately 61 inches. A linear displacement of 0.001 inch therefore corresponds to an angular displacement of 0.001 inch therefore corresponds to an angular displacement in verticality of 3.4 arc sec or 0.0009 deg. The radius of the Antares motor is 15 inches so that a displacement of the bench marks of 0.001 inch is produced by a rotation in azimuth of 13.8 arc sec, or 0.0038 deg.

Adjustment of verticality in yaw is accomplished by inserting or removing 1/64 inch shims under one bearing support on the elevation axis. Assuming the distance between supports is approximately 8 ft., the angular resolution due to shim thickness is 33.6 arc sec, or 0.0098 deg. The blockhouse elevation and azimuth encoder resolution is 0.01 deg.

With a properly graduated scale it is possible to estimate to within 1/2 to 1/5 of the smallest division. If statistical data on reading error is not available and it is necessary to assume a value for the standard deviation, this number should be some fraction of the smallest division. It seems reasonable to take the smallest division as being 3σ. The small fraction of the distribution outside the 3σ limits may represent the small but finite probability of misreading one whole division.

If the transit can be assumed to be the K&E 711010 and if the preceding philosophy is adopted we may write an error budget for the vertical alignment.

Yaw, transit reading error	0.0003 deg	(0.0009 deg = 3σ)
Adjustment error	0.0031	(0.0093 deg = 3σ)

Pitch or elevation, transit reading error	0.0003 deg
Adjustment error	0.0033 (0.01 deg = 3σ)

In Reference 9 (data sheets for vehicle 131) in the azimuth alignment procedure the azimuth ring reading with transit indications equal was given as 91.82 deg. This was apparently subtracted from 91° 52' 12" = 91.847 deg. Thus the azimuth deviation should be .03 deg although the 1 arc min difference is unexplained. It would seem reasonable that the azimuth deviation could normally be determined to an accuracy equal to that of reading the azimuth ring (.01 deg, 3σ). Reference 5 gives the azimuth ring calibration error at 126.5 deg as 7.8 arc sec = .0022 deg.

We can now list the azimuth (Roll) alignment errors.

Transit reading error	.0013 deg (.0038 deg = 3σ)
Azimuth deviation error	.0033
Adjustment error	.0033
Azimuth ring calibration	.0022

These figures do not include any misalignment between the actual gyro axes and the alignment marks on the outside of the vehicle. Table 5 summarizes the initial alignment errors.

The values of pitch program timing errors (TIM1, TIM2, TIM3, TIM4, TIM5, TIM6, TIM7) were also taken from S131 logbook data. The first step variation is considerably bigger than any of the subsequent steps (.078 seconds compared to .003 seconds). These differences were assumed to be one sigma errors in the analysis. The intervalometer error in amplitude was combined with the gyro scale factor to give a combined error in the amplitude of the pitch command. S131 logbook data was used to derive this figure.

TABLE 5. INITIAL ALIGNMENT ERRORS

Description (Symbol, Units)	Value (1σ)		
	Pitch (Elev.) (deg)	Roll (Az.) (deg)	Yaw (deg)
Launch Attitude			
IRP-Vehicle misalignment, deg.	.0062	.0111	.0062
Transit reading error	.0003	.0013	.0003
Adjustment error	.0033	.0033	.0031
Azimuth deviation error	-----	.0033	-----
Azimuth ring calibration	-----	.0022	-----
RSS sum	.0067	.0120	.0067

First stage fin position errors (CNDR, CYDQ, CLDR, CLDQ, CMDR, NDCQ) in both the force and moment equations were derived from assembly specifications for the Scout vehicle. For each pair of fins there are two error sources; the first is the misalignment of the pair causing a component of the force to appear in the other axis and the second is the unbalance between the members of a fin pair causing a roll couple. Since these two effects are uncorrelated, it was convenient to postulate individual roll and pitch coefficients for the yaw fins and roll and yaw coefficients for the pitch fins.

Scout stage misalignments due to nonparallelism are based on a diameter of 40 inches at sections A and B and 30 inches at section C. Since the relative directions of misalignment components due to nonparallelism and to nonconcentricity are random, these should be added in RSS fashion. One sigma values of these components and of their sum are as listed in Table 6.

TABLE 6. SCOUT FIN AND STAGE ALIGNMENT SPECS

Unit	Page (Ref.	Non-parallelism	Non-concentricity	Total
Base A	8	.0071 deg.	.0198 deg.	.0210 deg.
Lower B	9	.0048	.0367	.0370
C Section	10	.0064	.0125	.0140
IRP to Lower D	11	.0087		.0087

Fin dihedral tolerance	±.1667 deg (1σ)
Fin angle of incidence tolerance	±.0333
Parallelism between fin tip and jet vane	±.0833

Control motor misalignment on the second stage (C2PY, C2YP) were also based on Scout assembly specifications and are summarized in table 7.

TABLE 7

CONTROL MOTOR ALIGNMENT SPECIFICATIONS

Stage	Diameter	Length	Non-Parallelism	Non-Concentricity (Perpendicularity)	Total
1	40 in.	313 in.	$.0009^\circ$	$.0056^\circ$	$.0056^\circ$
2	31 in.	184.5 in.	$.0001^\circ$	$.0006^\circ$	$.0006^\circ$
3	30 in.	60.85 in.	$.0001^\circ$	$.0003^\circ$	$.0003^\circ$
4	18 in.	34.5 in.	$.0107^\circ$		

In Table (8), there is presented a complete list of all the error sources and their magnitudes and the symbol used in the analysis. Where no units appear in the one sigma magnitude, it is meant to be a fractional part of the nominal value.

Prior to investigating the errors, the validity of the Scout vehicle simulation was proved by matching a typical LTV trajectory with the TRW described in Appendix A using the data listed in Appendix B. The LTV trajectory was computed using 3 degrees of freedom for the second, third and fourth stages. The TRW simulation used six degrees of freedom from lift off to injection and therefore only in first stage was an exact comparison possible. Table 9 listing the trajectory comparisons are taken from Appendix A to which the interested reader is referrred for a detailed discussion.

TABLE 8. ERROR SOURCE LIST

I. Errors not Investigated

Description		Symbol	1σ Mag. Mag. *
IA	First Stage Errors		
1.	Propellant Weight Uncertainty	PW10	.0006
2.	First Stage Inert Weight	SIW1	.0083
3.	Second Stage Inert Weight	SIW2	.0041
4.	Third Stage Inert Weight	SIW3	.00093
5.	Fourth Stage Inert Weight	SIW3	.0024
6.	Specific Impulse	ISP1	.0018
7.	Mass Flow Rate	MFR1	.014
8.	Thrust Misalignment - Pitch	TMP1	1.67 mrad
9.	Thurst Misalignment - Yaw	TMY1	1.67 mrad
10.	Drag Coefficient (CAO)	CAO1	.01
11.	Normal Force Coefficients ($Cn\alpha$)	CNAL	.2
12.	Normal Force Coefficients ($Cn\delta q$)	CNDQ	.2
13.	Side Force Coefficients ($Cy\beta$)	CYBA	.33
14.	Side Force Coefficients ($Cy\delta r$)	CYDR	.33
15.	Roll Moment Coefficients ($C\ell\delta p$)	CLDP	.1
16.	Roll Moment Coefficients ($C\ell p$)	CLP1	.1
17.	Pitch Moment Coefficients (Cmo	CMO1	.002
18.	Pitch Moment Coefficients ($Cm\delta q$)	CMDQ	.002
19.	Pitch Moment Coefficients (Cmq)	CMQ1	.002
20.	Pitch Moment Coefficients ($Cm\alpha$)	CMAL	.002
21.	Yaw Moment Coefficients ($CN\beta$)	CNBA	.33
22.	Yaw Moment Coefficients ($CN\delta r$)	CNDR	.33
23.	Yaw Moment Coefficients (CNr	CNR1	.33
24.	Density Variation	DRHO	.0667
25.	Wind Profile	FWN1	-
26.	Jet Vane Drag Coefficient	CDV1	.1
27.	Jet Vane Drag Coefficient	CDV2	.1
28.	Jet Vane Drag Coefficient	CDV3	.1
29.	Jet Vane Side Force Coefficient	LDA2	.1

* Where no units appear, the magnitude is a percentage of nominal.

Description	Symbol	1σ Mag. Mag.
30. Roll Moment due to Yaw Axis Shift of Static Margin	LSMY	.01
31. Roll Moment due to Pitch Axis Shift of Static Margin	LSMP	.01
32. Pitch Moment due to Roll Axis Shift of Static Margin	MSMR	.1
33. Pitch Moment due to Yaw Axis Shift of Static Margin	MSMY	.1
34. Yaw Moment due to Pitch Axis Shift of Static Margin	NSMP	.1
35. Yaw Moment due to Roll Axis Shift of Static Margin	NSMR	.1
IB Second Stage Errors		
36. Propellant Wt Uncertainty	PW20	.00054
37. Specific Impulse	ISP2	.00094
38. Mass Flow Rate	MFR2	.01
39. Thrust Misalignment - Pitch	TMP2	1.67 mrad
40. Thrust Misalignment - Yaw	TMY2	1.67 mrad
41. Second Stage Aerodynamics (CDO)	CDO2	.1
42. Second Stage Aerodynamics ($C_{N\alpha}$)	CNA2	.1
43. Second Stage Aerodynamics (ξ)	ZET2	.1
IC Third Stage Errors		
44. Propellant Weight Uncertainty	PW30	.0006
45. Specific Impulse	ISP3	.0014
46. Mass Flow Rate	MFR3	.018
47. Thrust Misalignment - Pitch	TMP3	.557 mrad
48. Thrust Misalignment - Yaw	TMY3	.557 mrad
ID Fourth Stage Errors		
49. Propellant Weight Uncertainty	PW40	.00034
50. Specific Impulse	ISP4	.006

Description	Symbol	1σ Mag. Mag.
51. Mass Flow Rate	MFR4	.018
52. Thrust Misalignment - Pitch	TMP1	.5 mrad
53. Thrust Misalignment - Yaw	TMY1	.5 mrad
54. Coning Rate - Pitch	W4CP	.03 rad/sec
55. Coning Rate - Yaw	W4CY	.03 rad/sec

II Error Sources Investigated

Description and Reference		Symbol	1σ Mag.
IIA First Stage Errors			
56. Proportional Gain Error - Pitch	(Table 3)	KPP1	.0243
57. Proportional Gain Error - Yaw	(Table 3)	KPY1	.0306
58. Proportional Gain Error - Roll	(Table 3)	KPR1	.0233
59. Rate Gain Errors - Pitch	(Table 3)	KRP1	.044
60. Rate Gain Errors - Yaw	(Table 3)	KRY1	.021
61. Rate Gain Errors - Roll	(Table 3)	KRR1	.0262
62. Random Uncompensated Gyro Drift - Pitch	(Table 4)	DTEP	$.328\times10^{-5}$ rad/sec
63. Random Uncompensated Gyro Drift - Yaw	(Table 4)	DTEY	$.125\times10^{-5}$ rad/sec
64. Random Uncompensated Gyro Drift - Roll	(Table 4)	DTER	$.200\times10^{-5}$ rad/sec
65. Mass Unbalance Roll Gyro - Input Axis	(Table 4)	KRIA	1.03×10^{-7} rad/sec/ft/sec^2
66. Mass Unbalance Pitch Gyro - Spin Axis	(Table 4)	KPSA	1.08×10^{-7} rad/sec/ft/sec^2
67. Mass Unbalance Yaw Gyro - Input Axis	(Table 4)	KYIA	1.03×10^{-7} rad/sec/ft/sec^2
68. Anisoelastic Errors - Pitch	(Page 13)	KPAN	3.13×10^{-11} rad/sec/ft^2/sec^4
69. Anisoelastic Errors - Roll	(Page 13)	KYAN	3.13×10^{-11} rad/sec/ft^2/sec^4
70. Anisoelastic Errors - Yaw	(Page 13)	KRAN	3.13×10^{-11} rad/sec/ft^2/sec^4

			Symbol	1σ Mag.
71.	Rate Gyro Bias - Pitch		DPBE	3.57 mrad/sec
72.	Rate Gyro Bias - Yaw		DYBE	3.57 mrad/sec
73.	Rate Gyro Bias - Roll	(Page 13)	DRBE	3.57 mrad/sec
74.	Rate Gyro Misalignment - Yaw		TYRG	1.45 mrad
75.	Rate Gyro Misalignment - Roll		TRRG	1.45 mrad
76.	Vehicle Alignment Errors - Pitch		THOP	1.17×10^{-4} rad
77.	Vehicle Alignment Errors - Yaw	(Table 5)	THOY	2.10×10^{-4} rad
78.	Vehicle Alignment Errors - Roll		THOR	1.17×10^{-4} rad
79.	Intervalometer and Torquer Scale Factor	(Page 16)	DKSG	.0035

Fin Misalignment Errors

80.	Normal Force Error/Yaw Fins		CNDR	$.576 \times 10^{-4}$ rad
81.	Side Force Error/Pitch Fins		CYDQ	$.576 \times 10^{-4}$ rad
82.	Roll Moment Error/Yaw Fins		CLDR	$.576 \times 10^{-4}$ rad
83.	Roll Moment Error/Pitch Fins	(Table 6)	CLDQ	$.576 \times 10^{-4}$ rad
84.	Pitch Moment Error/Yaw Fins		CMDR	$.576 \times 10^{-4}$ rad
85.	Yaw Moment Error/Pitch Fins		NCDQ	$.576 \times 10^{-4}$ rad
86.	Timer Error - First Step		TIM1	.078 sec.
87.	Timer Error - Second Step		TIM2	.004 sec.
88.	Timer Error - Third Step	(Page 15)	TIM3	.003 sec.
89.	Timer Error - Fourth Step		TIM4	.003 sec.

IIB. Second Stage Errors

90.	Rate Gain Error - Pitch		KRP2	.044
91.	Rate Gain Error - Yaw		KRY2	.044
92.	Dead Band Error - Pitch	(Table 3)	DBP2	.1
93.	Dead Band Error - Yaw		DBY2	.1
94.	Yaw Offset		ROE2	.25 deg.
95.	Control Motor Misalignment - Pitch axis	(Table 17)	C2PY	.0033 deg.
96.	Control Motor Misalignment - Yaw axis		C2YP	.0033 deg.
97.	Timer Error - Sixth Step		TIM6	.003 sec.
98.	Timer Error - Seventh Step		TIM7	.003 sec.

IIC. Third Stage Errors

			Symbol	1σ Mag.
99.	Rate Gain Error - Pitch		KRP3	.044
100.	Rate Gain Error - Yaw		KRY3	.021
101.	Dead Zone Error - Pitch	(Table 3)	DBP3	.1
102.	Dead Zone Error - Yaw		DBY3	.1
103.	Roll Offset		ROE3	.25 deg.

TABLE 9

COMPARISON OF TRAJECTORY PARAMETERS AT END OF FIRST STAGE (t=76.46 sec)

Variable	TRW (N-Stage)	LTV (NEMAR)	Δ
V_I - ft/sec	4059.2	4060.5	1.3
XL - ft	81680.	81755.	75
YL - ft	-993.	-993.	0.0
ZL - ft	132302.	132379.	77
$\dot{X}L$ - ft/sec	2118.2	2119.2	1.0
$\dot{Y}L$ - ft/sec	-31.1	-31.1	0.0
$\dot{Z}L$ - ft/sec	2537.7	2538.5	0.8
θ - deg	50.34	50.22	0.12
ψ - deg	127.14	127.13	0.01
ϕ - deg	.234	.231	0.003

METHOD OF STATISTICAL ANALYSIS

In this section, the methods used to statistically analyze the effects on injection parameters of the error sources evaluated in the previous section are described.

The Scout simulation equations were assumed to be a quadratic form using coefficients previously calculated in the TRW N-Stage Trajectory Program (MVNS). There were three component parts:

Linear Errors:

$$\underline{X}_L = \sum_{\substack{i=1 \\ \text{linear}}}^{95} \underline{C}_i \, \Delta_i \qquad (1)$$

where $\underline{X}_L$ is the state vector at a stage time

$\underline{C}_i$ is the vector of linear sensitivity coefficients associated with the i^{th} error source

Δ_i is a random number with standard deviation equal to σ_i

Non-linear Errors:

$$\underline{X}_{NL} = \sum_{j=1}^{8} \underline{f}_j(\Delta_j) \qquad (2)$$

where $\underline{X}_{NL}$ is the non-linear state vector

$\underline{f}_j(\Delta_j)$ is the piece-wise linear function for the non-linear source j, formed by its effect at $\pm 1\sigma$, $\pm 2\sigma$, $\pm 3\sigma$.

Cross-term Errors:

$$\underline{X}_{CT} = \sum_{k=1}^{11} \sum_{l=k+1}^{12} \underline{C}_{kl} \, \Delta_k \, \Delta_l \qquad (3)$$

where $\underline{X}_{CT}$ is the cross-term vector

$\underline{C}_{kl}$ is the cross-term sensitivity

finally:

$$\underline{X} = \underline{X}_L + \underline{X}_{NL} + \underline{X}_{CT} \qquad (4)$$

The procedure is divided into three consecutive steps: (1) the generation of sensitivity coefficients of the state vector at the stage ignition times and at burnout with respect to error sources deviations; (2) the generation of cumulative distribution functions of desired orbital and reentry parameters using the sensitivity coefficients and the statistic of the error sources; (3) the analysis of these distribution functions. In Figure 2 , a block diagram describes the relationship between the TRW programs which will be used in the analysis. Each step will be discussed separately in some detail.

Sensitivity Coefficient Generation

The state of any system, as a function of time, may be considered as a function of initial state as well as a number of performance parameters (thrust, commanded turning rates, aerodynamic properties, etc.). The effects caused by nominal values of these parameters serve to define a nominal state at some time of interest, t_k, i.e.,

$$X_N (t_k) = f (X_o, P, t_o; t_k) \tag{5}$$

However, if these parameters are allowed to depart from their nominal values, a perturbed state vector is generated:

$$X (t_k) = f (X_o, P + \delta P, t_o; t_k) \tag{6}$$

If the difference in the two state vectors is expanded into a Taylor series about the nominal value:

$$\delta X_i = \sum_{j=1}^{q} C_{ij} \, \delta P_j + \frac{1}{2} \sum_{\substack{k=1 \\ j=1}}^{q} C_{ijk}^{(2)} \, \delta P_j \, \delta P_k + \ldots \qquad i = 1, 2, \ldots 6 \tag{7}$$

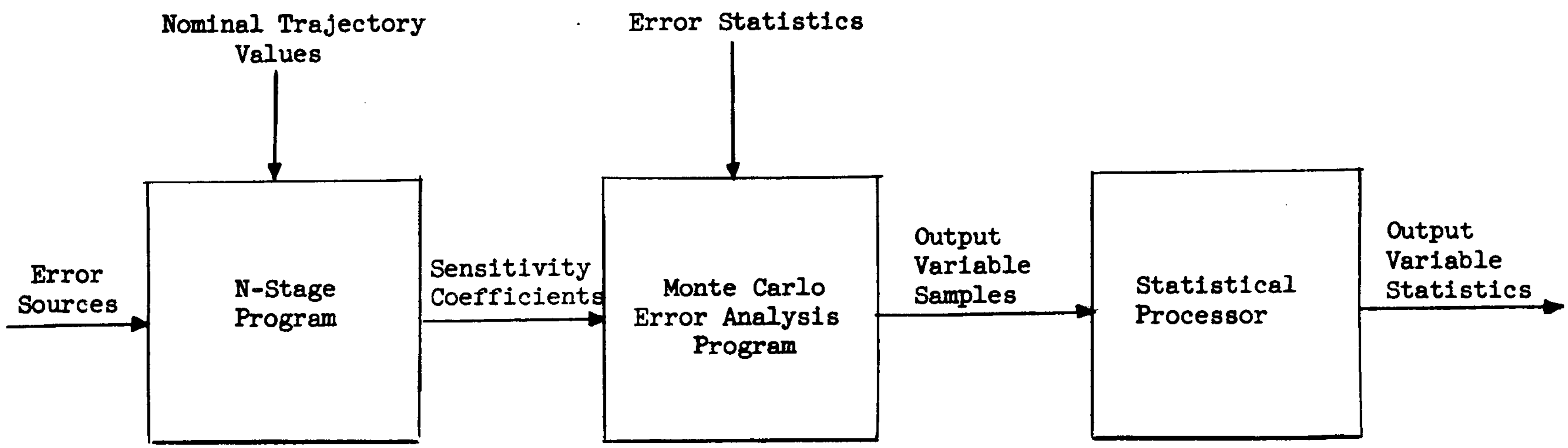

Figure 2. Programs to be Used in the Scout Error Analysis Program

where:

δX_i = the i^{th} component of the difference between perturbed and nominal state vectors

q is the dimension of the performance variation vector

C_{ij} is the partial derivative $\partial X_i/\partial P_j$

$C^{(2)}_{ijk}$ is the second partial derivative $\partial^2 X_i/\partial P_j P_k$

The number of terms in the expansion is sufficient to adequately represent the functional dependence of the state variation with respect to these parameters. If this expansion is truncated to include only second order terms, there are q first order parameters and $\frac{q(q+1)}{2}$ second order coefficients. This would necessitate $\frac{q(q+3)}{2}$ computer runs which for the values of q modelled for the Scout analysis (~100) is unrealistic.

However, it is certainly true that certain error sources will contribute more to the state vector dispersion than others and only these major contributors need be investigated for nonlinear effects. Thus, if the linear effect of an error source on the dependent variables was found to be negligible in relation to that of more significant error sources, no attempt was made to investigate such minor sources in any greater detail. This procedure has been found by TRW Systems to be most efficient, since the time spent in modeling any error sources is roughly proportional to its overall contribution to the output. The procedure for generation of sensitivity coefficients was as follows:

1. Using the MVNS simulation of the nominal mission, perturb the system with a +3 sigma variation for each error source. Take the square root of the sum of the squares of the deviations and compare each deviation with the RSS total. If the individual deviation is less than 0.3 of the RSS total, the effect of the error source will be represented by a linear sensitivity function. This criterion guarantees that the error source deviation, when squared has a contribution of magnitude less than the total sum of the squares.

2. The selected sources were perturbed by $\pm 1\sigma$ and $\pm 2\sigma$ and -3σ to determine their degree of nonlinearity. Both postive and negative perturbations are required, since it is possible for the curve to be symmetrical while still nonlinear. If it were found that the sensitivity curve had a nonlinear shape, a straightline approximation was used to represent the partial as shown in Figure 3.

3. The next relationship to be found was the cross-correlations between these most significant variables. The difficulty of this problem is increased by the fact that the important combinations are not all known a priori. TRW Systems isolated and identified several combinations for the Phase I reference mission, so that it was not necessary to use the corresponding large amounts of machine time for each subsequent mission.

The non-linear sources investigated in this analysis were thrust misalignments and coning rate errors, since not only were these sources large contributors to the combined errors, but it is clear that major effects such as velocity loss will be the same whether the misalignment is positive or negative. Conversely, a large effect such as specific impulse tends to be linear, more impulse produces more velocity and vice-versa. In addition, this type of error source has no out of plane or in plane directional effects. To summarize, the non-linear sources used in the Scout analysis were

Thrust misalignments, first stage (TMP1)
Thrust misalignments, first stage (TMY1)
Thrust misalignments, second stage (TMP2)
Thrust misalignments, second stage (TMY2)
Thrust misalignments, third stage (TMP3)
Thrust misalignments, third stage (TMY3)
Coning impulse, fourth stage (WC4P)
Coning impulse, fourth stage (WC4Y)

The cross correlations used in the Scout analysis were those combining thrust misalignments at second and third stages with their respective control system errors. These combinations are necessary to discover any of the effects of control system errors since if they are operating on a trajectory with no upsetting moments as second and third stage are, there will be no reason for any control system activity and the nominal burnout values will be reproduced. Therefore it was necessary to provide a large and relatively constant upsetting force which led logically to the choice of thrust misalignments. The pairings which were used in the simulation were:

Second Stage:

Thrust Misalignment, Pitch:	Rate Gain, Pitch
Thrust Misalignment, Pitch:	Dead Band, Pitch
Thrust Misalignment, Pitch:	Roll Offset
Thrust Misalignment, Yaw:	Rate Gain, Yaw
Thrust Misalignment, Yaw:	Dead Band, Yaw
Thrust Misalignment, Yaw:	Roll Offset

Third Stage:

Thrust Misalignment, Pitch;	Rate Gain, Pitch
Thrust Misalignment, Pitch:	Dead Band, Pitch
Thrust Misalignment, Pitch:	Roll Offset
Thrust Misalignment, Yaw:	Rate Gain, Yaw
Thrust Misalignment, Yaw:	Dead Band, Yaw
Thrust Misalignment, Yaw:	Roll Offset

It can be assumed that an output variable is related to two independent variables by the relation

$$\delta w = f(\delta x, \delta y) = C_x \delta x + C_y \delta y + C_{xx} \delta x^2 + C_{yy} \delta y^2 + C_{xy} \delta x \delta y \tag{8}$$

$$\delta w = \underbrace{C_x \delta x + C_{xx} \delta x^2}_{f_1(x)} + \underbrace{C_y \delta y + C_{yy} \delta y^2}_{f_2(y)} + C_{xy} \delta x \delta y \tag{9}$$

$$C_{xy} = \frac{\delta w - f_1(x) - f_2(y)}{\delta x \delta y} \tag{10}$$

In this equation $f_1(x)$ and $f_2(y)$ are represented by the piecewise linear functions described in the previous paragraph.

The effect of carrying out the three-step procedure outlined above has to reduce the nonlinear process (i.e., the system and its environment) to a polynomial approximation. This procedure reduced machine running time per sample from 2 to 3 minutes on the TRW Systems N-Stage program to 2 seconds on the Monte Carlo Error Analysis Program, while still including all significant non-linearities.

This polynomial fit was used to relate the input quantities to the state vector at burnout, and any unpowered propagations to other points on the trajectory were calculated by an analytical ephemeris generator.

Monte Carlo Analysis

Using the nomenclature of the previous section, let us assume that there are q error sources, of which p are found to have either nonlinear, cross-coupling terms or both. Since the nonlinear terms have $\pm 1\sigma$, $\pm 2\sigma$ and $\pm 3\sigma$ deviations, each nonlinear error source will have a 6x6 matrix of sensitivity coefficients, i.e., the value of the output state vector as a function of $\pm n_\sigma$. These values will be used to construct a piece-wise linear function as seen in Figure 3 and replace the square terms $C^{(2)}_{ijk}\ \delta P^2_j$ in Eq. 7. The advantage of this approach is that it is not necessary to fit an arbitrarily truncated power series when the curve may contain higher components.

For each cross coupling pair of error sources, there will be a single coefficient for each output state vector component or a 6x1 vector for the output state vector. The error sources which have only linear terms can all be compressed into a single equivalent variable by the following steps. Given that:

$$X = [C]\ P \tag{11}$$

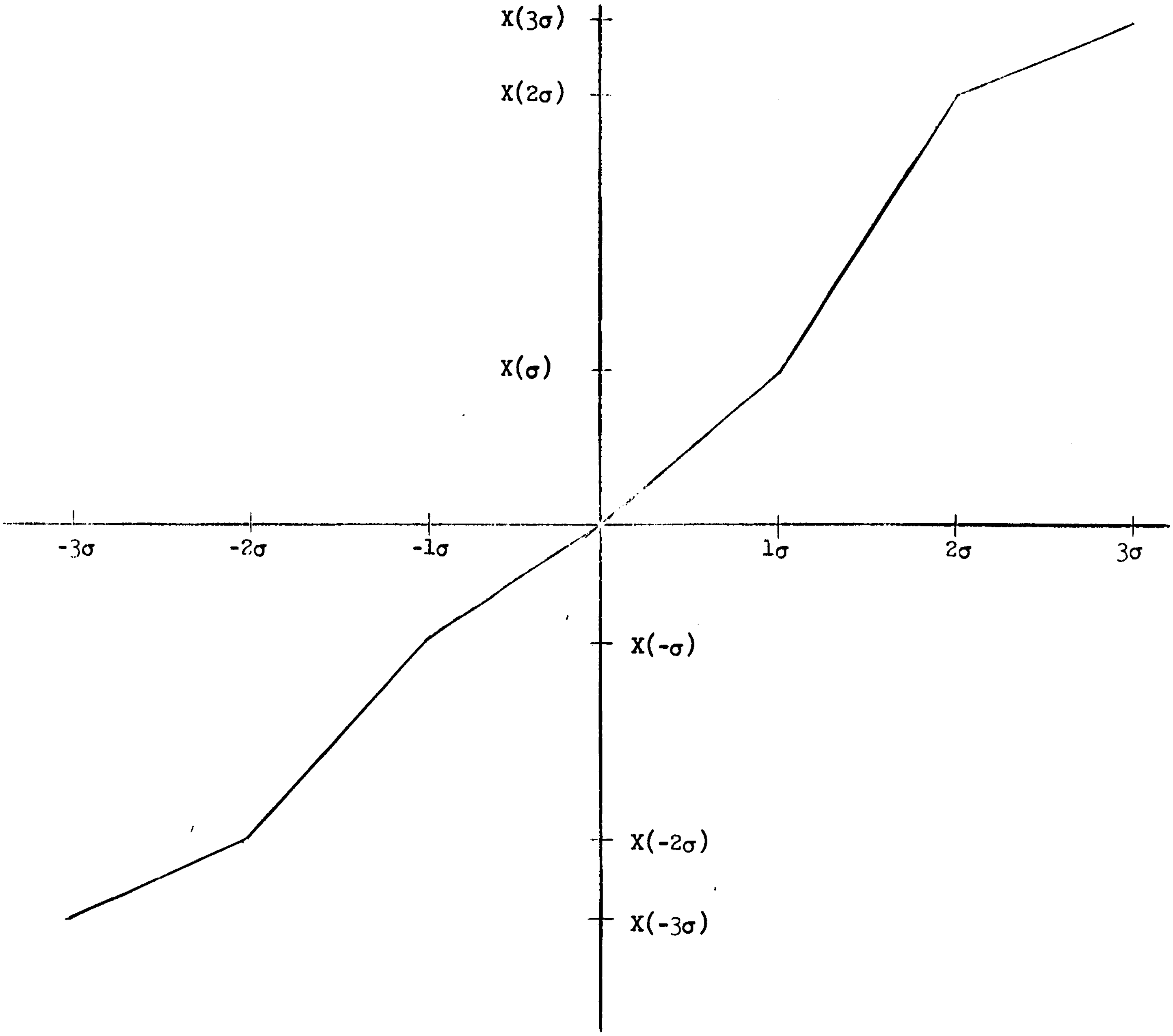

Figure 3. Piecewise Nonlinear Function

where

X is the output 6x1 state vector.

P is the linear error source vector of dimension q-p,

C is the 6 x (q-p) matrix of sensitivity coefficients,

then $XX^T = CPP^TC^T$.

Taking the expectation of each side gives

$$\Sigma_X = C \Sigma_P C^T \tag{12}$$

where

Σ_X is the covariance matrix of the output state vector due to linear error sources;

Σ_P is the covariance matrix of the linear error sources.

Thus, all the linear error sources and their statistics can be compressed into a single 6x6 covariance matrix.

The Monte Carlo analysis progresses through the following steps:

(1) Using the equivalent linear covariance matrix and a random vector generator, choose a random output vector from this covariance matrix Σ_X.

(2) Using the statistics of each nonlinear source, choose a random value of this error source. Enter the piecewise linear function associated with the source and calculate the value of the output state vector dispersion due to this nonlinear effect.

(3) Using the statistics of each pair of cross coupling error sources choose pair random values. Multiply the product of these values by the cross coupling sensitivity coefficient vector to calculate the dispersion due to the combined effects of these sources.

(4) Add the three dispersions due to linear, nonlinear and cross coupling effects to the nominal state vector at burnout to calculate one sample of the analysis. Using this perturbed vector calculate the variables of interest. For the Scout analysis, the following variables were calculated and compared with their nominal values:

a. Geocentric Radius Vector

b. Inertial Velocity

c. Inertial Flight Path Angle
d. Relative Velocity
e. Flight Path Angle w/r to the Air Mass
f. Semi-major Axis
g. Eccentricity
h. Inclination
i. Longitude of the Ascending Node
j. Argument of Perigee
k. Downrange Distance from Launch Site
l. Apogee Altitude
m. Perigee Altitude
n. Period
o. Longitude
p. Latitude
q. Altitude

Statistical Analysis of Samples

The analysis of the sample statistics is relatively straightforward. The samples of any variable are used to calculate a mean and second central moment. The samples are then ordered by size and a cumulative distribution is plotted. This curve shows the correct percentile levels for the variable even though the distribution may be highly non-Gaussian.

The equations which are used in the Statistical Processor program (PROC) will be presented here. The same equations apply to both scalars and vectors unless a distinction is made in the description of the sample statistic. All computations are performed in double precision.

AVERAGE OR MEAN VALUE

The sample mean of a random vector X, denoted by X, is computed by PROC using the following equation:

$$\bar{X} = \frac{1}{N} \sum_{i=1}^{N} X_i$$

In this and all following equations, N is the total number of samples used in the computation and X_i is the value of the random vector X for the i^{th} sample of the Monte Carlo simulation.

COVARIANCE MATRIX AND CORRELATION MATRIX

The covariance matrix of a random vector X, denoted by Σ_{XX}, is defined by the following equation in which E indicates the expectation operator.

$$\Sigma_{XX} = E(X - \bar{X})(X - \bar{X})^T$$

This equation can be expanded and rewritten as follows:

$$\Sigma_{XX} = E(XX^T) - (\bar{X})(\bar{X})^T$$

The equation used by PROC to compute a sample covariance matrix is similar to Equation and can be written

$$\Sigma_{XX} = \frac{1}{N-1}\left[\sum_{i=1}^{N} X_i X_i^T - \frac{1}{N}\left(\sum_{i=1}^{N} X_i\right)\left(\sum_{i=1}^{N} X_i\right)^T\right]$$

CUMULATIVE DISTRIBUTION FUNCTION

A cumulative distribution function (CDF) is the probability that a random variable, X, is less than a specified number. This information is displayed by PROC as a graph of the probability that the random variable is less than the specified number versus the specified number. This is accomplished by ordering all of the samples in the order of increasing numerical value and plotting the percentage of the samples that are less than a given value, say ν, as a function of ν.

DISCUSSION OF THE ERROR ANALYSIS RESULTS

The mission which was analyzed was a 300 pound payload placed in a polar orbit. The pitch profile used and the corresponding nominal values at burnout are listed in TABLE 10. The simulation was run with 95 linear sources, 8 non-linear sources, and 12 cross term combinations. The non-linear and cross term sources were described in the previous section. Thus, the effect of the control system errors could be measured in the presence of the strongest upsetting moment and the possible non-linearities of the largest error sources are also considered.

The results are summarized by TABLE 11 which lists the mean and one sigma value of each output parameters. The most important quantities are inclination with dispersion of .258 degree (1σ), inertial velocity with a dispersion of 72.9 ft/sec (1σ) and an altitude dispersion of 6.5 n.mi. at burnout (1σ).

Along track distance is defined to be the nominal equatorial radius of the earth (2.092×10^7) ft) multiplied by the angular in plane variation of the burnout point which represents the subsatellite along track variation at burnout.

The air speed and atmospheric flight path angle are the same as the inertial pair except that they are computed in an Earth fixed rotating coordinate system.

The other parameters are defined as shown in Figure 4.

The results are an example of the usefulness of the Monte-Carlo method which disclosed a bias in the distribution of the burnout velocity vector of 13 ft/sec, result validated by the flight history of the Scout Vehicle. This effect could not have been calculated by linear RMS techniques.

A complete listing of the error analysis results is presented. At each stage ignition time for each error source there is a table showing the equivalent range, velocity flight-path and inclination dispersion caused by each THREE sigma error variation.

Following these, there is a statistical summary of the results of 551 Monte Carlo samples for each of 19 trajectory parameters. Every summary contains the mean, standard deviation, largest and smallest sample, second, fifth, ninety-fifth and ninety-eighth percentiles of the variable.

Table 10. NOMINAL POLAR TRAJECTORY PARAMETERS

(1) PITCH PROGRAM:

TIME (sec)	PITCH RATE (deg/sec)
0.0	0.0
3.0	-3.45665
8.0	- .70750
32.0	- .50000
41.0	- .36364
74.0	- .41579
93.0	- .28125
109.0	- .17619
130.0	- .12167
190.0	-1.00000
225.75	0.0

(2) IGNITION TIMES:

Stage 2 - 82.00 sec
Stage 3 - 134.77 sec
Stage 4 - 567.56 sec

(3) LAUNCH AZIMUTH: 182 deg

(4) PAYLOAD WEIGHT: 300 lbs

(5) TIME AT BURNOUT: 600.68 sec

(6) CONDITIONS AT BURNOUT:

ALTITUDE - 1744825.25 ft

VELOCITY - 26107 ft/sec

FLIGHT PATH ANGLE - -.39226 deg

PERIGEE - 288.9 n.mi.

APOGEE - 1096.7 n.mi.

ECCENTRICITY - .0977 n.mi.

PERIOD - 111.07 sec

Table 11. SUMMARY OF ORBITAL PARAMETER VARIATIONS

	MEAN	1 σ VALUE
SEMI-MAJOR AXIS	38491 ft	185,579 ft
ECCENTRICITY	1.307×10^{-3}	6.128×10^{-3}
INCLINATION	8.099×10^{-3} deg	.258 deg
LONG OF ASCENDING NODE	.0413 deg	.157 deg
ARGUMENT OF PERIGEE	.345 deg	2.93 deg
ALONG TRACK DISTANCE	.918 n.mi	4.22 n.mi.
RADIUS VECTOR	2447 ft	39,554 ft
INERTIAL VELOCITY	13.2 ft/sec	72.9 ft/sec
AIR SPEED	13.5 ft/sec	72.9 ft/sec
INERTIAL FLIGHT PATH ANGLE	-.0324 deg	.262 deg
ATMOSPHERE FLIGHT PATH ANGLE	-.0323 deg	.262 deg
APOGEE	12.5 n.mi.	58.4 n.mi.
PERIGEE	.122 n.mi	7.2 n.mi.
PERIOD	15.4 sec	73.9sec
LONGITUDE	.0437 deg	.109 deg
LATITUDE	.0155 deg	.070 deg
ALTITUDE	.402 n.mi	6.5 n.mi.

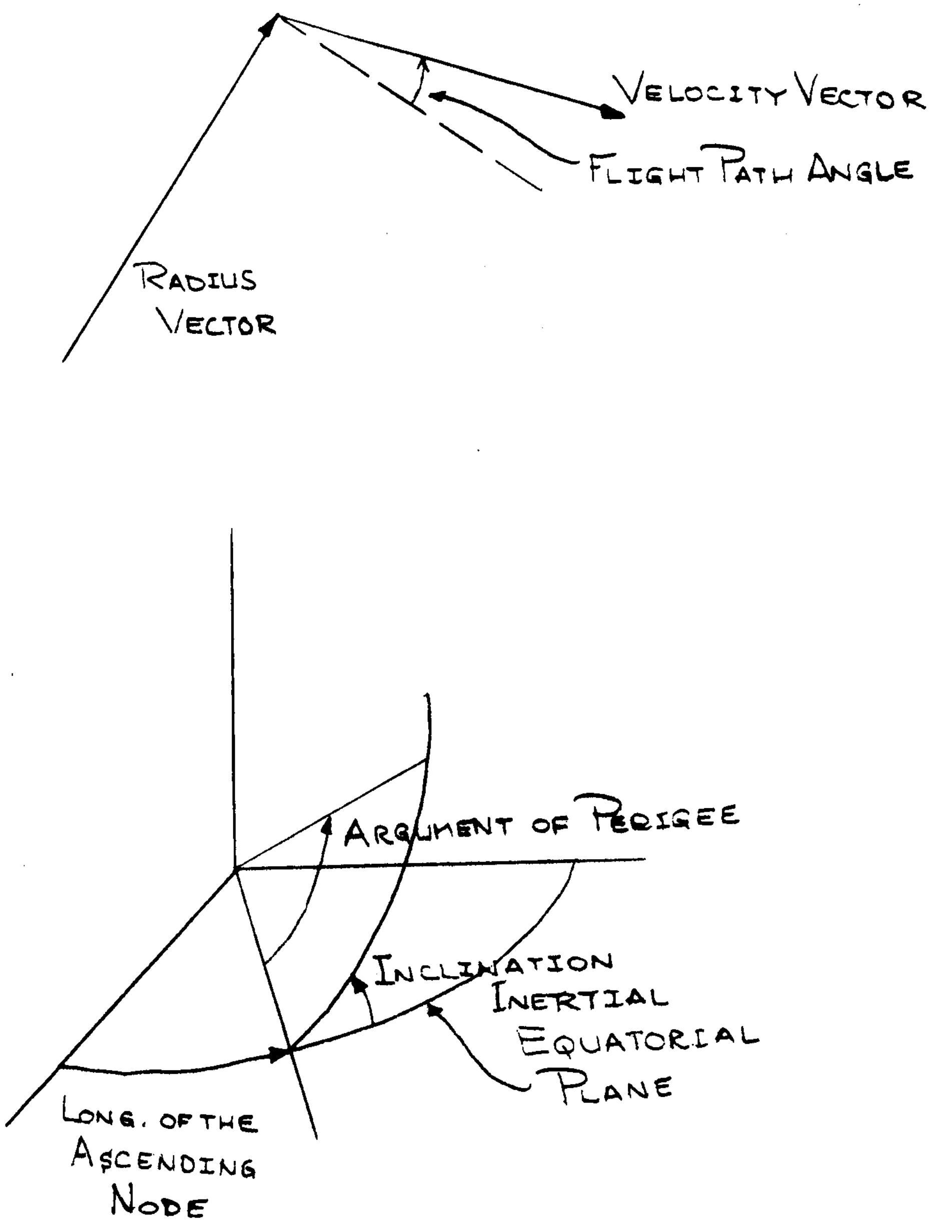

Figure 4. Output Parameter Definition.

Table 12. 3σ ERRORS AT SECOND STAGE IGNITION

	CODE	STND.DEV.	RANGE DEVIATION (FT)	VELOCITY DEV. (FPS)	FLT. PATH ANGLE DEV. (DEG)	INCL.DEV. (DEG)
1	PWIO	6.000000E-04	1.597500E 02	1.820679E-01	5.395209E-02	-1.172914E-02
2	SIW1	8.300000E-03	7.160000E 02	-1.755981E-01	3.016766E-01	-7.285165E-02
3	SIW2	4.100000E-03	2.365000E 02	-6.930542E-02	9.952098E-02	-2.397567E-02
4	SIW3	9.300000E-04	8.575000E 01	-2.664185E-02	3.620000E-02	-8.716175E-03
5	SIW4	2.400000E-03	1.750000E 01	-5.554199E-03	7.399556E-03	-1.780972E-03
6	ISP1	1.800000E-03	1.384000E 03	3.103793E 01	2.133858E-01	1.254457E-01
7	WFR1	1.400000E-02	1.591750E 03	3.287717E 01	2.346435E-01	1.346039E-01
8	KRIA	1.030000E-07	-2.500000E-01	2.132874E-01	-2.250793E-03	-8.575194E-03
9	KPSA	1.080000E-07	1.750000E 01	-1.213074E-01	1.096331E-02	-1.164939E-03
10	KYIA	1.030000E-07	0.	2.309875E-01	-2.470394E-03	9.363335E-03
11	THOR	9.250000E-05	2.500000E-01	2.591553E-01	-2.802085E-03	1.037506E-02
12	THOP	5.760000E-05	2.400000E 01	7.687073E-01	2.388005E-03	3.574642E-03
13	THOY	5.430000E-05	5.000000E-01	2.248535E-01	-2.309885E-03	8.563241E-03
14	DTER	3.280000E-06	0.	1.458811E-01	-1.598264E-03	5.955925E-03
15	DTEP	1.250000E-06	1.750000E 01	6.266785E-01	2.202736E-03	2.951495E-03
16	DTEY	2.000000E-06	2.500000E-01	3.532104E-01	-3.839847E-03	1.422728E-02
17	DKSG	3.500000E-03	8.415000E 02	2.831396E 01	1.018189E-01	1.314615E-01
18	DRBE	3.570000E-03	2.000000E 00	3.993378E 00	-4.201804E-02	-1.500561E-01
19	DYBE	3.570000E-03	7.500000E-01	5.692749E 00	-6.113489E-02	-2.281471E-01
20	DPBE	3.570000E-03	5.955000E 02	-4.015320E 00	3.073295E-01	-9.221182E-02
21	TYRG	1.450000E-03	0.	5.484009E-02	-5.895307E-04	-2.224934E-03
22	TRRG	1.450000E-03	0.	0.	0.	-1.707547E-06
23	KPP1	2.430000E-02	2.750000E 01	5.818481E-01	1.050142E-04	3.095783E-03
24	KPR1	3.060000E-02	0.	0.	0.	-8.537736E-07
25	KPY1	2.330000E-02	0.	4.379272E-02	-4.729906E-04	-1.789510E-03
26	KRP1	4.400000E-02	9.100000E 01	-5.484619E-01	3.925993E-02	-1.181537E-02
27	KRY1	2.100000E-02	-2.500000E-01	3.662109E-04	-2.134434E-06	-1.792925E-05
28	KRR1	2.620000E-02	0.	0.	0.	-8.537736E-07
29	KPAN	3.130000E-11	2.500000E-01	1.318359E-02	4.823821E-05	-6.403302E-05
30	KRAN	3.120000E-11	0.	3.265381E-03	-3.372406E-05	-1.374576E-04
31	KYAN	3.130000E-11	-2.500000E-01	4.730225E-03	-4.866510E-05	-1.946504E-04
32	TMP1	1.670000E-03	3.123750E 03	-3.939929E 01	1.800545E 00	-6.518673E-01
33	TMY1	1.670000E-03	7.625000E 02	3.381491E 01	-9.099861E-02	-1.336811E 00
34	CA01	10.000000E-03	4.690000E 02	-5.892029E-01	2.337252E-01	-5.847069E-02
35	CNAL	2.000000E-01	4.827500E 02	-1.490173E 00	2.211556E-01	-5.840665E-02
36	CNDQ	2.000000E-01	-6.800000E 01	1.635742E-01	-2.522750E-02	6.747373E-03
37	CYBA	3.300000E-01	1.750000E 00	7.492371E-01	-7.257503E-03	-2.839310E-02
38	CYDR	3.300000E-01	-7.500000E-01	1.002502E-01	-1.268281E-03	4.040911E-03
39	CLDP	1.000000E-01	0.	0.	0.	-8.537736E-07

40	CLP1	1.000000E-01	0.	0.	0.	-8.537736E-07
41	CMDQ	2.000000E-03	1.750000E 00	5.184937E-02	2.428986E-04	-2.271038E-04
42	CMQ1	2.000000E-03	5.000000E-01	1.593018E-02	5.037264E-05	-7.513208E-05
43	CMAL	2.000000E-03	2.750000E 00	7.452393E-02	5.088491E-04	-2.971132E-04
44	CM01	9.000000E-02	3.105000E 02	-2.455838E 00	1.911296E-01	-5.309930E-02
45	NCBA	3.300000E-01	-5.000000E 00	7.510071E-01	-1.027260E-02	3.001356E-02
46	NCDR	3.300000E-01	7.500000E-01	3.293152E-01	-3.056510E-03	-1.210907E-02
47	NCR1	3.300000E-01	-2.500000E-01	1.647949E-03	-1.408726E-05	-5.976415E-05
48	DRHO	6.670000E-02	2.836500E 03	-1.144641E 01	1.520371E 00	-4.519434E-01
49	FWN1	10.000000E-01	2.250000E 01	2.798157E 00	-1.054368E-02	-7.941743E-01
50	CNDR	5.760000E-05	5.000000E-01	1.455688E-02	6.275236E-05	-6.830189E-05
51	CYDQ	5.760000E-05	0.	5.706787E-03	-5.165330E-05	-2.142972E-04
52	CLDR	5.760000E-05	0.	2.715064E-03	-2.860142E-05	-1.161132E-04
53	CLDQ	5.760000E-05	0.	2.273550E-02	-2.433255E-04	-9.408585E-04
54	CMDR	5.760000E-05	-2.500000E-01	2.135230E-04	1.280560E-06	-1.707547E-06
55	NCDQ	5.760000E-05	0.	5.187988E-04	-5.976415E-06	-2.390556E-05
56	LSMY	10.000000E-03	2.500000E-01	1.221313E-01	-9.895236E-04	4.048595E-03
57	LSMP	10.000000E-03	7.000000E 00	-4.722595E-01	1.043397E-02	1.511925E-02
58	MSMP	1.000000E-01	3.475000E 01	-1.640320E-01	2.018790E-02	-5.497448E-03
59	MSMR	1.000000E-01	3.590000E 02	-1.912292E 00	2.123775E-01	-5.904955E-02
60	NSMY	1.000000E-01	-2.500000E-01	5.624390E-02	-7.035095E-04	-2.309458E-03
61	NSMR	1.000000E-01	-2.000000E 00	4.550760E 00	-5.056901E-02	-1.887002E-01
62	CDV1	1.000000E-01	-4.017500E 02	-8.793793E 00	-6.234810E-02	-3.564163E-02
63	CDV2	1.000000E-01	-1.895000E 02	-4.182190E 00	-2.940653E-02	-1.597729E-02
64	CDV3	1.000000E-01	-1.895000E 02	-4.182190E 00	-2.940653E-02	-1.597729E-02
65	LDA2	1.000000E-01	4.850000E 01	4.521790E-01	2.080646E-02	-6.246208E-03
66	TIM1	7.800000E-02	1.916750E 03	-1.183105E 01	9.926322E-01	-2.965250E-01
67	TIM2	4.000000E-03	7.400000E 01	2.353210E 00	8.520661E-03	1.098465E-02
68	TIM3	3.000000E-03	2.500000E 00	1.049500E-01	3.671227E-04	-5.045802E-04
69	TIM4	3.000000E-03	1.250000E 00	5.197144E-02	1.827076E-04	-2.501557E-04

Table 13. 3σ ERROR SOURCE DEVIATIONS AT THIRD STAGE IGNITION

	CODE	STND.DEV.	RANGE DEVIATION (FT)	VELOCITY DEV. (FPS)	FLT. PATH ANGLE DEV. (DEG)	INCL.DEV. (DEG)
1	PW10	6.000000E-04	3.142500E 02	-5.344238E-01	1.943317E-02	-1.283222E-03
2	SIW1	8.300000E-03	1.544000E 03	-4.210815E 00	1.071405E-01	-7.829104E-03
3	SIW2	4.100000E-03	5.095000E 02	-1.392578E 00	3.533257E-02	-2.580104E-03
4	SIW3	9.300000E-04	1.850000E 02	-5.072021E-01	1.285079E-02	-9.382972E-04
5	SIW4	2.400000E-03	3.775000E 01	-1.036377E-01	2.625140E-03	-1.912453E-04
6	ISP1	1.800000E-03	2.909500E 03	3.010425E 01	1.099767E-01	1.333424E-02
7	MFR1	1.400000E-02	3.529750E 03	3.286829E 01	1.172793E-01	1.521083E-02
8	KRIA	1.030000E-07	2.500000E-01	6.982422E-02	-1.340425E-04	-2.948080E-03
9	KPSA	1.080000E-07	4.275000E 01	-2.644043E-01	3.601644E-03	-2.843066E-04
10	KYIA	1.030000E-07	2.500000E-01	7.641602E-02	-1.948738E-04	-3.499618E-03
11	THOR	9.250000E-05	5.000000E-01	8.740234E-02	-2.115224E-04	-3.895769E-03
12	THOP	5.760000E-05	5.175000E 01	7.552490E-01	1.628573E-03	3.235802E-04
13	THOY	5.430000E-05	1.250000E 00	8.044434E-02	-1.555002E-04	-3.283613E-03
14	DTER	3.280000E-06	0.	4.833984E-02	-1.195283E-04	-2.227495E-03
15	DTEP	1.250000E-06	4.075000E 01	6.132813E-01	1.395493E-03	2.638161E-04
16	DTEY	2.000000E-06	5.000000E-01	1.177979E-01	-2.924175E-04	4.834920E-03
17	DKSG	3.500000E-03	1.902750E 03	2.761035E 01	6.430687E-02	1.169158E-02
18	DRBE	3.570000E-03	8.250000E 00	1.326904E 00	-2.471675E-03	-5.438111E-02
19	DYBE	3.570000E-03	4.500000E 00	1.881836E 00	-3.908362E-03	-7.722809E-02
20	DPBE	3.570000E-03	1.277000E 03	-8.035278E 00	9.976452E-02	-8.109996E-03
21	TYRG	1.450000E-03	0.	1.867676E-02	-4.396934E-05	-8.213302E-04
22	TRRG	1.450000E-03	0.	0.	2.134434E-07	-8.537736E-07
23	KPP1	2.430000E-02	4.275000E 01	5.883789E-01	7.585779E-04	2.527170E-04
24	KPR1	3.060000E-02	0.	0.	0.	0.
25	KPY1	2.330000E-02	0.	1.428223E-02	-3.030896E-05	-6.061793E-04
26	KRP1	4.400000E-02	1.770000E 02	-1.047852E 00	1.263286E-02	-1.015137E-03
27	KRY1	2.100000E-02	0.	0.	4.268868E-07	-5.976415E-06
28	KRR1	2.620000E-02	0.	0.	0.	0.
29	KPAN	3.130000E-11	7.500000E-01	1.293945E-02	2.965863E-05	-5.976415E-06
30	KRAN	3.120000E-11	0.	9.765625E-04	-1.920991E-06	-4.610378E-05
31	KYAN	3.130000E-11	0.	1.464844E-03	-2.774764E-06	-6.574057E-05
32	TMP1	1.670000E-03	6.535000E 03	-6.512329E 01	5.617845E-01	-5.731809E-02
33	TMY1	1.670000E-03	1.482000E 03	7.849854E 00	5.965982E-02	-4.412464E-01
34	CA01	10.000000E-03	1.097250E 03	-3.705566E 00	8.236418E-02	-6.155708E-03
35	CNAL	2.000000E-01	1.018250E 03	-4.285767E 00	7.370457E-02	-5.069708E-03
36	CNDO	2.000000E-01	-1.320000E 02	4.840088E-01	-8.711479E-03	5.660519E-04
37	CYBA	3.300000E-01	4.750000E 00	2.745582E-01	-3.171769E-04	-9.638250E-03
38	CYDR	3.300000E-01	-1.000000E 00	3.393555E-02	-1.541061E-04	-1.539354E-03
39	CLDP	1.000000E-01	0.	0.	0.	0.

40 CLP1	1.000000E-01	0.	0.	0.	0.
41 CMDQ	2.000000E-03	4.000000E 00	4.980469E-02	1.205955E-04	-1.963679E-05
42 CMQ1	2.000000E-03	1.250000E 00	1.550293E-02	2.838797E-05	-6.830189E-06
43 CMAL	2.000000E-03	6.500000E 00	6.958008E-02	2.537842E-04	-2.732076E-05
44 CM01	9.000000E-02	7.372500E 02	-5.033325E 00	6.260978E-02	-5.182406E-03
45 NCBA	3.300000E-01	-1.075000E 01	-3.502197E-01	1.344693E-04	1.021369E-02
46 NCDR	3.300000E-01	2.500000E 00	1.268311E-01	-1.101368E-04	-4.139095E-03
47 NCR1	3.300000E-01	0.	6.103516E-04	-6.403302E-07	-2.049057E-05
48 DRHO	6.670000E-02	6.681750E 03	-3.351758E 01	5.312786E-01	-5.003455E-02
49 FWN1	10.000000E-01	1.495000E 02	1.906372E 00	[illegible]	-3.194514E-01
50 CNDR	5.760000E-05	1.000000E 00	1.403809E-02	3.795260E-05	-6.830189E-06
51 CYDQ	5.760000E-05	0.	2.197266E-03	-1.920991E-06	-7.940095E-05
52 CLDR	5.760000E-05	0.	8.544922E-04	-1.280660E-06	-3.927359E-05
53 CLDQ	5.760000E-05	0.	7.202148E-03	-1.472760E-05	-3.201651E-04
54 CMDR	5.760000E-05	0.	1.220703E-04	6.403302E-07	0.
55 NCDQ	5.760000E-05	0.	1.220703E-04	0.	-7.683963E-06
56 LSMY	10.000000E-03	1.500000E 00	5.358887E-02	-2.582665E-05	-1.527401E-03
57 LSMP	10.000000E-03	2.175000E 01	-2.551270E-01	2.338913E-03	5.910675E-03
58 MSMP	1.000000E-01	8.275000E 01	-4.240723E-01	6.708313E-03	-4.909198E-04
59 MSMR	1.000000E-01	8.580000E 02	-4.676514E 00	7.024828E-02	-5.250708E-03
60 NSMY	1.000000E-01	-7.500000E-01	1.916504E-02	-8.281604E-05	-8.537736E-04
61 NSMR	1.000000E-01	-2.000000E 00	1.432495E 00	-3.459491E-03	-6.416450E-02
62 CDV1	1.000000E-01	-8.372500E 02	-8.585693E 00	-3.149827E-02	-3.830882E-03
63 CDV2	1.000000E-01	-3.960000E 02	-4.084106E 00	-1.490347E-02	-1.823660E-03
64 CDV3	1.000000E-01	-3.960000E 02	-4.084106E 00	-1.490347E-02	-1.823660E-03
65 LDA2	1.000000E-01	1.175000E 02	1.461182E-01	7.886734E-03	-1.374576E-03
66 TIM1	7.800000E-02	4.138750E 03	-2.511023E 01	3.237469E-01	-2.599911E-02
67 TIM2	4.000000E-03	1.620000E 02	2.296875E 00	5.382829E-03	9.690331E-04
68 TIM3	3.000000E-03	6.500000E 00	1.027832E-01	2.320130E-04	-4.951887E-05
69 TIM4	3.000000E-03	3.250000E 00	5.090332E-02	1.141922E-04	-2.475944E-05
70 PW20	5.400000E-04	-7.050000E 01	-3.320190E 00	-4.607816E-03	-1.881973E-02
71 ISP2	9.400000E-04	3.172500E 02	2.079040E 01	1.435044E-02	-9.733019E-04
72 MFR2	10.000000E-03	3.492500E 02	2.120642E 01	9.614345E-03	-5.822736E-04
73 KRP2	4.400000E-02	1.725000E 01	-1.645825E 01	-2.592633E-02	2.467423E-01
74 DBP2	1.000000E-01	-3.070000E 02	2.280518E 00	-1.381111E-01	-6.044376E-02
75 KRY2	2.620000E-02	0.	4.713135E-01	-1.094965E-03	-1.987158E-02
76 DBY2	1.000000E-01	3.250000E 00	5.214722E 00	-1.322367E-02	-2.214911E-01
77 ROF2	2.500000E-01	-3.325000E 01	-1.262329E 00	-4.178155E-03	5.963182E-02
78 TMP2	1.670000E-03	-4.708000E 03	1.955579E 01	-1.057977E 00	3.450014E-02
79 TMY2	1.670000E-03	-7.750000E 01	-2.150891E 01	3.752890E-02	8.900821E-01
80 C2PY	3.300000E-03	0.	1.848149E-01	-4.463102E-04	-7.779585E-03
81 C2YP	3.300000E-03	0.	2.036133E-01	-4.887854E-04	-8.524930E-03

82	CD02	1.000000E-01	-5.750000E 01	-2.739624E 00	-3.363014E-03	-1.000708E-02
83	CNA2	1.000000E-01	-1.200000E 01	6.671143E-01	-9.035059E-03	-2.823429E-02
84	ZET2	1.000000E-01	-4.750000E 00	5.822754E-01	-5.694884E-03	-2.555771E-02
85	TIM6	3.000000E-03	0.	1.545410E-01	-3.694705E-04	-6.465628E-03
86	TIM7	3.000000E-03	0.	1.220703E-04	-2.134434E-07	-8.537736E-07

Table 14. ERROR SOURCE DEVIATION AT FOURTH STAGE IGNITION

CODE	STND.DEV.	RANGE DEVIATION (FT)	VELOCITY DEV. (FPS)	FLT. PATH ANGLE DEV. (DEG)	INCL.DEV. (DEG)
1 PW10	6.000000E-04	2.002000E 03	-5.699463E-01	1.529466E-02	-3.537076E-04
2 SIW1	8.300000E-03	1.077575E 04	-4.248047E 00	8.123437E-02	-2.205297E-03
3 SIW2	4.100000E-03	3.554000E 03	-1.402954E 00	2.678367E-02	-7.265614E-04
4 SIW3	9.300000E-04	1.293000E 03	-5.115967E-01	9.743510E-03	-2.646698E-04
5 SIW4	2.400000E-03	2.637500E 02	-1.041260E-01	1.990545E-03	-5.293397E-05
6 ISP1	1.800000E-03	1.971525E 04	6.753540E 00	1.725302E-01	3.742090E-03
7 MFR1	1.400000E-02	2.147025E 04	6.956543E 00	1.858900E-01	9.085859E-03
8 KPIA	1.030000E-07	8.500000E 00	2.722168E-02	1.080757E-04	-1.499226E-03
9 KPSA	1.080000E-07	1.845000E 02	-5.521240E-01	7.993597E-04	-6.574057E-05
10 KYIA	1.030000E-07	8.750000E 00	3.088379E-02	2.162032E-05	-2.148094E-03
11 THOR	9.250000E-05	1.125000E 01	3.503418E-02	3.511894E-05	-2.379467E-03
12 THOP	5.760000E-05	2.012500E 02	6.276855E-01	2.730311E-03	7.427831E-05
13 THOY	5.430000E-05	1.450000E 01	3.063965E-02	6.398717E-05	-1.986731E-03
14 DTER	3.280000E-06	5.750000E 00	1.904297E-02	1.635177E-05	-1.365184E-03
15 DTEP	1.250000E-06	1.720000E 02	5.129395E-01	2.267534E-03	6.147170E-05
16 DTEY	2.000000E-06	1.450000E 01	4.748535E-02	4.071683E-05	-3.263977E-03
17 DKSG	3.500000E-03	7.917500E 03	2.304248E 01	1.034874E-01	2.685118E-03
18 DRBE	3.570000E-03	1.692500E 02	5.234375E-01	2.140221E-03	-2.758457E-02
19 DYBE	3.570000E-03	2.052500E 02	7.786865E-01	2.801054E-03	-3.894403E-02
20 DPBE	3.570000E-03	4.943750E 03	-1.567053E 01	1.941299E-02	-1.844151E-03
21 TYRG	1.450000E-03	2.500000E 00	7.324219E-03	8.487711E-06	-4.994576E-04
22 TRRG	1.450000E-03	0.	0.	1.625838E-07	0.
23 KPP1	2.430000E-02	9.275000E 01	4.691162E-01	1.749616E-03	5.122642E-05
24 KPR1	3.060000E-02	0.	0.	-0.	0.
25 KPY1	2.330000E-02	1.250000E 00	5.859375E-03	2.031881E-05	-3.065047E-04
26 KRP1	4.400000E-02	6.302500E 02	-1.993652E 00	2.355800E-03	-2.219811E-04
27 KRY1	2.100000E-02	0.	1.220703E-04	3.260015E-07	-2.561321E-06
28 KRR1	2.620000E-02	0.	0.	-0.	0.
29 KPAN	3.130000E-11	3.500000E 00	1.086426E-02	4.744947E-05	-1.707547E-06
30 KRAN	3.120000E-11	0.	4.882813E-04	6.520029E-07	-2.305189E-05
31 KYAN	3.130000E-11	0.	6.103516E-04	1.464922E-06	-3.329717E-05
32 TMP1	1.670000E-03	2.030925E 04	-1.001678E 02	2.943705E-02	-1.321300E-02
33 TMY1	1.670000E-03	8.617750E 03	1.463013E 00	7.283455E-02	-2.196811E-01
34 CA01	10.000000E-03	8.164500E 03	-3.671265E 00	6.121730E-02	-1.946945E-02
35 CNAL	2.000000E-01	4.288250E 03	-1.059216E 01	2.093910E-02	-1.134665E-03
36 CNDQ	2.000000E-01	-5.250000E 02	1.232056E 00	-2.575617E-03	1.203821E-04
37 CYBA	3.300000E-01	5.400000E 01	1.038818E-01	5.931342E-04	-4.869925E-03
38 CYDR	3.300000E-01	-9.000000E 00	1.525879E-02	-9.535167E-05	-9.289057E-04
39 CLDP	1.000000E-01	0.	0.	-0.	0.

40	CLP1	1.000000E-01	0.	0.	-0.	0.
41	CMDQ	2.000000E-03	1.700000E 01	4.125977E-02	8.401166E-05	-4.268868E-06
42	CMQ1	2.000000E-03	4.500000E 00	1.269531E-02	1.858375E-05	-8.537736E-07
43	CMAL	2.000000E-03	3.025000E 01	5.822754E-02	3.380685E-04	-6.830189E-06
44	CMO1	9.000000E-02	3.047000E 03	-9.868408E 00	1.216321E-02	-1.209797E-03
45	NCBA	3.300000E-01	-9.450000E 01	-1.241455E-01	-9.594448E-04	5.147401E-03
46	NCDR	3.300000E-01	2.825000E 01	4.748535E-02	3.031197E-04	-2.103698E-03
47	NCR1	3.300000E-01	2.500000E-01	1.220703E-04	2.436256E-06	-9.391510E-06
48	DRHO	6.670000E-02	5.195925E 04	-3.184485E 01	3.760770E-01	-1.459355E-02
49	FWN1	10.000000E-01	2.710000E 02	1.050903E 00	8.142977E-03	-2.404013E-01
50	CNDR	5.760000E-05	4.500000E 00	1.171875E-02	5.719283E-05	-1.707547E-06
51	CYDQ	5.760000E-05	5.000000E-01	8.544922E-04	2.765593E-06	-4.781132E-05
52	CLDR	5.760000E-05	0.	1.220703E-04	1.137253E-06	-2.561321E-05
53	CLDQ	5.760000E-05	7.500000E-01	2.807617E-03	1.072720E-05	-1.622170E-04
54	CMDR	5.760000E-05	0.	2.441406E-04	8.137530E-07	0.
55	NCDQ	5.760000E-05	0.	0.	-1.617501E-07	-3.415095E-06
56	LSMY	10.000000E-03	1.550000E 01	1.916504E-02	1.007578E-04	-9.468350E-04
57	LSMP	10.000000E-03	2.035000E 02	-1.734619E-01	1.437174E-03	3.083830E-03
58	MSMP	1.000000E-01	3.695000E 02	-9.869385E-01	1.760512E-03	-1.135519E-04
59	MSMR	1.000000E-01	3.772000E 03	-1.046826E 01	1.742943E-02	-1.209797E-03
60	NSMY	1.000000E-01	-4.500000E 00	8.666992E-03	-5.123892E-05	-5.242170E-04
61	NSMR	1.000000E-01	1.115000E 02	5.957031E-01	1.746312E-03	-3.263037E-02
62	CDV1	1.000000E-01	-5.636500E 03	-1.894775E 00	-4.937603E-02	-1.073193E-03
63	CDV2	1.000000E-01	-2.673750E 03	-9.108887E-01	-2.344402E-02	-5.105566E-04
64	CDV3	1.000000E-01	-2.673750E 03	-9.108887E-01	-2.344402E-02	-5.105566E-04
65	LDA2	1.000000E-01	6.685000E 02	-7.862549E-01	4.573528E-03	-6.232548E-04
66	TIM1	7.800000E-02	1.630500E 04	-5.028137E 01	6.639660E-02	-5.920066E-03
67	TIM2	4.000000E-03	6.607500E 02	1.912231E 00	8.653793E-03	2.211274E-04
68	TIM3	3.000000E-03	2.875000E 01	8.618164E-02	3.776414E-04	-1.366038E-05
69	TIM4	3.000000E-03	1.425000E 01	4.284668E-02	1.863861E-04	-6.830189E-06
70	PW20	5.400000E-04	-1.428750E 03	-1.799438E 00	-1.513143E-02	-9.359067E-03
71	ISP2	9.400000E-04	7.672500E 03	1.152637E 01	8.373832E-02	-3.785632E-03
72	MFR2	10.000000E-03	7.993750E 03	1.390637E 01	9.984564E-02	-6.333293E-03
73	KRP2	4.400000E-02	2.095000E 02	-2.890625E-01	1.537976E-03	-6.720352E-03
74	DBP2	1.000000E-01	-8.146000E 03	1.519263E 01	-5.852703E-02	-3.386237E-02
75	KRY2	2.620000E-02	4.050000E 01	1.889648E-01	5.982510E-04	-1.049117E-02
76	DBY2	1.000000E-01	3.825000E 02	2.223633E 00	6.128105E-03	-1.167331E-01
77	ROE2	2.500000E-01	-5.695000E 02	3.308105E-01	-4.810672E-03	3.123616E-02
78	TMP2	1.670000E-03	-6.467925E 04	1.265763E 02	-4.358729E-01	1.354939E-03
79	TMY2	1.670000E-03	-2.835250E 03	-8.119019E 00	-3.562557E-02	4.665907E-01
80	C2PY	3.300000E-03	1.500000E 01	7.617188E-02	2.271330E-04	-4.109212E-03
81	C2YP	3.300000E-03	1.650000E 01	8.422852E-02	2.531422E-04	-4.504510E-03

82	CDO2	1.000000E-01	-1.140750E 03	-1.469360E 00	-1.210769E-02	-4.824675E-03
83	CNA2	1.000000E-01	-4.165000E 02	1.073364E 00	-2.687729E-03	-1.496324E-02
84	ZET2	1.000000E-01	-2.242500E 02	6.901855E-01	-1.336858E-03	-1.350841E-02
85	TIM6	3.000000E-03	1.300000E 01	6.384277E-02	1.929862E-04	-3.415948E-03
86	TIM7	3.000000E-03	0.	0.	3.251677E-07	0.
87	PW3C	6.000000E-04	1.612500E 03	-3.701050E 00	1.120457E-02	-9.869623E-04
88	ISP3	1.400000E-03	1.019950E 04	2.414673E 01	1.264097E-01	6.410986E-03
89	MFR3	1.800000E-02	1.297325E 04	2.014209E 01	1.054485E-01	4.029812E-04
90	KRP3	4.400000E-02	0.	0.	4.869178E-07	0.
91	DRP3	1.000000E-01	0.	0.	-0.	0.
92	KRY3	2.100000E-02	0.	0.	-0.	0.
93	DRY3	1.000000E-01	0.	0.	-0.	0.
94	PDF3	2.500000E-01	-4.675000E 01	-2.480469E-01	-7.300398E-04	1.197161E-02
95	TMP3	5.570000E-04	1.837650E 04	3.201086E 01	2.177926E-01	2.163462E-03
96	TMY3	5.570000E-04	7.255000E 02	-2.738892E 00	3.813403E-03	1.397405E-01

Table 15. 3σ ERROR SOURCE DEVIATIONS AT BURNOUT

CODE	STND.DEV.	RANGE DEVIATION (FT)	VELOCITY DEV. (FPS)	FLT. PATH ANGLE DEV. (DEG)	INCL.DEV. (DEG)
1 PWIC	6.000000E-04	2.166000E 03	-4.443359E-01	9.470217E-03	-1.810000E-04
2 SIW1	8.300000E-03	1.168925E 04	-3.543701E 00	4.955629E-02	-1.067217E-03
3 SIW2	4.100000E-03	3.854250E 03	-1.168945E 00	1.634123E-02	-3.517547E-04
4 SIW3	9.300000E-04	1.402250E 03	-4.265137E-01	5.944682E-03	-1.280660E-04
5 SIW4	2.400000E-03	2.865000E 02	-8.666992E-02	1.214526E-03	-2.561321E-05
6 TSP1	1.800000E-03	2.136075E 04	4.957275E 00	1.129225E-01	1.830491E-03
7 MER1	1.400000E-02	2.463000E 04	6.944092E 00	1.132234E-01	2.228349E-03
8 KRIA	1.030000E-07	9.250000E 00	1.440430E-02	6.839527E-05	-8.204765E-04
9 KPSA	1.080000E-07	1.892500E 02	-5.549316E-01	1.018292E-04	-1.536793E-05
10 KYIA	1.030000E-07	9.750000E 00	1.684570E-02	1.668194E-05	-1.383967E-03
11 THOR	9.250000E-05	1.250000E 01	1.904297E-02	2.508961E-05	-1.533377E-03
12 THOP	5.760000E-05	2.052500E 02	6.245117E-01	2.113166E-03	1.622170E-05
13 THOY	5.430000E-05	1.575000E 01	1.684570E-02	4.276872E-05	-1.281514E-03
14 DTER	3.280000E-06	6.250000E 00	1.025391E-02	1.215960E-05	-8.802406E-04
15 DTEP	1.250000E-06	1.762500E 02	5.109863E-01	1.741331E-03	1.451415E-05
16 DTEY	2.000000E-06	1.600000E 01	2.587891E-02	3.021225E-05	-2.103698E-03
17 DKSG	3.500000E-03	8.128000E 03	2.295094E 01	7.939207E-02	5.984953E-04
18 DRBF	3.570000E-03	1.892500E 02	2.824707E-01	1.358774E-03	-1.505118E-02
19 DYBF	3.570000E-03	2.317500E 02	4.384766E-01	1.806051E-03	-2.116761E-02
20 DPBF	3.570000E-03	5.048000E 03	-1.571606E 01	4.958791E-04	-4.157878E-04
21 TYRG	1.450000E-03	2.500000E 00	3.906250E-03	5.655250E-06	-3.218727E-04
22 TPRG	1.450000E-03	0.	0.	-0.	0.
23 KPP1	2.420000E-02	9.000000E 01	4.609375E-01	1.444018E-03	1.024528E-05
24 KPR1	3.060000E-02	0.	0.	-0.	0.
25 KPY1	2.320000E-02	1.500000E 00	3.173828E-03	1.296335E-05	-1.673396E-04
26 KRP1	4.400000E-02	6.415000E 02	-1.997559E 00	-5.778647E-05	-4.610378E-05
27 KRY1	2.100000E-02	-2.500000E-01	0.	1.934331E-07	-1.707547E-06
28 KRR1	2.620000E-02	0.	0.	-0.	0.
29 KPAN	3.130000E-11	3.500000E 00	1.074219E-02	3.651550E-05	0.
30 KRAN	3.120000E-11	-2.500000E-01	2.441406E-04	3.968713E-07	-1.280660E-05
31 KYAN	3.130000E-11	-2.500000E-01	0.	1.187279E-06	-1.792925E-05
32 CAC1	10.000000E-03	8.868250E 03	-3.121582E 00	3.706063E-02	-8.076699E-04
33 CNAL	2.000000E-01	4.432500E 03	-1.070288E 01	5.351510E-03	-2.194198E-04
34 CNDQ	2.000000E-01	-5.432500E 02	1.245117E 00	-6.811946E-04	1.878302E-05
35 CYBA	3.300000E-01	5.925000E 01	5.883789E-02	3.836512E-04	-2.649260E-03
36 CYDR	3.300000E-01	-1.000000E 01	8.789063E-03	-6.132162E-05	-5.993491E-04
37 CLDP	1.000000E-01	0.	0.	-0.	0.

38	CLP1	1.000000E-01	0.	0.	-0.	0.
39	CMDQ	2.000000E-03	1.750000E 01	4.077148E-02	2.312526E-05	-8.537736E-07
40	CMQ1	2.000000E-03	4.250000E 00	1.269531E-02	2.244491E-06	0.
41	CMAL	2.000000E-03	3.150000E 01	5.834961E-02	2.483181E-04	-8.537736E-07
42	CMO1	9.000000E-02	3.112250E 03	-9.899170E 00	4.745747E-04	-2.928444E-04
43	NCBA	3.300000E-01	-1.040000E 02	-7.348633E-02	-6.242153E-04	-4.476335E-03
44	NCDR	3.300000E-01	3.125000E 01	2.783203E-02	1.970850E-04	-1.149179E-03
45	NCR1	3.300000E-01	-2.500000E-01	-2.441406E-04	1.180609E-06	-5.122642E-06
46	DRHO	6.670000E-02	5.659825E 04	-2.827368E 01	2.219846E-01	-6.870316E-03
47	FWN1	10.000000E-01	9.425000E 01	1.183350E 00	2.220739E-03	-8.420342E-02
48	CNDR	5.760000E-05	4.250000E 00	1.147461E-02	4.347575E-05	0.
49	CYDQ	5.760000E-05	2.500000E-01	4.882813E-04	1.597491E-06	-3.073585E-05
50	CLDR	5.760000E-05	-2.500000E-01	-2.441406E-04	3.868662E-07	-1.024528E-05
51	CLDQ	5.760000E-05	7.500000E-01	9.765625E-04	6.373287E-06	-8.879246E-05
52	CMDR	5.760000E-05	0.	0.	5.969745E-07	0.
53	NCDQ	5.760000E-05	-2.500000E-01	0.	-3.335053E-09	-1.707547E-06
54	LSMY	10.000000E-03	1.675000E 01	1.147461E-02	6.253225E-05	-6.104481E-04
55	LSMP	10.000000E-03	2.220000E 02	-1.340332E-01	8.605038E-04	1.703278E-03
56	MSMP	1.000000E-01	3.810000E 02	-9.956055E-01	3.940099E-04	-2.475944E-05
57	MSMR	1.000000E-01	3.884500E 03	-1.054687E 01	3.337304E-03	-2.655236E-04
58	NSMY	1.000000E-01	-5.750000E 00	5.126953E-03	-3.333719E-05	-3.380944E-04
59	NSMR	1.000000E-01	1.275000E 02	3.193359E-01	1.099674E-03	-1.783704E-02
60	CDV1	1.000000E-01	-6.107750E 03	-1.387695E 00	-3.230810E-02	-5.250708E-04
61	CDV2	1.000000E-01	-2.897750E 03	-6.696777E-01	-1.534753E-02	-2.493019E-04
62	CDV3	1.000000E-01	-2.897750E 03	-6.696777E-01	-1.534753E-02	-2.493019E-04
63	LDA2	1.000000E-01	7.080000E 02	-8.305664E-01	2.351930E-03	-3.082123E-04
64	TIM1	7.800000E-02	1.667775E 04	-5.048364E 01	4.248901E-03	-1.331033E-03
65	TIM2	4.000000E-03	6.782500E 02	1.905518E 00	6.638253E-03	4.866510E-05
66	TIM3	3.000000E-03	2.925000E 01	8.569336E-02	2.903331E-04	-3.415095E-06
67	TIM4	3.000000E-03	1.425000E 01	4.248047E-02	1.430738E-04	-1.707547E-06
68	PW20	5.400000E-04	-1.579000E 03	-1.711914E 00	-1.073390E-02	-5.151670E-03
69	ISP2	9.400000E-04	8.502500E 03	1.054443E 01	5.953024E-02	-2.614255E-03
70	MFR2	10.000000E-03	9.223500E 03	1.110107E 01	7.374287E-02	-4.072500E-03
71	KRP2	4.400000E-02	2.217500E 02	-3.598633E-01	5.873645E-04	-3.739529E-03
72	DBP2	1.000000E-01	-8.688250E 03	1.535449E 01	-2.721539E-02	-1.964789E-02
73	KRY2	2.620000E-02	4.550000E 01	9.082031E-02	3.648582E-04	-5.867132E-03
74	DBY2	1.000000E-01	4.347500E 02	1.147949E 00	3.764064E-03	-6.512158E-02
75	ROF2	2.500000E-01	-6.110000E 02	6.437988E-01	-2.404423E-03	1.738710E-02
76	C2PY	3.300000E-03	1.650000E 01	3.784180E-02	1.398688E-04	-2.299212E-03
77	C2YP	3.300000E-03	1.875000E 01	4.174805E-02	1.560305E-04	-2.520340E-03
78	CD02	1.000000E-01	-1.260750E 03	-1.375977E 00	-8.574729E-03	-2.631330E-03
79	CNA2	1.000000E-01	-4.390000E 02	9.616699E-01	-1.198065E-03	-8.391741E-03

80	ZET2	1.000000E-01	-2.355000E 02	5.810547E-01	-5.757903E-04	-7.562727E-03
81	TIM6	3.000000E-03	1.425000E 01	3.198242E-02	1.189213E-04	-1.910745E-03
82	TIM7	3.000000E-03	0.	0.	-0.	0.
83	PW30	6.000000E-04	1.811500E 03	-3.528809E 00	5.496805E-03	-4.123727E-04
84	ISP3	1.400000E-03	1.147275E 04	2.272168E 01	9.293049E-02	2.675727E-03
85	MFR3	1.800000E-02	1.023550E 04	2.265967E 01	5.998991E-02	7.385142E-04
86	KPP3	4.400000E-02	0.	0.	2.001032E-07	0.
87	DBP3	1.000000E-01	0.	0.	-0.	0.
88	KRY3	2.100000E-02	0.	0.	-0.	0.
89	DBY3	1.000000E-01	0.	0.	-0.	0.
90	RCF3	2.500000E-01	-5.425000E 01	-1.499023E-01	-4.856871E-04	6.766156E-03
91	PW4C	3.400000E-04	2.000000E 00	-4.106201E 00	-1.565140E-05	-3.107736E-04
92	ISP4	6.000000E-03	7.450000E 01	1.826553E 02	2.045298E-02	1.376112E-02
93	MFR4	1.800000E-02	9.225000E 01	9.743552E 00	1.489861E-02	2.825991E-03
94	TMP4	5.000000E-04	9.675000E 01	1.118164E-01	1.410644E-02	-1.157888E-02
95	TMY4	5.000000E-04	9.050000E 01	-3.117676E-01	1.217123E-02	1.339571E-02
96	TMP1	1.670000E-03	2.008425E 04	-9.952222E 01	-5.722424E-02	-3.425340E-03
97	TMY1	1.670000E-03	9.277000E 03	1.311035E-01	4.384546E-02	1.919889E-01
98	TMP2	1.670000E-03	-6.825100E 04	1.295133E 02	-1.923391E-01	-4.929689E-03
99	TMY2	1.670000E-03	-3.162250E 03	-3.954346 00	-2.203015E-02	2.599877E-01
100	TMP3	5.570000E-04	1.962625E 04	3.266087E 01	1.525493E-01	-7.683963E-05
101	TMY3	5.570000E-04	8.217500E 02	-1.625732E 00	2.373941E-03	7.888015E-02
102	W4CP	3.000000E-02	-4.607500E 02	-1.079858E 01	-5.500703E-02	5.645245E-01
103	W4CY	3.000000E-02	-4.000250E 03	-1.227246E 01	5.781016E-01	6.029008E-02

Table 16. SUMMARY OF STATISTICAL OUTPUT AND CUMULATIVE DISTRIBUTION FUNCTIONS

DISPERSED STATE (ORBITAL PLANE)

MEAN MAGNITUDE OF POSITION	=	1.7798697D 04
MEAN MAGNITUDE OF VELOCITY	=	1.4884561D 01
RST OF POSITION	=	6.3716131D 04
RST OF VELOCITY	=	1.9305753D 02

DISPERSED STATE(ECI)

MEAN MAGNITUDE OF POSITION	=	1.7798697D 04
MEAN MAGNITUDE OF VELOCITY	=	1.4884561D 01
RST OF POSITION	=	6.3716130D 04
RST OF VELOCITY	=	1.9305753D 02

DISPERSION OF THE SEMIMAJOR AXIS(FT.)

MEAN	=	3.8491378D 04
STANDARD DEVIATION	=	1.8557913D 05
SMALLEST SAMPLE	=	-5.1307974E 05
2ND PERCENTILE SAMPLE	=	-3.5150600E 05
5TH PERCENTILE SAMPLE	=	-2.6366000E 05
95TH PERCENTILE SAMPLE	=	3.5333775E 05
98TH PERCENTILE SAMPLE	=	4.4065275E 05
LARGEST SAMPLE	=	7.5662674E 05

ECCENTRICITY DISPERSION

MEAN	=	1.3077680D-03
STANDARD DEVIATION	=	6.1285438D-03
SMALLEST SAMPLE	=	-1.6527190E-02
2ND PERCENTILE SAMPLE	=	-1.2076994E-02
5TH PERCENTILE SAMPLE	=	-8.9474627E-03
95TH PERCENTILE SAMPLE	=	1.1209779E-02
98TH PERCENTILE SAMPLE	=	1.4431600E-02
LARGEST SAMPLE	=	2.3213425E-02

INCLINATION DISPERSION (DEGREES)

MEAN	=	8.0994435D-03
STANDARD DEVIATION	=	2.5838917D-01
SMALLEST SAMPLE	=	-7.4547482E-01
2ND PERCENTILE SAMPLE	=	-5.0601196E-01
5TH PERCENTILE SAMPLE	=	-3.8473511E-01
95TH PERCENTILE SAMPLE	=	3.8161469E-01
98TH PERCENTILE SAMPLE	=	4.6471500E-01
LARGEST SAMPLE	=	1.7465315E 00

LONG. OF ASCENDING NODE DISPERSION (DEGREES)

MEAN	=	4.1299455D-02
STANDARD DEVIATION	=	1.5704708D-01
SMALLEST SAMPLE	=	-4.5805550E-01
2ND PERCENTILE SAMPLE	=	-2.7197170E-01
5TH PERCENTILE SAMPLE	=	-2.0540047E-01
95TH PERCENTILE SAMPLE	=	3.0354500E-01
98TH PERCENTILE SAMPLE	=	3.6755562E-01
LARGEST SAMPLE	=	5.6257439E-01

ARGUMENT OF PERIGEE DISPERSION (DEGREES)

MEAN	=	-3.4490963D-01
STANDARD DEVIATION	=	2.9371286D 00
SMALLEST SAMPLE	=	-1.0077705E 01
2ND PERCENTILE SAMPLE	=	-6.4568195E 00
5TH PERCENTILE SAMPLE	=	-5.5474358E 00
95TH PERCENTILE SAMPLE	=	4.3334522E 00
98TH PERCENTILE SAMPLE	=	5.6094685E 00
LARGEST SAMPLE	=	7.3938828E 00

DISPERSION OF ARC LENGTH ALONG ORBIT (NM)

MEAN	=	9.1870450D-01
STANDARD DEVIATION	=	4.2207398D 00
SMALLEST SAMPLE	=	-9.4426270E 00
2ND PERCENTILE SAMPLE	=	-7.4941406E 00
5TH PERCENTILE SAMPLE	=	-6.1430664E 00
95TH PERCENTILE SAMPLE	=	8.1850586E 00
98TH PERCENTILE SAMPLE	=	9.7133789E 00
LARGEST SAMPLE	=	1.9013183E 01

RADIUS VECTOR DISPERSION (FT)

MEAN	=	2.4473049D 03
STANDARD DEVIATION	=	3.9553746D 04
SMALLEST SAMPLE	=	-1.7844325E 05
2ND PERCENTILE SAMPLE	=	-6.9691000E 04
5TH PERCENTILE SAMPLE	=	-5.9351250E 04
95TH PERCENTILE SAMPLE	=	6.6545750E 04
98TH PERCENTILE SAMPLE	=	8.0538750E 04
LARGEST SAMPLE	=	1.2315425E 05

INERTIAL VELOCITY DISPERSION (FPS)

MEAN	=	1.3246368D 01
STANDARD DEVIATION	=	7.2937789D 01
SMALLEST SAMPLE	=	-2.1023291E 02
2ND PERCENTILE SAMPLE	=	-1.4189087E 02
5TH PERCENTILE SAMPLE	=	-1.0268628E 02
95TH PERCENTILE SAMPLE	=	1.3124414E 02
93TH PERCENTILE SAMPLE	=	1.6086157E 02
LARGEST SAMPLE	=	3.4003442E 02

AIRSPEED DISPERSION (FPS)

MEAN	=	1.3473233D 01
STANDARD DEVIATION	=	7.2858531D 01
SMALLEST SAMPLE	=	-2.1471704E 02
2ND PERCENTILE SAMPLE	=	-1.4149658E 02
5TH PERCENTILE SAMPLE	=	-1.0914844E 02
95TH PERCENTILE SAMPLE	=	1.3444019E 02
98TH PERCENTILE SAMPLE	=	1.6157568E 02
LARGEST SAMPLE	=	3.4847974E 02

INERTIAL FLIGHT PATH ANGLE DISPERSION (DEGREES)

MEAN	=	-3.2424376D-02
STANDARD DEVIATION	=	2.6268104D-01
SMALLEST SAMPLE	=	-9.5562365E-01
2ND PERCENTILE SAMPLE	=	-5.8515211E-01
5TH PERCENTILE SAMPLE	=	-5.0663142E-01
95TH PERCENTILE SAMPLE	=	3.6175275E-01
98TH PERCENTILE SAMPLE	=	4.9200977E-01
LARGEST SAMPLE	=	7.0523432E-01

ATMOSPHERIC FLIGHT PATH ANGLE DISPERSION (DEGREES)

MEAN	=	-3.2360883D-02
STANDARD DEVIATION	=	2.6215581D-01
SMALLEST SAMPLE	=	-9.5368574E-01
2ND PERCENTILE SAMPLE	=	-5.8399298E-01
5TH PERCENTILE SAMPLE	=	-5.0556389E-01
95TH PERCENTILE SAMPLE	=	3.6120283E-01
98TH PERCENTILE SAMPLE	=	4.9066618E-01
LARGEST SAMPLE	=	7.0389846E-01

APOGEE DISPERSION (NM)

MEAN	=	1.2547468D 01
STANDARD DEVIATION	=	5.8448690D 01
SMALLEST SAMPLE	=	-1.5819611E 02
2ND PERCENTILE SAMPLE	=	-1.1271759E 02
5TH PERCENTILE SAMPLE	=	-8.3956237E 01
95TH PERCENTILE SAMPLE	=	1.0781769E 02
98TH PERCENTILE SAMPLE	=	1.3700702E 02
LARGEST SAMPLE	=	2.3552209E 02

PERIGEE DISPERSION (NM)

MEAN	=	1.2229629D-01
STANDARD DEVIATION	=	7.2492862D 00
SMALLEST SAMPLE	=	-3.4590271E 01
2ND PERCENTILE SAMPLE	=	-1.3997986E 01
5TH PERCENTILE SAMPLE	=	-1.1578247E 01
95TH PERCENTILE SAMPLE	=	1.1613537E 01
98TH PERCENTILE SAMPLE	=	1.3657440E 01
LARGEST SAMPLE	=	2.0620911E 01

PERIOD DISPERSION (SEC)

MEAN	=	1.5464455D 01
STANDARD DEVIATION	=	7.3949864D 01
SMALLEST SAMPLE	=	-2.0319794E 02
2ND PERCENTILE SAMPLE	=	-1.3943524E 02
5TH PERCENTILE SAMPLE	=	-1.0468079E 02
95TH PERCENTILE SAMPLE	=	1.4114880E 02
98TH PERCENTILE SAMPLE	=	1.7618054E 02
LARGEST SAMPLE	=	3.0345239E 02

LONGITUDE DISPERSION (DEGREES)

MEAN	=	4.3711517D-02
STANDARD DEVIATION	=	1.0965521D-01
SMALLEST SAMPLE	=	-2.7001095E-01
2ND PERCENTILE SAMPLE	=	-1.7365456E-01
5TH PERCENTILE SAMPLE	=	-1.2997913E-01
95TH PERCENTILE SAMPLE	=	2.2935390E-01
98TH PERCENTILE SAMPLE	=	2.9844093E-01
LARGEST SAMPLE	=	4.7781944E-01

LATITUDE DISPERSION (DGREES)

MEAN	=	-1.5469372D-02
STANDARD DEVIATION	=	7.0195739D-02
SMALLEST SAMPLE	=	-3.1692839E-01
2ND PERCENTILE SAMPLE	=	-1.6178918E-01
5TH PERCENTILE SAMPLE	=	-1.3615537E-01
95TH PERCENTILE SAMPLE	=	1.0227585E-01
98TH PERCENTILE SAMPLE	=	1.2464929E-01
LARGEST SAMPLE	=	1.5712571E-01

ALTITUDE DISPERSION (NM)

MEAN	=	4.0275635D-01
STANDARD DEVIATION	=	6.5096974D 00
SMALLEST SAMPLE	=	-2.9367775E 01
2ND PERCENTILE SAMPLE	=	-1.1469662E 01
5TH PERCENTILE SAMPLE	=	-9.7680016E 00
95TH PERCENTILE SAMPLE	=	1.0952022E 01
98TH PERCENTILE SAMPLE	=	1.3254890E 01
LARGEST SAMPLE	=	2.0268623E 01

The final charts are cumulative distribution functions for each of the variables in the summary. Every tenth point after being sorted is plotted against its corresponding frequency. The solid line of the figures is a Gaussian distribution with equivalent mean and standard deviation.

Figure 5.

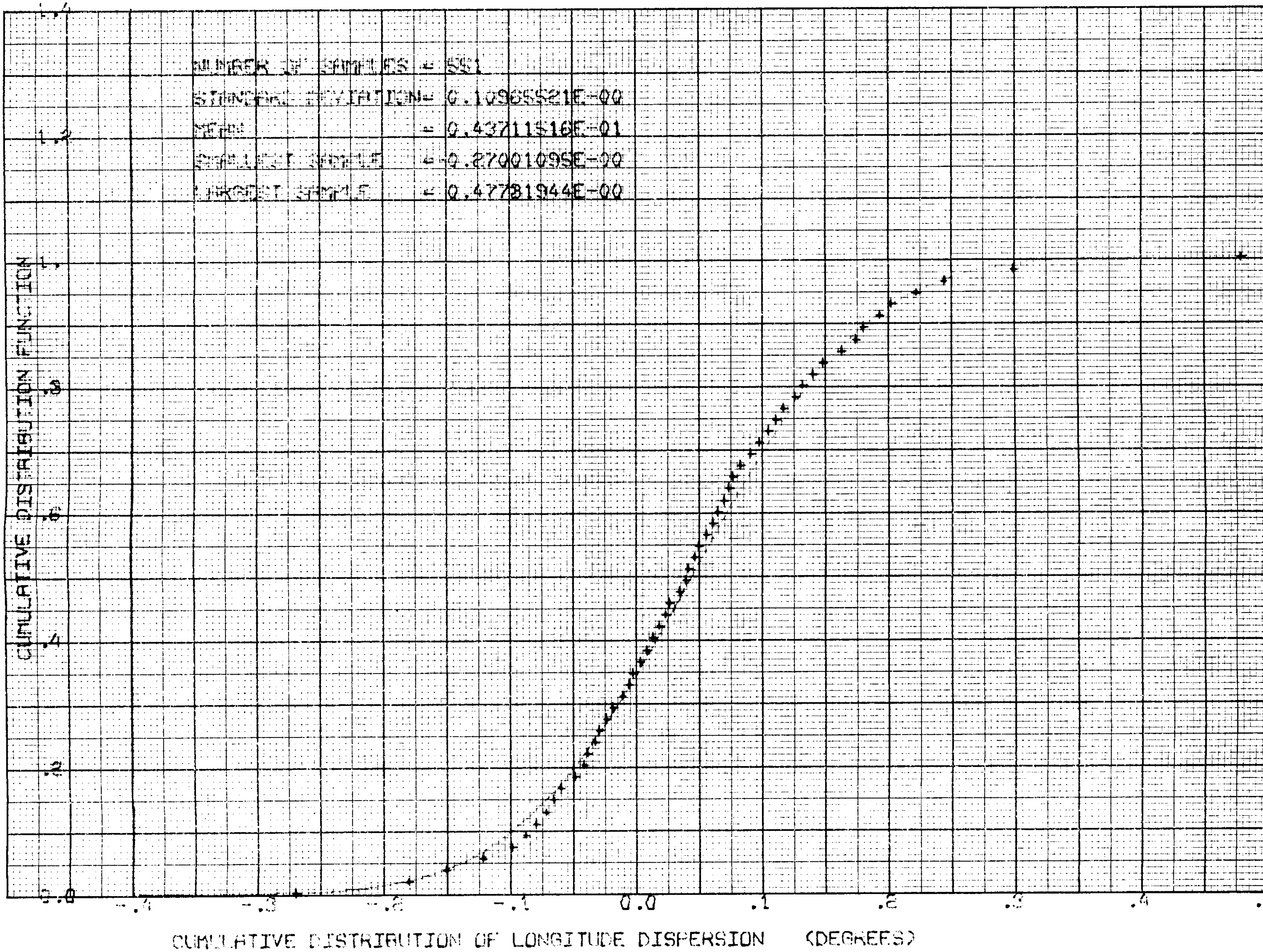
NUMBER OF SAMPLES = 551
STANDARD DEVIATION= 0.10965521E-00
MEAN = 0.43711516E-01
SMALLEST SAMPLE = -0.27001095E-00
LARGEST SAMPLE = 0.47781944E-00
CUMULATIVE DISTRIBUTION FUNCTION
CUMULATIVE DISTRIBUTION OF LONGITUDE DISPERSION (DEGREES)
0.0
.2
.4
.6
.8
1.
1.2
-.4
-.3
-.2
-.1
0.0
.1
.2
.3
.4
.5

Figure 6

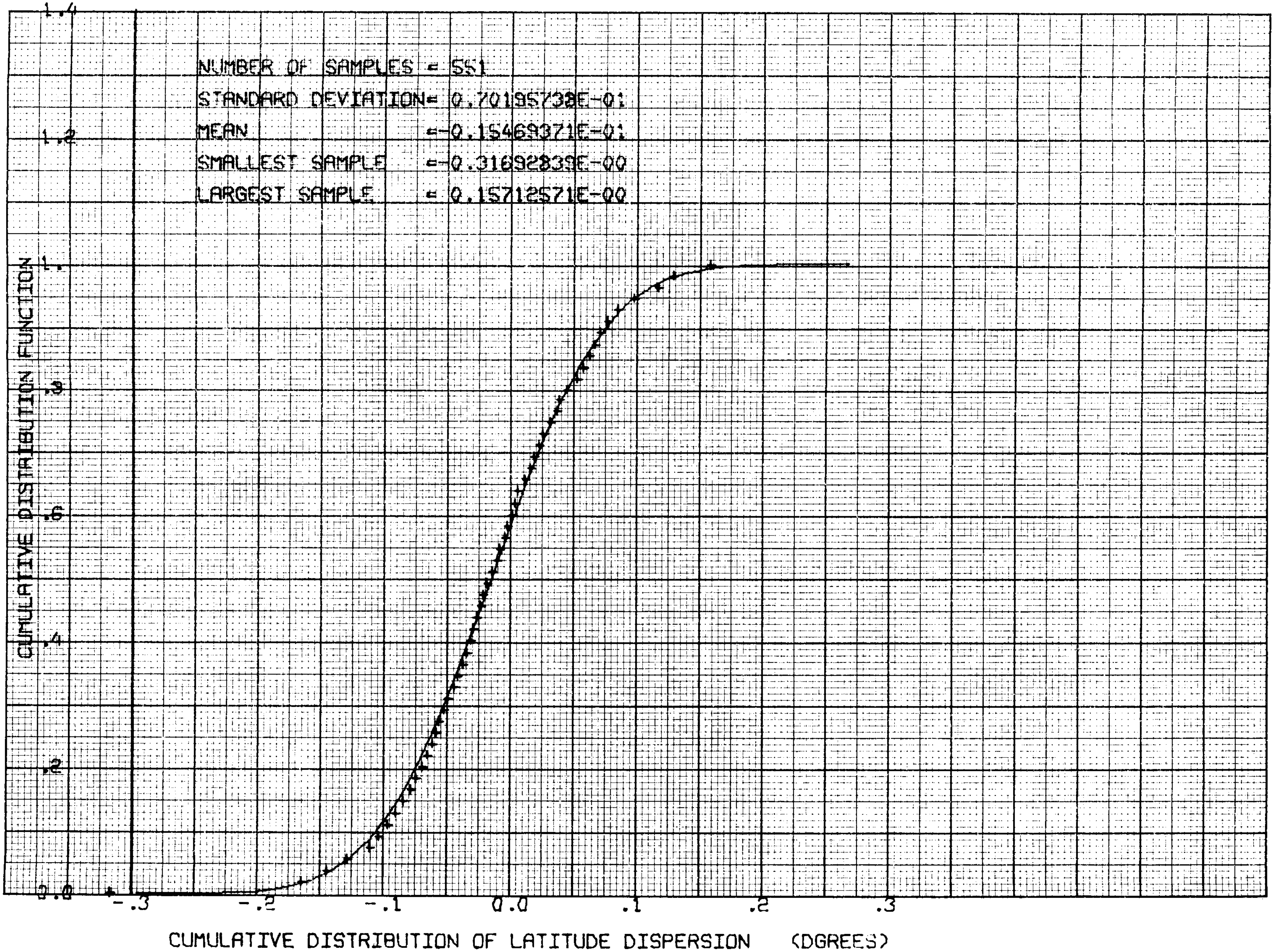
NUMBER OF SAMPLES = 551
STANDARD DEVIATION= 0.70195738E-01
MEAN =-0.15469371E-01
SMALLEST SAMPLE =-0.31692839E-00
LARGEST SAMPLE = 0.15712571E-00
CUMULATIVE DISTRIBUTION FUNCTION
1.4
1.2
1.
.8
.6
.4
.2
0.0
-.3
-.2
-.1
0.0
.1
.2
.3
CUMULATIVE DISTRIBUTION OF LATITUDE DISPERSION (DGREES)

Figure 7

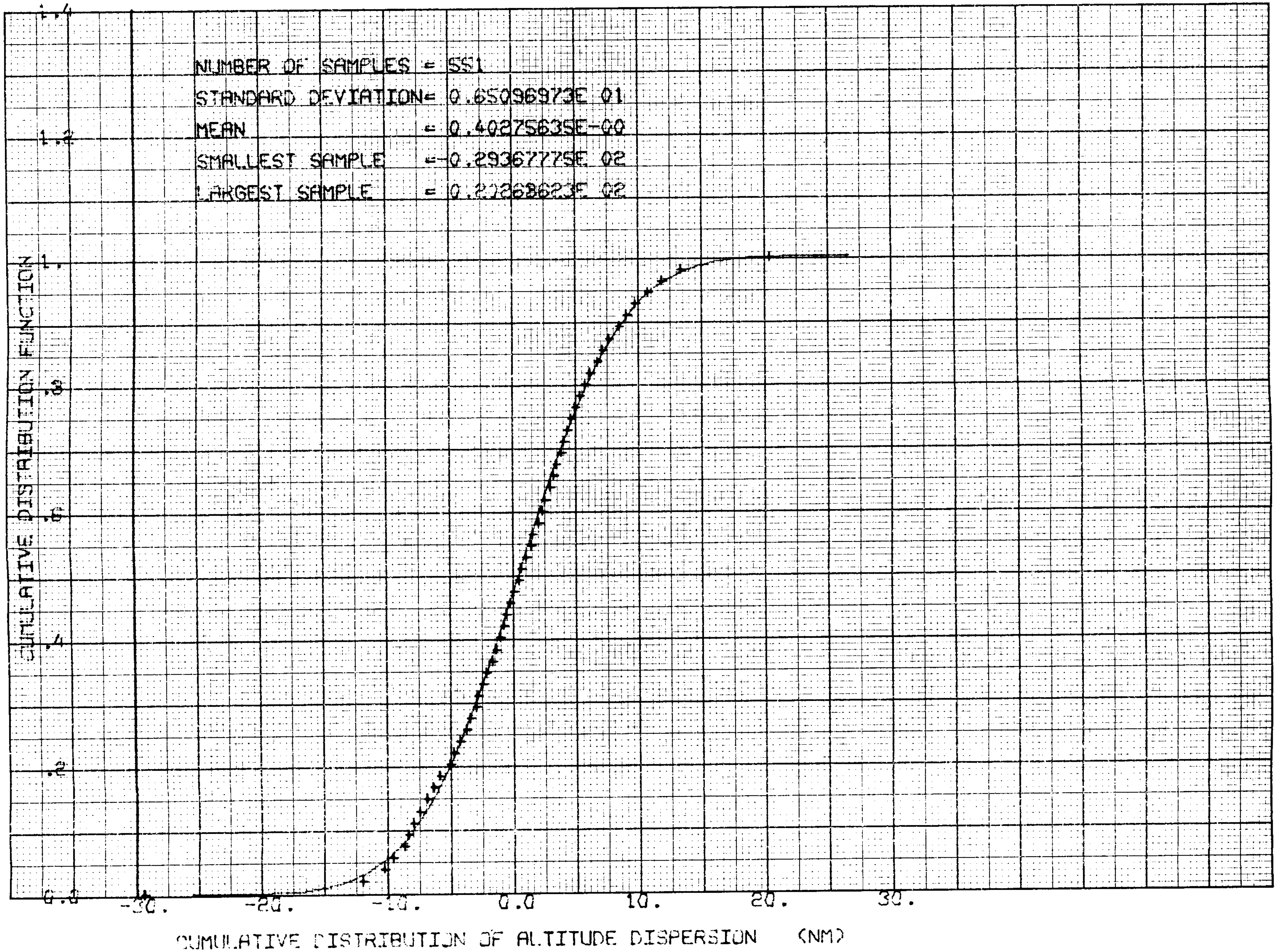
NUMBER OF SAMPLES = 551
STANDARD DEVIATION= 0.65096973E 01
MEAN = 0.40275635E-00
SMALLEST SAMPLE =-0.29367775E 02
LARGEST SAMPLE =
CUMULATIVE DISTRIBUTION FUNCTION
1.4
1.2
1.
.8
.6
.4
.2
0.0
-30.
-20.
-10.
0.0
10.
20.
30.
CUMULATIVE DISTRIBUTION OF ALTITUDE DISPERSION (NM)

Figure 8

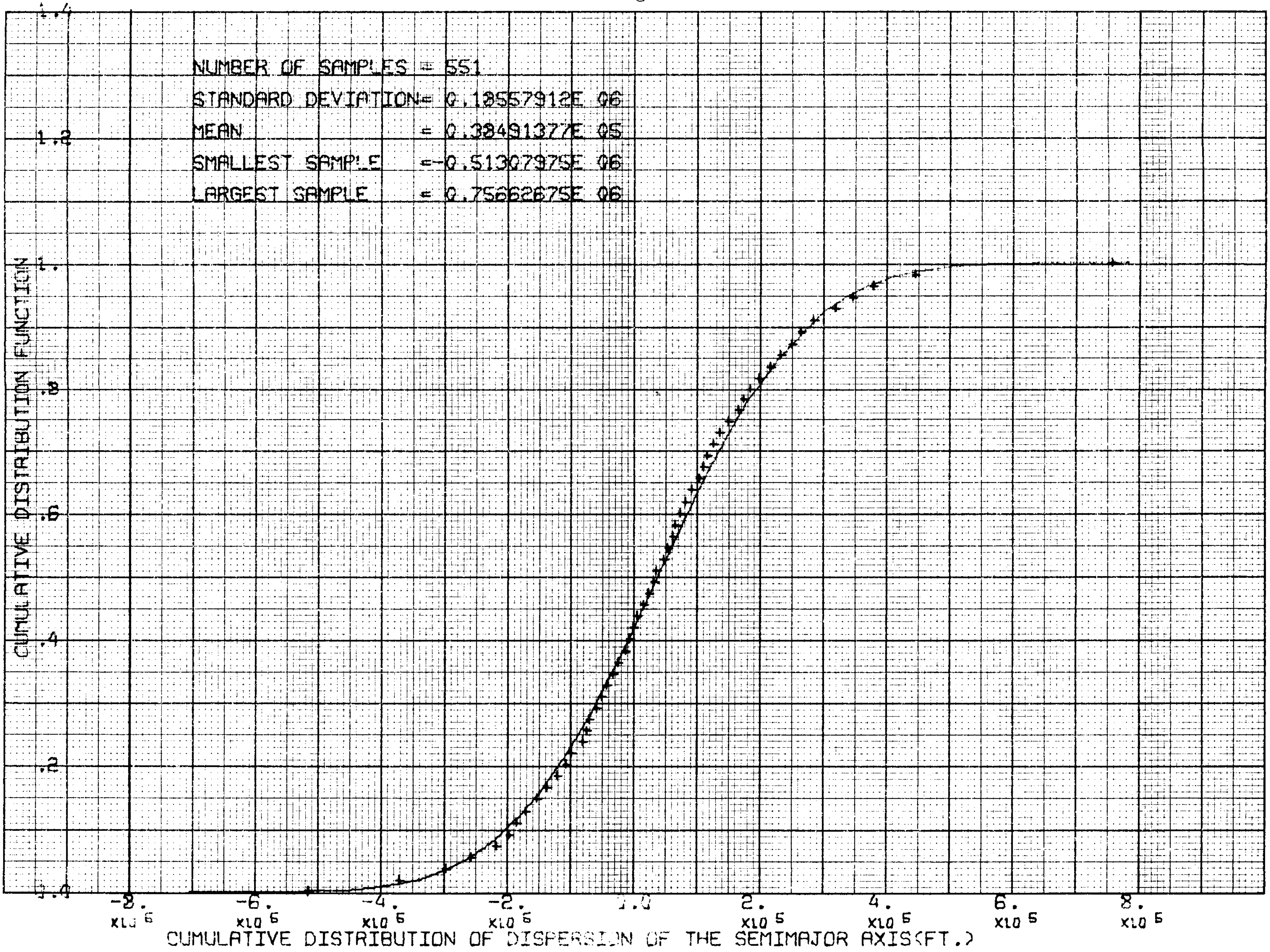
NUMBER OF SAMPLES = 551
STANDARD DEVIATION= 0.18557912E 06
MEAN = 0.38491377E 05
SMALLEST SAMPLE =-0.51307975E 06
LARGEST SAMPLE = 0.75662675E 06
CUMULATIVE DISTRIBUTION FUNCTION
CUMULATIVE DISTRIBUTION OF DISPERSION OF THE SEMIMAJOR AXIS(FT.)

Figure 9

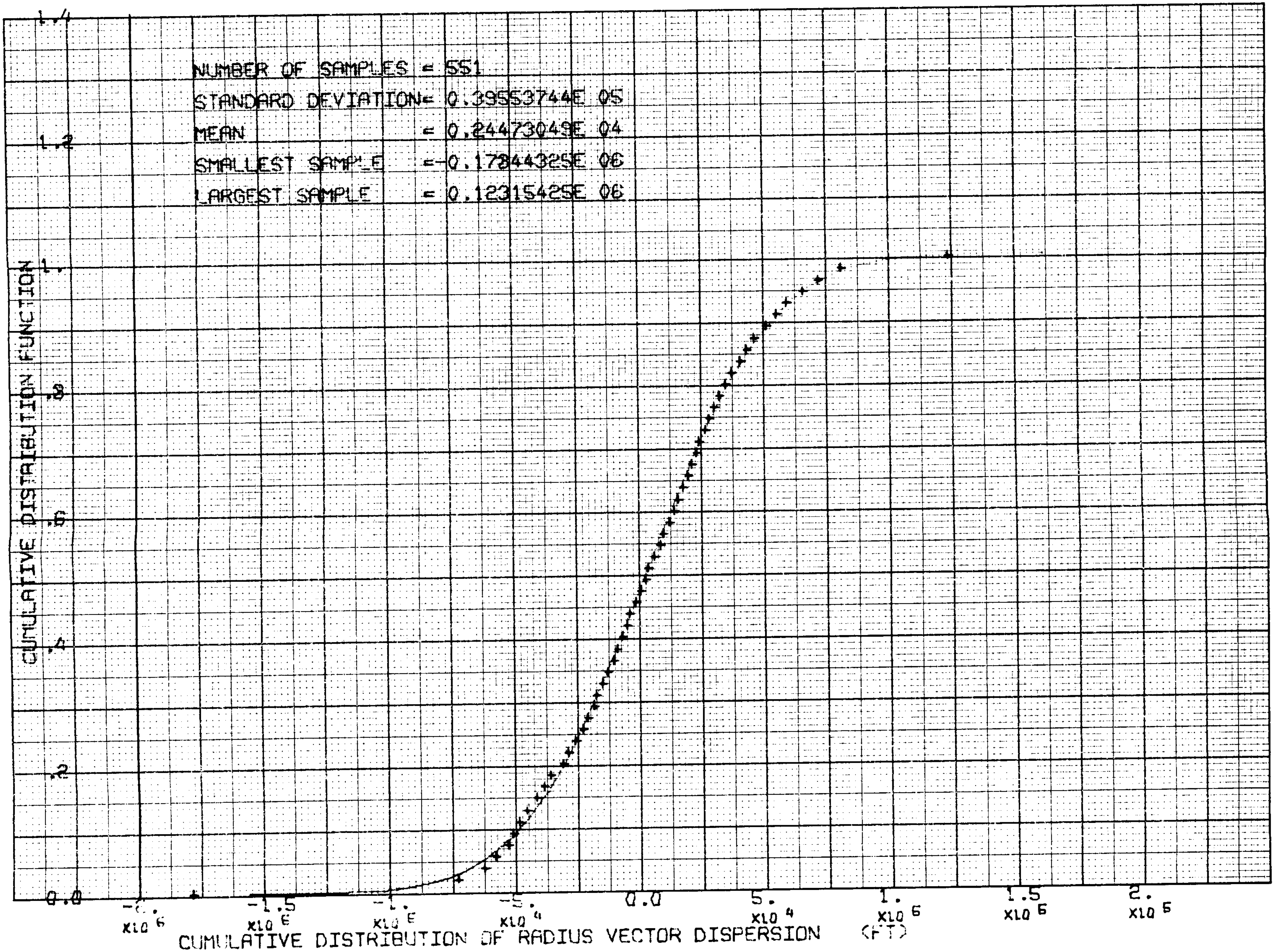
NUMBER OF SAMPLES = 551
STANDARD DEVIATION= 0.39553744E 05
MEAN = 0.24473049E 04
SMALLEST SAMPLE =-0.17844325E 06
LARGEST SAMPLE = 0.12315425E 06
CUMULATIVE DISTRIBUTION FUNCTION
0.0
.2
.4
.6
.8
1.
1.2
1.4
-1.5 X10 5
-1. X10 5
-5. X10 4
0.0
5. X10 4
1. X10 5
1.5 X10 5
2. X10 5
CUMULATIVE DISTRIBUTION OF RADIUS VECTOR DISPERSION (FT)

Figure 10

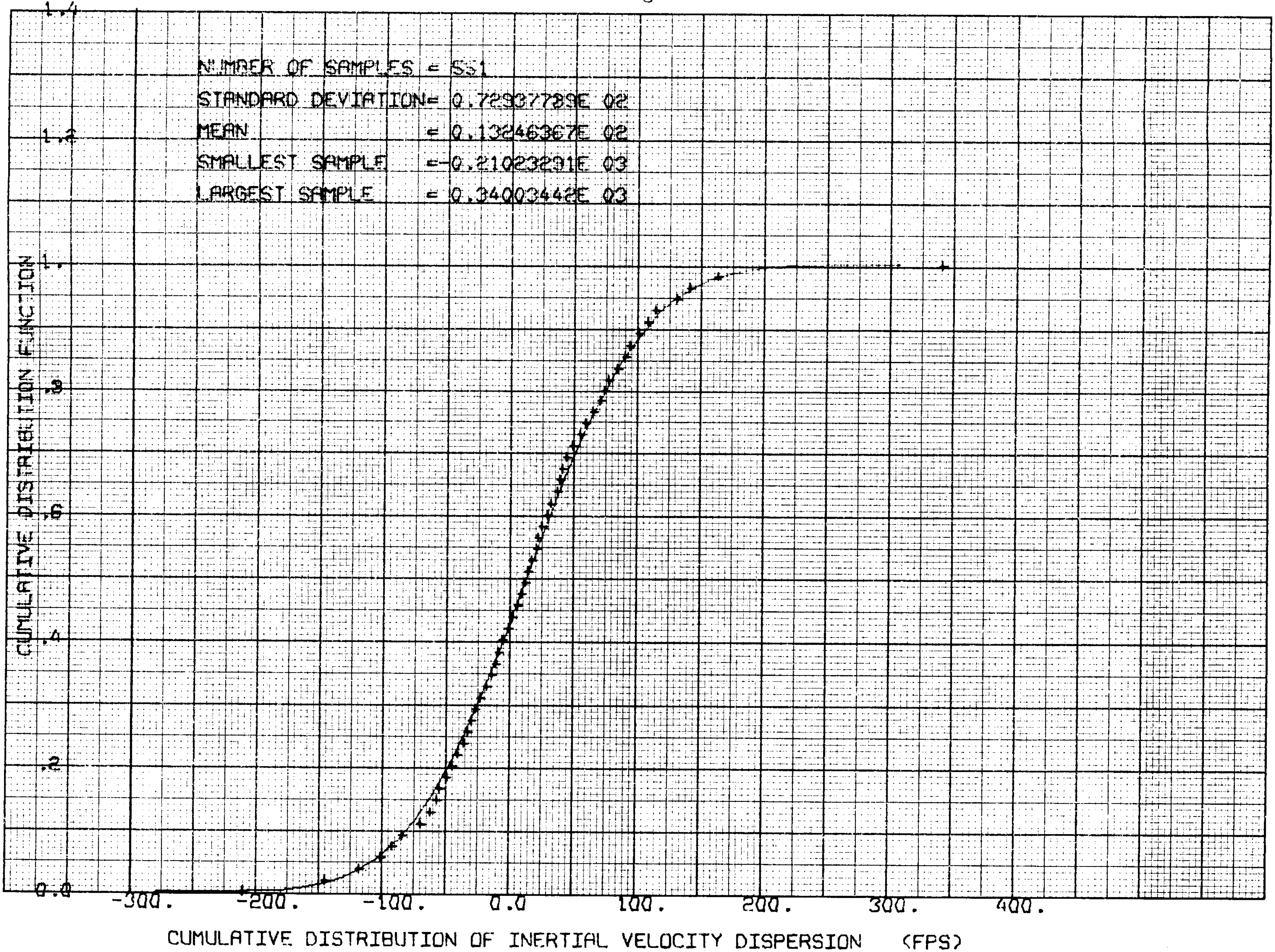
NUMBER OF SAMPLES = 551
STANDARD DEVIATION= 0.72937789E 02
MEAN = 0.13246367E 02
SMALLEST SAMPLE =-0.21023291E 03
LARGEST SAMPLE = 0.34003442E 03
CUMULATIVE DISTRIBUTION FUNCTION
0.0
.2
.4
.6
.8
1.
1.2
1.4
-300.
-200.
-100.
0.0
100.
200.
300.
400.
CUMULATIVE DISTRIBUTION OF INERTIAL VELOCITY DISPERSION (FPS)

Figure 11

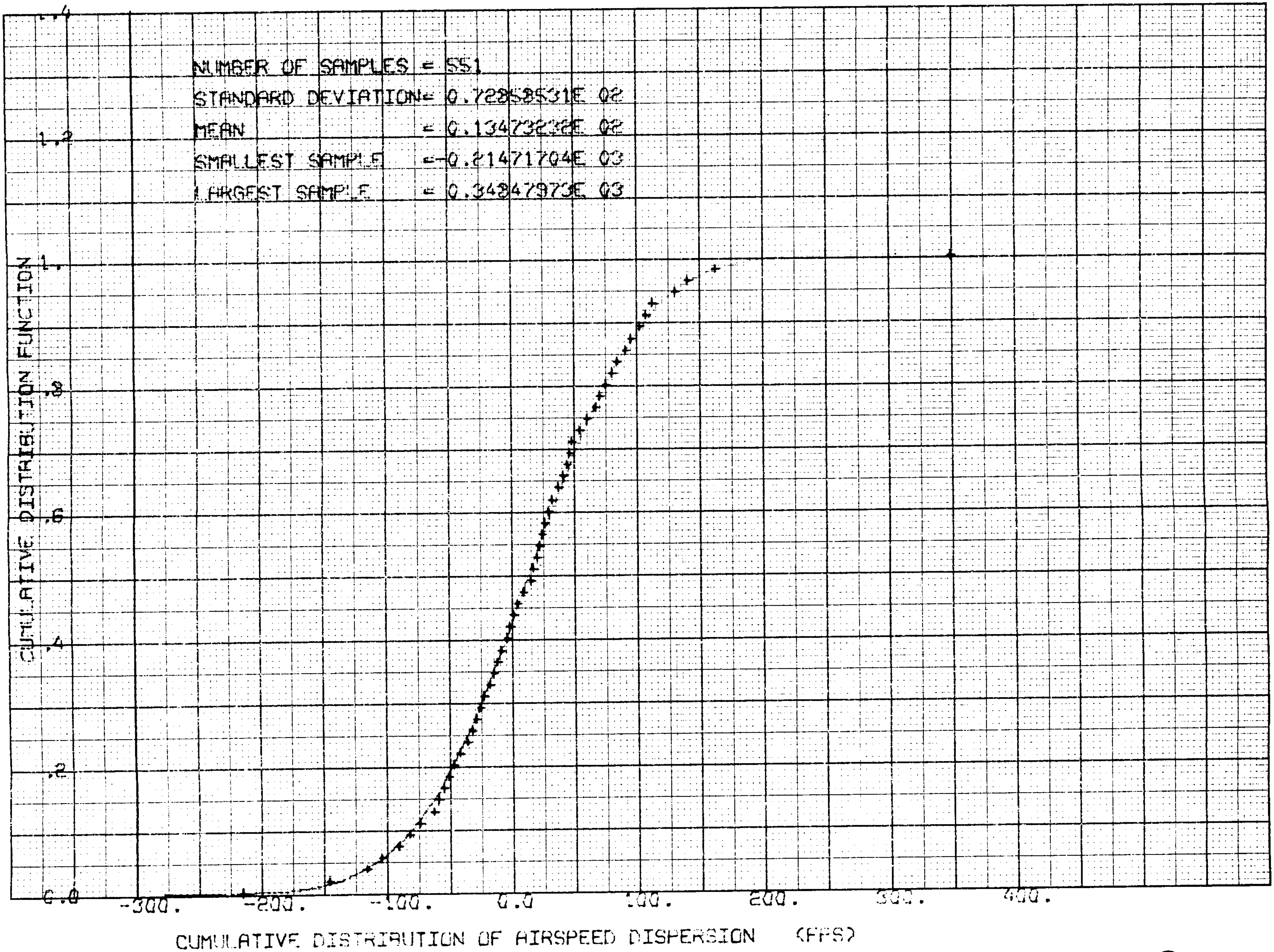
NUMBER OF SAMPLES = 551
STANDARD DEVIATION= 0.72858531E 02
MEAN = 0.13473232E 02
SMALLEST SAMPLE =-0.21471704E 03
LARGEST SAMPLE = 0.34847973E 03
CUMULATIVE DISTRIBUTION FUNCTION
0.0
.2
.4
.6
.8
1.
1.2
1.4
-300.
-200.
-100.
0.0
100.
200.
300.
400.
CUMULATIVE DISTRIBUTION OF AIRSPEED DISPERSION (FPS)

Figure 12

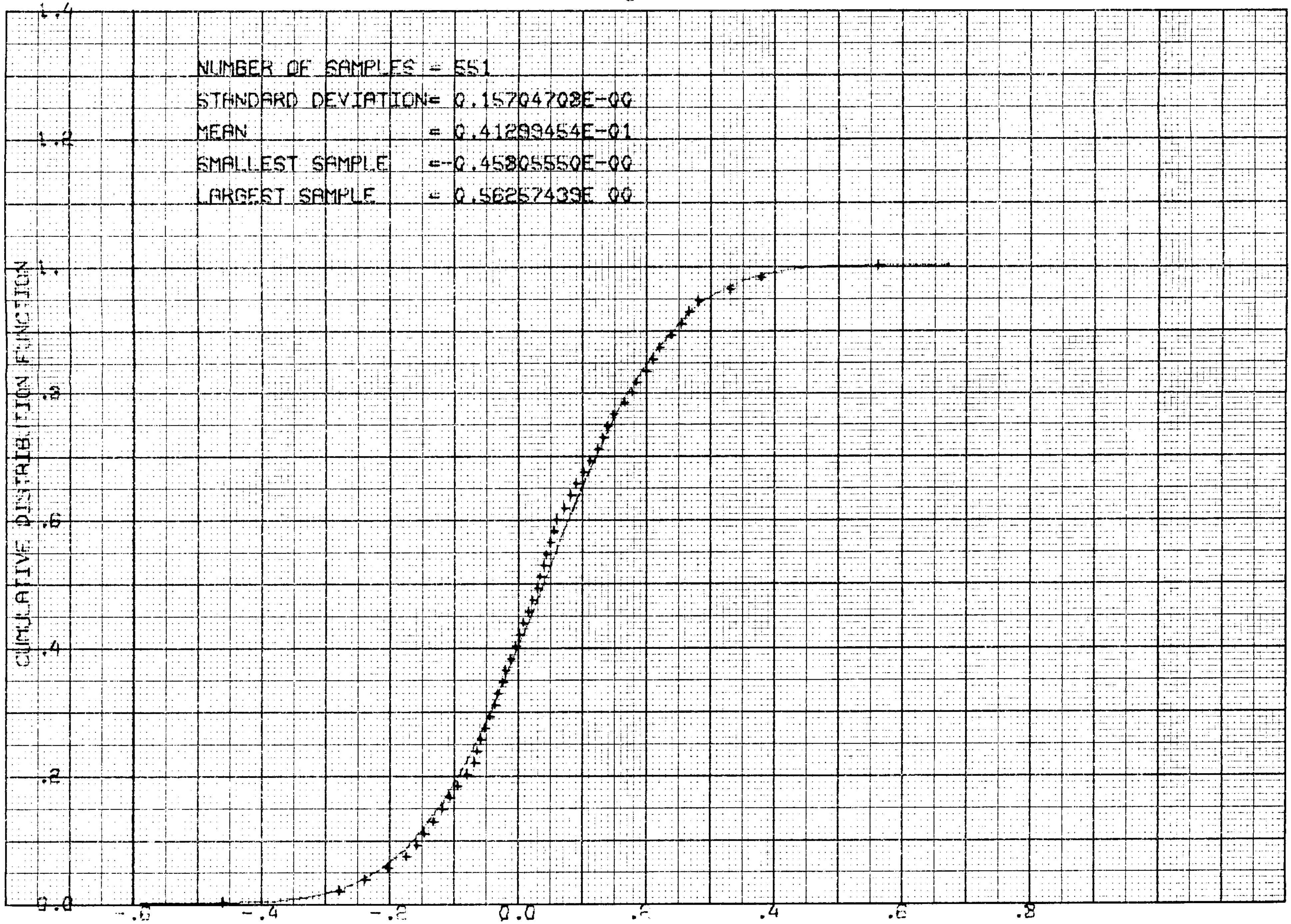
NUMBER OF SAMPLES = 551
STANDARD DEVIATION= 0.15704702E-00
MEAN = 0.41209454E-01
SMALLEST SAMPLE =-0.45805550E-00
LARGEST SAMPLE = 0.56257439E 00
CUMULATIVE DISTRIBUTION FUNCTION
0.0
.2
.4
.6
.8
1.
1.2
1.4
-.6
-.4
-.2
0.0
.2
.4
.6
.8
CUMULATIVE DISTRIBUTION OF LONG. OF ASCENDING NODE DISPERSION (DEGREES)

Figure 13

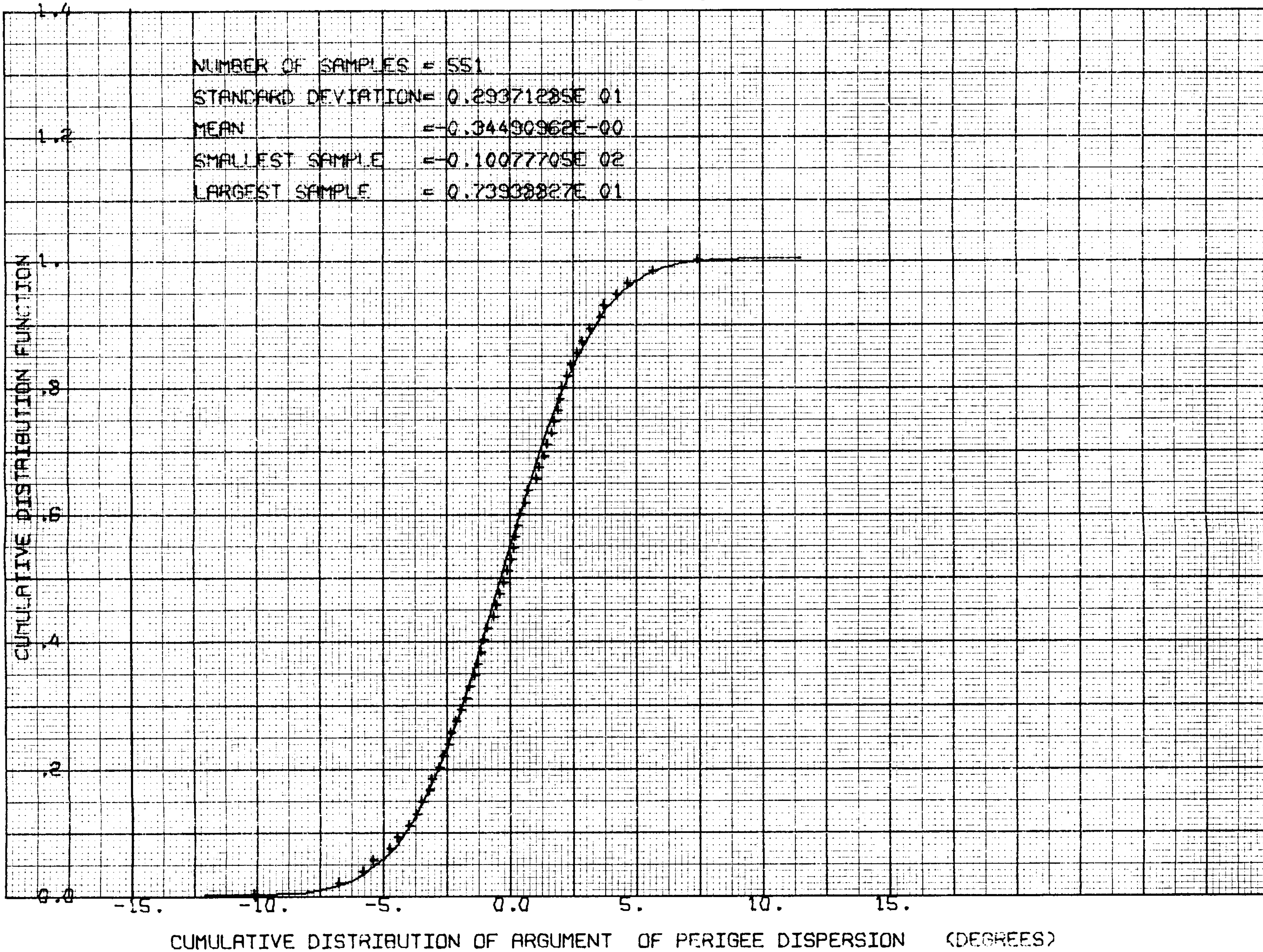
NUMBER OF SAMPLES = 551
STANDARD DEVIATION= 0.29371285E 01
MEAN = -0.34490962E-00
SMALLEST SAMPLE = -0.10077705E 02
LARGEST SAMPLE = 0.73938827E 01
CUMULATIVE DISTRIBUTION FUNCTION
1.4
1.2
1.
.8
.6
.4
.2
0.0
-15.
-10.
-5.
0.0
5.
10.
15.
CUMULATIVE DISTRIBUTION OF ARGUMENT OF PERIGEE DISPERSION (DEGREES)

Figure 14

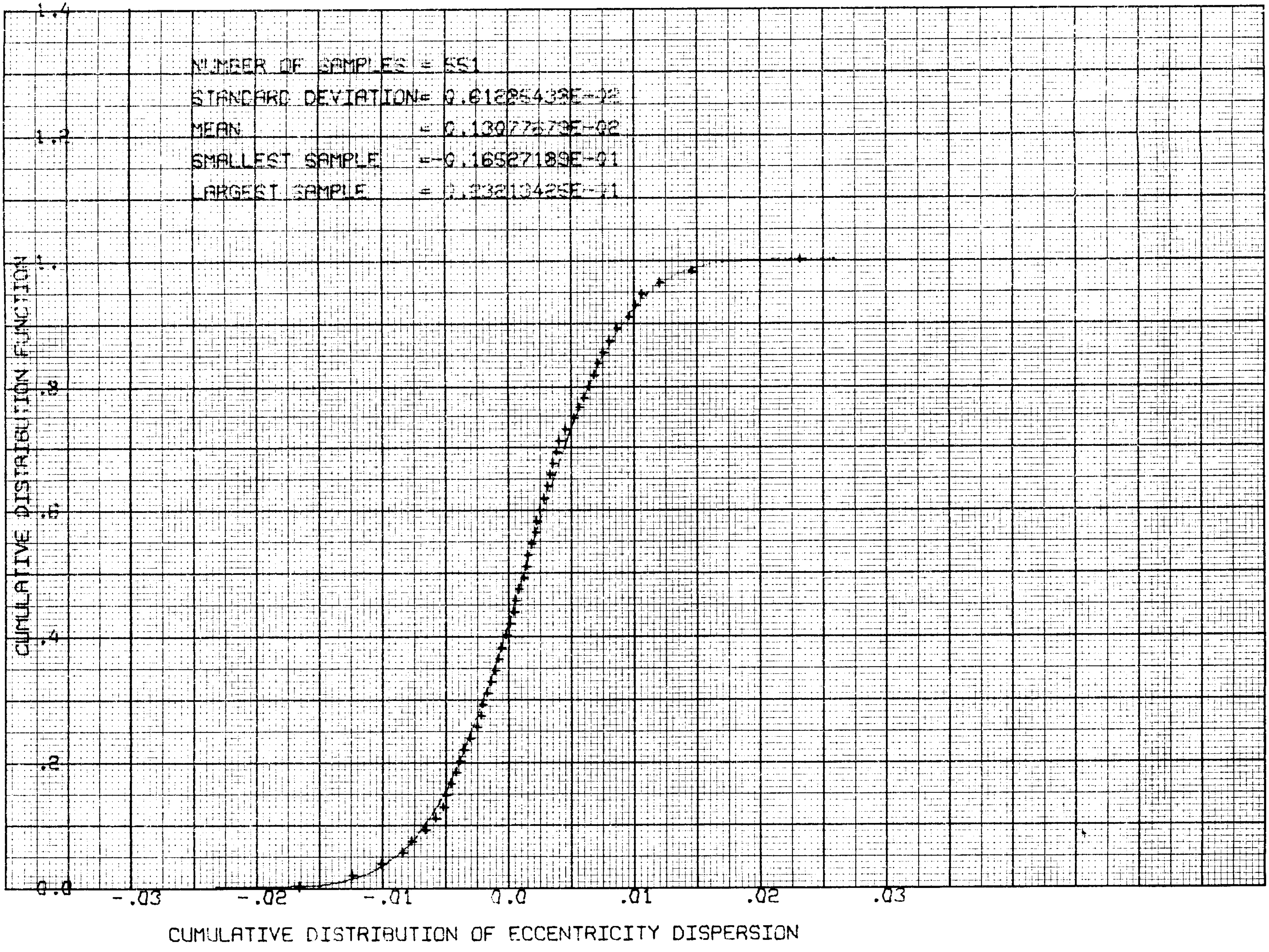
NUMBER OF SAMPLES = 551
STANDARD DEVIATION= 0.61285433E-02
MEAN = 0.13077573E-02
SMALLEST SAMPLE =-0.16527189E-01
LARGEST SAMPLE = 0.23213425E-01
CUMULATIVE DISTRIBUTION FUNCTION
0.0
.2
.4
.6
.8
1.
1.2
1.4
-.03
-.02
-.01
0.0
.01
.02
.03
CUMULATIVE DISTRIBUTION OF ECCENTRICITY DISPERSION

Figure 15

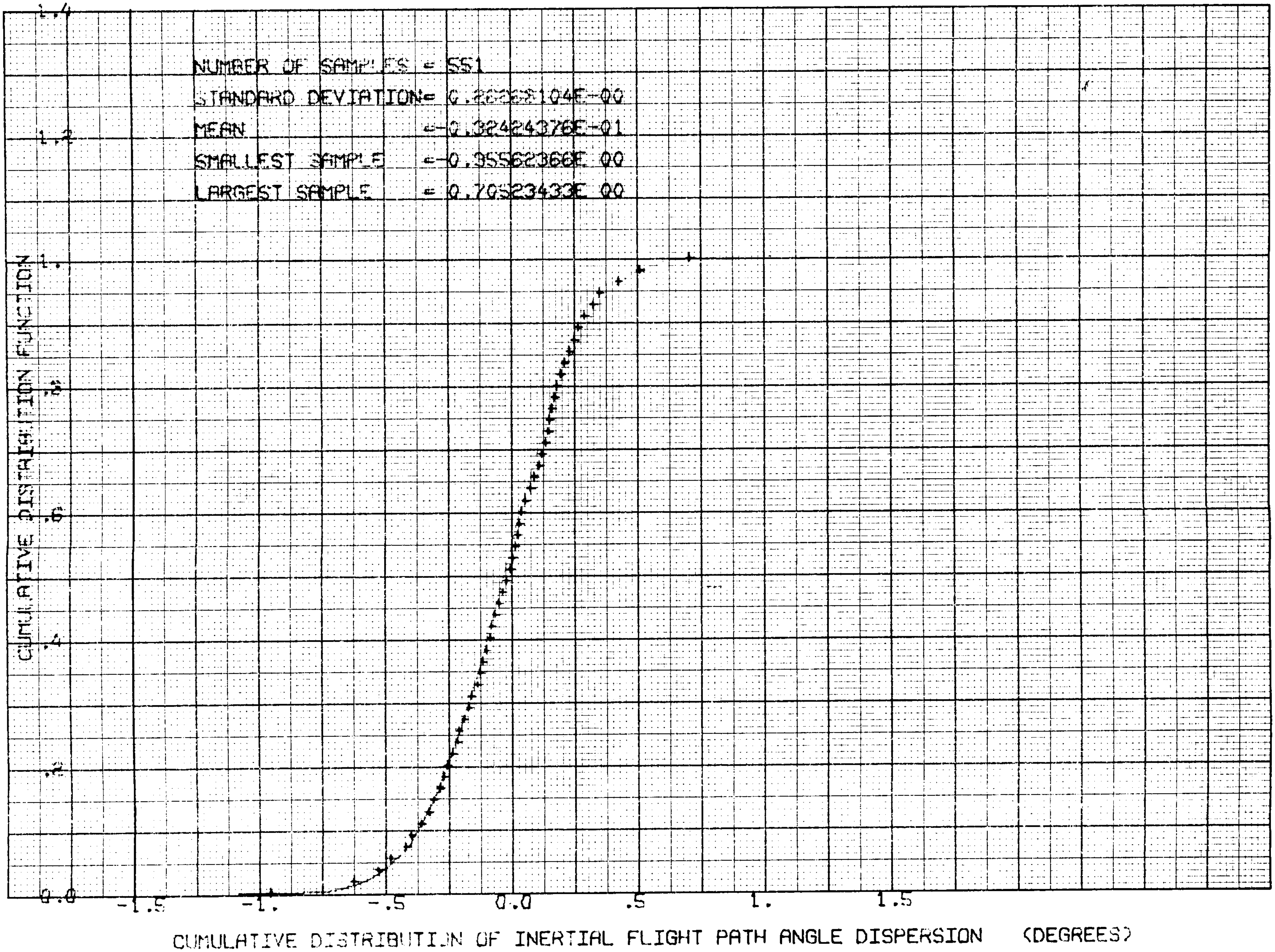
NUMBER OF SAMPLES = 551
MEAN =-0.32424376E-01
SMALLEST SAMPLE =-0.35562366E 00
LARGEST SAMPLE = 0.70523433E 00
CUMULATIVE DISTRIBUTION FUNCTION
CUMULATIVE DISTRIBUTION OF INERTIAL FLIGHT PATH ANGLE DISPERSION (DEGREES)

Figure 16

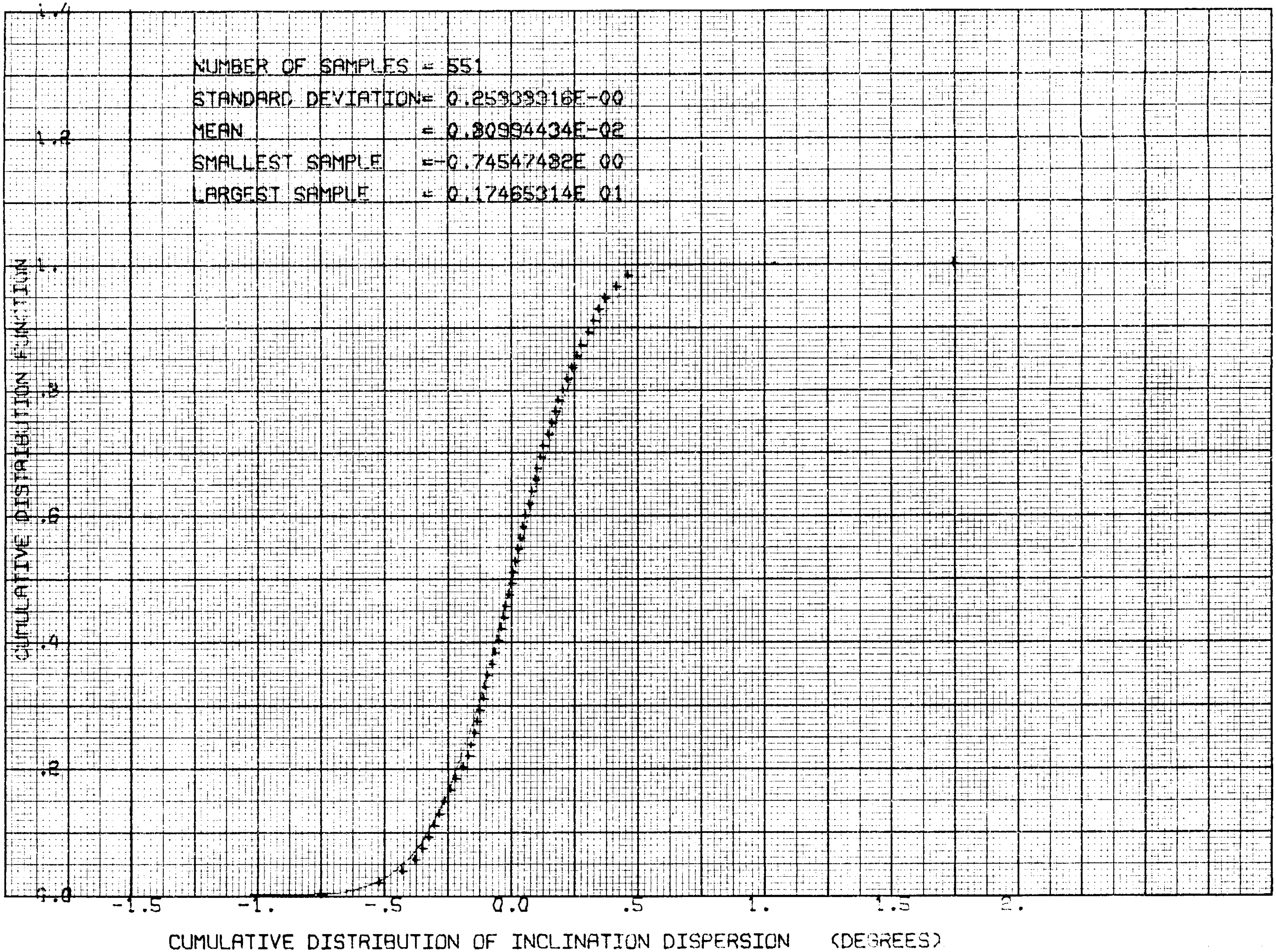
NUMBER OF SAMPLES = 551
STANDARD DEVIATION= 0.25939316E-00
MEAN = 0.30994434E-02
SMALLEST SAMPLE =-0.74547482E 00
LARGEST SAMPLE = 0.17465314E 01
CUMULATIVE DISTRIBUTION FUNCTION
0.0
.2
.4
.6
.8
1.
1.2
1.4
-1.5
-1.
-.5
0.0
.5
1.
1.5
2.
CUMULATIVE DISTRIBUTION OF INCLINATION DISPERSION (DEGREES)

Figure 17

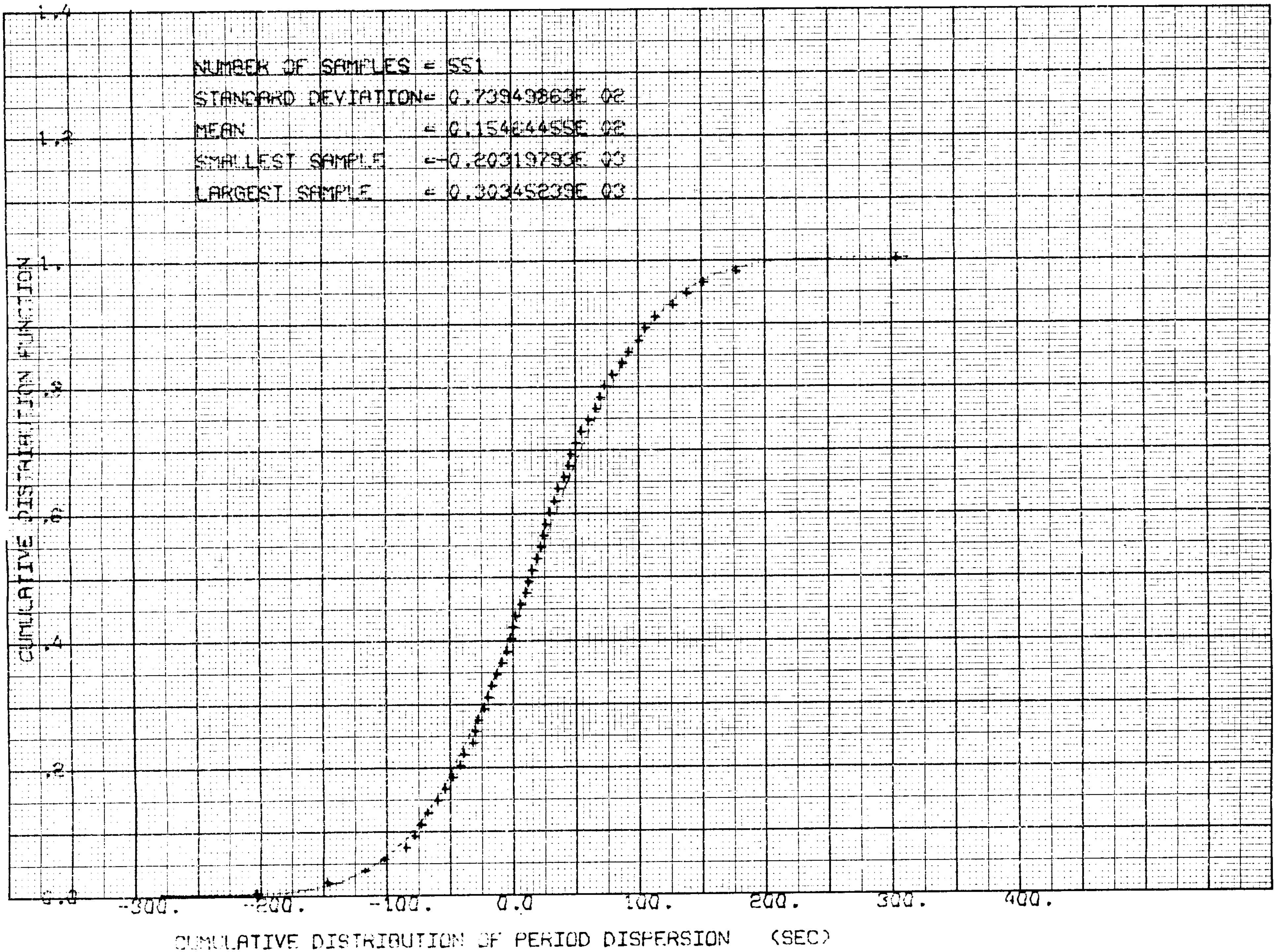
NUMBER OF SAMPLES = 551
STANDARD DEVIATION= 0.73943863E 02
MEAN = 0.15464455E 02
SMALLEST SAMPLE =-0.20319793E 03
LARGEST SAMPLE = 0.30345239E 03
CUMULATIVE DISTRIBUTION FUNCTION
1.4
1.2
1.
.8
.6
.4
.2
0.0
-300.
-200.
-100.
0.0
100.
200.
300.
400.
CUMULATIVE DISTRIBUTION OF PERIOD DISPERSION (SEC)

Figure 18

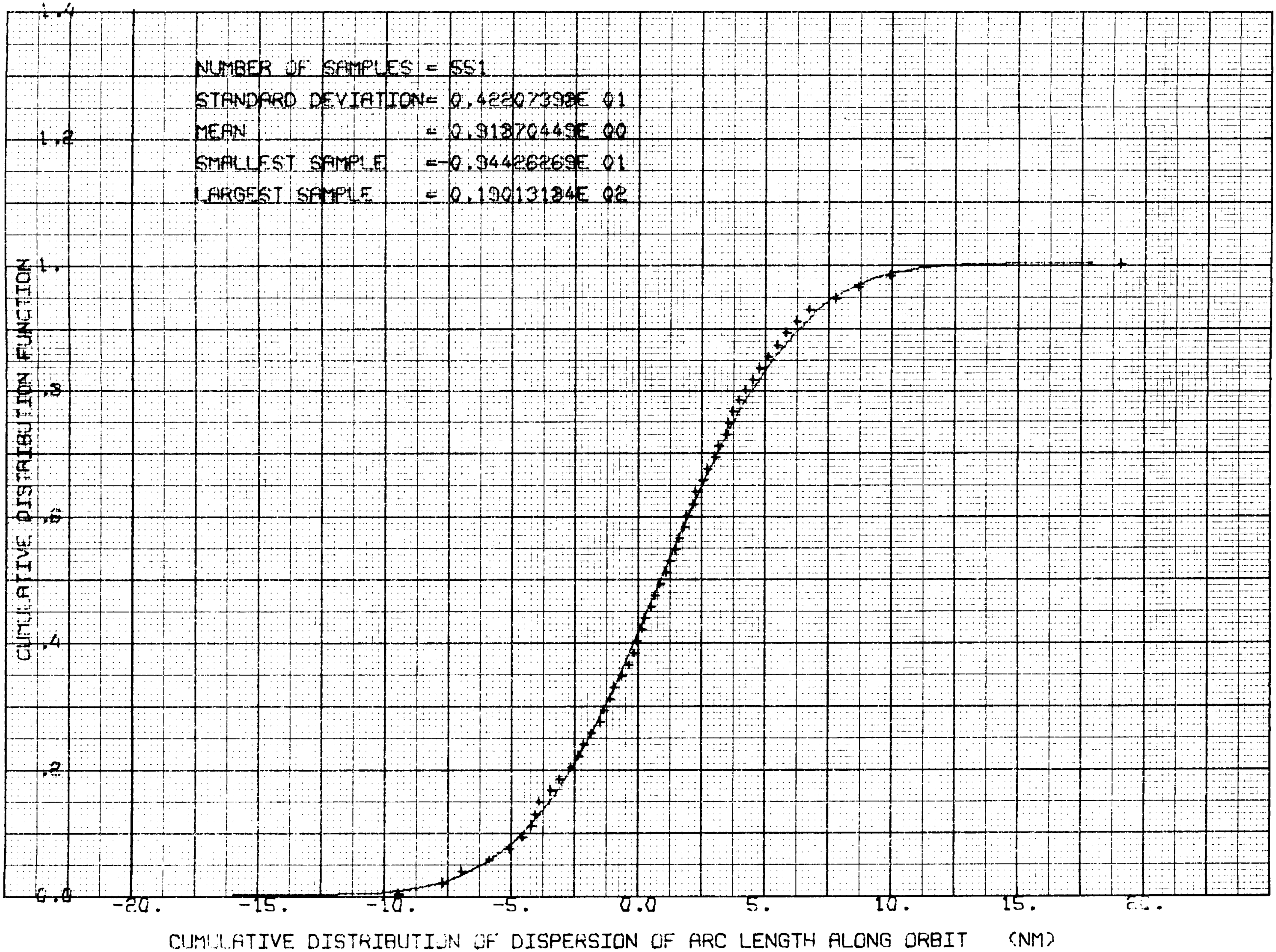
NUMBER OF SAMPLES = 551
STANDARD DEVIATION= 0.42207398E 01
MEAN = 0.91370449E 00
SMALLEST SAMPLE =-0.94426269E 01
LARGEST SAMPLE = 0.19013134E 02
CUMULATIVE DISTRIBUTION FUNCTION
0.0
.2
.4
.6
.8
1.
1.2
1.4
-20.
-15.
-10.
-5.
0.0
5.
10.
15.
CUMULATIVE DISTRIBUTION OF DISPERSION OF ARC LENGTH ALONG ORBIT (NM)

Figure 19

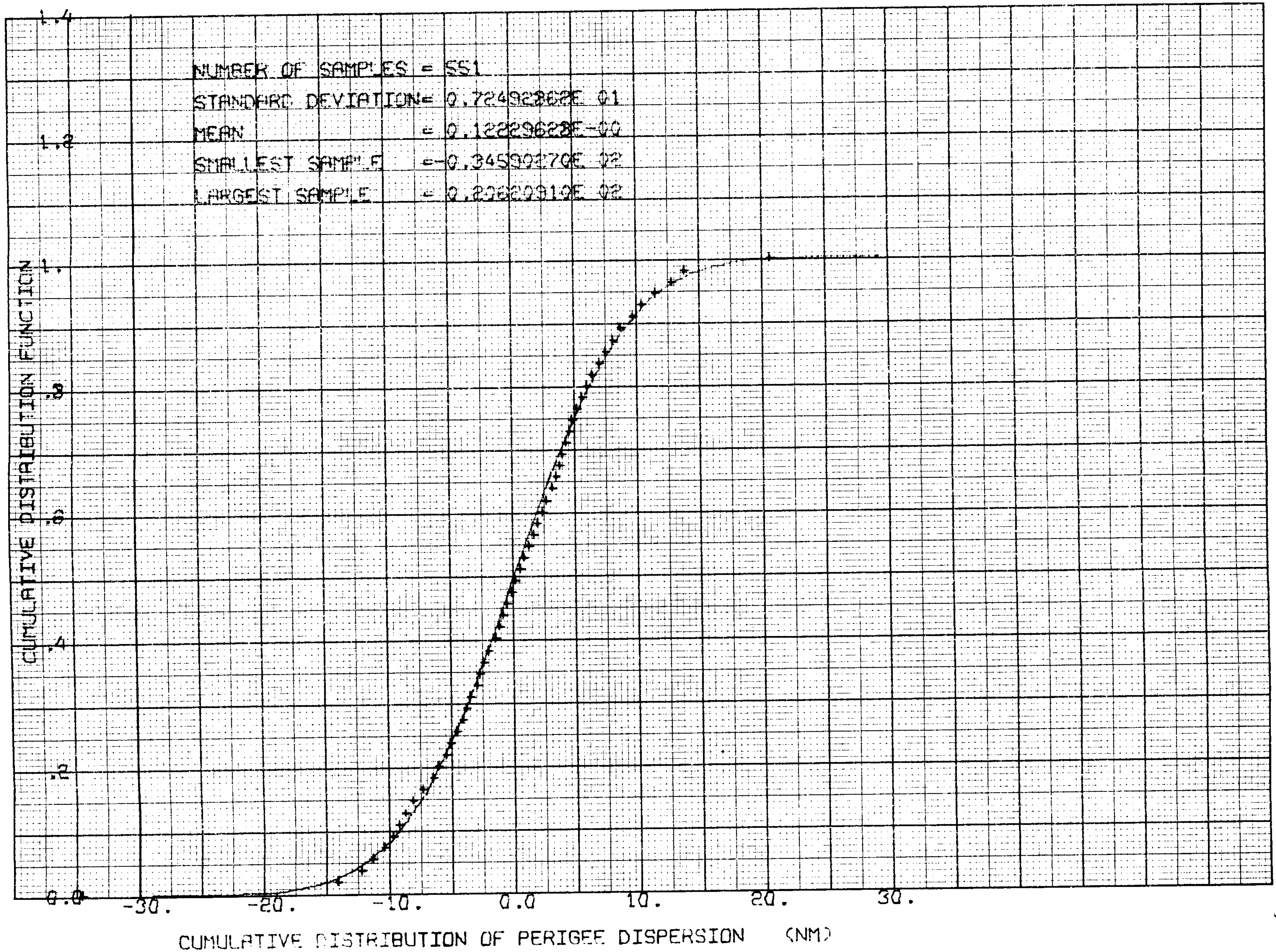
NUMBER OF SAMPLES = 551
STANDARD DEVIATION= 0.72492862E 01
MEAN = 0.12229623E-00
SMALLEST SAMPLE =-0.34599170E 02
LARGEST SAMPLE = 0.22629919E 02
CUMULATIVE DISTRIBUTION FUNCTION
0.0
.2
.4
.6
.8
1.
1.2
1.4
-30.
-20.
-10.
0.0
10.
20.
30.
CUMULATIVE DISTRIBUTION OF PERIGEE DISPERSION (NM)

Figure 20

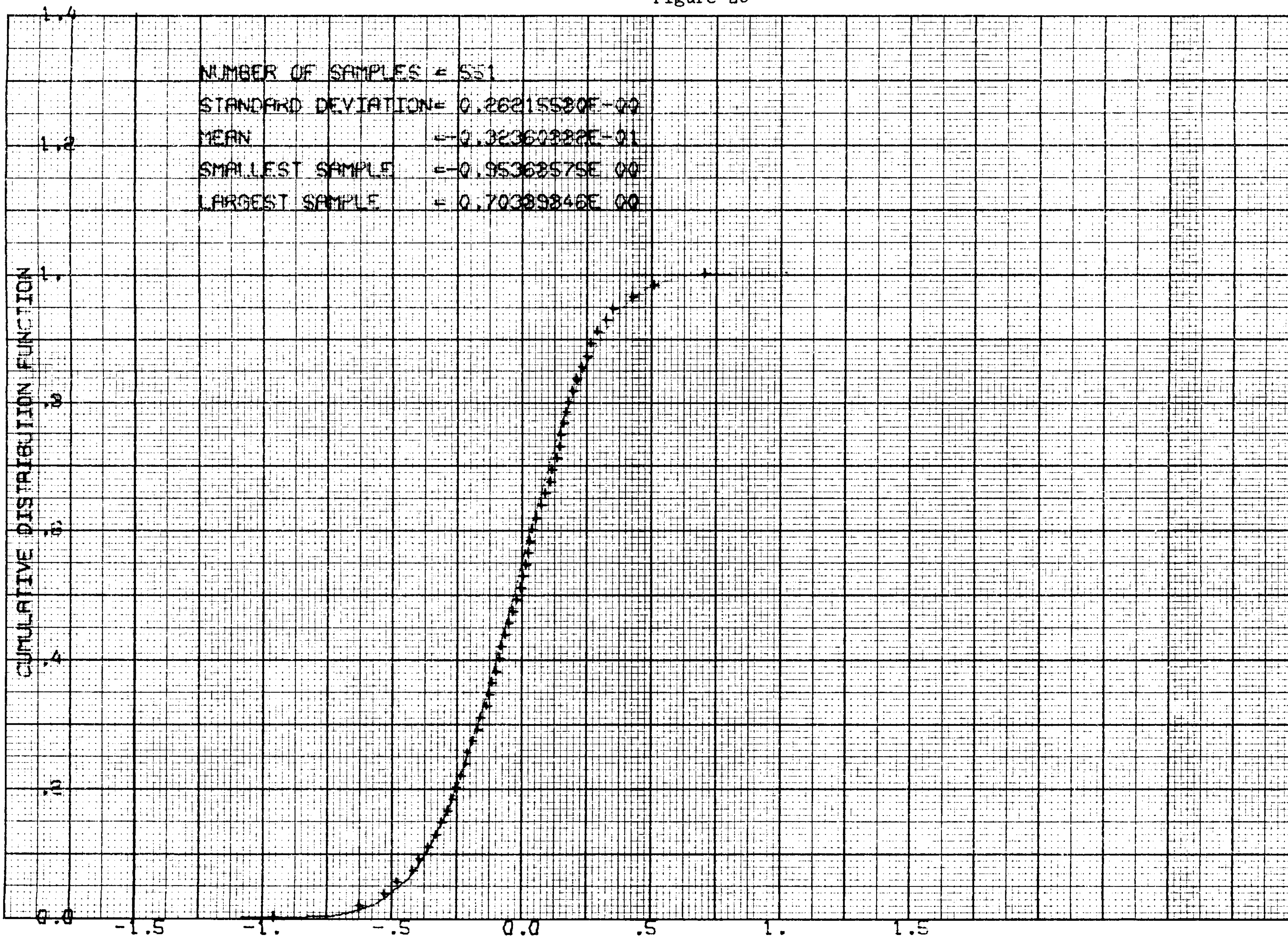

CUMULATIVE DISTRIBUTION OF ATMOSPHERIC FLIGHT PATH ANGLE DISPERSION (DEGREES)

Figure 21

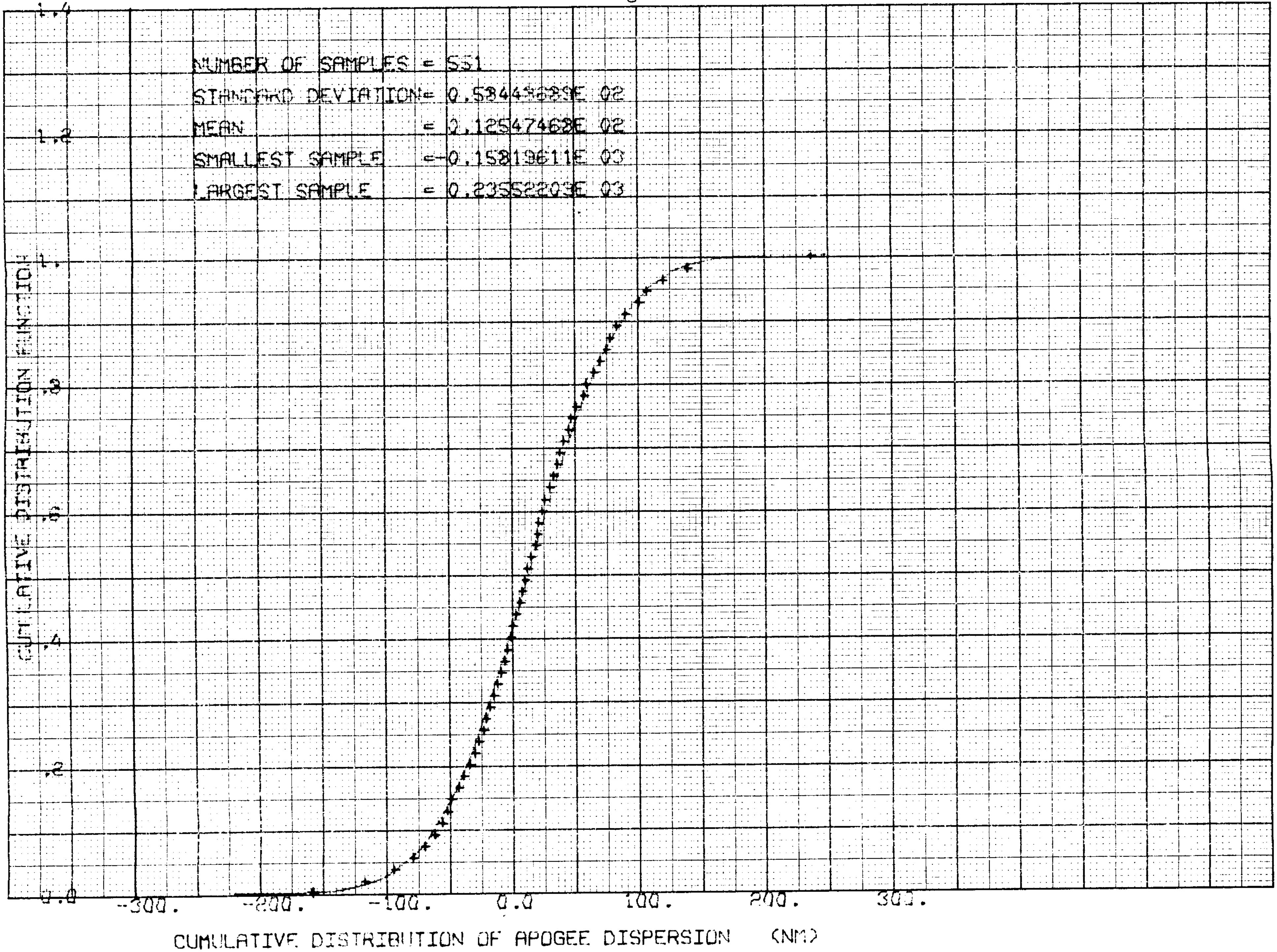

NUMBER OF SAMPLES = 551
STANDARD DEVIATION=
MEAN = 0.12547468E 02
SMALLEST SAMPLE =-0.15819611E 03
LARGEST SAMPLE = 0.23552203E 03
CUMULATIVE DISTRIBUTION FUNCTION
0.0
.2
.4
.6
.8
1.
1.2
1.4
-300.
-200.
-100.
0.0
100.
200.
300.
CUMULATIVE DISTRIBUTION OF APOGEE DISPERSION (NM)

TABLE 17. SIGNIFICANT ERROR SOURCES AND THEIR 3σ DISPERSIONS

	NAME	ALTITUDE (FT)	VELOCITY (FT/SEC)	FLT PATH ANGLE (DEG)	INCLINATION (DEG)
1	SIW1	11689		.0496	
	SIW2	3854			
	ISP1	21360		.1129	
	MFR1	24630		.1132	
5	DKSG	8128	22.9	.0794	
	DPBE	5048	15.7		
	TMP1	20084	99.5	.0572	
	TMY1	9277		.0438	.1919
	CA01	8868		.0371	
10	CNAL	4432	10.7		
	CM01	3112			
	DRHO	56598	28.3	.2220	
	FWN1				.0842
	MSMR	3884	10.5		
15	CDV1	6107		.0323	
	TIM1	16677	50.5		
	ISP2	8502	10.5	.0596	
	MFR2	9223	11.1	.0737	
	DBP2	8688	15.4	.0272	
20	DBY2				.0651
	TMP2	68251	129.5	.1923	
	TMY2	3166			.2600
	ISP3	11472	22.7	.0929	
	MFR3	10235	22.7	.0700	
25	TMP3	19620	32.6	.1525	
	TMY3				.0789
	ISP4		18.3		
	W4CP		10.8	.0650	.5645
29	W4CY	4000	12.3	.5781	.0603

Examining the individual error sources, it was discovered that the largest 3σ variation in altitude was 68,251 ft. It was assumed that any error source that contributed less than 3000 ft (approx 5%) would be called negligible. Using the same reasoning with respect to velocity (<10 ft/sec), flight path angle and inclination (<.025 deg.) a list of twenty-nine error sources were sifted out and presented with their contributions in Table 17 Some of the less predictable ones were: pitch rate gyro bias (DPBE), pitch torquer scale factor (DKSG) which also includes amplitude variation in the intervalometer, jet vane effects (CDV1) and dead band error in pitch and yaw in the second stage (DBP2, DBY2). However, it should be remembered that a value of .1 was used for these last two sources which is considerably larger than the log book data would indicate (.012).

A non-statistical result of this study was the determination of the effect on the state vector at burnout of the inclusion of a pitch moment aerodynamic coefficient (C_{MO}) which had previously been neglected in computing the nominal trajectories. The curve used was supplied by the Scout Project Office and is presented on Page 5 of Appendix B. A trajectory was run using it and the state vector at insertion was compared to the previous nominal trajectory. The results are summarized in Table 17. It is evident that neglecting this constant in the production of the nominal trajectory will lead to substantial biases in the velocity vector (37 feet for this particular trajectory).

Table 18. TRAJECTORY COMPARISON USING C_{MO}

	With C_{MO}	Without C_{MO}	Difference
Altitude (ft)	1,690,425	1,677,923	12,502
Velocity (ft/sec)	26,192	26,229	-37
Flight Path Angle (deg)	-.845	-.850	.005
Apogee Ht. (n.mi.)	1130	1150	2
Perigee Ht. (n.mi.)	276	274	-20

It is instructive to compare the results of this study with a previously published analysis by Woodling, et al., (Reference 2). In this report, only 26 errors were considered, and the results were basically a linear two dimensional analysis of the system. The authors presented results for circular orbits of 120, 300 and 600 n.mi. which are reprinted here for comparison:

	Perigee-apogee	1σ altitude (n.mi.)	1σ velocity (ft/sec)	Flt path angle (deg)
Woodling	120 - 120	4.35	67.5	.595
	300 - 300	6.00	62.5	.700
	600 - 600	9.80	70.0	.920
TRW	289 - 1096	6.50	72.9	.262

The altitude and velocity dispersions are in very good agreement. However, the Woodling flight path angle dispersion is 3 or 4 times greater. Further investigation shows that 95% of the flight path error in the Woodling study is due to fourth stage tip-off error which is taken to be 1.75 degrees (1 sigma). That simulation assumes that the vehicle holds this constant angle for the remainder of the fourth stage burning.

The TRW study simulated the six dimensional coning motion that results from an impulsive force applied at the separation plane at separation. In addition, the damping effects of the thrust vector have been taken into account. The assumed error was .2 lb-sec (one sigma) in both the pitch and yaw axes which results in a total impulse of .28 lb-sec applied in a random direction in the stage separation plane. There is no easily computed relationship between the error expressed as a fixed angle or as an impulsive force because of the complicated gyroscopic motion and the strong effect of the jet damping, but the authors of the NASA report admit that their choice is greater than flight results would indicate. Based on the present study, the equivalent angle would be approximately .5 degrees.

Out-of-plane effects were not considered in the NASA report nor was any significant non-linear effect discovered.

CONCLUSIONS

The conclusions which can be drawn from this analysis are:

1) The guidance and control system errors as measured in the field are well within the specifications and do not contribute appreciably to the total vehicle dispersions.

2) Design of any nominal trajectory which does not include C_{MO} (Pitching moment) will produce results that have a substantial velocity bias at burnout. For the trajectory analyzed in this report the bias was 37 ft/sec.

3) Non-linear effects cause a velocity bias of 13 ft/sec for the example used in this report. The error source contributing most of this effect was the fourth stage coning caused by tipoff at separation.

APPENDIX A

DESCRIPTION OF THE SCOUT SIMULATION

This section will describe the methods that were used to simulate the Scout.

The description of the models used is divided into the following sections:

First Stage Aerodynamics
First Stage Control System
On-off Control System
Guidance System and Error Model
Fourth Stage Dynamics

The appendix then presents a comparison of the results of the simulation with a trajectory calculated by the LTV Scout program.

FIRST STAGE AERODYNAMICS

Pitch Angle of Attack $$\alpha = \mathrm{TAN}^{-1} \frac{-V_\eta}{V_\xi} \tag{1}$$

Yaw Angle of Attack $$\beta = \mathrm{SIN}^{-1} \frac{V_\zeta}{V_A} \tag{2}$$

<u>Aero coefficients (for right handed ξ, η, ζ system)</u>

$$C_A = C_{A_O} \tag{3}$$

$$C_N = C_{N_\alpha} \alpha + C_{N_{\delta q}} \delta q \tag{4}$$

$$C_Y = C_{Y_\beta} |\beta| + C_{Y_{\delta r}} \delta r \tag{5}$$

Note: δp, δq, δr indicate control surface deflections causing moments about the roll, pitch, and yaw axis, respectively.

$$C_l = C_{l_{\delta p}} \delta p + C_{l_p} \left(\frac{-pb}{2V_A}\right) + \frac{\Delta\eta}{b} C_Y - \frac{\Delta\zeta}{b} C_N \tag{6}$$

$$C_m = C_{m_o} + C_{m_\alpha} \alpha + C_{m_{\delta q}} \delta q + C_{m_q} \left(\frac{-qb}{2V_A}\right) + \frac{\Delta\xi}{b} C_N \tag{7}$$

$$+ \frac{\Delta\eta}{b} C_A$$

$$C_n = C_{n_\beta} \beta + C_{n_{\delta r}} \delta r + C_{n_r} \left(\frac{rb}{2V_a}\right) - \frac{\Delta\zeta}{b} C_A - \frac{\Delta\xi}{b} C_Y \tag{8}$$

$$\dot{V}_\xi = - \frac{\rho V_A^2 S}{2 M} C_A \tag{9}$$

$$\dot{V}_\eta = \frac{\rho V_A^2 S}{2 M} C_N \tag{10}$$

$$\dot{V}_\zeta = \frac{\rho V_A^2 S}{2 M} C_Y \tag{11}$$

Valid for ξ, η, ζ with L. H. Rotations

$$M_\xi = - \frac{\rho V_A^2 Sb}{2} C_l \tag{12}$$

$$M_\eta = \frac{\rho V_A^2 Sb}{2} C_n \tag{13}$$

$$M_\zeta = - \frac{\rho V_A^2 Sb}{2} C_m \tag{14}$$

Valid for ξ, η, ζ with L. H. Rotation

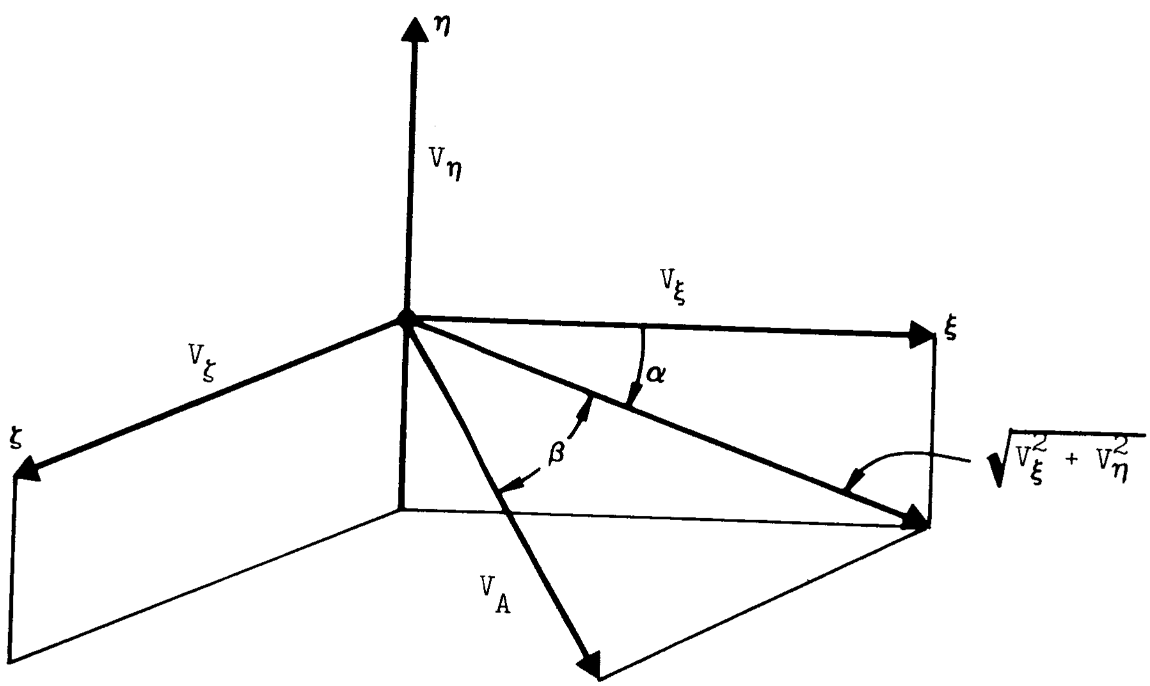

Figure A. Definition of Pitch and Yaw Angles of Attack

FIRST STAGE CONTROL SYSTEM

The Scout first stage employs a combination of jet vanes and aerodynamic tip control surfaces to provide control moments. A proportional feedback control system is used to maintain the desired pitch and yaw rates. High frequency servo dynamics and body bending were not simulated. A block diagram of the system as it is presently being simulated is shown below in Figure A2

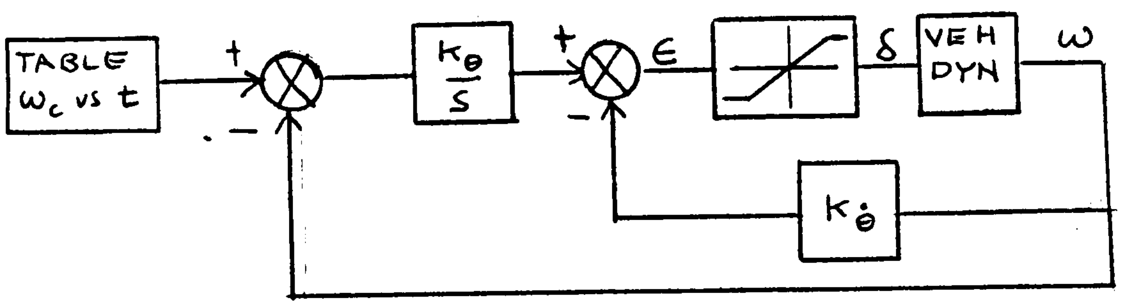

Figure A2

Simulation of this system is carried out by simply computing the pitch, yaw, and roll error signals with appropriate position limits as follows:

$$\delta q = \epsilon \Big|_{LIM\ \pm 19^{o}} = K_{PP} \int_{0}^{t} (\dot{\theta}_{PC} - \dot{\theta}_{P})\, dt - K_{RP}\, \dot{\theta}_{P} \tag{15}$$

$$\delta r = \epsilon \Big|_{LIM\ \pm 19^{o}} = K_{PY} \int_{0}^{t} (\dot{\theta}_{YC} - \dot{\theta}_{Y})\, dt - K_{RY}\, \dot{\theta}_{Y} \tag{16}$$

$$\delta p = \epsilon \Big|_{LIM\ \pm 19^{o}} = K_{PR} \int_{0}^{t} (\dot{\theta}_{RC} - \dot{\theta}_{R})\, dt - K_{RR}\, \dot{\theta}_{R} \tag{17}$$

ON-OFF CONTROL SYSTEM

Efficient digital simulation of on-off control systems has continued to be an unsolved problem since the advent of high speed digital computers. As a consequence of this, simulation of on-off control is either done on an analog machine or at extremely slow speeds (step size of .01 sec.) on digital computers. This memo describes a method for efficient digital simulation of on-off control systems. The equations and logic developed herein are presently programmed and checked out on the MVNS εD program. Results have shown that computer time savings of more than 36% are realized using this method.

A typical on-off control loop is shown in Figure A3.

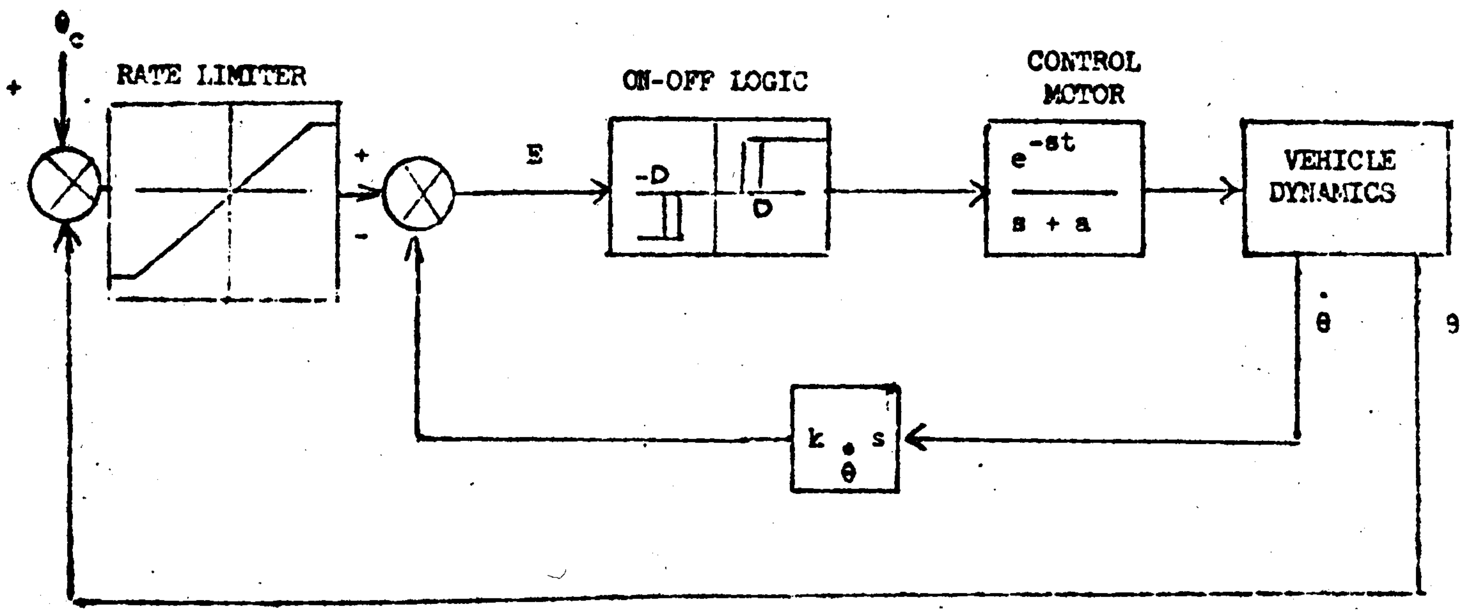

Figure A3

The on-off logic works so that an engine is turned on whenever the error signal $|E|$ is greater than the deadband $|D|$. It is therefore necessary to compute $|E|$ very accurately, and to predict the discontinuity at $|E| = |D|$. Since E is being computed only at discrete intervals, it is possible to miss the discontinuity by ±h where h is the integration step size. This would cause the attitude time history to be in error and even make a normally stable system unstable. A typical phase plane trajectory for a continuous and discrete on-off system is shown in Figure A4.

The effect of discretizing the system is to cause delays in the system which do not really exist. These delays effectively rotate the on-off switching lines resulting in incorrect response characteristics. In order to minimize this effect, it is necessary to use very small computing increments which, in turn, increase computing time and cost. The following development shows how the step size may be increased without loss of accuracy.

The method basically consists of expanding the error signal in a Taylor series about each integration point. If a discontinuity (switch point) is sensed within the next integration interval, the step size is modified accordingly.

The error signal of the system in Figure A3 may be written as

$$E = \theta + K_{\dot{\theta}}\dot{\theta} \tag{18}$$

On-off control is almost always used when external torques are very small compared to the control torque. Therefore, it is safe to assume that the external torque on the body is constant over an integration step. With this assumption we may write:

$$\ddot{\theta} = K = \text{CONST} \tag{19}$$

Ignoring initial conditions

$$\dot{\theta} = Kt \tag{20}$$

and

$$\theta = \frac{Kt^2}{2} \tag{21}$$

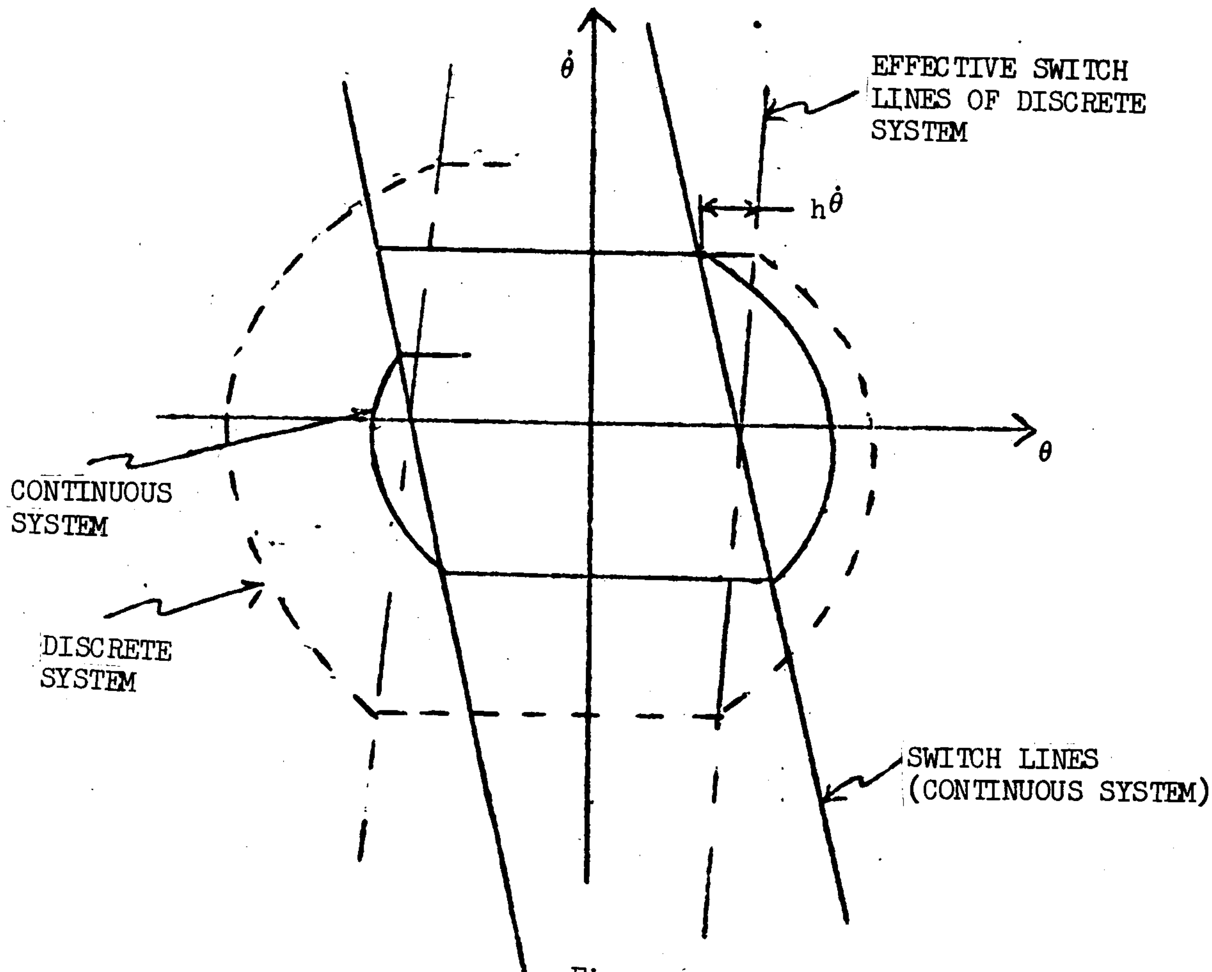

Figure A4

Substituting equation (6) into (7) gives the relation between θ and $\dot{\theta}$

$$\theta = \frac{\dot{\theta}^2}{2\ddot{\theta}} \tag{22}$$

Substitute equation (8) into (4)

$$E = C_1 \dot{\theta}^2 + C_2\dot{\theta} \tag{23}$$

As long as $\dot{\theta}$ is assumed constant, $\ddot{\theta}$ is a linear function of time

$$E = K_1 t + K_2 t^2 \tag{24}$$

It follows that a second order Taylor series in E should represent the function well in the majority of cases. Writing E as a Taylor series and retaining terms up to t^2 we obtain:

$$E(t) = E(t_n) + \dot{E}(t_n)(t - t_n) + \frac{\ddot{E}}{2}(t - t_n)^2 \tag{25}$$

where t_n is the present value of time in the computation. Let $E(t_s)$ be the value of error signal at a switch point and t_s be the time when $E(t) = E(t_s)$.

$$E(t_s) = E(t_n) + \dot{E}(t_n)(t_s - t_n) + \frac{\ddot{E}}{2}(t_s - t_n)^2 \tag{26}$$

Let $\Delta t = t_s - t_n$, the time to a switch point. Solving equation (26) for Δt we obtain:

$$\Delta t = \frac{-\dot{E}(t_n) \pm \sqrt{\dot{E}(t_n)^2 + 2\ddot{E}\Delta E}}{\ddot{E}} \tag{27}$$

where

$$E = -\theta - K_{\dot{\theta}}\dot{\theta} \tag{28}$$

$$\dot{E} = -\dot{\theta} - K_{\dot{\theta}}\ddot{\theta} \tag{29}$$

$$\ddot{E} = -\ddot{\theta}\,^{*} \tag{30}$$

$$\Delta E = E(t_s) - E(t) \tag{31}$$

If the on-off system does not have hysteresis, $E(t_s) = \pm D$ (see Figure A5).

---

* $\dddot{\theta} = 0$ since we are assuming constant torque.

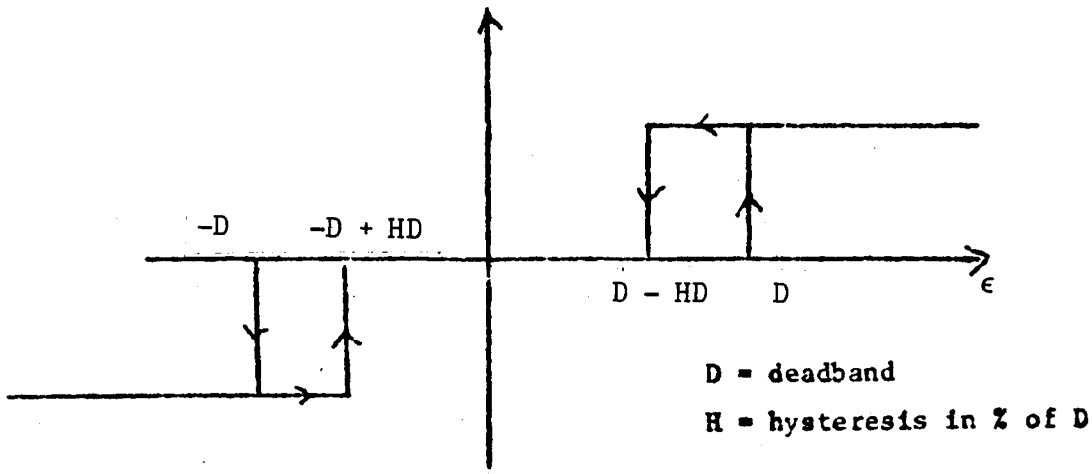

Figure A5

The sign of D to be used to compute $E(t_s)$ depends on the sign of E. Likewise, if hysterysis is present, $E(t_s)$ also depends on $\dot{E}$. The following equations summarize the logic used to compute $E(t_s)$.

if $E \geq 0$.

$$E(t_s) = \begin{cases} D; \ \frac{dE}{dt} \geq 0 \\ D-DH; \ \frac{dE}{dt} < 0 \end{cases} \tag{32}$$

if $E < 0$

$$E(t_s) = \begin{cases} -D; \ \frac{dE}{dt} \leq 0 \\ -D + DH; \ \frac{dE}{dt} > 0 \end{cases}$$

Equation (10) has two solutions corresponding to the roots of the second order Taylor series,

$$\frac{\ddot{E}}{2} \ \Delta t^2 + \dot{E}\Delta t - \Delta E = f(\Delta t) = 0 \tag{33}$$

$f(\Delta t)$ will have the form shown in Figure (A6).

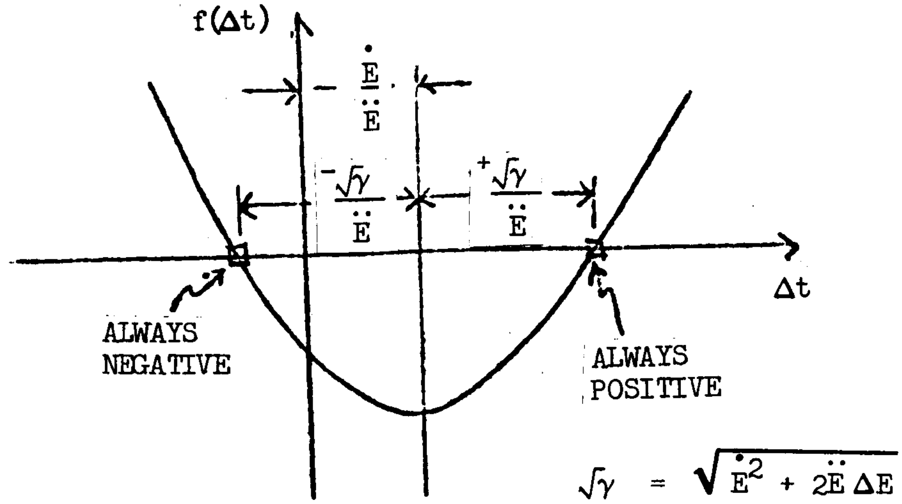

Figure A6

Assuming a stable system, the sign of ΔE will always be the same as the sign of $\ddot{E}$ so that $2\hat{E}\Delta E$ is always a positive quantity. Therefore, one root of $f(\Delta t)$ is always negative and can be discarded. The correct value of Δt is obtained by computing equation (27) as:

$$\Delta t = -\frac{\dot{E}}{\ddot{E}} + \frac{\sqrt{\dot{E}^2 + 2\ddot{E}\Delta E}}{|\ddot{E}|} \tag{34}$$

The absolute value sign on $\ddot{E}$ insures that the quantity

$$\frac{\sqrt{\dot{E}^2 + 2\ddot{E}\Delta E}}{|\ddot{E}|}$$

is always added as shown in Figure A6.

If the external torques on the vehicle are zero, $\ddot{\theta}$ is zero and equation is undefined. However, if we consider the fact that zero external torque implies a linear relationship between t and θ, it is apparent that only two terms of the Taylor series are necessary. For $\hat{\theta} = 0$,

$$E(t_s) = E(t_n) + E(t_n)\,\Delta t \tag{35}$$

$$\Delta t = \frac{E(t_s) - E(t_n)}{\dot{E}(t_n)} \tag{36}$$

When $\ddot{\theta}$ is finite, Δt is computed from equation (20) and when $\ddot{\theta}$ is zero we use equation (36). The logic used to compute the modified computing increment is given in Figure A3.

It is necessary to have at least two data points between E $= -$D and D to determine $E(t_s)$. Therefore, the minimum step size is dictated by the magnitude of D and the highest expected frequency.

$$h_{max} \leqq \frac{D}{2\omega_{max}} \tag{37}$$

Other step size restrictions are imposed by frequency considerations (Shannon's Sampling Theorem) and numerical integration stability. Shannon's Sampling Theorem states that the sampling frequency must be equal to or greater than twice the highest frequency or:

$$h_{max} \leq \frac{1}{2f_{max}} \tag{38}$$

Runge Kutta numerical integration of the direction cosine rates requires that

$$h_{max} \leq \frac{2}{\omega} \tag{39}$$

$\omega \sim$ deg/sec

The maximum allowable step size for the 6D portion of the run is taken as the smallest value of h_{max} obtained by solving equations (37), (38), and (39).

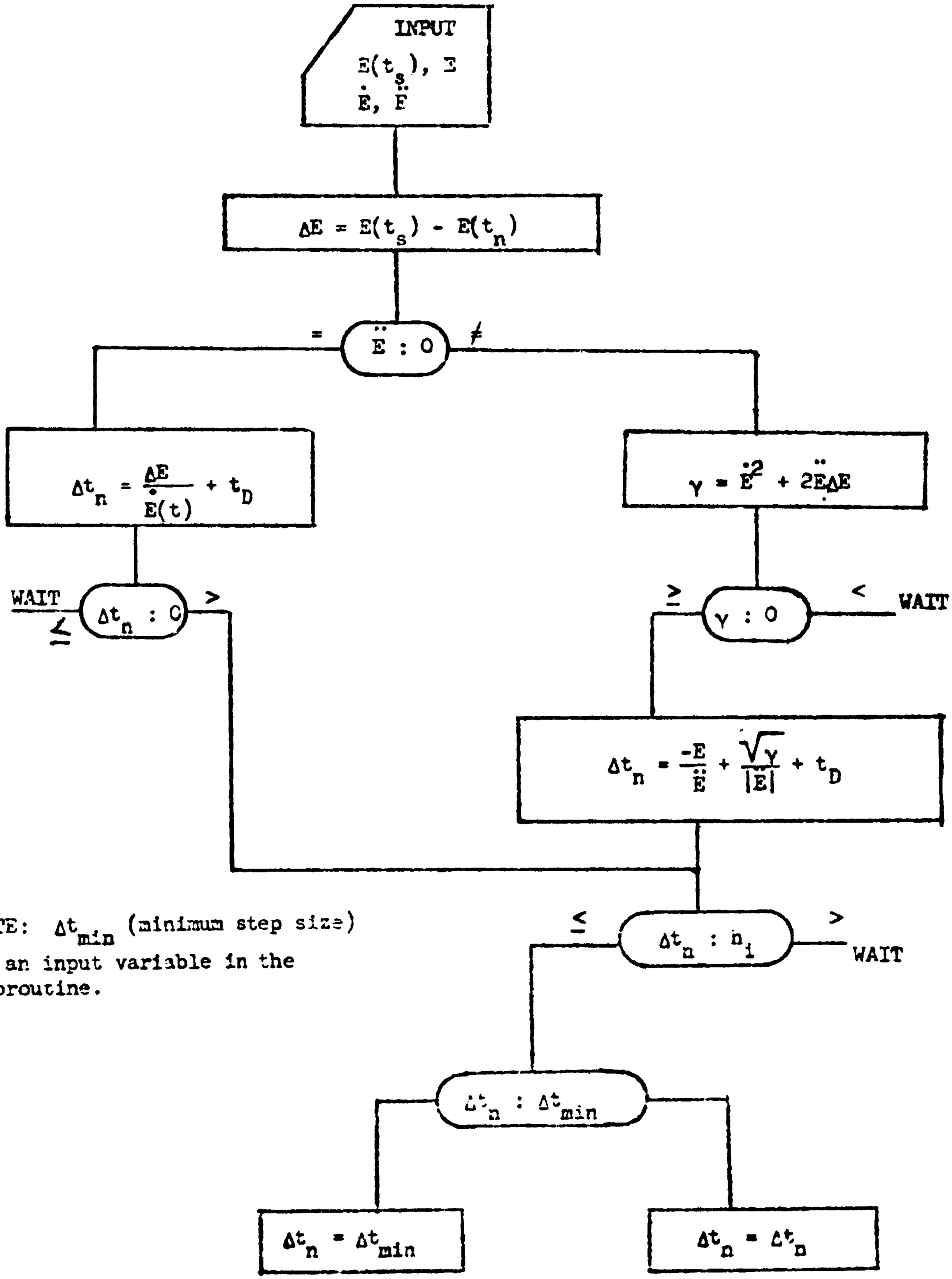

NOTE: Δt_{min} (minimum step size) is an input variable in the subroutine.

NOTE: h_i = nominal step $\begin{cases} i = 1 \text{ even step} \\ i = 2 \text{ discontinuity} \\ i = 3 \text{ staging} \end{cases}$

Figure A7

SCOUT GUIDANCE SYSTEM AND ERROR MODELS

Integrating Gyro Model

The gyro package for the Scout Vehicle consists of three mutually orthogonal rate-integrating single degree-of-freedom gyros aligned as in Figure A8. The equation for the output of any gyro signal generator in terms of vehicle rotational rates and linear accelerations expressed in gyro coordinates

$$\dot{\theta} = W_{IA} + K_T - K_{OA} - K_{SO}\,\theta\, W_{SA} - K_{AI}\, W_{SA}\, W_{IA}$$

$$- K_{IA}\, a_{IA} + K_{SA}\, a_{SA} - K_A\, a_{IA}\, a_{SA} + \dot{\theta}_E \qquad (40)$$

where: $\dot{\theta}$ is the output signal

$\dot{\theta}_E$ is the random drift

W_{SA}, W_{IA}, W_{OA} are the inertial angular rates of the gyro package about the spin, input and output axes

a_{IA}, a_{SA} are accelerations along the input and spin axes

K_T is the commanded rate while the other K's are scale factors.

It is assumed that the only command rate is about the pitch axis. Neglecting the third, fourth and fifth terms as insignificant and referring to Figure A8, noting, for example, that W_{OA} for the roll gyro is $-W_y$, the following equations can be written:

$$\dot{\theta}_{ROLL} = \dot{\theta}_{ER} - K_{RIA}\, A_R + W_R + K_{RSA}\, A_P - K_{RA}\, A_R\, A_P \qquad (41)$$

$$\dot{\theta}_{PITCH} = \dot{\theta}_{EP} + K_{PSA}\, A_Y + (W_{PC} - W_P) + \Delta K_{SG}\, W_{PC} \qquad (42)$$

$$+ K_{PMIA}\, A_P - K_{PA}\, A_P\, A_Y$$

$$\dot{\theta}_{YAW} = \dot{\theta}_{EY} - K_{YIA}\, A_Y + W_Y - K_{YSA}\, A_P + K_{YA}\, A_Y\, A_P \qquad (43)$$

where $K_T = (1 + \Delta K_{SG})W_{PC}$ and W_{PC} is the commanded pitch rate. The output signal from each gyro is:

$$\theta_{ROLL} = \int^{t} \dot{\theta}_{ROLL}\, dt + \theta_{OR} \tag{44}$$

$$\theta_{PITCH} = \int^{t} \dot{\theta}_{PITCH}\, dt + \theta_{OP} \tag{45}$$

$$\theta_{YAW} = \int^{t} \dot{\theta}_{YAW}\, dt + \theta_{OY} \tag{46}$$

where θ_{OR}, θ_{OP}, θ_{OY} are the initial guidance axis misalignments.

In conclusion, the following quantities are input as perturbations:

KRSA - Roll gyro mass unbalance - spin axis
KRIA - Roll gyro mass unbalance - input axis
KPSA - Pitch gyro mass unbalance - spin axis
KPIA - Pitch gyro mass unbalance - input axis
KYIA - Yaw gyro mass unbalance - input axis
KYSA - Yaw gyro mass unbalance - spin axis
THOR - Initial roll misalignment
THOP - Initial pitch misalignment
THOY - Initial yaw misalignment
DKSG - Torquer and intervalometer scale factor error
DTER - Roll random drift
DTEP - Pitch random drift
DTEY - Yaw random drift

The following variables are calculated in the trajectory analysis program

A_P, A_R, A_Y - inertial acceleration coordinates in the body axes

Equations (41)-(46) were programed.

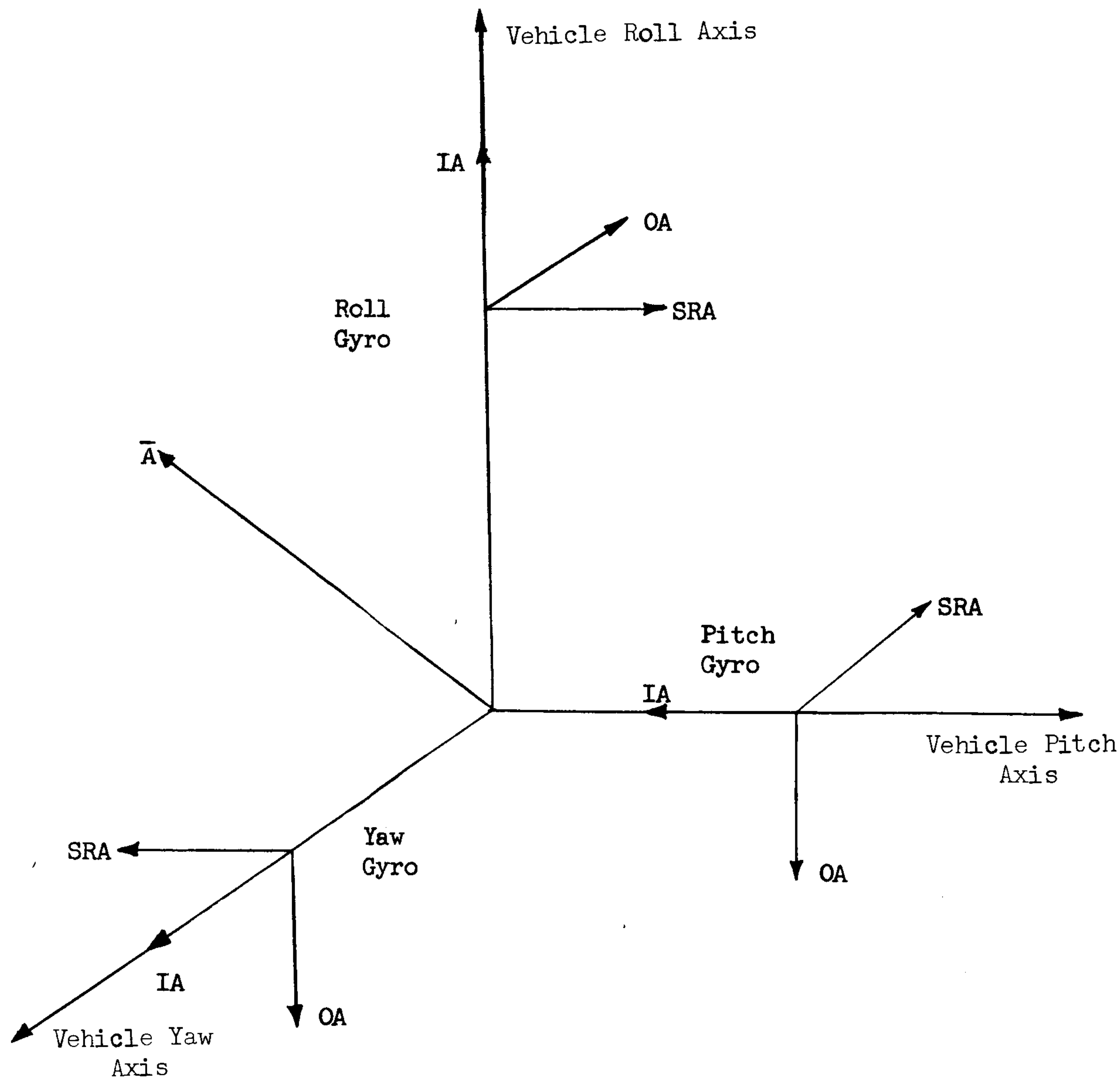

Figure A8 **Scout Gyroscope Orientation.**

Rate Gyro Model

The error sources of the rate gyro package are misalignment with respect to the body axes and a bias error. (The scale factor error shall be absorbed into the rate gain variation.) The equations programmed are:

$$\dot{\theta}_R = W_R + DRBE - (TYRG)\, W_P \qquad (47)$$

$$\dot{\theta}_Y = W_Y + DYBE + (TRRG)\, W_P \qquad (48)$$

$$\dot{\theta}_P = W_P + DPBE \qquad (49)$$

where the perturbations are:

DRBE - Roll rate gyro bias error
DYBE - Yaw rate gyro bias error
DPBE - Pitch rate gyro bias error
TYRG - Yaw axis misalignment
TRRG - Roll axis misalignment

and W_P, W_R, W_Y are pitch, roll and yaw body rates.

Error Signal Model

The first stage error signal for any axis is:

$$\epsilon_J = K_{PJ}\,\theta_J + K_{RJ}\,\dot{\theta}_J \qquad J = P, Y, R \qquad (50)$$

Assuming perturbations in each gain the following error sources exist:

KPP1 - Pitch proportional gain variation as a function of nominal
KPY1 - Yaw proportional gain variation as a fraction of nominal
KPR1 - Roll proportional gain variation as a fraction of nominal
KRR1 - Roll rate gain variation as a fraction of nominal
KPY1 - Yaw rate gain variation as a function of nominal

The equations mechanized are

$$\epsilon_P = K_{PP}(1 + KPP1)\,\theta_P + K_{PR}(1 + KRP1)\,\dot{\theta}_P \tag{51}$$

with analogous expressions for yaw and roll.

The second and third stage error signals have the same form with the addition of a dead zone variation, consequently, the perturbations are listed without further comment.

$$\left.\begin{array}{l} \text{KPP2, KPP3} \\ \text{KPR2, KPR3} \\ \text{KPY2, KPY3} \end{array}\right\} \textbf{Proportional gain errors}$$

$$\left.\begin{array}{l} \text{KRP2, KRP3} \\ \text{KRR2, KRR3} \\ \text{KPY2, KRY3} \end{array}\right\} \textbf{Rate gain errors}$$

$$\left.\begin{array}{l} \text{DBP2, DBP3} \\ \text{DBR2, DBR3} \\ \text{DBY2, DBY3} \end{array}\right\} \textbf{Dead-band errors}$$

SPINNING FOURTH STAGE SIMULATION

The N-stage program integrates six direction cosine rates to obtain body orientation as a function of time. If the body is spinning, the direction cosines change very rapidly requiring an extremely small integration step size. In order to avoid this problem, an additional coordinate system was defined. This system is fixed in the body but does not roll with it. It is convenient to visualize this system in the following way: Let the non-rolling reference frame be fixed in a non-rolling rigid body which contains the missile as a spinning rotor. The angular momentum is made up of contributions from the spinning rotor (H_R) and the rigid body (H_{RB}).

$$\bar{H} < \bar{H}_R + \bar{H}_{RB} \tag{52}$$

Differentiating with respect to time;

$$\dot{H} = \dot{H}_R + \dot{H}_{RB}$$

$$= [I_R\omega_R - \dot{\overline{\omega}}_{RB} \times I_R\overline{\omega}_R] + [I_{RB}\overline{\omega}_{RB} - \overline{\omega}_{RB} \times I_{RB}\overline{\omega}_{RB}] \qquad (53)$$

Note that the minus signs are compatable with left handed rotations. The Scout is designed to be symmetrical about its longitudinal axis and has zero cross products of inertia. The rate change of rotor angular momentum becomes:

$$\begin{pmatrix} \dot{H}_\xi \\ \dot{H}_\eta \\ \dot{H}_\zeta \end{pmatrix}_{\text{ROTOR}} = \begin{pmatrix} I_\xi & 0 & 0 & \dot{\Omega} \\ 0 & I_\eta & 0 & 0 \\ 0 & 0 & I_\zeta & 0 \end{pmatrix} - \begin{pmatrix} 0 & -\omega_\zeta & \omega_\eta \\ \omega_\zeta & 0 & -\omega_\xi \\ -\omega_\eta & +\omega_\xi & 0 \end{pmatrix} \begin{pmatrix} I_\xi & \Omega \\ 0 & \\ 0 & \end{pmatrix} \qquad (54)$$

It has been assumed that all of the angular velocity of the rotor is about the foll (ζ) axis of the rigid body.

The rate change of angular momentum of the nom-rolling rigid body is:

$$\begin{pmatrix} \dot{H}_\xi \\ \dot{H}_\eta \\ \dot{H}_\zeta \end{pmatrix} = \begin{pmatrix} I_\xi\dot{\omega}_\xi + \omega_\eta\omega_\zeta (I_\eta - I_\zeta) \\ I_\eta\dot{\omega}_\eta + \omega_\xi\omega_\zeta (I_\zeta - I_\xi) \\ I_\zeta\dot{\omega}_\zeta + \omega_\xi\omega_\eta (I_\eta - I_\xi) \end{pmatrix} \qquad (55)$$

Substituting equations (53) and (54) into equation (55) and solving for the angular acceleration of the system:

$$\begin{pmatrix} \dot{\omega}_\xi \\ \dot{\omega}_\eta \\ \dot{\omega}_\zeta \end{pmatrix} = [I]^{-1} \left\{ \begin{pmatrix} M_\xi \\ M_\eta \\ M_\zeta \end{pmatrix} + \begin{pmatrix} \omega_\eta\omega_\zeta (I_\zeta - I_\eta) \\ \omega_\xi\omega_\eta (I_\xi - I_\zeta) \\ \omega_\xi\omega_\eta (I_\xi - I_\eta) \end{pmatrix} + \begin{pmatrix} I_\xi\dot{\Omega} \\ I_\xi\Omega\omega_\zeta \\ -I_\xi\Omega\omega_\eta \end{pmatrix} \right. \qquad (56)$$

The oscillations exhibit an exponential decay due to the jet damping effect of the solid rocket engine. These results were obtained by using an integration step size of .25 sec. It is interesting to note that a step of .002 sec. is required to obtain these same results by straight forward integration of the equations of motion. The precession frequency can be verified by comparison with the following expression:

$$\dot{\psi} = \frac{I_{xx}\omega_x}{I_{zz}\cos\theta}$$

where θ is the cone angle.

Substituting the following fourth stage data:

$$\begin{aligned} I_{xx} &= 8.64 \text{ slug-ft}^2 \\ I_{zz} &= 46.91 \text{ slug-ft}^2 \\ \omega_x &= 3.0 \text{ cycles/sec} \\ \cos\theta &= 1 \end{aligned}$$

gives a precession frequency of .56 cycles/sec. which agrees with Figure A9.

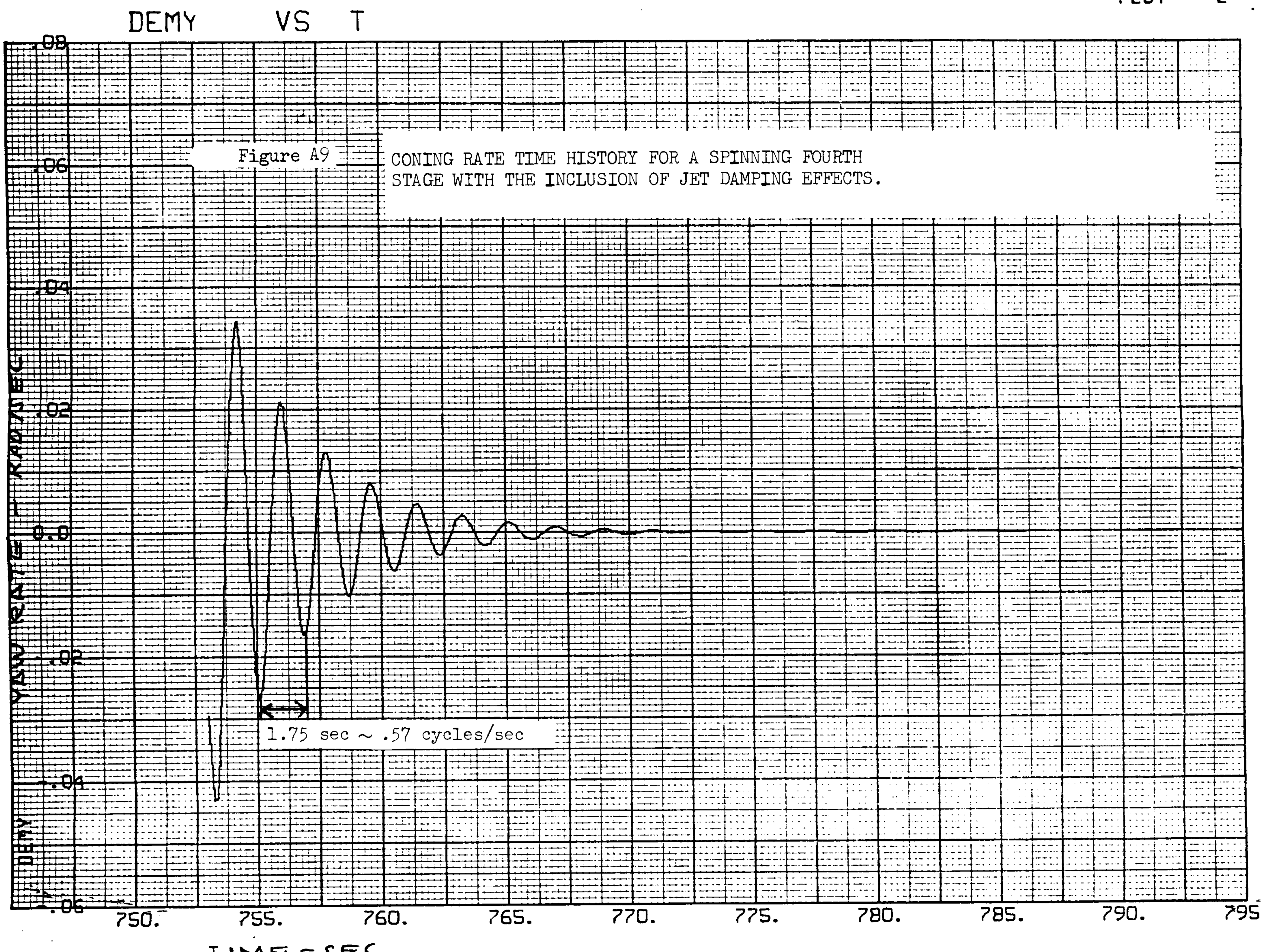

Figure A9

CONING RATE TIME HISTORY FOR A SPINNING FOURTH STAGE WITH THE INCLUSION OF JET DAMPING EFFECTS.

TABLE A

COMPARISON OF TRAJECTORY PARAMETERS AT END OF FIRST STAGE (t=76.46 sec)

Variable	TRW (N-Stage)	LTV (NEMAR)	Δ
V_I - ft/sec	4059.2	4060.5	1.3
XL - ft	81680.	81755.	75
YL - ft	-993.	-993.	0.0
ZL - ft	132302.	132379.	77
$\dot{X}L$ - ft/sec	2118.2	2119.2	1.0
$\dot{Y}L$ - ft/sec	-31.1	-31.1	0.0
$\dot{Z}L$ - ft/sec	2537.7	2538.5	0.8
θ - deg	50.34	50.22	0.12
ψ - deg	127.14	127.13	0.01
φ - deg	.234	.231	0.003

The small difference in inertial velocity at staging is probably due to the fact that N-stage uses a different technique to compute jet vane drag as shown below.

LTV jet vane drag

$$F_{\xi_V} = -(\delta p^2 + \delta q^2 + \delta r^2)^{1/2} K_F T_{VAC} \tag{57}$$

TRW jet vane drag

$$F_{\xi_V} = -T_{VAC}\left[2CD_{V_{f(|\delta q|)}} + CD_{V_{f(|\delta r + \delta p|)}} + CD_{V_{f(|\delta r - \delta p|)}}\right] \tag{58}$$

where

δp, δq, δr = jet vane deflection angles in roll, pitch, and yaw, respectively

K_F = constant to relate jet vane drag to vacuum thrust

$CD_{V_{f(|\delta|)}}$ = jet vane drag coefficient per vane. It is determined from a table lookup routine.

The TRW method involves a straight forward table lookup routine with an argument of vane deflection angle for each vane. Since the drag due to each vane is defined in the ξ direction, the individual drag components from each vane may be summed directly to obtain the total jet vane drag.

Time histories of the vehicle motion up to second stage coast are shown in Figures A10 through A15. Results from the NEMAR simulation are plotted where available to show comparison of results in the first stage motion.

Inspection of Table I and Figures A10 through A15 reveals that the LTV and TRW results are in good agreement for the first stage 6D portion of the Scout trajectory.

A rough measure of validity of the second and third stage 6D simulation was obtained by matching LTV's modified 3D with the 3D and 6D N-stage results. A comparison of the state vectors at third stage separation is given in Table AII.

	TRW N-STAGE 6D	TRW N-STAGE 3D	LTV NEMAR 3D
h -ft	3692901	3704088	3704346
V_I-ft/sec	13192.8	13172.3	13172.0
γ_I-deg	1.136	1.198	1.200
θ -deg	.232	.457	.455
Ψ -deg	178.93	178.73	178.730
ϕ -deg	.993	1.024	1.026

Table AII. Comparison of trajectory parameters at third stage separation (t = 753.07)

The N-stage 3D results were obtained by ignoring the rotational dynamics equations and autopilot in the 6D model. Table II indicates that the TRW and LTV 3D programs are in excellent agreement and therefore are probably valid simulations of a point mass trajectory.* It should be noted that the transition

* It should be noted that 3D refers to the dynamical degrees of freedom and that the simulation actually involves 6D kinematics with 3D dynamics.

from 6D to 3D at the end of first stage involves an instantaneous change in attitude. This arises from the fact that the 3D simulation assumes perfect control ($\dot{\theta}_c = \dot{\theta}$) or zero error signal in the autopilot. The error signal in pitch may be written as follows:

$$\epsilon = \int_0^t (\dot{\theta}_c - \dot{\theta})\, dt - K_{\dot{\theta}}\dot{\theta}$$

$$= \theta_c - \theta - K_{\dot{\theta}}\dot{\theta}$$

At the end of first stage, ϵ has some finite value which is instantaneously set to zero by perturbing the attitude so that $\theta_c = \theta$. Since $K_{\dot{\theta}}\dot{\theta}$ serves only to stablize the autopilot, it is considered to be zero for 3D computations. The 3D N-stage data in Table II was obtained by setting $\theta = \theta_c$ at the end of first stage.

The rotational dynamics of the second and third stage may be verified by consideration of the phase plane trajectories in pitch and yaw (angular rate vs position). Consider the phase trajectories of the second stage burn period shown in Figure A10 and A11. Note that a restoring impulse, $\Delta\omega$, is applied each time the phase trajectory comes in contact with a switch line indicating that the proper engines are firing when the error signal exceeds the deadband. In this case, the hysteresis is 10% of the deadband and is indicated by dashed lines parallel to the switch lines. The thrusters turn off at the hysteresis line. The external moment due to atmospheric forces causes a limit cycle on one side of the deadband until the vehicle leaves the atmosphere at which time the attitude is observed to oscillate back and forth between ± D. It can be shown that the shape of the phase trajectory with external moment is a parabola.

$$\theta = \frac{\dot{\theta}^2}{2(\frac{M}{I})} \tag{59}$$

The appropriate aerodynamic moment and moment of inertia was substituted into equation (59) to obtain a check on the rotational dynamics. Comparison of the resulting parabola with one oscillation of this biased limit cycle is shown in Figure 18.

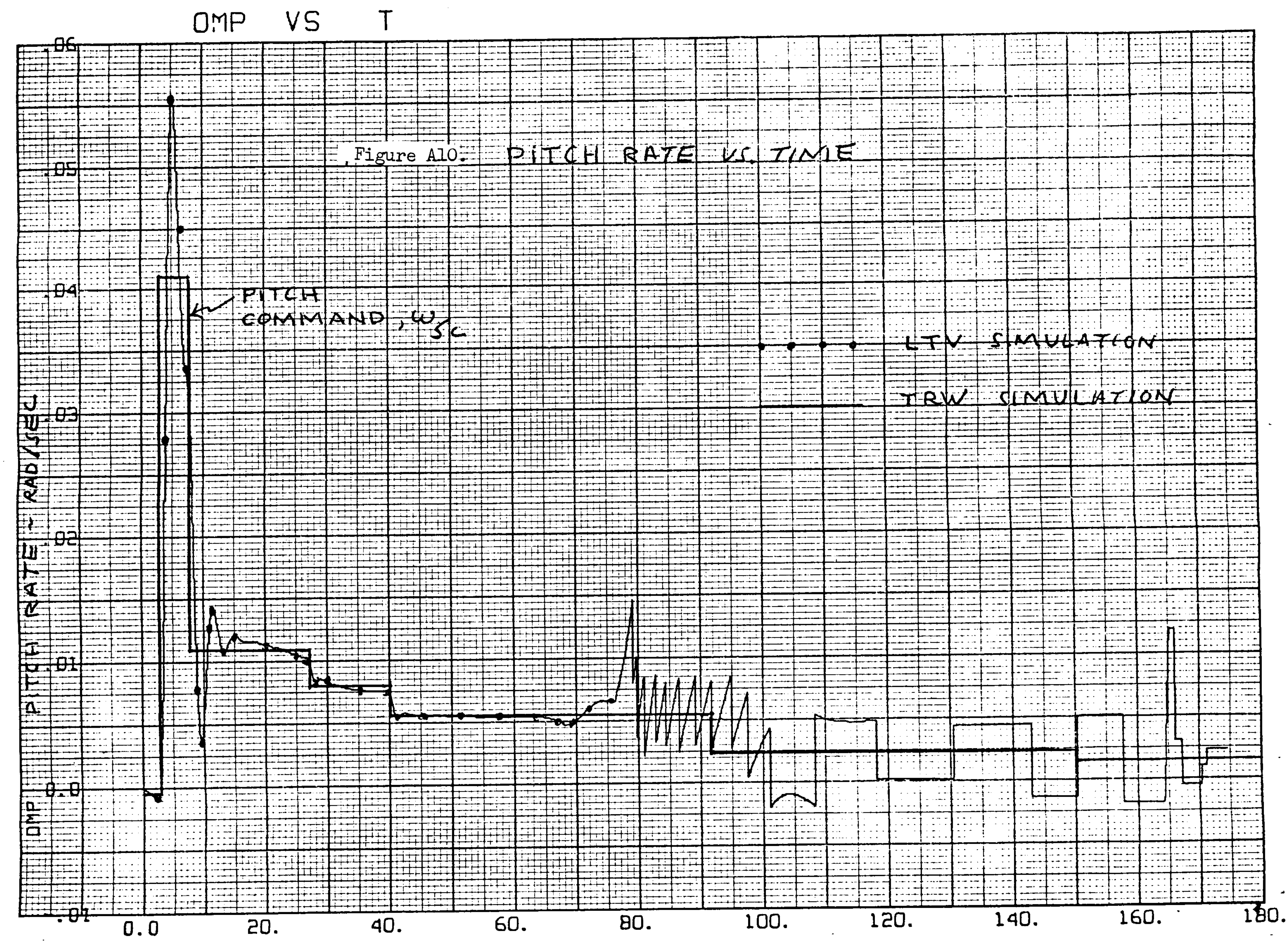

Figure A10. PITCH RATE VS. TIME

PLOT 2

OMY VS T

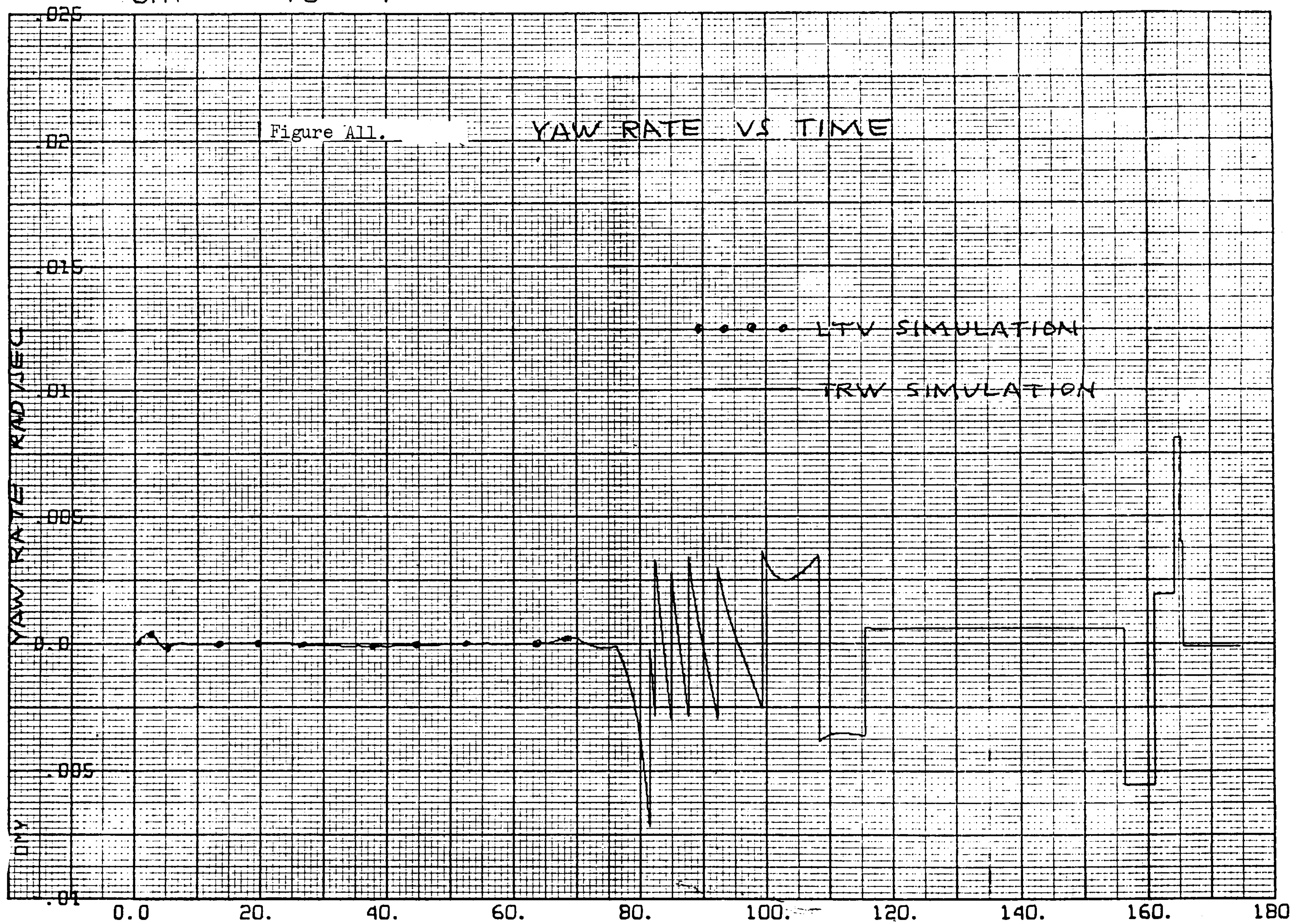

Figure A11.

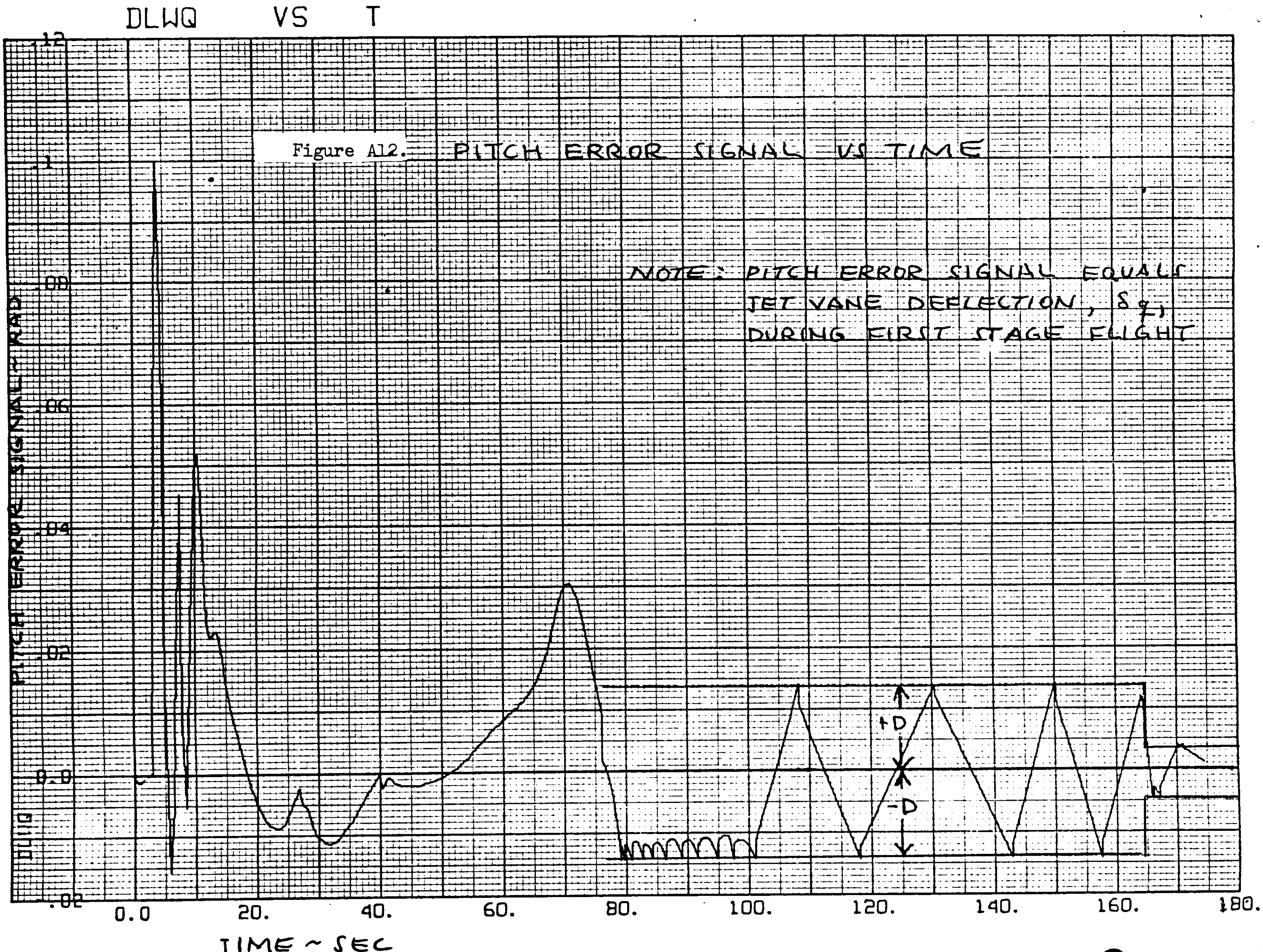

Figure A12. PITCH ERROR SIGNAL VS TIME

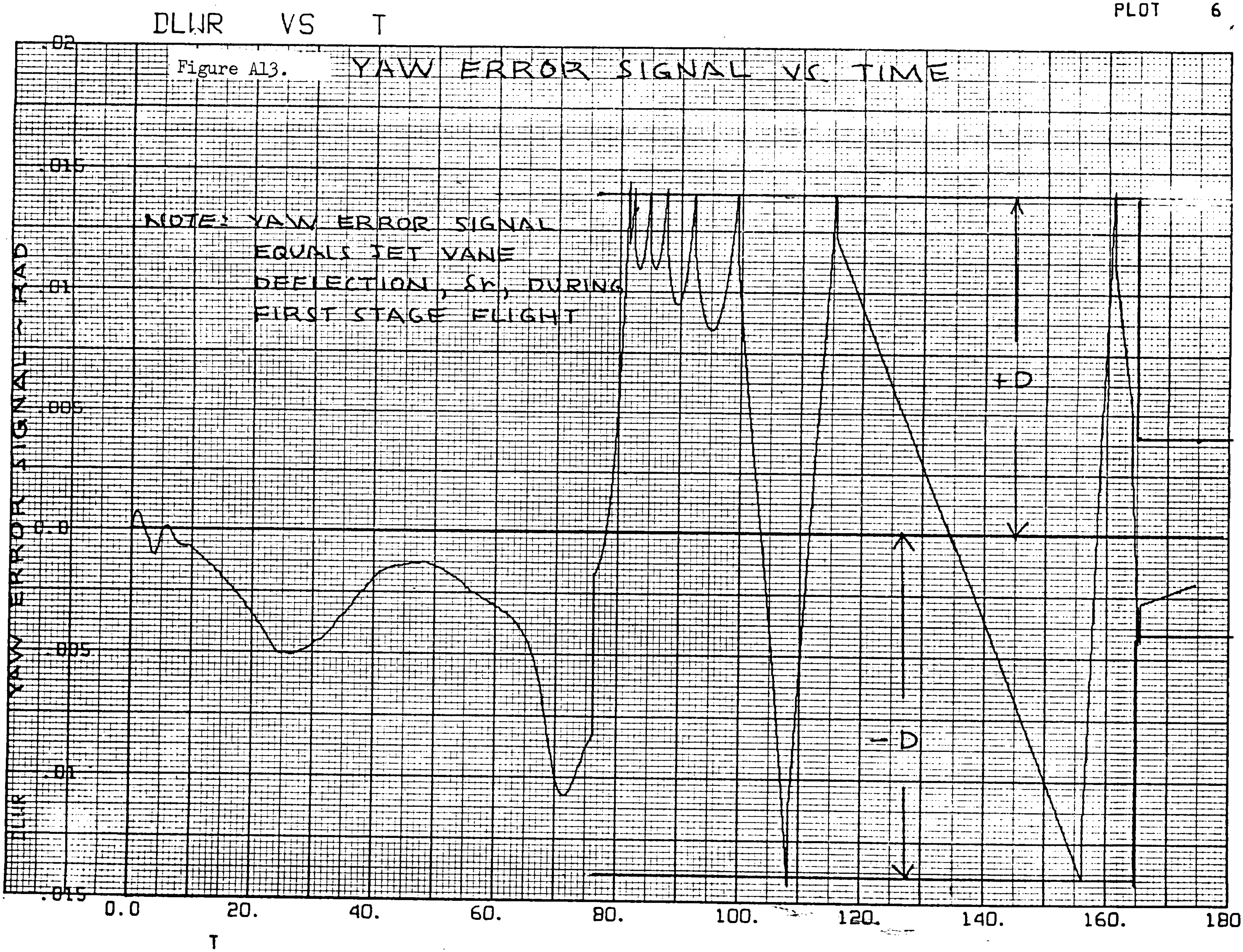
PLOT 6
DLWR VS T
YAW ERROR SIGNAL VS TIME
NOTE: YAW ERROR SIGNAL
EQUALS JET VANE
DEFLECTION, δr, DURING
FIRST STAGE FLIGHT
+D
-D
YAW ERROR SIGNAL ~ RAD
DLWR
.02
.015
.01
.005
0.0
-.005
-.01
-.015
0.0
20.
40.
60.
80.
100.
120.
140.
160.
180.
T
Figure A13.

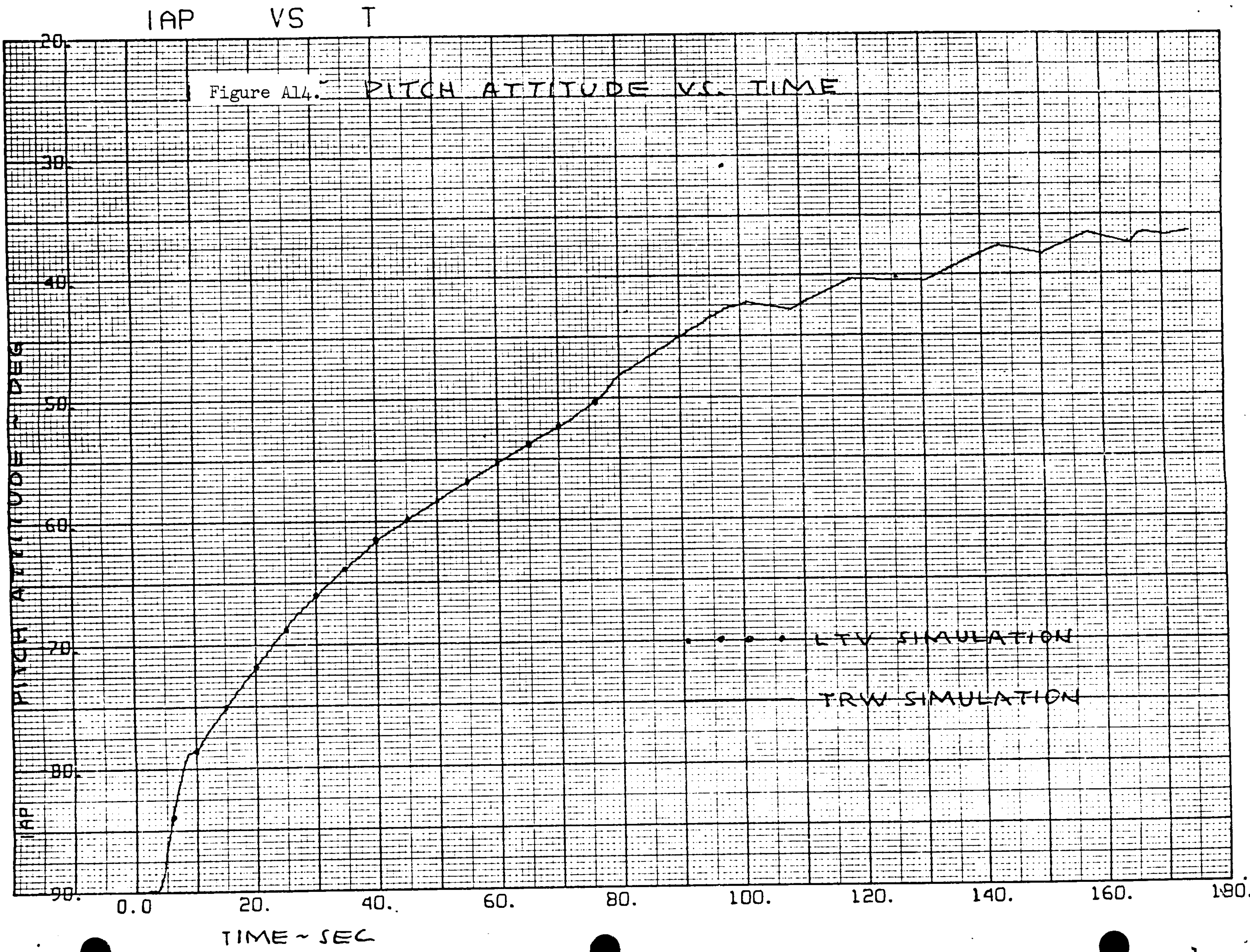

Figure A14. PITCH ATTITUDE VS. TIME

PLOT 4

IAY VS T

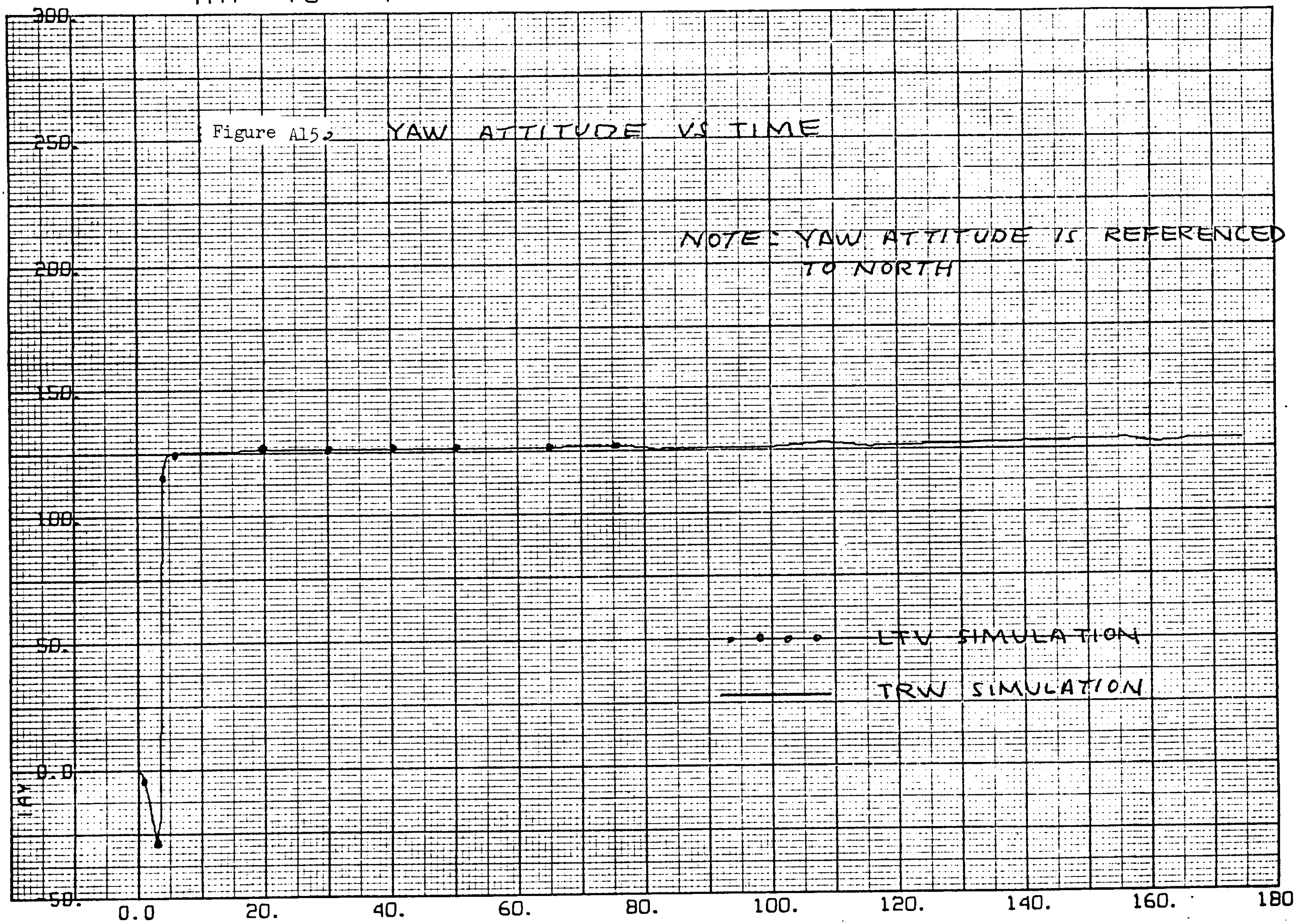

Figure A15. YAW ATTITUDE VS TIME

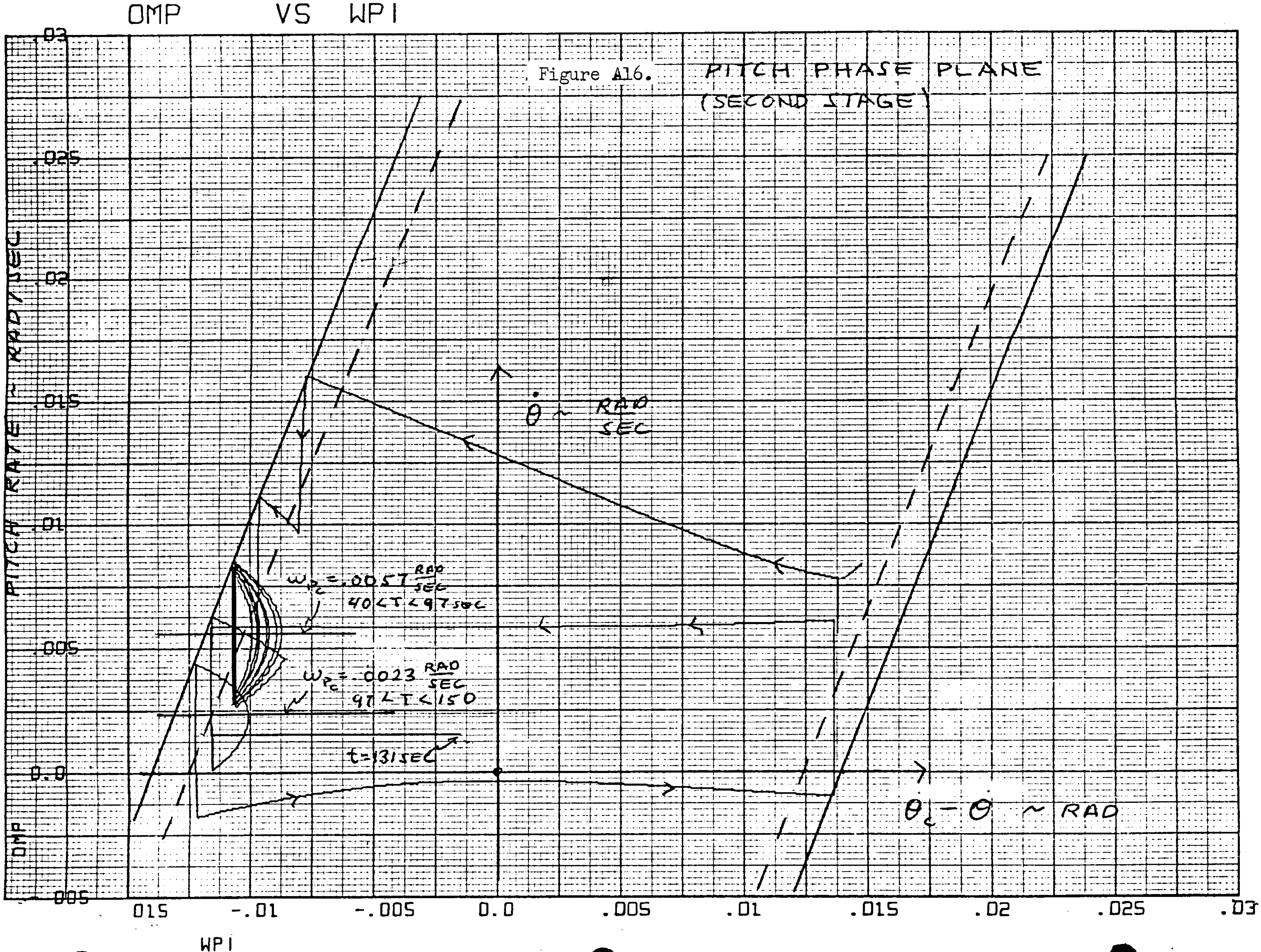
OMP VS WPI
Figure A16.
PITCH PHASE PLANE
(SECOND STAGE)
PITCH RATE ~ RAD/SEC
OMP
.03
.025
.02
.015
.01
.005
0.0
.005
$\dot{\theta}$ ~ RAD/SEC
ω_{P_C} = .0057 RAD/SEC
40 < T < 97 SEC
ω_{P_C} = .0023 RAD/SEC
97 < T < 150
t=131 SEC
$\theta_c - \theta$ ~ RAD
015
-.01
-.005
0.0
.005
.01
.015
.02
.025
.03
WPI

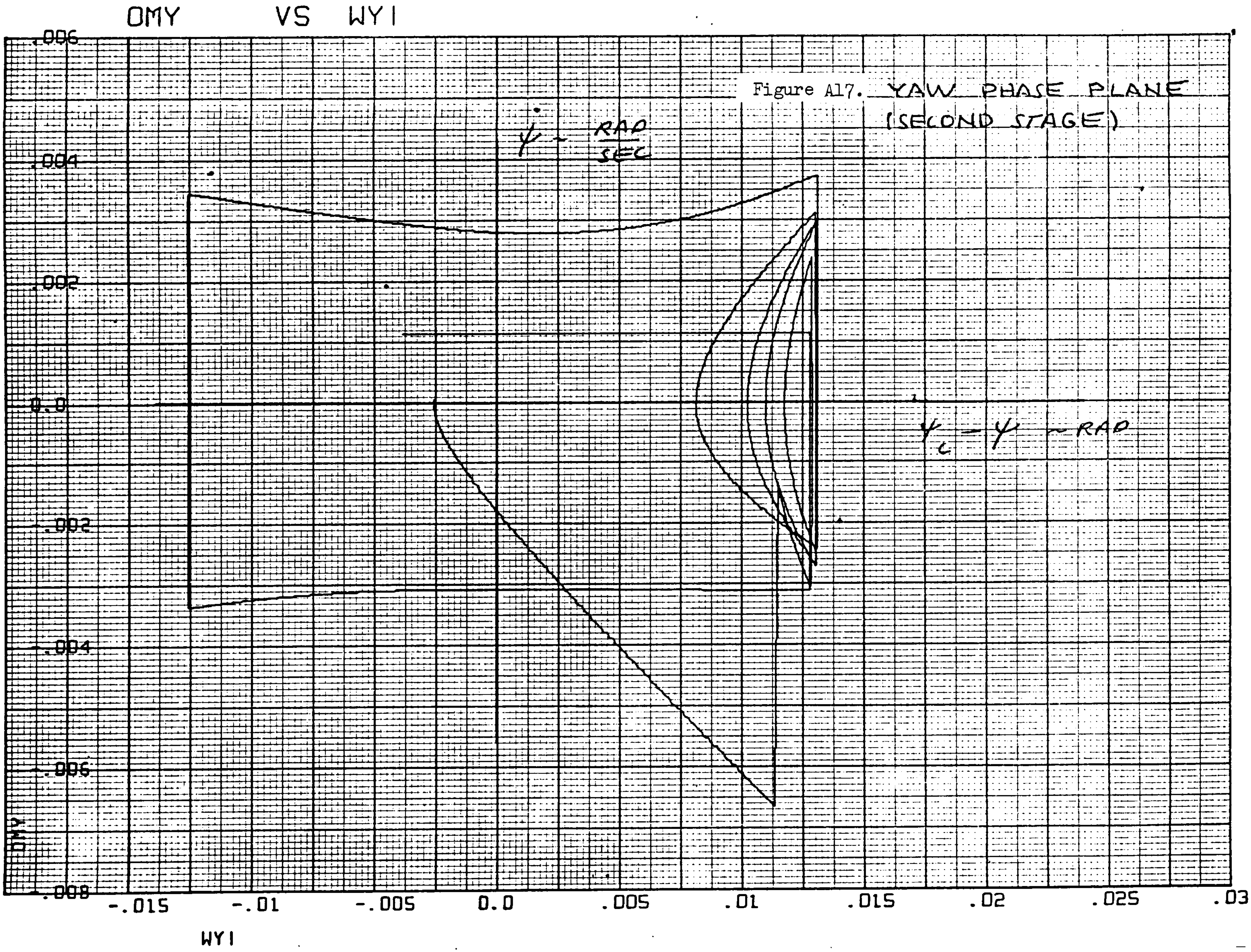

Figure A17. YAW PHASE PLANE (SECOND STAGE)

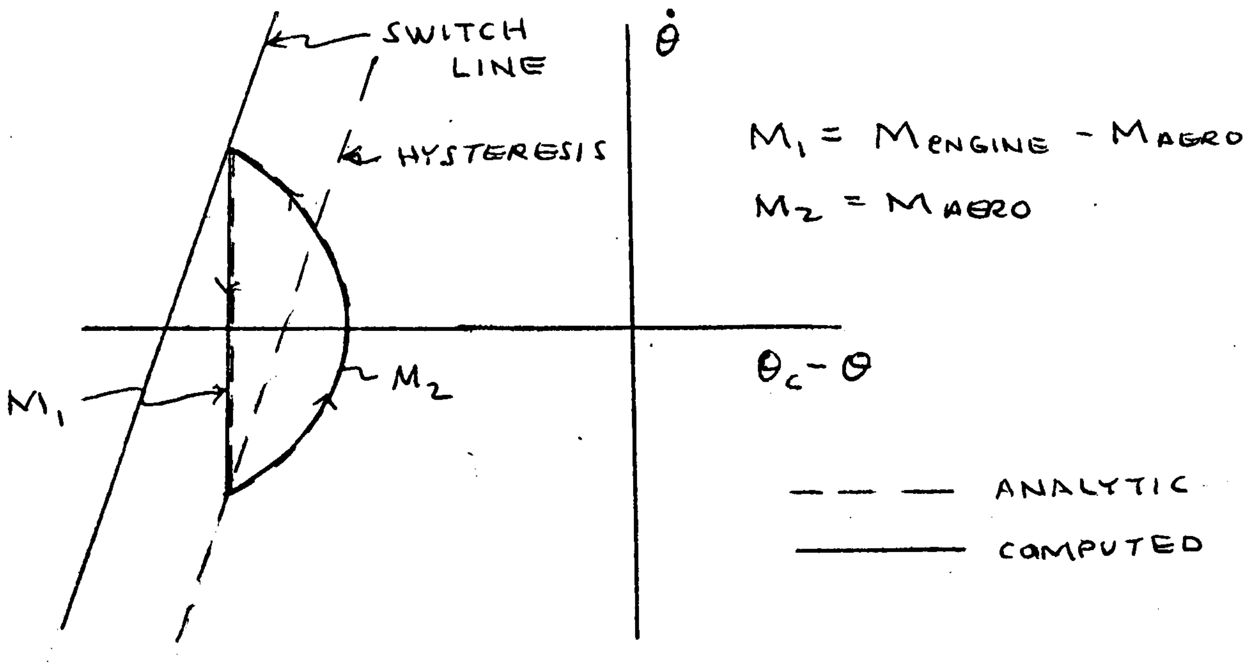

Figure A18. **Comparison of analytic and simulated limit cycle with aerodynamic moment.**

It should be noted that the limit cycle is symmetrical about the commanded angular rate in Figures 10 and 16. The error signal time histories in Figures 12 and 13 also reflect the limit cycle characteristics and the effect of aerodynamic moment along with a change in deadband width at 164.68 seconds.

The above discussion indicates that the autopilot and rotational dynamics simulation gives the expected results as predicted by non-linear control theory. Therefore, since the 3D simulation was previously shown to be valid (TRW - LTV match) the 6D simulation is also valid in the sense that the rotational dynamics plus autopilot act according to theory. However, this does not imply that the motion inside the deadband is an exact simulation of the actual vehicle. Addition of high frequency effects such as body bending, thrust lags, and time delays will alter the motion inside the deadband. However, it is characteristic of systems utilizing on-off control that motion inside the deadband is of no consequence to system performance.

APPENDIX B
SCOUT SIMULATION INPUT DATA

This appendix will present the data tables used in the initial verification of the simulation.

The aerodynamic coefficient programed was available in the LTV S-131R trajectory printout. Those for which data was available are listed below with symbolic designations for both LTV and TRW and the number of the table in which each may be found. In the case of those data which are functions of mach number and dynamic pressure the data have been converted from LTV form (which gives coefficient value per radian) to TRW form which gives the coefficient value per degree.

Those for which data are available:

LTV Equation Symbol	LTV Program Symbol	TRW Equation Symbol	TRW Program Symbol
C_{Ao}	CAO	C_{Ao}	CD
$C_{N\alpha}$	CNA	$C_{N\alpha}$	CNPI
$C_{Y\beta}$	CNA	$C_{Y\beta}$	CNYI
C_{1p}	CLP	C_{1p}	CMRV
$C_{m\alpha}$	-CNB	$C_{m\alpha}$	CMP
C_{mq}	CMQ	C_{mq}	CMPV
$C_{n\beta}$	CNB	$C_{n\beta}$	CMY
C_{nR}	CMQ	C_{nr}	CMRV
$C_{N\delta}$	-CYD	$C_{N\delta q}$	CNPD
$C_{y\delta}$	CYD	$C_{y\delta q}$	CNYD
$C_{m\delta}$	CMD	$C_{m\delta q}$	CMPD
$C_{m\delta}$	CMD	$C_{m\delta r}$	CMYD
$C_{1\delta}$	CLD	$C_{1\delta p}$	CMRD
--	--	C_{mo}	CM

TABLE B-1

C_{AO}, $C_{\ell\delta_p}$, AND $C_{\ell p}$ VERSUS MACH NUMBER

MACH NUMBER	C_{AO}	$C_{\ell\delta p}$	$C_{\ell p}$
0	.495	.0138	-.0285
.2	.522	.0142	-.0289
.4	.5525	.0152	-.03
.6	.6	.0167	-.0314
.7	.635	.0174	-.0325
.8	.714	.0182	-.0336
.9	.809	.0188	-.035
1.	1.238	.0192	-.0359
1.1	1.465	.0184	-.0355
1.2	1.458	.0154	-.0343
1.4	1.377	.0128	-.0313
1.7	1.238	.0104	-.0269
2.	1.12	.0088	-.0233
2.3	1.025	.0076	-.0205
2.6	.952	.0066	-.018
3.2	.85	.0051	-.0146
3.8	.794	.0042	-.0124
4.2	.781	.0038	-.0114
4.6	.791	.0034	-.0105
100.	.791	.0034	-.0105

TABLE B-2

*C_{N_α} VERSUS MACH NUMBER AND DYNAMIC PRESSURE

MACH NUMBER	Q = 0, $C_{N\alpha}$ =	Q = 1500, $C_{N\alpha}$ =	Q = 2500, $C_{N\alpha}$ =	Q = 3500, $C_{N\alpha}$ =
0	.2566	.2539	.2520	.2487
.2	.2597	.2566	.2545	.2513
.4	.2653	.2618	.2597	.2562
.6	.2754	.2714	.2693	.2658
.7	.2836	.2793	.2763	.2728
.8	.2957	.2897	.2862	.2819
.9	.3176	.3063	.3019	.2976
1.	.3438	.3316	.3264	.3211
1.1	.3351	.3176	.3229	.3124
1.2	.3063	.3011	.2985	.2985
1.4	.2635	.2662	.2688	.2714
1.7	.2234	.2295	.2339	.2400
2.	.1981	.2051	.2108	.2182
2.3	.1812	.1885	.1954	.2042
2.6	.1693	.1780	.1850	.1937
3.2	.1553	.1641	.1710	.1798
3.8	.1466	.1553	.1623	.1710
4.2	.1431	.1518	.1588	.1676
4.6	.1422	.1501	.1571	.1658
100.	.1422	.1501	.1571	.1658

* FOR SYMMETRIC VEHICLE $C_{Y\beta} = C_{N\alpha}$

TABLE B-3

*C_{n_β} VERSUS MACH NUMBER AND DYNAMIC PRESSURE

MACH NUMBER	Q = 0, C_{n_β} =	Q = 1500, C_{n_β} =	Q = 2500, C_{n_β} =	Q = 3500, C_{n_β} =
0	1.9722	1.7453	1.5708	1.3963
.2	2.0071	1.7802	1.6057	1.4137
.4	2.0944	1.8675	1.6755	1.4835
.6	2.2427	2.0246	1.8239	1.6232
.7	2.3736	2.1468	1.9286	1.7191
.8	2.5307	2.3038	2.0857	1.8675
.9	2.7925	2.5307	2.2689	2.0769
1.	3.1590	2.8187	2.5307	2.3213
1.1	2.8449	2.5045	2.2340	1.9548
1.2	2.4173	2.0944	1.8151	1.5708
1.4	1.7628	1.5010	1.2741	1.0036
1.7	1.1519	.9338	.7330	.4887
2.	.7854	.5934	.4189	.1920
2.3	.5760	.3840	.2269	.0175
2.6	.4276	.2531	.1047	-.1047
3.2	.2269	.0698	-.0698	-.2618
3.8	.1047	-.0436	-.1833	-.3491
4.2	.0611	-.1047	-.2269	-.3927
4.6	.0436	-.1222	-.2443	-.4014
100.	.0436	-.1222	-.2443	-.4014

* FOR SYMMETRIC VEHICLE $C_{m_\alpha} = -C_{n_\beta}$

TABLE B-4

PITCHING MOMENT C_{MO}

M	C_{MO}
0	.1
.4	.13
.8	.17
1.0	.23
1.2	.35
1.4	.57
1.5	.63
1.6	.65
1.7	.66
1.8	.64
2.0	.58
2.2	.50
2.4	.45
2.6	.42
2.8	.38
3.2	.34
4.0	.27
4.5	.25
100	.25

TABLE B-5

*C_{m_q} VERSUS MACH NUMBER AND DYNAMIC PRESSURE

MACH NUMBER	Q = 0, C_{m_q} =	Q = 1500, C_{m_q} =	Q = 2500, C_{m_q} =	Q = 3500, C_{m_q} =
0	-80.983	-80.285	-79.587	-78.889
.2	-81.158	-80.634	-79.936	-79.412
.4	-82.729	-82.030	-81.332	-80.809
.6	-86.568	-85.696	-84.823	-84.299
.7	-89.710	-88.488	-87.616	-87.092
.8	-94.073	-92.502	-91.804	-90.757
.9	-101.055	-99.135	-98.262	-96.866
1.	-111.701	-110.828	-109.956	-108.559
1.1	-105.941	-104.720	-104.720	-103.847
1.2	-96.866	-96.866	-97.040	-97.215
1.4	-83.252	-84.299	-85.347	-86.743
1.7	-69.813	-71.558	-73.478	-75.747
2.	-61.261	-63.879	-66.323	-68.941
2.3	-55.851	-58.818	-61.087	-64.403
2.6	-51.836	-54.978	-57.421	-60.912
3.2	-46.426	-49.567	-52.185	-55.851
3.8	-43.284	-46.251	-49.044	-52.534
4.2	-41.888	-44.680	-47.997	-51.313
4.6	-41.539	-44.157	-47.298	-50.964
100.	-41.539	-44.157	-47.298	-50.964

*FOR SYMMETRIC VEHICLE $C_{m_r} = C_{m_q}$

TABLE B-6

*$C_{y\delta_r}$ VERSUS MACH NUMBER AND DYNAMIC PRESSURE

MACH NUMBER	Q = 0, $C_{Y\delta r}$ =	Q = 1500, $C_{Y\delta r}$ =	Q = 2500, $C_{Y\delta r}$ =	Q = 3500, $C_{Y\delta r}$ =
0	.00869	.00846	.00820	.00803
.2	.00894	.00864	.00841	.00820
.4	.00942	.00904	.00873	.00855
.6	.01021	.00960	.00925	.00899
.7	.01065	.00995	.00967	.00937
.8	.01117	.01038	.01009	.00977
.9	.01169	.01082	.01056	.01021
1.	.01187	.01117	.01091	.01065
1.1	.01143	.01073	.01047	.01012
1.2	.00986	.00969	.00960	.00925
1.4	.00803	.00794	.00794	.00785
1.7	.00637	.00637	.00637	.00620
2.	.00524	.00524	.00524	.00524
2.3	.00450	.00450	.00450	.00450
2.6	.00384	.00384	.00384	.00384
3.2	.00314	.00314	.00314	.00314
3.8	.00271	.00271	.00271	.00271
4.2	.00253	.00253	.00253	.00253
4.6	.00244	.00244	.00244	.00244
100.	.00244	.00244	.00244	.00244

* FOR SYMMETRIC VEHICLE $C_{N\delta_\ell} = -C_{Y\delta_r}$

TABLE B-7

*$C_{m\delta_q}$ VERSUS MACH NUMBER AND DYNAMIC PRESSURE

MACH NUMBER	Q = 0, $C_{m\delta q}$ =	Q = 1500, $C_{m\delta q}$ =	Q = 2500, $C_{m\delta q}$ =	Q = 3500, $C_{m\delta q}$ =
0	.1178	.1152	.1129	.1100
.2	.1239	.1210	.1187	.1159
.4	.1318	.1274	.1248	.1218
.6	.1405	.1358	.1318	.1283
.7	.1457	.1405	.1361	.1323
.8	.1510	.1449	.1414	.1370
.9	.1580	.1501	.1459	.1414
1.	.1623	.1553	.1501	.1449
1.1	.1553	.1463	.1405	.1340
1.2	.1396	.1318	.1274	.1222
1.4	.1152	.1108	.1073	.1047
1.7	.0899	.0890	.0873	.0846
2.	.0742	.0733	.0733	.0716
2.3	.0625	.0625	.0625	.0625
2.6	.0541	.0541	.0541	.0541
3.2	.0436	.0436	.0436	.0436
3.8	.0367	.0367	.0367	.0367
4.2	.0340	.0340	.0340	.0340
4.6	.0332	.0332	.0332	.0332
100.	.0332	.0332	.0332	.0332

* FOR SYMMETRIC VEHICLE $C_{m\delta r} = C_{m\delta q}$

TABLE B-8

STAGE ONE PROPULSION DATA

TIME (sec)	VACUUM THRUST (lbs)	PROPELLANT WEIGHT (lbs)
.0	51730.16	21341.
.203	98966.4	21303.02
.506	94025.43	21190.1
.709	91490.25	21117.15
1.316	89763.34	20905.29
2.734	89829.44	20422.6
5.063	89487.01	19624.13
9.114	92207.68	18189.07
13.57	96610.88	16533.15
19.241	98432.55	14348.59
25.823	98835.18	11768.28
34.431	101966.37	8313.55
43.14	106703.11	4655.95
46.279	106422.59	3307.83
46.988	103914.35	3008.03
48.102	98105.91	2554.32
49.013	91274.14	2208.55
52.051	60834.63	1295.15
55.495	32147.7	662.57
57.52	23072.89	440.71
59.95	16839.13	262.83
66.837	3271.31	23.98
67.95	1070.7	9.99
68.052	973.01	8.99
81.014	.0	.0

Notes: 1. Nozzle exit area is 813.168 sq. in.

2. Time is measured from motor ignition.

TABLE B-9

STAGE TWO PROPULSION DATA

TIME (sec)	VACUUM THRUST (lbs)	PROPELLANT WEIGHT (lbs)
.0	43156.52	8294.2
.402	40214.03	8234.09
2.011	41685.27	7997.89
4.022	44627.76	7686.82
8.044	50512.74	7001.39
12.066	57084.3	6226.69
14.077	59928.71	5805.59
16.088	62773.12	5364.11
18.099	64930.94	4904.69
20.109	66696.44	4431.22
22.12	67971.52	3946.85
24.131	68658.1	3455.44
28.153	69344.68	2462.8
29.159	69148.51	2213.76
30.164	67971.52	1967.18
31.17	66304.11	1725.7
32.175	66206.02	1487.38
36.197	66402.19	533.41
37.202	66206.02	294.92
37.705	64440.53	177.42
38.007	55907.31	112.47
38.811	8827.47	18.97
39.213	3923.32	9.49
40.42	.0	.0
40.5	.0	.0

Notes: 1. Nozzle exit area is 1167.84 sq. in.

2. Time is measured from motor ignition.

TABLE B-10

STAGE THREE PROPULSION DATA

TIME (sec)	VACUUM THRUST (lbs)	PROPELLANT WEIGHT (lbs)
.0	.0	2594.5
.1	22996.72	2581.29
2.	21454.66	2437.29
3.	21588.75	2359.28
5.	21838.92	2201.96
7.	22428.33	2041.55
10.	23393.99	1792.54
12.	23674.18	1621.92
14.	23821.28	1449.92
16.	23750.23	1277.51
19.	23465.04	1017.3
21.	23069.77	848.69
24.	22956.69	598.48
27.	22524.39	351.26
28.	22147.13	270.36
29.	21629.78	191.0[illegible]
30.	20628.1	114.44
31.	18213.45	44.13
32.	3509.4	6.51
32.8	.0	.0
33.	.0	.0

Note: Time is measured from motor ignition.

TABLE B-11

STAGE FOUR PROPULSION DATA

TIME (sec)	VACUUM THRUST (lbs)	PROPELLANT WEIGHT (lbs)
.0	.0	612.2
.31	4374.91	609.81
.414	4423.52	608.21
.621	4326.3	605.02
3.105	5395.72	562.51
4.14	5784.6	542.14
4.554	5881.82	533.64
5.175	5687.38	521.
9.315	6076.26	435.28
11.902	6222.09	379.27
15.007	6222.09	311.26
17.077	6124.87	266.27
21.735	5784.6	168.64
24.84	5444.33	10[illegible].27
28.98	5347.11	28.64
29.29	5249.89	22.85
29.601	4958.23	17.27
30.105	4131.86	10.64
30.636	1847.18	4.11
31.05	972.2	2.05
31.671	340.27	.62
32.085	145.83	.27
33.12	.0	.0
34.	.0	.0

Note: Time is measured from motor ignition

TABLE B-12

C.G. LOCATION AND MOMENTS OF INERTIA

VERSUS WEIGHT HISTORY

STAGE	WEIGHT (lbs)	C.G. LOCATION (in.)	I_x (slug ft^2)	$I_y = I_z$ (slug ft^2)
1	39700.5	520.77	1684.6	367652.
	34365.3	500.68	1577.33	336176.99
	29030.	473.2	1382.38	296476.97
	23694.7	433.36	1090.	242983.31
	18359.5	370.35	709.92	163772.32
2	14822.	290.14	416.05	43311.08
	12748.5	281.19	396.01	40889.11
	10874.9	268.75	352.19	37343.36
	8601.4	250.32	286.61	32730.58
	6527.8	220.17	197.12	26043.11
3	4165.6	143.5	89.67	2054.3
	3517.	140.33	82.04	1946.63
	2868.4	135.71	69.71	1814.31
	2219.7	128.41	52.72	1635.15
	1571.1	115.07	31.01	1360.04
4	782.8	62.61	8.64	46.91
	629.8	61.87	7.85	42.29
	476.7	60.64	6.44	37.22
	323.7	58.26	4.52	31.19
	170.6	51.61	1.97	22.74

Note: C.G. locations are measured from reference Station 0.

TABLE E-13

PITCH, YAW, AND ROLL PROGRAMS

TIME (sec)	PITCH RATE (deg./sec.)	ROLL RATE (deg./sec.)	YAW RATE (deg./sec.)
0 TO 3.	-.0265	.0256	.0196
3. TO 7.6	2.38047	0	0
7.6 TO 27.	.62124	0	0
27. TO 40.	.45833	0	0
40. TO 97.	.32466	0	0
97. TO 150.	.13147	0	0
150. TO 190.	.09643	0	0
190. TO 243.6	1.	0	0
243.6 TO 255.	0	0	0
255. TO 283.	0	0	1.5
283. TO 7000.	0	0	0

Notes:

1. Time is measured from Stage One ignition.
2. Positive pitch rate moves vehicle nose down (opposite to LTV convention).
3. Positive roll rate rolls vehicle in a counter-clockwise direction when viewed from rear and looking forward (also opposite to LTV convention).
4. Positive yaw rate moves vehicle nose to the right when viewed from the rear (equivalent to LTV convention).

TABLE B-14

STAGE TWO AXIAL AND NORMAL

FORCE COEFFICIENTS VS MACH NUMBER

MACH NUMBER	$C_D = C_{AO}$	$C_{NPI} = C_{NA}$
0	.724	.0705
2.5	.724	
3.	.705	
3.5	.692	
4.	.686	
20.	.686	.0705

TABLE B-15

SEQUENCE OF TRAJECTORY EVENTS

TIME (sec)	EVENT	VEHICLE WEIGHT (lbs)	VEHICLE LENGTH (ft)	CRITERION FOR INITIATION
0	Stage One Ignition Begin Roll Program	39700 39700	71.38	Launch
3.0	End Roll Program Begin Pitch Program	38691 38691		
76.5	Stage Two Ignition Stage One Thrust Ends Stage One Jettisoned	18363 18363 14822	 71.38 40.57	Dynamic pressure less than 40 lbs/sq.ft.
116.9	Stage Two Burnout Begin Coast	6528 6528		Burnout
131.9	End Coast Stage Three Ignition Stage Two Jettisoned	6528 6528 4166	 40.57 19.85	Time Lapse of 15 sec. after Stage Two burnout
164.7	Stage Three Burnout Begin Coast to Apogee	1571 1571		Burnout
753.1	End Coast Stage Three Jettisoned Stage Four Ignition	1571 783 783	19.85 10.7 10.7	Inertial Flight Path Angle γ = 1.2 deg.
786.2	Stage Four Burnout Orbit Injection	171 171	10.7 10.7	Burnout

Notes: 1. Vehicle Length measured from Station zero to stage separation plane location. Data extracted from Reference 2.

2. Vehicle Reference Area for all stages is 5.25 sq. ft.

APPENDIX C

SCOUT AEROELASTIC BENDING

INTRODUCTION

This appendix summarizes an analysis to evaluate the effects of aeroelastic bending of the Scout Missile on the total aerodynamic normal force coefficient and the center of pressure. A comparison of these effects with the results of a similar analysis by LTV is also presented.

STATEMENT OF PROBLEM

A launch vehicle, during its ascent through the atmosphere, is subjected to varying lateral loads. Some of these loads are oscillatory, as those produced by the dynamic response of the flexible vehicle to a gust. Other loads are slowly varying and may continue to act in one direction for some time. These latter loads may be caused by the vehicle flying at an angle of attack (as induced by winds or the trajectory) or by the vehicle being unsymmetrical (i.e., pods on one side or stage misalignments).

Any load imposed on the flexible vehicle will cause deflection or bending of the structure. If these deflections are of sufficient magnitude, they will affect the distribution of aerodynamic force along the vehicle. For instance, large lateral loads may cause the vehicle longitudinal axis to assume a banana shape. This would increase the local angle of attack at the front end of the vehicle and decrease it at the aft end. The local aerodynamic forces, which are a function of local angle of attack, would also increase in the front and decrease in the rear. The change in local aerodynamic forces would induce changes in the loads and cause further bending of the structure until an equilibrium was reached. The total lateral aerodynamic force in this deflected shape may increase or decrease depending on the rigid body (i.e., undeflected) aerodynamic distribution. The center of pressure would generally shift forward. This change to the vehicle stability derivatives (i.e., normal force and center of pressure) could, if sufficiently large, affect the response, and, therefore, the trajectory of the vehicle.

ANALYTICAL PROCEDURE

Two different aeroelastic bending situations were evaluated for the Scout vehicle. The first considered the vehicle longitudinal axis to be perfectly aligned prior to bending under the influence of lateral loads. The second bending situation considered the vehicle axis to be straight over each distinct section of the vehicle (i.e., first stage motor, interstage, second stage motor, etc.) with rotations at the joints representing misalignments during assembly. These misalignments were considered for a "worst case" situation in which all joint rotations were additive.

The technique used for evaluating the aeroelastic bending due to a given lateral loading condition was as follows:

1. Calculate deflections of the missile fixed at the aft end.
2. Release the fixed point using energy considerations (conservation of angular and linear momentum) and determine deflections with respect to the original axis.
3. Determine the new load distribution for the bent vehicle.
4. Iterate the procedure until no additional bending is induced.

It should be noted that additional bending induced by axial loads (i.e., beam column effect) is not included in this analysis. This effect was assumed small in comparison with the lateral load effects and was, therefore, neglected. Rotary inertia effects were considered negligible since the vehicle is in a trimmed condition. However, shear deformation was taken into account.

The effects of the aeroelastic bending on the total aerodynamic normal force coefficient and the center of pressure were found by calculating a new angle of attack at various points (X_i) along the missile due to the aeroelastic bending. The effect of this new angle of attack on the aerodynamic coefficient at each point was taken into account by the following equation:

$$C_{n_i} = C_{n_{\alpha_i}} (\alpha + \theta_i) \qquad (1)$$

where C_{n_i} is the aerodynamic normal force coefficient at the i^{th} point

$C_{n_{\alpha_i}}$ is the slope of the rigid body aerodynamic normal force coefficient at the i^{th} point.

α is the original angle of attack, and

θ_i is the bending angle from the original missile axis at the i^{th} point.

The total normal force coefficient and center of pressure are then determined by the following:

$$C_N' = \sum C_{n_i}' \tag{2}$$

$$C.P.' = \frac{\sum C_{n_i}' X_i}{C_N'} \tag{3}$$

INPUT DATA

The vehicle stiffness distributions, obtained from Reference 13 were available at only three discrete times of flight; 10, 19, and 31 seconds from liftoff. Since no other stiffness data could be obtained, this analysis was limited to these three flight times. The vehicle mass distributions at these times were obtained from Reference 14.

The aerodynamic distributions at Mach numbers corresponding to these flight times were obtained from Reference 13. Since this reference did not contain the aerodynamic distributions on the payload section or the fins, these distributions were generated by TRW aerodynamics personnel. The resulting rigid body total normal aerodynamic coefficients and the rigid body centers of pressure from this mixed data were approximately 10% to 15% higher than those reported in Reference 13.

The joint rotations for the analysis considering misalignment were obtained from Reference 13.

RESULTS

As previously mentioned, this analysis was limited by the available input to flight times of 10, 19, and 31 seconds after liftoff. These flight times corresponded to Mach numbers of 0.31, 0.71, and 1.44 respectively. The bending effects were determined for dynamic pressures of 1500, 2500, and 3500 PSF at each Mach number. Rigid body angles of attack of 0.25, 0.5, 1.0, 1.5, 2.0, 3.0, and 4.0 degrees were investigated.

The results of the analysis are presented in Figures C1 through C22. Figure C1 illustrates a typical aeroelastic bending shape for the Scout missile. Figures C2 through C10 present the total aerodynamic coefficient slopes (C_{N_α}) versus α for the rigid body, aeroelastic bending only, and aeroelastic bending including misalignment. These data were presented as slopes of a total C_N versus α curve (i.e., C_{N_α}) to facilitate later comparisons with the data presently used for Scout error analysis trajectory simulations.

The flexible body C_{N_α} determined for the pure bending situation is constant with angle of attack. This is illustrated by the local aeroelastic normal force equation.

$$C_{n_i} = C_{n_{\alpha_i}} (\alpha + \theta_i) \tag{4}$$

Since θ_i, the bending angle, is proportional to α, each local normal force, and, therefore, the total normal force is proportional to α.

The bending situation considering initial joint rotations represents the effects of an unsymmetrical vehicle. That is, the front of the vehicle is at a positive α while the rear is at a negative α; thus, a finite normal force exists for a zero rigid body α. The bending angle (θ_i) is then made up of (1) a component induced by and proportional to α and (2) a component due to the original misalignment. The total coefficient is then determined by the following expression:

$$C_N' = C_{N_\alpha}' \alpha + C_{N_o}$$

This is illustrated in the following sketch:

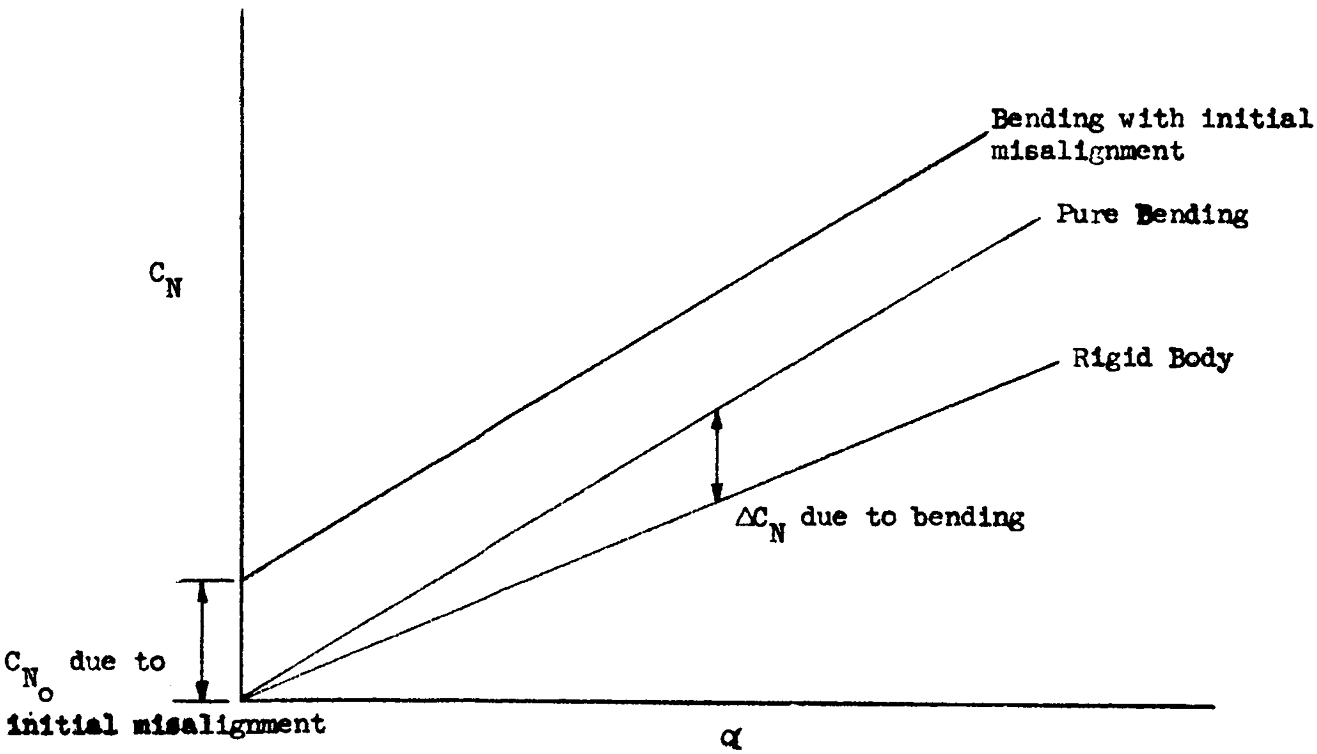

It should be noted in Figures C2 through C10 that, defining C_{N_α} as the total normal force coefficient divided by α results in very large values for small α's (i.e., less than one degree). However, defining C_{N_α} as the total coefficient minus the portion due to initial misalignments (C_{N_o}) divided by α gives the same constant C_{N_α} as the pure bending situation. The values of C_{N_o} for the conditions investigated in this study are shown in Table C1.

The actual change in normal force coefficient due to bending, even with misalignments included, is so small that it could be neglected. Figure C11 shows a typical plot of total C_N (rather than C_{N_α}) versus angle of attack which shows that the change cannot be detected when plotted on a reasonable scale. This is due to the increase in aerodynamic force over the front of the vehicle being approximately offset by the decrease over the aft portion.

This re-distribution of the airload, however, has a very significant effect on the center of pressure (C.P.). Figures C12 through C20 present the C.P. versus angle of attack for the rigid body, aeroelastic bending only, and aeroelastic bending including misalignment. As with the C_N data, the C.P. for the pure bending situation is constant with α while the misalignments induce large changes especially for α less than one degree. The C.P. for the portion of the normal force due to misalignment (i.e., $C.P._o$) lies off the vehicle since the distribution of this force applies a couple to the vehicle.

Pitching moment coefficients about station 478 of the vehicle were also computed for later comparisons. The portion of this coefficient due to misalignments (C_{M_o}) and the portion which is linear with α (C_{M_α}) are presented in Table C2 The total pitching moment about station 428 is then:

$$C_M = C_{M_\alpha} + C_{M_o} \tag{5}$$

COMPARISON OF RESULTS

Appendix B presents flexible body C_{N_α} and C.P. values which were used in the Scout error analysis trajectory simulations. These data were taken from an LTV trajectory printout (LTV Dir No. 23-DIR-56). Nothing is known of the analysis procedure or input data used to derive these values; however, an attempt was made to compare them with the results of this analysis. The C_{N_α} and C.P. data from Appendix are shown in Figures C21 and C22. It may be seen that the effects of bending are very small on the slope of the normal force coefficient (C_{N_α}). The maximum change is less than 5% at the Mach numbers investigated in this study (.31,.71,1.44). The change of the aerodynamic moment coefficient about station 428 is much more significant. The maximum change in this parameter is in excess of 45%. A better evaluation of this change may be made by examining the shift in aerodynamic center of pressure (C.P.).

Table C2 presents the incremental effects of aeroelastic bending on C_{N_α} and C.P. for both Reference 6 data and the effects as determined by this analysis. As indicated, both sets have extremely small incremental values that result from the differences between the increase in aerodynamic force at the front end of the vehicle and the decrease at the aft end. Thus, the correlation between the two sets of data is reasonable considering the inconsistencies and the unknowns involved. It can, therefore, be concluded that the aeroelastic bending has negligible effects on the aerodynamic normal force.

The incremental effect on C.P. location shows fair correlation between the two sets of data. The Appendix data gives much larger C.P. shifts than this analysis when only pure bending was considered. If the effects of misalignment are considered, the correlation improves for α equal to one degree. This could infer that the analysis for the Appendix B data considered misalignments for a unit α and neglected the non-linear effects. As was pointed out, this could lead to larger errors. However, it is also quite possible that differences in the analysis data and procedures could have caused variations of this magnitude for the pure bending situation.

The primary result of the comparison of these data is that both sets show negligible aeroelastic bending effects on total aerodynamic normal force and significant effect on center of pressure.

CONCLUSIONS

The following conclusions can be made as a result of this study:

- The changes in the total aerodynamic normal force coefficient (C_N) for the Scout vehicle are insignificant for the range of dynamic pressures and Mach numbers considered in this study.
- There is a significant change in C.P. location due to the aeroelastic bending effects.
- This effect on C.P. location is more pronounced and becomes nonlinear with α if vehicle misalignments are considered.
- It appears that the non-linearities of C.P. with α are neglected in the Reference 6 data presently being used in the Scout error analysis trajectory simulation.

If the change in C.P. locations reported here are determined to be significant, a thorough examination should be made of the LTV analysis used to derive the Appendix B′ data. In addition, an independent study with more complete and accurate data would be in order.

TABLE C-1

SCOUT VEHICLE STABILITY DERIVATIVES

$$\text{Pitching Moment} = (C_{M_\alpha}\,\alpha + C_{M_o})\; q\; A_R\; L_{REF}$$

$$\text{Normal Force} = (C_{N_\alpha}\,\alpha + C_{N_o})\; q\; A_R$$

$$\text{where } A_R = 5.25\ FT^2$$

$$L_{REF} = 2.58\ FT$$

Dynamic Pressure (lb/ft^2)	RIGID BODY DATA C_{N_α}	C_{M_α}	FLEXIBLE BODY DATA C_{N_o} *	C_{N_α}	C_{M_o} *	C_{M_α}
			Time of Flight = 10 secs Mach Number = 0.31			
1500	.286556	.313812	0.00131	.286477	-0.04111	.30139
2500	↓	↓	0.00130	.286422	-0.04115	.29252
3500	↓	↓	0.00129	.286302	-0.04473	.28365
			Time of Flight = 19 secs Mach Number = 0.71			
1500	.309244	.302509	0.00377	.310119	-0.05062	.28429
2500	↓	↓	0.00391	.310771	-0.05276	.26959
3500	↓	↓	0.00367	.311503	-0.05711	.25489
			Time of Flight = 31 secs Mach Number = 1.44			
1500	.358356	.315276	0.00367	.360151	-0.05969	.292481
2500	↓	↓	0.00389	.361510	-0.06227	.271344
3500	↓	↓	0.00415	.363031	-0.06719	.247917

* Applicable for bending with misalignments considered only

TABLE C-2

COMPARISON OF STATIC AEROELASTIC BENDING EFFECTS

Dynamic Pressure (lb/Ft^2)	Present Scout Data		Results of this analysis: Aeroelastic Bending Only		Results of this analysis: Aeroelastic Bending Including Misalignment at $\alpha = 1.0^{\circ}$	
	ΔC_{N_α}	ΔC.P. (in.)	ΔC_{N_α}	ΔC.P.	ΔC_{N_α}	ΔC.P. (in.)
	Time of Flight = 10 secs, Mach Number = 0.31					
1500	-.0033	-24.	-.0001	-7.	+.0012	-31.
2500	-.0054	-44.	-.0001	-12.	+.0012	-36.
3500	-.0088	-65.	-.0002	-27.	+.0011	-43.
	Time of Flight = 19 secs, Mach Number = 0.71					
1500	-.0045	-21.	+.0008	-10.	+.0046	-38.
2500	-.0076	-43.	+.0015	-18.	+.0054	-47.
3500	-.0111	-64	+.023	-26.	+.0059	-57.
	Time of Flight = 31 secs, Mach Number = 1.44					
1500	+.0032	-33.	+.0018	-11.	+.0055	-39.
2500	+.0060	-61.	+.0032	-21.	+.0071	-50.
3500	+.0109	-93.	+.0047	-42	+.0088	-63.

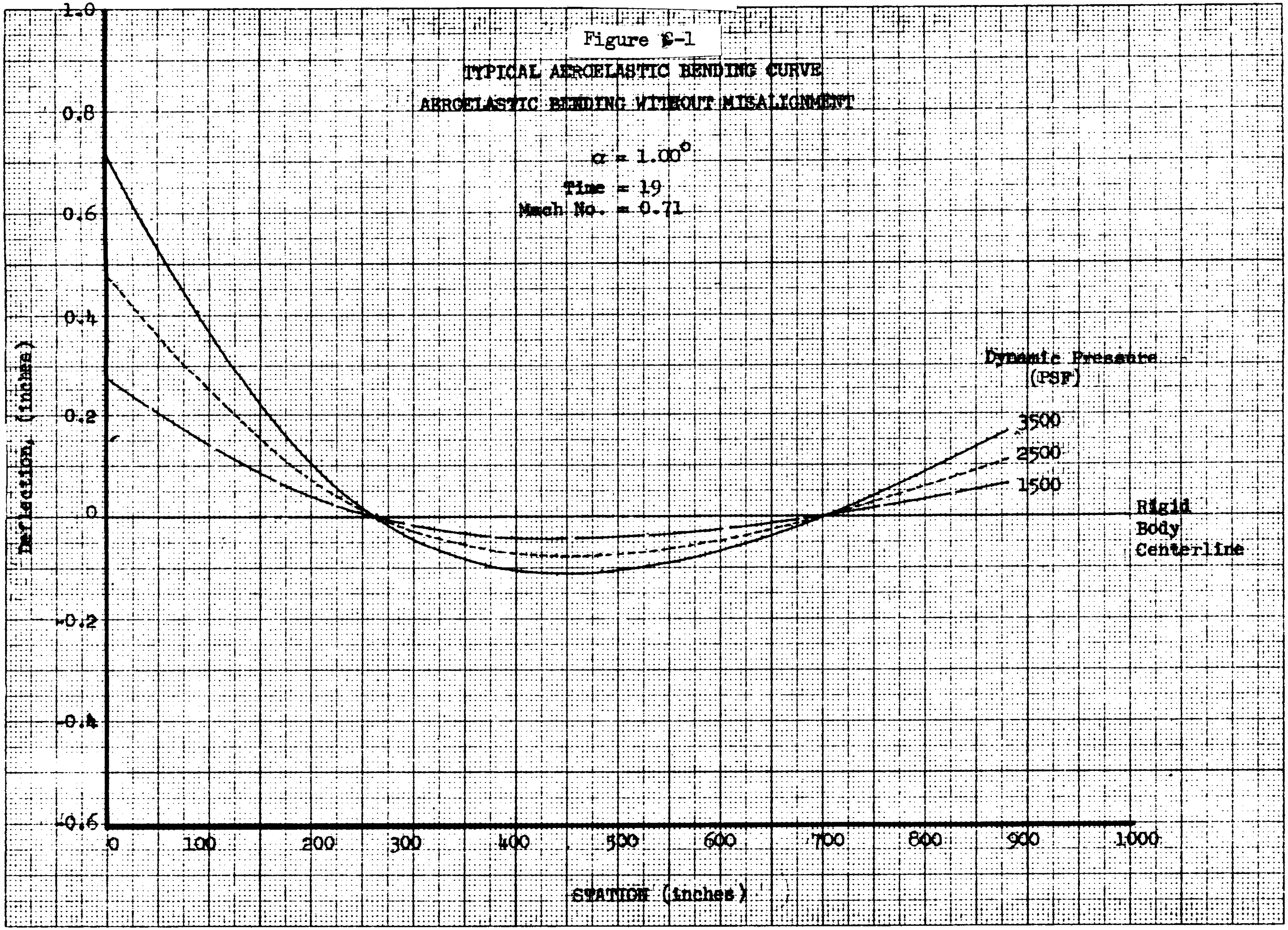

Figure C-1

TYPICAL AEROELASTIC BENDING CURVE

AEROELASTIC BENDING WITHOUT MISALIGNMENT

$\alpha = 1.00^{\circ}$

Time = 19
Mach No. = 0.71

Figure C-2

AEROELASTIC BENDING EFFECT ON NORMAL FORCE

Mach Number = 0.31
Dynamic Pressure = 1500 PSF

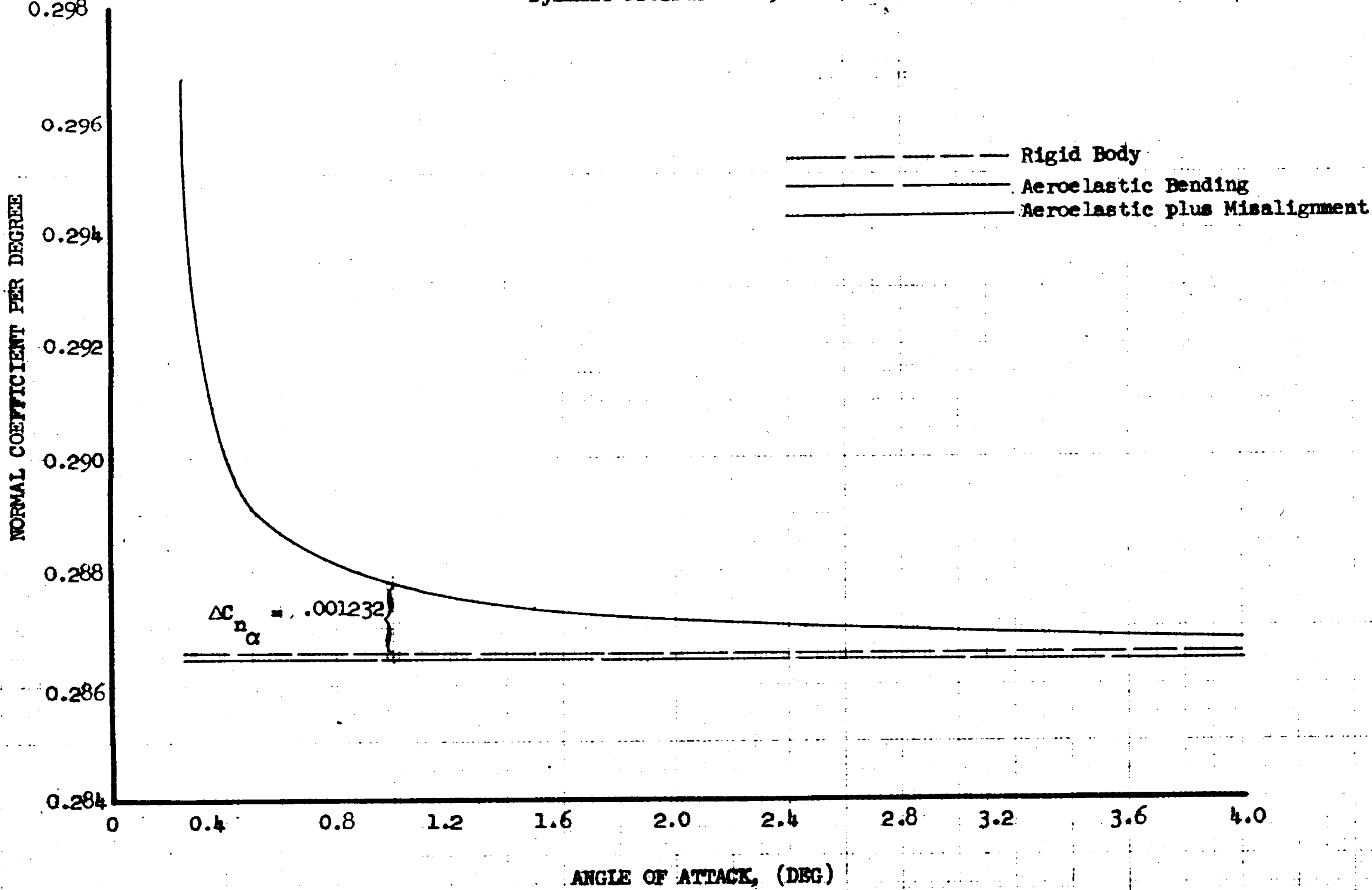

Figure C-3
AEROELASTIC BENDING EFFECT ON NORMAL FORCE
Mach Number = 0.31
Dynamic Pressure = 2500 PSF

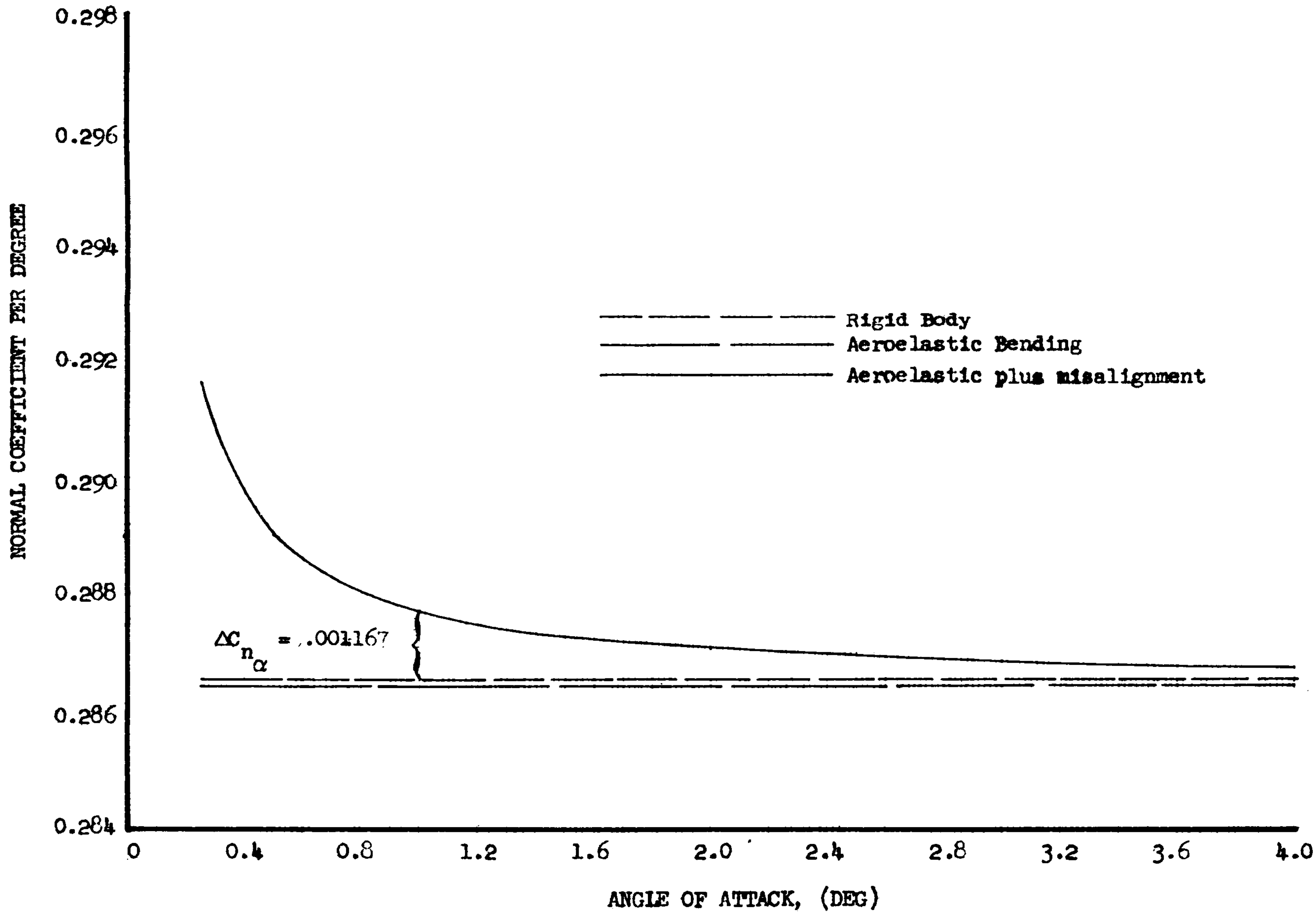

Figure 8-4

AEROELASTIC BENDING EFFECT ON NORMAL FORCE

Mach Number = 0.31
Dynamic Pressure = 3500 PSF

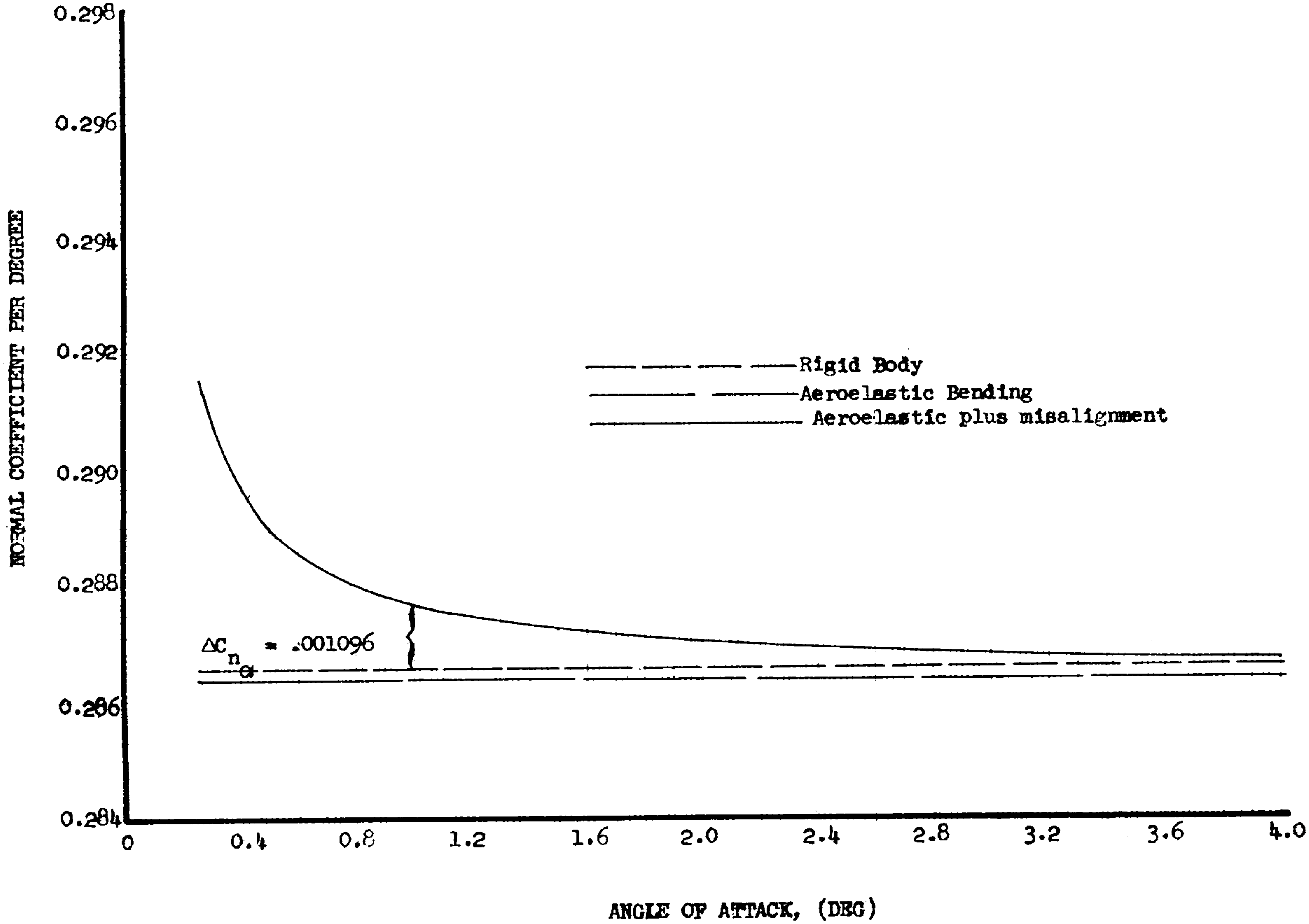

Figure C-5

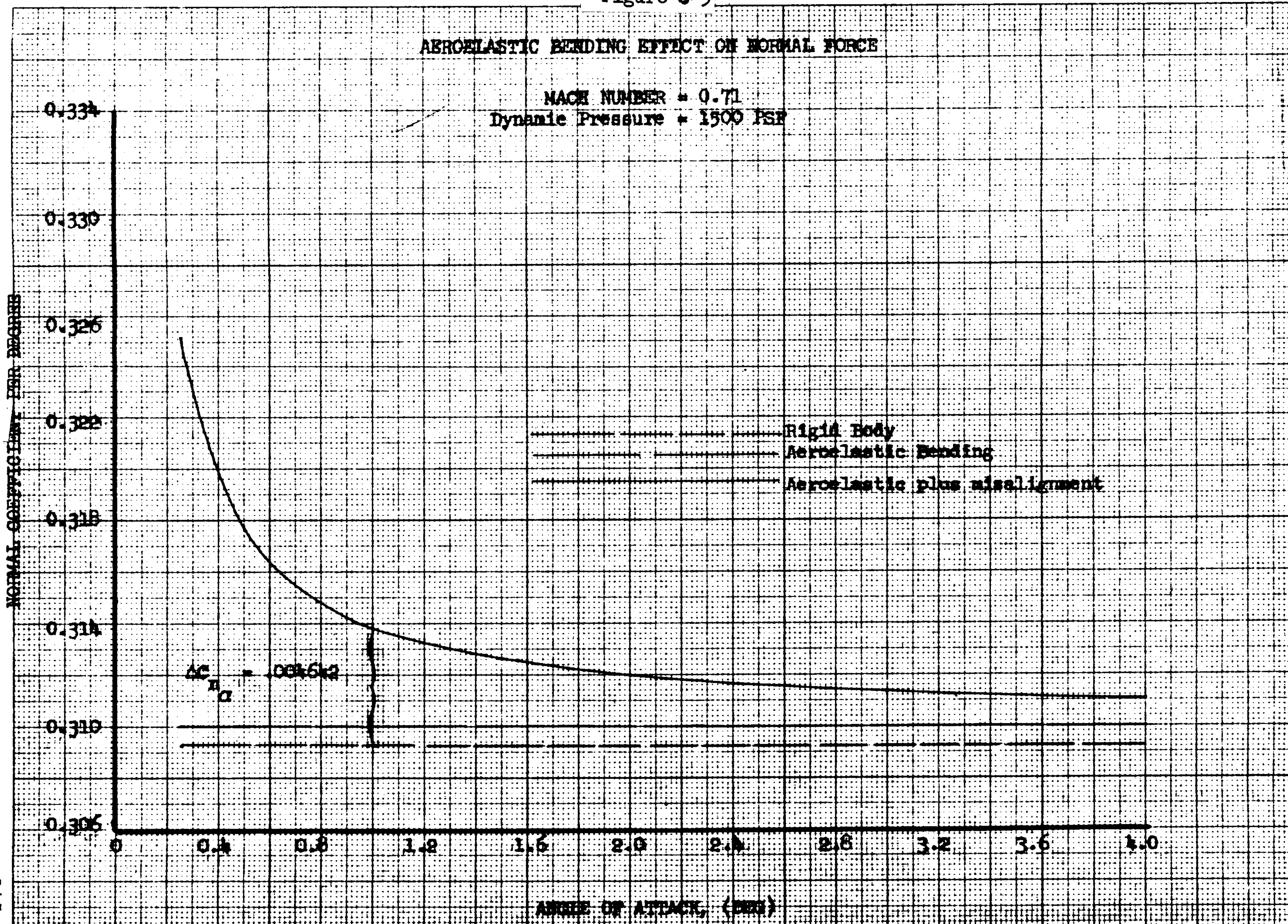
AEROELASTIC BENDING EFFECT ON NORMAL FORCE
MACH NUMBER = 0.71
Dynamic Pressure = 1500 PSF
Rigid Body
Aeroelastic Bending
Aeroelastic plus misalignment
ΔC_{n_α} = .004642
0.334
0.330
0.326
0.322
0.318
0.314
0.310
0.306
NORMAL COEFFICIENT PER DEGREE
0
0.4
0.8
1.2
1.6
2.0
2.4
2.8
3.2
3.6
4.0
ANGLE OF ATTACK, (DEG)

Figure C-6

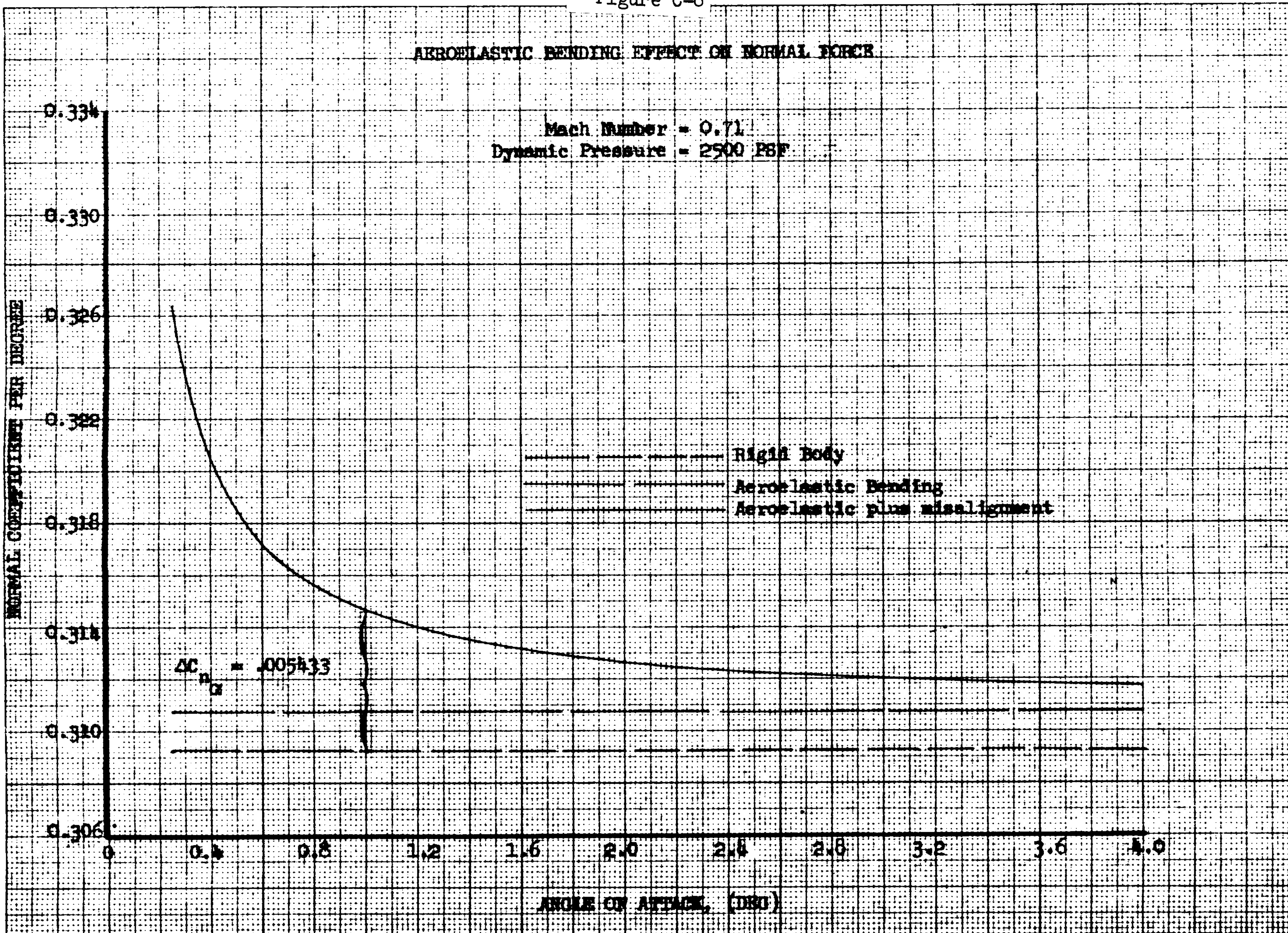

AEROELASTIC BENDING EFFECT ON NORMAL FORCE
Mach Number = 0.71
Dynamic Pressure = 2900 PSF
Rigid Body
Aeroelastic Bending
Aeroelastic plus misaligment
ΔC_{n_α} = .005433
NORMAL COEFFICIENT PER DEGREE
0.334
0.330
0.326
0.322
0.318
0.314
0.310
0.306
0
0.4
0.8
1.2
1.6
2.0
2.4
2.8
3.2
3.6
4.0
ANGLE OF ATTACK, (DEG)

Figure C-7

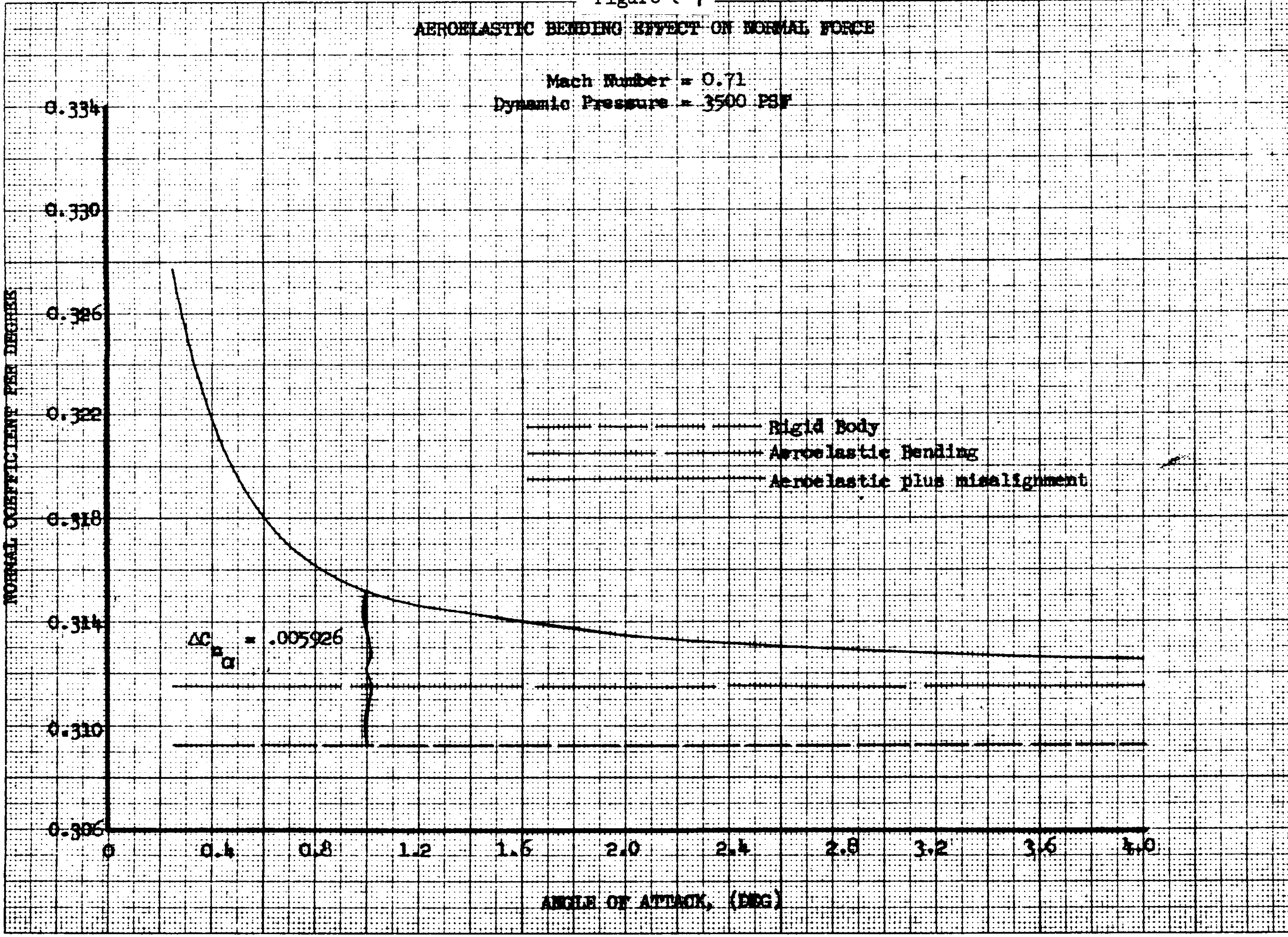

AEROELASTIC BENDING EFFECT ON NORMAL FORCE
Mach Number = 0.71
Dynamic Pressure = 3500 PSF
Rigid Body
Aeroelastic Bending
Aeroelastic plus misalignment
ΔC_{n_α} = .005926
0.334
0.330
0.326
0.322
0.318
0.314
0.310
0.306
0
0.4
0.8
1.2
1.6
2.0
2.4
2.8
3.2
3.6
4.0
NORMAL COEFFICIENT PER DEGREE
ANGLE OF ATTACK, (DEG)

Figure C-8

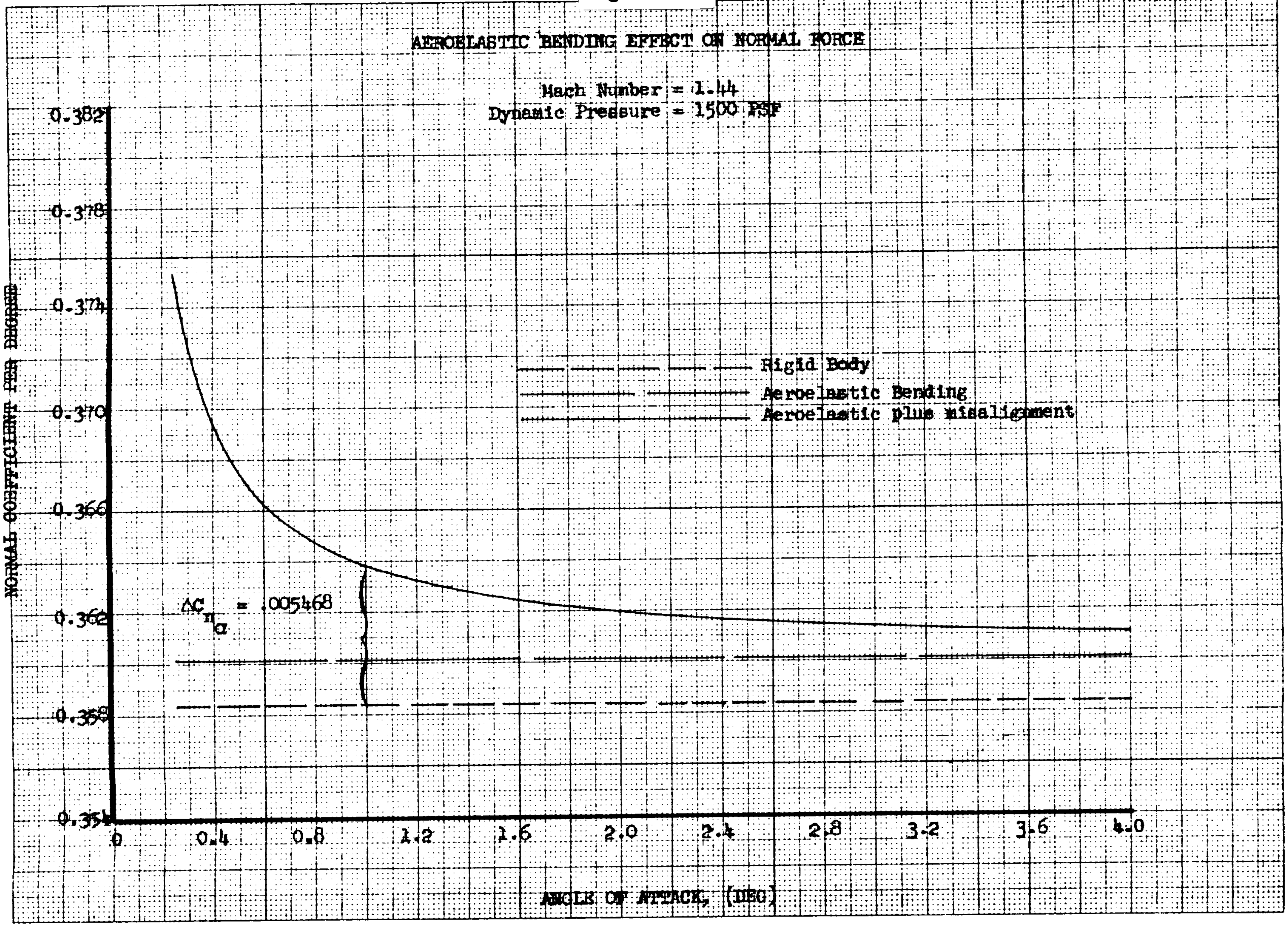
AEROELASTIC BENDING EFFECT ON NORMAL FORCE
Mach Number = 1.44
Dynamic Pressure = 1500 PSF
Rigid Body
Aeroelastic Bending
Aeroelastic plus misalignment
ΔC_{n_α} = .005468
0.382
0.378
0.374
0.370
0.366
0.362
0.358
0.354
0
0.4
0.8
1.2
1.6
2.0
2.4
2.8
3.2
3.6
4.0
NORMAL COEFFICIENT PER DEGREE
ANGLE OF ATTACK, (DEG)

Figure C-9

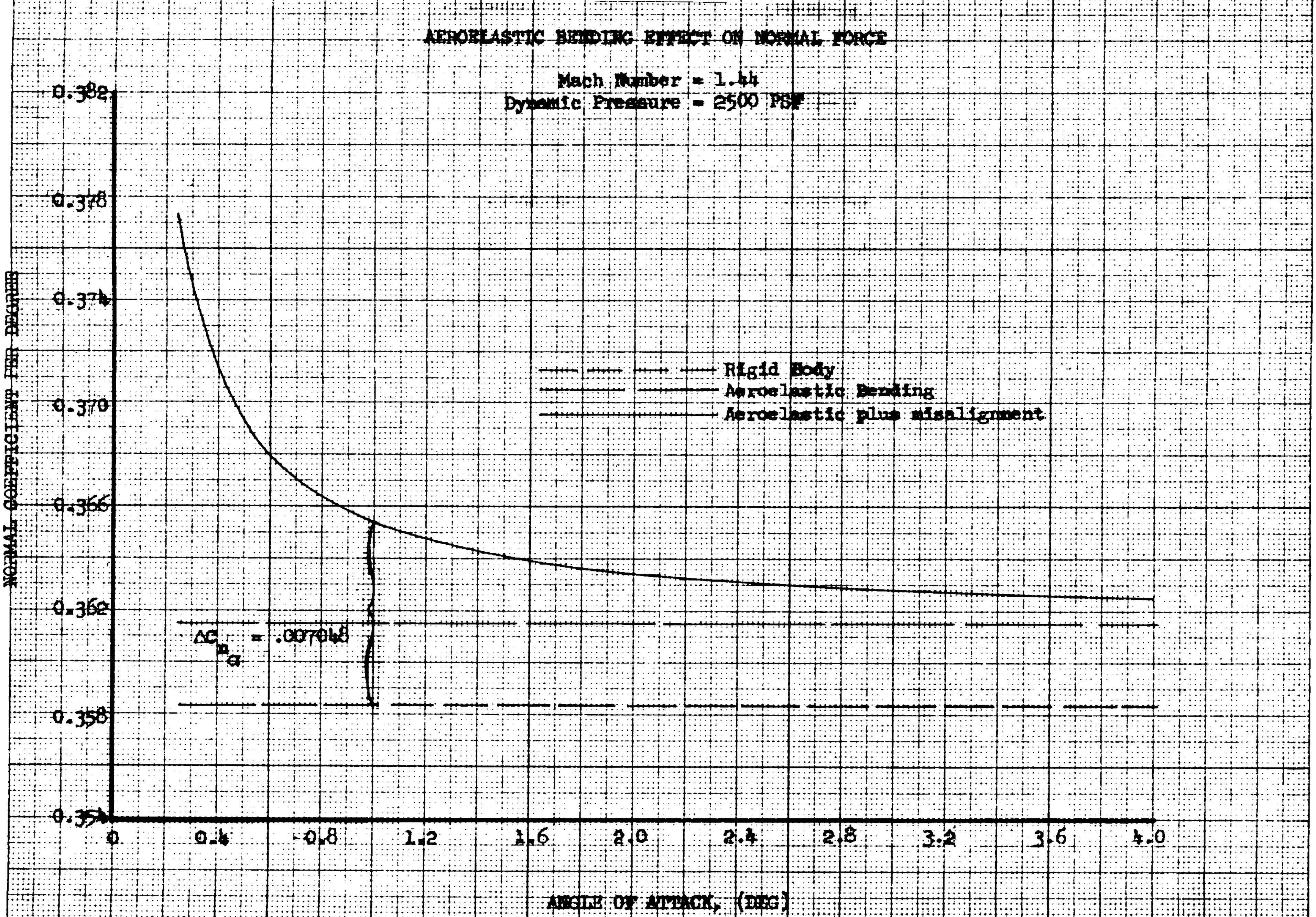

AEROELASTIC BENDING EFFECT ON NORMAL FORCE
Mach Number = 1.44
Dynamic Pressure = 2500 PSF
Rigid Body
Aeroelastic Bending
Aeroelastic plus misalignment
ΔC_{n_α} = .007048
NORMAL COEFFICIENT PER DEGREE
0.382
0.378
0.374
0.370
0.366
0.362
0.358
0.354
0
0.4
0.8
1.2
1.6
2.0
2.4
2.8
3.2
3.6
4.0
ANGLE OF ATTACK, (DEG)

Figure C-10

AEROELASTIC BENDING EFFECT ON NORMAL FORCE

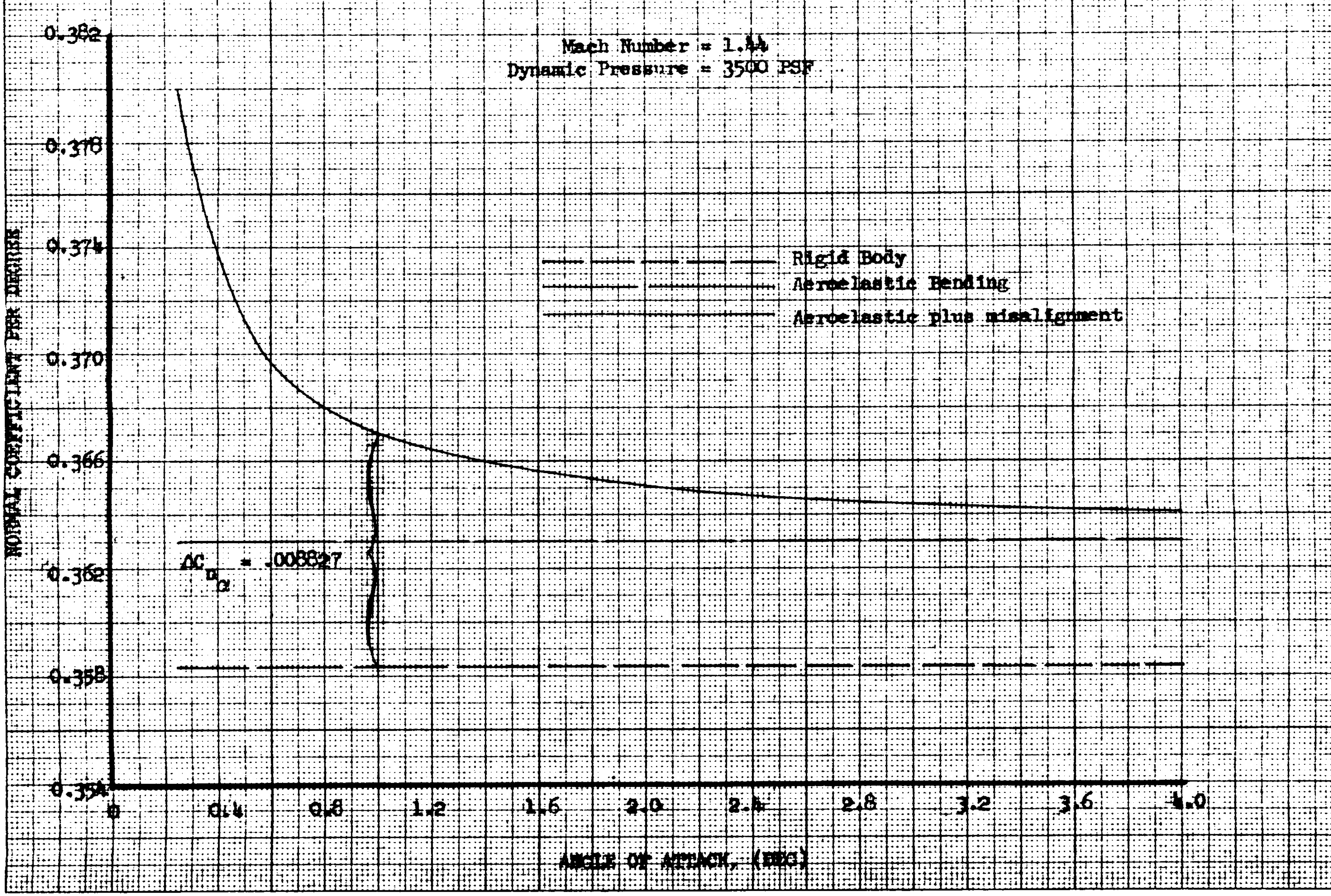

Figure C-11

TOTAL C_N VS. ANGLE OF ATTACK

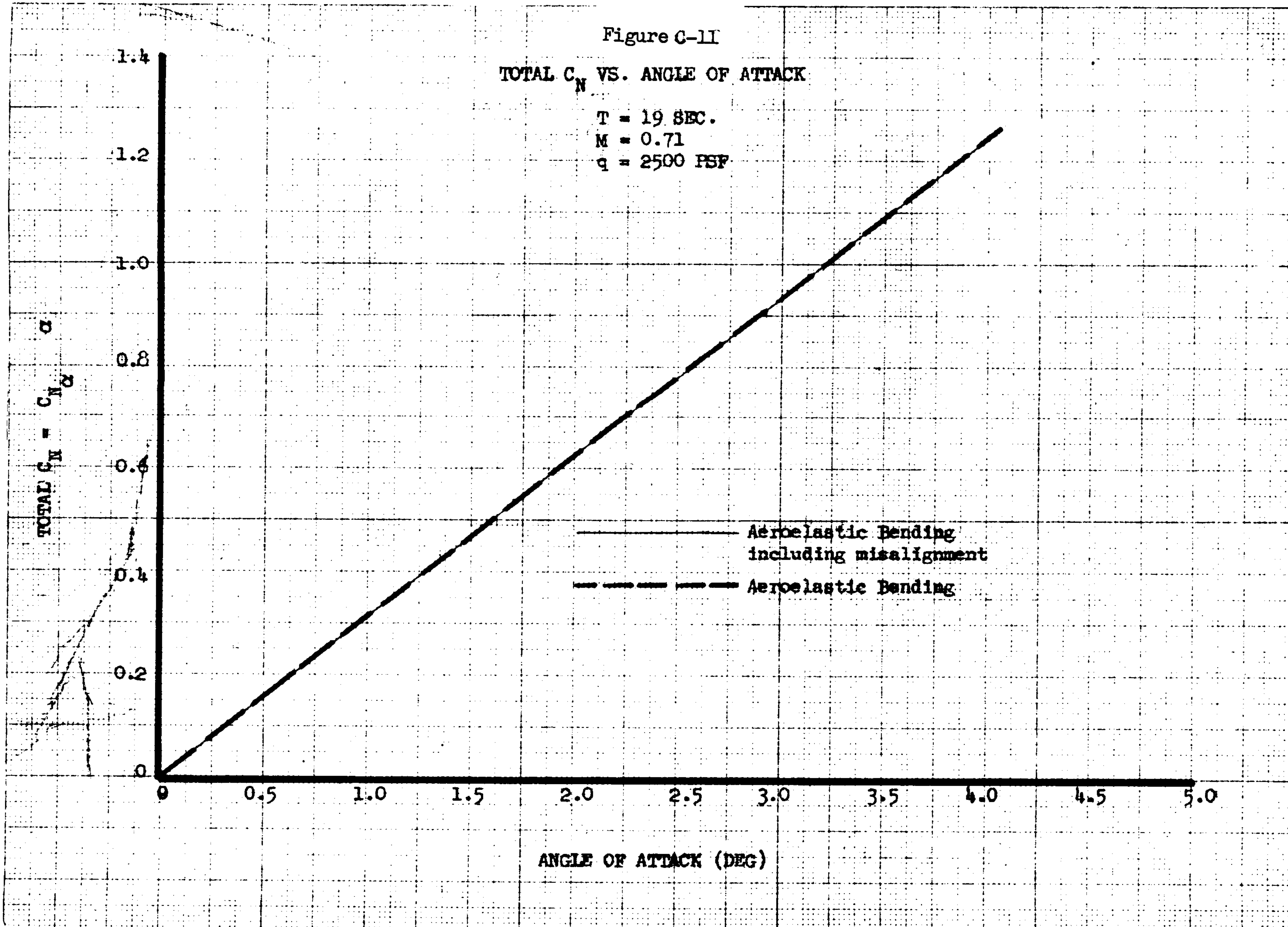

Figure C-12

AEROELASTIC BENDING EFFECT ON CENTER OF PRESSURE

Mach Number = 0.31
Dynamic Pressure = 1500 PSF

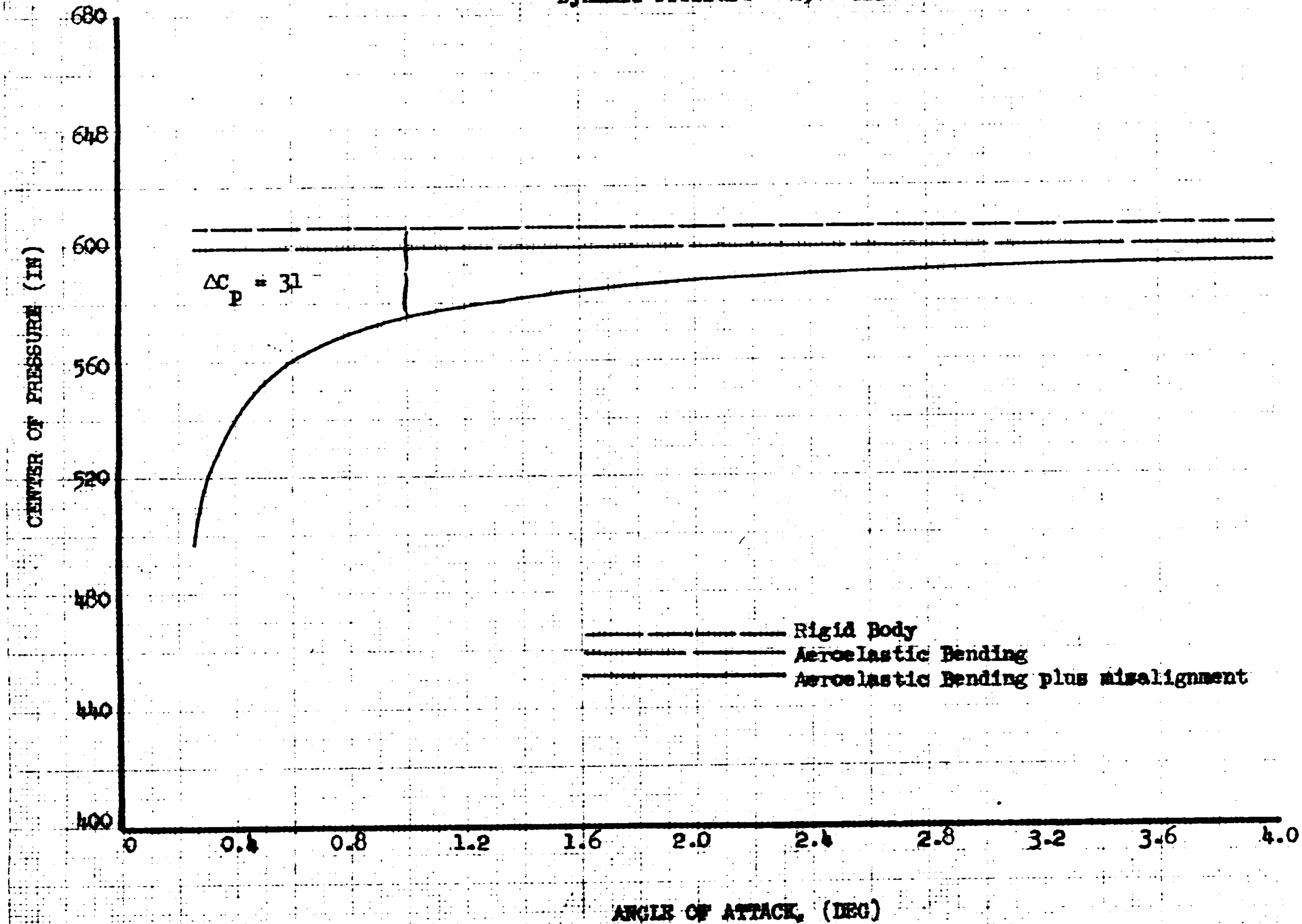

Figure C-13

AEROELASTIC BENDING EFFECT ON CENTER OF PRESSURE

Mach Number = 0.31

Dynamic Pressure = 2500 PSF

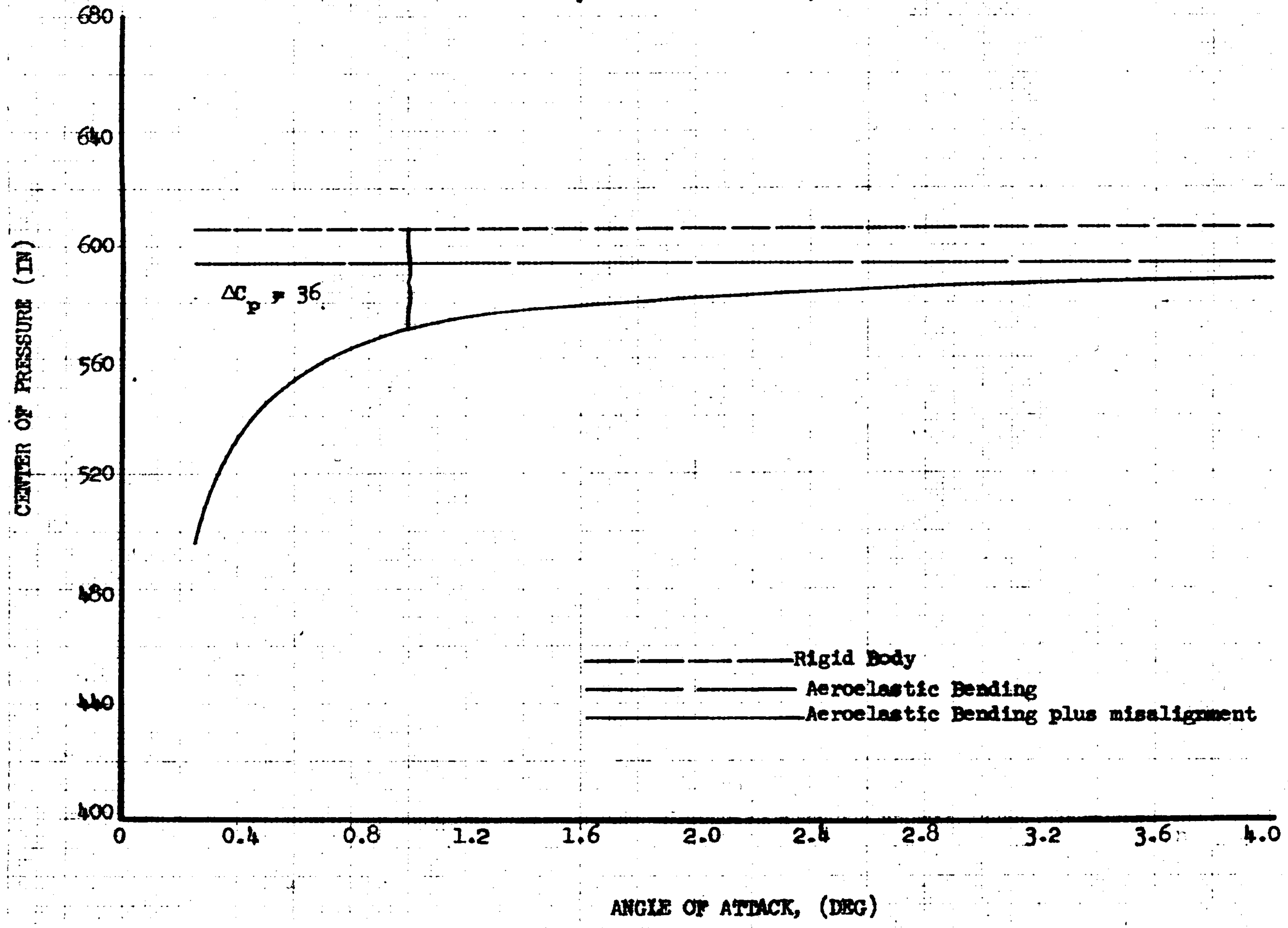

Figure C-14

AEROELASTIC BENDING EFFECT ON CENTER OF PRESSURE

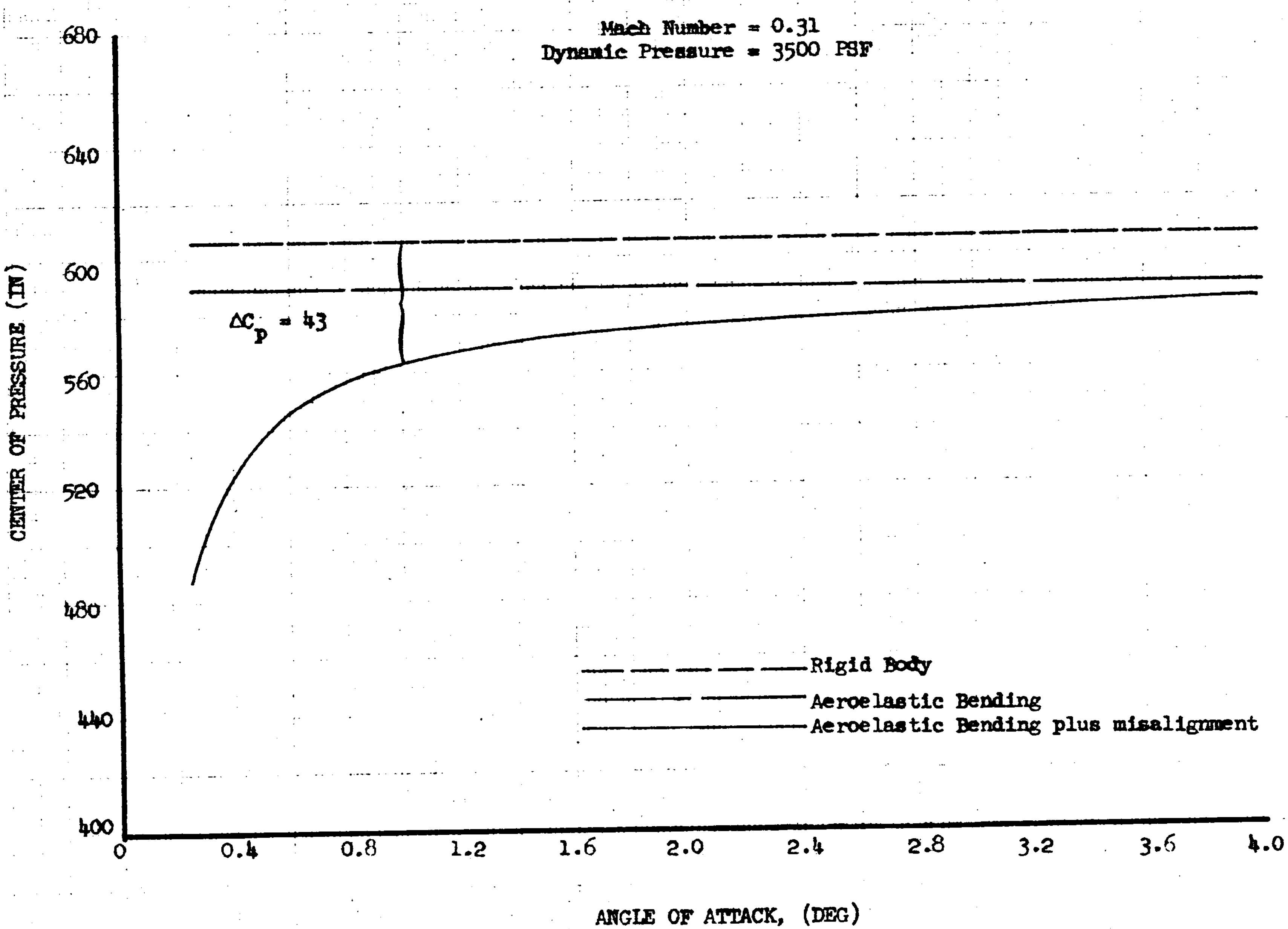

Figure C-15

AEROELASTIC BENDING EFFECT ON CENTER OF PRESSURE

Mach Number = 0.71
Dynamic Pressure = 1500 PSF

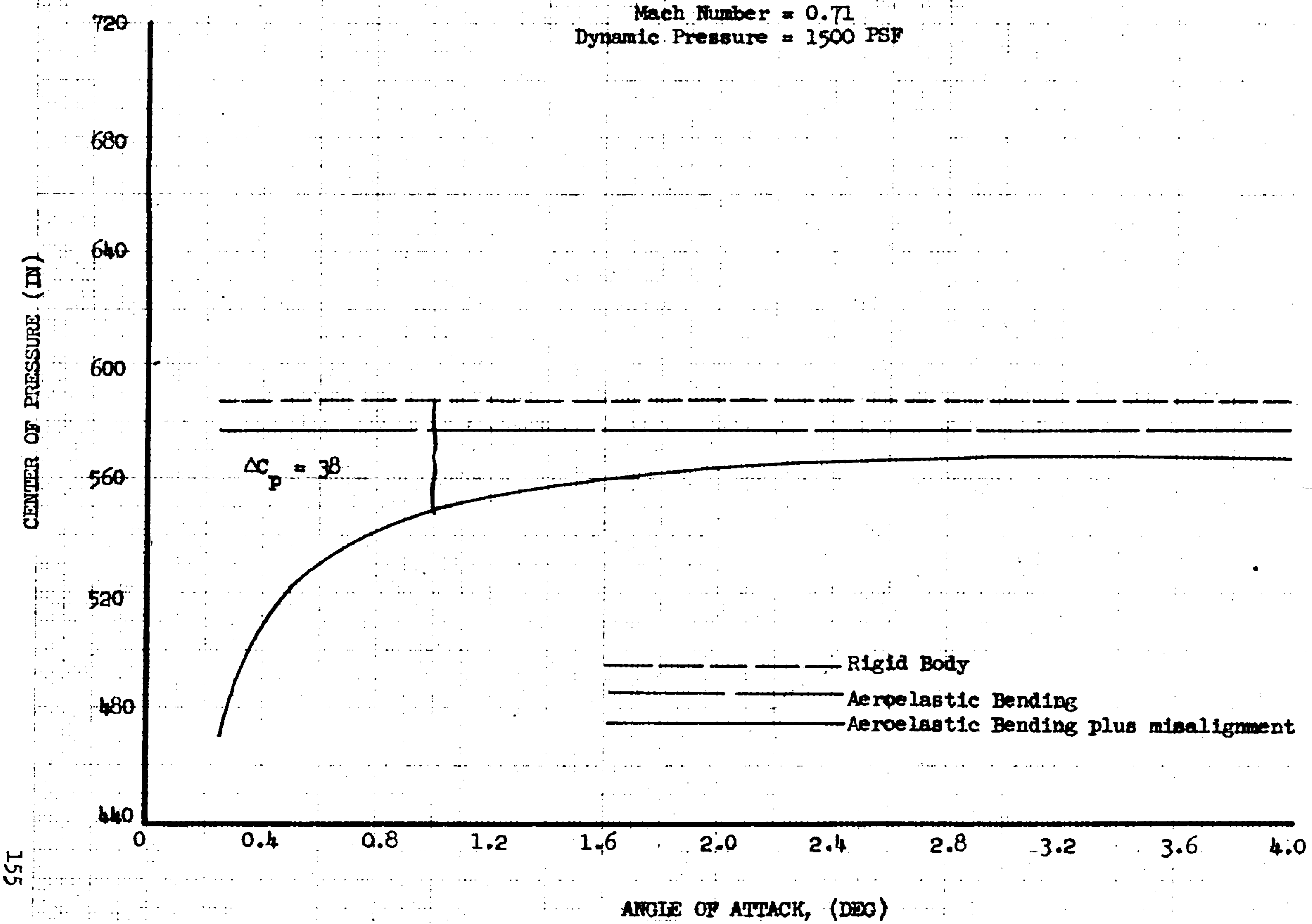

Figure C-16

AEROELASTIC BENDING EFFECT ON CENTER OF PRESSURE

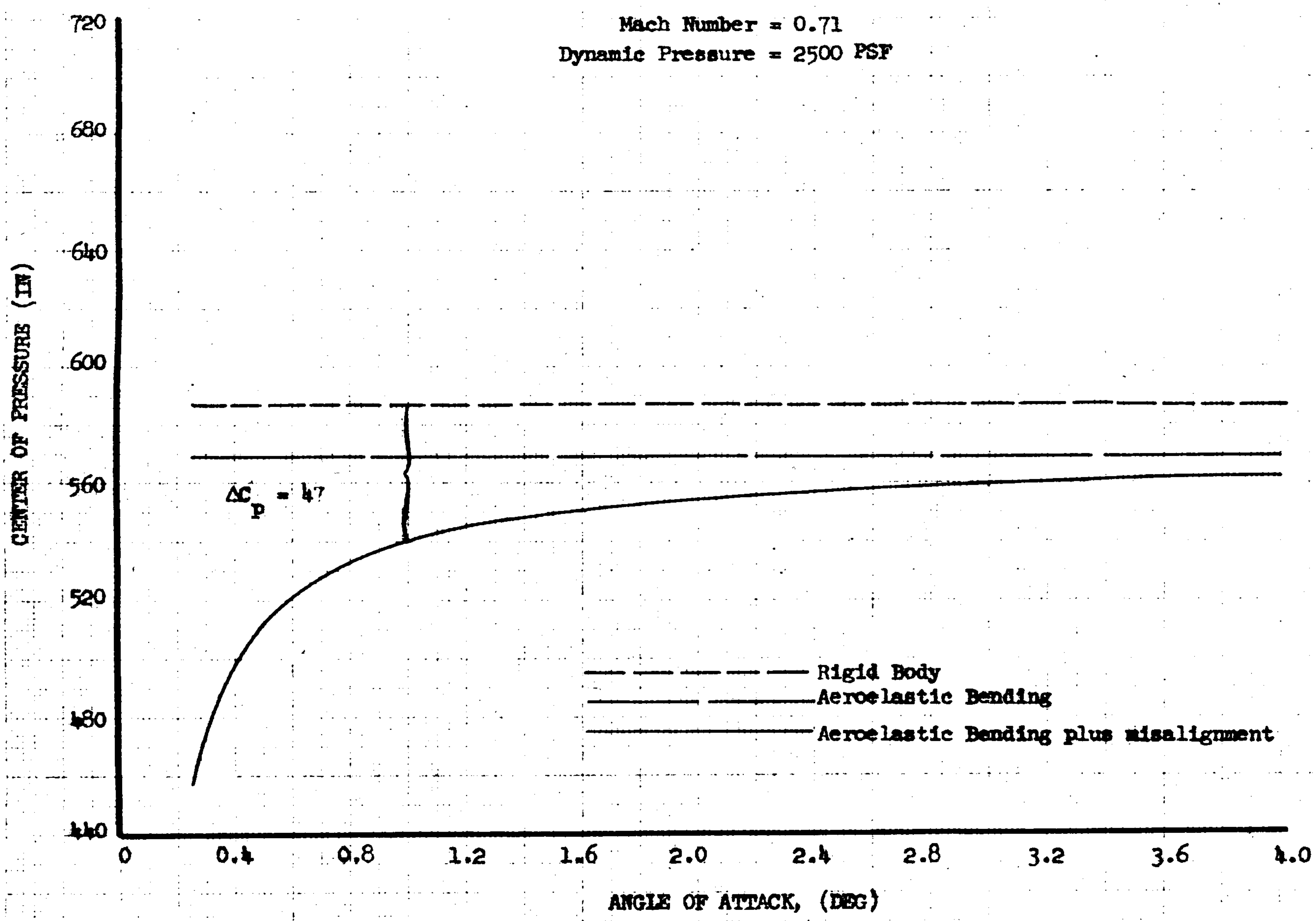

Figure C-17

AEROELASTIC BENDING EFFECT ON CENTER OF PRESSURE

Mach Number = 0.71
Dynamic Pressure = 3500 PSF

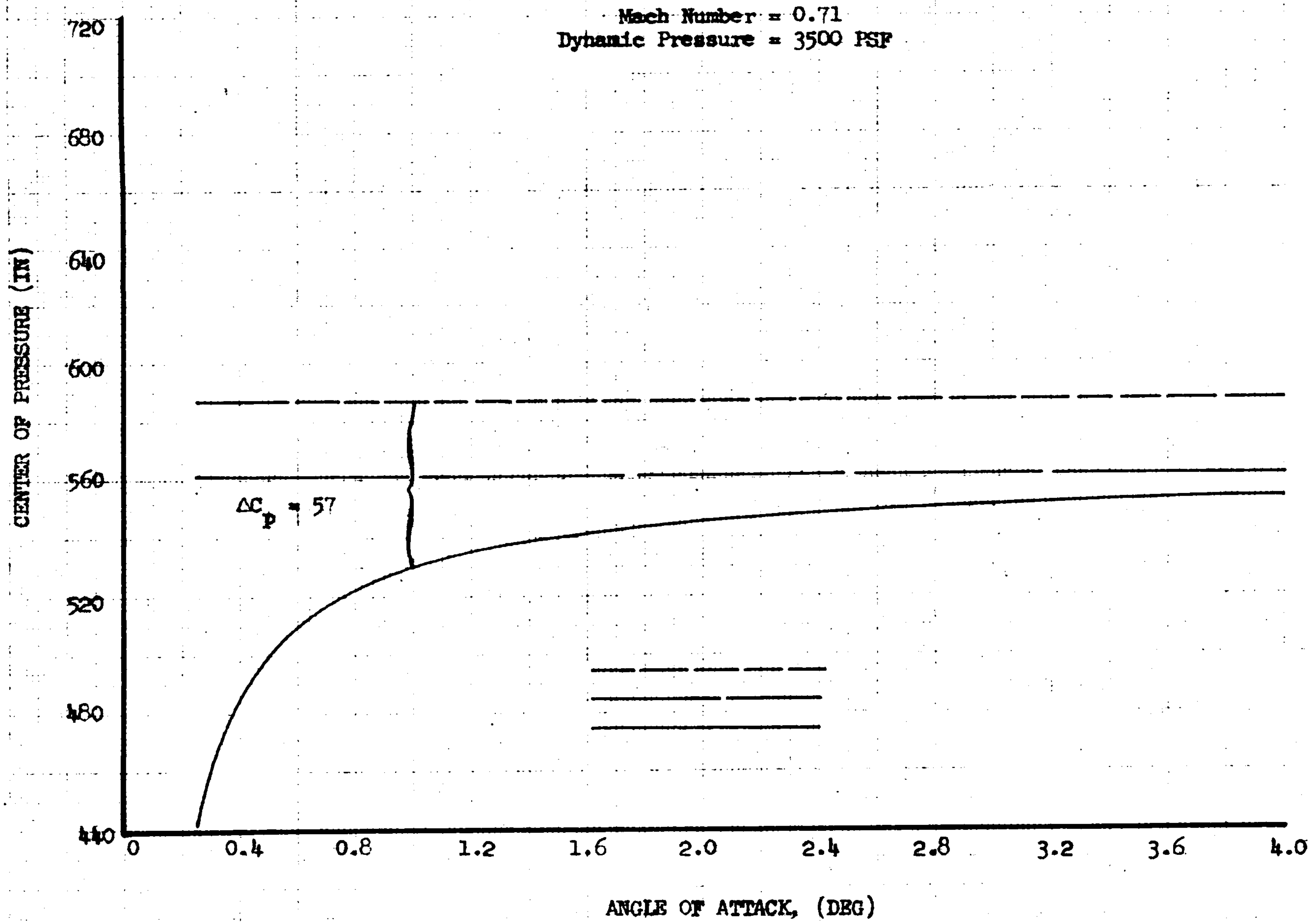

Figure C-18

AEROELASTIC BENDING EFFECT ON CENTER OF PRESSURE

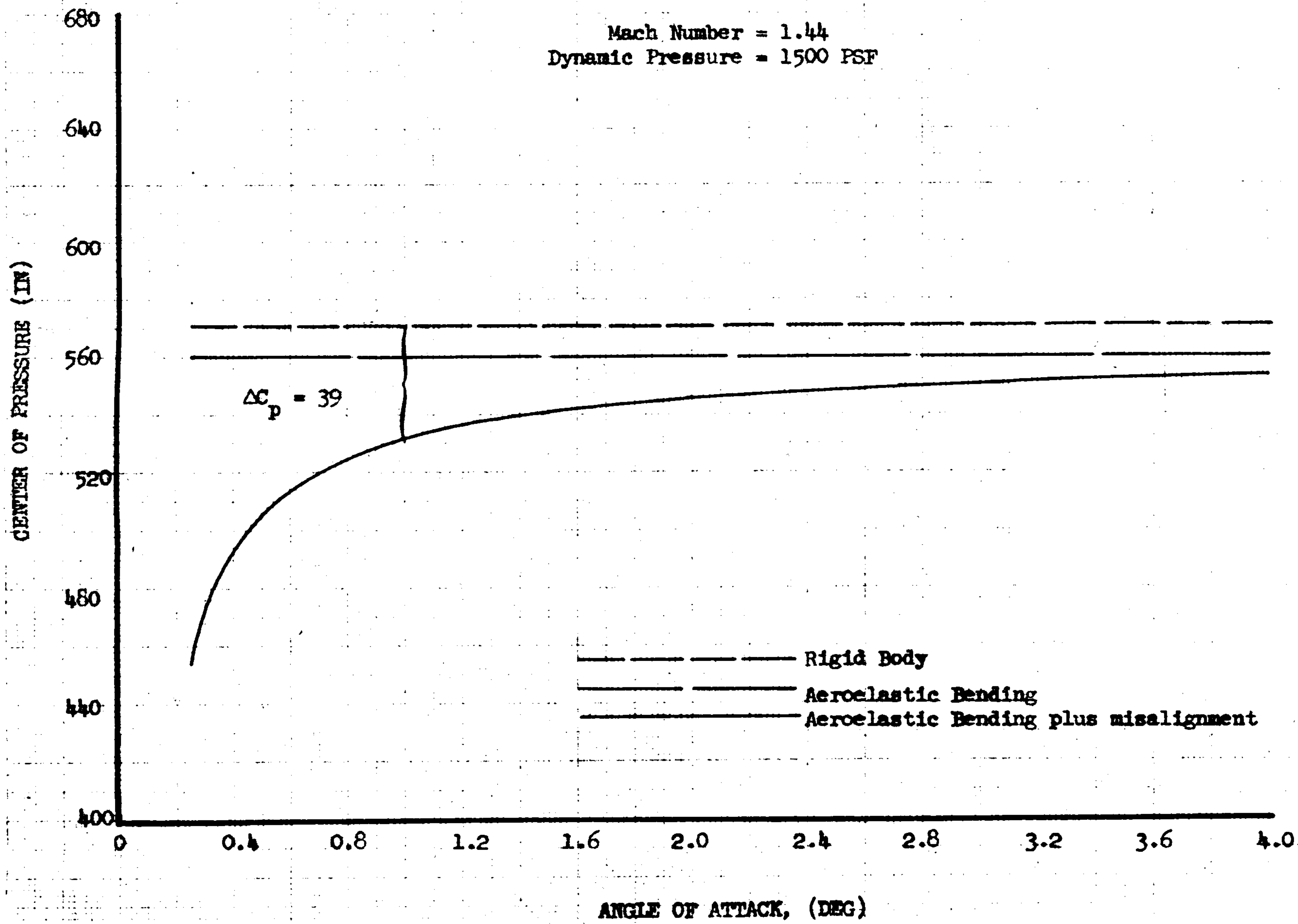

Figure C-19

AEROELASTIC BENDING EFFECT ON CENTER OF PRESSURE

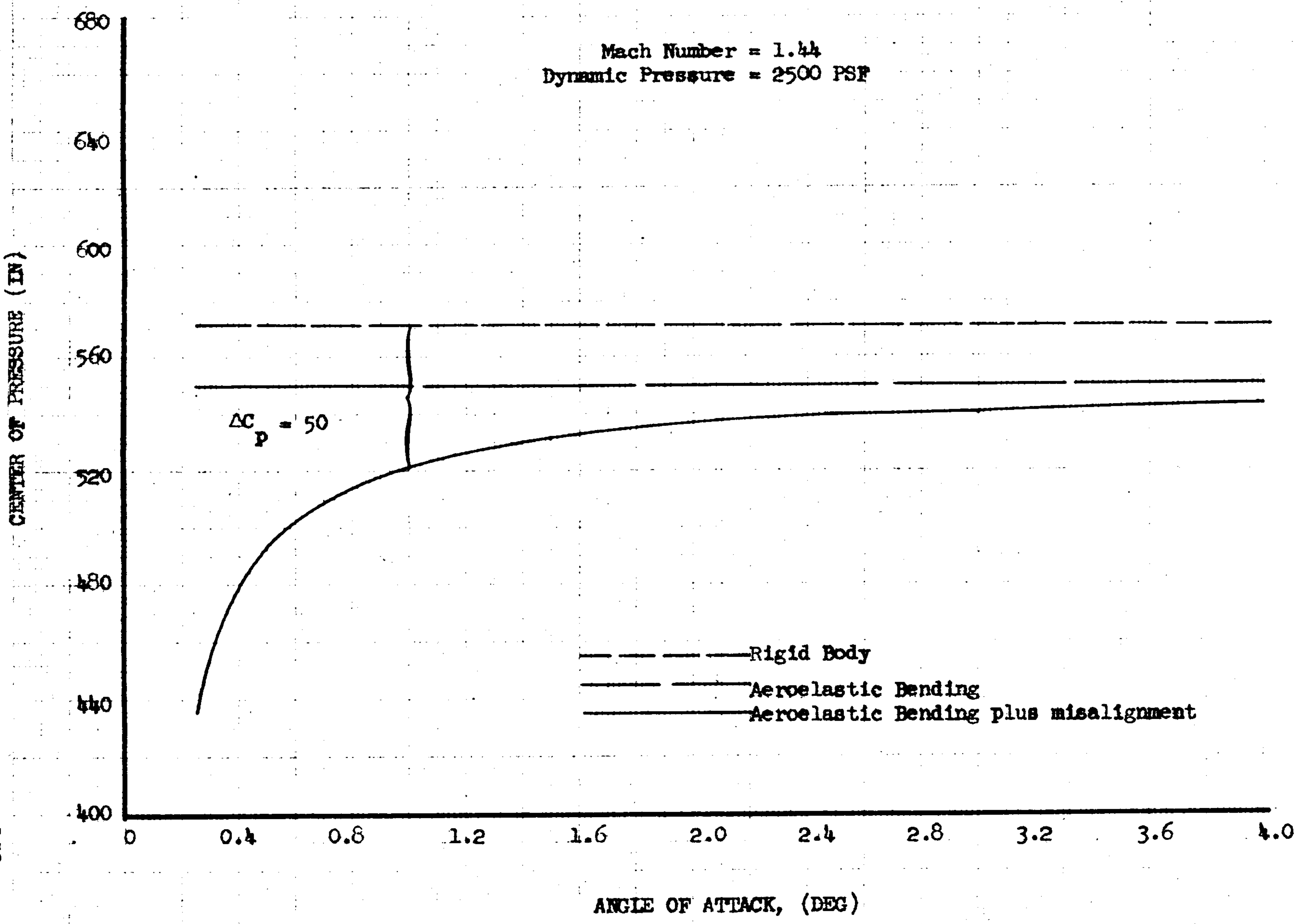

Figure C-20

AEROELASTIC BENDING EFFECT ON CENTER OF PRESSURE

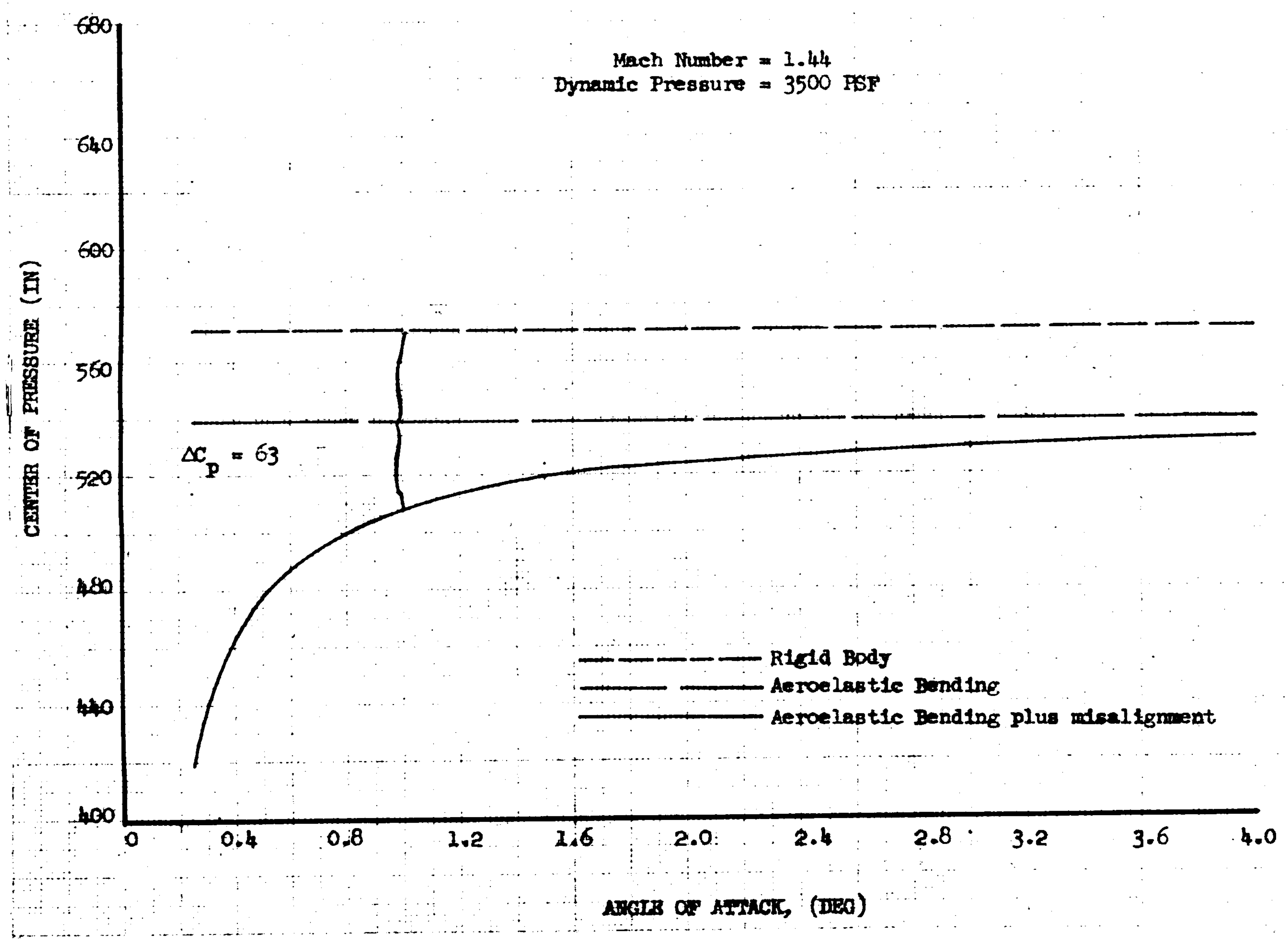

Figure C-21

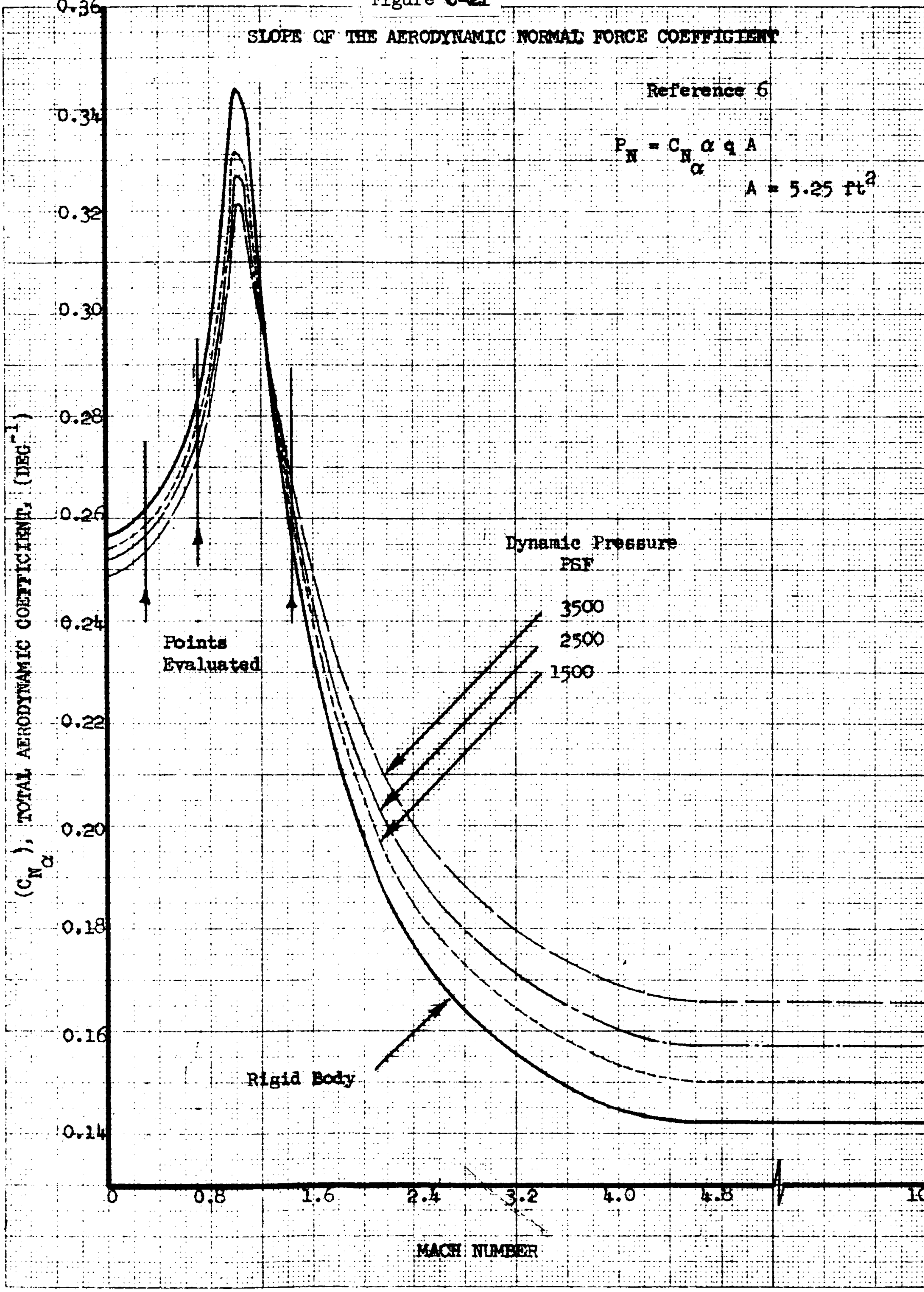

SLOPE OF THE AERODYNAMIC NORMAL FORCE COEFFICIENT
Reference 6
$P_N = C_{N_\alpha} \alpha q A$
$A = 5.25 \text{ ft}^2$
Dynamic Pressure PSF
3500
2500
1500
Points Evaluated
Rigid Body
(C_{N_α}), TOTAL AERODYNAMIC COEFFICIENT, (DEG^{-1})
MACH NUMBER
0.36
0.34
0.32
0.30
0.28
0.26
0.24
0.22
0.20
0.18
0.16
0.14
0
0.8
1.6
2.4
3.2
4.0
4.8
100

Figure C-22

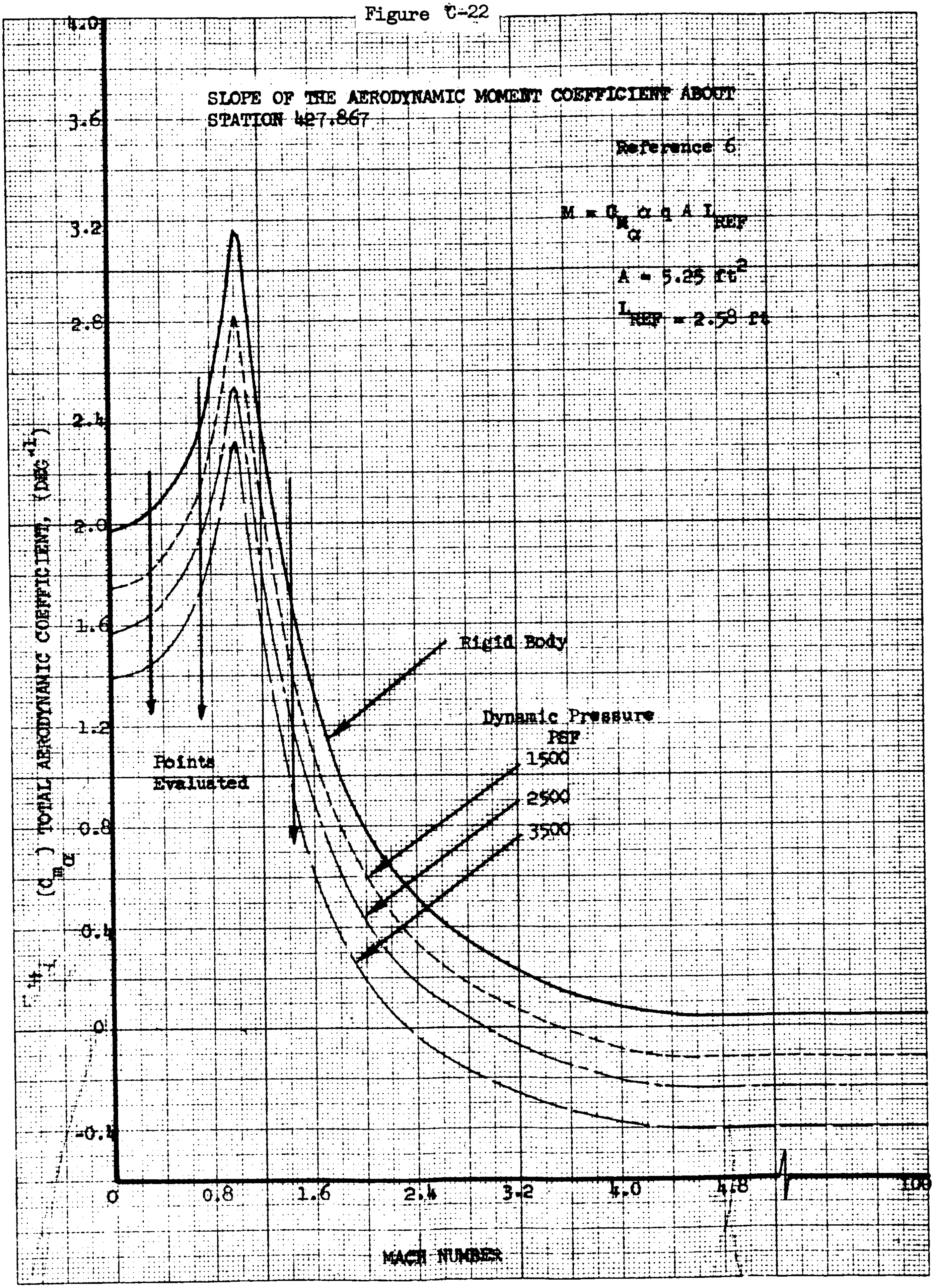

SLOPE OF THE AERODYNAMIC MOMENT COEFFICIENT ABOUT STATION 427.867
Reference 6
M = C$_{M_\alpha}$ α q A L$_{REF}$
A = 5.25 ft^2
L$_{REF}$ = 2.58 ft
Rigid Body
Dynamic Pressure PSF
1500
2500
3500
Points Evaluated
(C_{m_α}) TOTAL AERODYNAMIC COEFFICIENT, (DEG^{-1})
4.0
3.6
3.2
2.8
2.4
2.0
1.6
1.2
0.8
0.4
0
-0.4
0
0.8
1.6
2.4
3.2
4.0
4.8
MACH NUMBER

REFERENCES

1. C.K. Whitney, T.F. Owens, J. Paskind, and M.B. Rubin, "Scout Motor Performance Analysis and Prediction Study," NASA Contractor Report CR-336 dated December 1965.

2. J.R. Elliott, P.J. Stull, and C.H. Woodling, "Orbital Error Analysis of the Scout Research Vehicle," NASA Technical Note TND-1639 dated May 1963.

3. "Scout S-131 Final Flight Report," LTV Report 3-30000/6R-19.

4. NASA Drawing No. LC-926112.

5. "Survey Results, etc." Coast and Geodetic Survey letter 405.2.1.

6. "Section Assembly," LTV Specification 309-2B.

7. "Scout Guidance," Honeywell brochure.

8. "Accuracy Tolerance on Scout Aerodynamic Coefficients," letter from R.D. English SL-891/RJK.

9. Vehicle 131 Date Log.

10. Procedure No 6-3-7, Vehicle Alignment

11. Ground Support Equipment Manual (Vol. II).

12. LTV Specification 305-716.

13. "Matrix Method for Determining Missile Flight Divergence Characteristics with Specific Application to the Research Vehicle Scout," NASA-Langley Engineering Report No. 1002 for Engineering Service Division files.

14. LTV Astronautics Division, Scout Vehicle 131R - Pre-Flight Weight Report, 24 June 1967.

15. "Pacific Missile Range Reference Atmosphere for Pt. Arguello, Calif; Part I - August 1965. Prepared by Inter-Range Instrumentation Group IRIG Document 104-63.

16. NASA Scout S-131R(SEV), Secor Mission Pre-Flight Trajectory, LTV Astronautics Division, Enclosure 1 to LTV Letter No. 3-15000/5L-4248.

17. A Study to Determine the Performance Capabilities of the Scout Vehicle with a Velocity Package, LTV Report No. 23.242, dated 28 September 1965.

ERRATA

NASA CR-66596

ERROR ANALYSIS OF THE SCOUT LAUNCH VEHICLE

By Lester Cohen

TRW INC.
TRW Systems Group
One Space Park
Redondo Beach, California 90278

NASA Contract NAS1-6969

Issue date: 8-23-68

SEP 1968
RECEIVED
NASA STI FACILITY
INPUT BRANCH

Errata Sheet for Phase I Error Analysis Report

Page 10 - Include these words in the second paragraph after the first sentence, "The uncertainties in the tunnel data were absolute values on the coefficient itself. An estimate of the coefficient's variation as a function of angle of attack was obtained in terms of a fraction of the nominal value." After "...Table 8" add "the jet vane lift and drag simulation described in Appendix A are a result of tests during Algol IIB firings."

Page 13 - After last sentence in top paragraph add these words, "Since the only significant turning was about the pitch axis only the mass unbalance about the pitch spin axis, and yaw and roll input axes were considered."

Page 14 - In the third paragraph, second sentence, strike out the words, "...therefore corresponds to an angular displacement of 0.001 in..."

Page 16 - Add after Table 5 "The errors associated with the IRP were not included at the time of the first runs. Since the errors from this source were small, no further runs were made after the receipt of the IRP errors."

Page 17 - Table 6 - Eliminate all numbers and heading under column heading page (ref. sic.

Page 18 - In first paragraph eliminate words "...and are summarized in Table 7..." and add "These were 3-sigma values of .01 degree based on machine tolerances. No third-stage motor tolerances were used due to the lack of any manuever during that period of time in the mission analyzed." Change title in Table 7 from "Control Motor..." to "...Stage Motor..."

Page 19 - Change the title, "I. Errors not investigated: to "I. Errors from previous investigations."

Change the symbols in brackets for errors 11, 12, 21, 22, and 23, from $Cn\alpha$, $Cn\delta q$, $CN\beta$, $CN\delta r$, CNr, to $CN\alpha$, $CN\delta q$, $Cn\beta$, $Cn\delta r$, Cnr respectively.

Change the 1-sigma mag values of errors 17 - CM01 and 20 - CMAL from .002 to .05 for both errors.

Change word "percentage" to "fraction" in asterisk note at bottom of page.

Change errors 19 and 23 to pitch moment and yaw moment damping coefficients.

Page 21 - Change title in II. to "II. Error Sources Resulting from Investigation."

Change 1-sigma mag values for errors 62, 63, and 64, to .125 X 10^{-5} rad/sec; .200 X 10^{-5} rad/sec; and .328 X 10^{-5} rad/sec respectively.

Change reference for errors 68, 69, 70 from page 13 to catalog data.

Page 22 - Change reference for erros 71-75 frompage 13 to catalog data.

Change values for errors 76,77,78, to 5.76 X 10^{-5}; 5.43 X 10^{-5}; and 9.25 X 10^{-5} respectively.

Change reference for error 79 from page 16 to page 15.

Change value for error 91 to .026.

Bracket on errors 90 to 93 only - does not include number 94.

Change 94 from yaw to roll offset.

Change reference for errors 95 and 96 to Table 7.

Page 34 - In fourth paragraph eliminate words "...is similar to equation and..."

Pages 41, 44, 48 - Eliminate error #43 CMAL as a valid value.

Page 52 - Change values for error 41 CMAL to read as follows: 5.000000E-02; 7.89000E02; 1.927000E00; 6.542701E-03; -4.439623E-05.

Page 79 - Replace Table 17 with enclosed Table 17.

Page 80 - Add after Table 18, "Table 19 presents a summary of the dispersions in orbital elements as a result of a Monte Carlo analysis in which C_{M_0} is used as a bias error instead of an aerodynamic parameter."

Page 81 - Change last paragraph to read "Out of plane effects in NASA report. The most significant non-linear effect discovered was fourth-stage coning." Add the following after page 81, "Table 20 is a listing of the 3-sigma dispersions caused by the 12 cross term combinations mentioned on page 29. These results show that the dispersions caused by the cross term combinations of these errors are approximately equal to the sum of their individual effects."

Page 91 - In the last paragraph change "Equation (10)..." to "Equation 27..."

Page 93 - First paragraph change "..equation (20)..." to "...equation (34)..."

Page 100 - Matrix brackets are required between the diagonal inertial matrix and the column matrix containing the angular acceleration about the roll axis.

Add Reference 2A - "Introduction to Space Dynamics" Thompson, W.T. pp117, John Wiley 1964.

Page 101 - Add at end of first paragraph "(reference 2A)". In back reference 2A -"Introduction to Space Dynamics", Thompson, W. R. pp 117, John Wiley 1964.

Page 104 - After first paragraph add the following: "In addition, the normal and transverse lift on the vanes are computed from the following:

$$F_{\eta_v} = 2L_{\delta f(T_{vac})}\delta q$$

$$F_{\zeta_v} = -2L_{\delta f(T_{vac})}\,\delta r$$

Where:

$L_{\delta f}$ - jet vane lift (lbs) per degree vane deflection - $f(T_{vac})$

The values for jet vane drag $(C_{D_{V_f}})$ and lift $\left(L_{\delta f}\right)$ are shown in figures A-10 and A-11." Change the numbers of figures on page 106 to 114 accordingly.

Page 115 - In Table change the "TRW Equation Symbol" for LTV program symbol of CYD and CMD to "$C_{y\delta r}$ and $C_{n\delta r}$." Also, change all "TRW Program Symbol" listings to the following symbols in the following order from top to bottom. "CA01; CNAL; CYBA; CLP1; CMAL; CMQ1; CNBA; CNR1, CNDQ; CYDR; CMDQ; CNDR; CLDP; CM01."

Page 129 - Table B-14; change $C_{NPI} = C_{NA}$ to $C_{NAL} = C_{N\alpha}$

Page 137 - In first paragraph, last sentence add "B" after word "Appendix." Do the same in second sentence of last paragraph.

Page 139 - After listing "Rigid Body Data" add a double asterisk. At bottom of page add a double asterisk followed by the words "reference 14."

Page 163 - Reference 9 should read "Vehicle 131 Field Data Logbook." Reference 12 should read "Scout Assembly LTV Spec 305-716."

Add reference 13, "Final Report Algol IIB-31 Static Test, Aerojet General Corporation, Contract NAS1-3833, dated 23 November 1964."

Change all subsequent reference by one, i.e., current reference 13 becomes reference 14, etc.

TABLE 17 SIGNIFICANT ERROR SOURCES AND THEIR 3-SIGMA DISPERSIONS

NAME	1σ Error Mag. Fraction of nominal or as noted	3σ Dispersions Alt. (ft)	Vel. (ft/sec)	Flight Path Angle (deg)	Incl (deg)
I. MOTORS AND STRUCTURES					
First-stage inert weight (SIW1)	.0083	11689		.0496	
Second-stage inert weight (SIW2)	.0041	3854			
First-stage specific impulse (ISP1)	.0018	21360		.1129	
Second-stage specific impulse (ISP2)	.00094	8502	10.5	.0596	
Third-stage specific impulse (ISP3)	.0014	11472	22.7	.0929	
Fourth-stage specific impulse (ISP4)	.006		18.3		
First-stage mass flow rate (MFR1)	.014	24630		.1132	
Second-stage mass flow rate (MFR2)	.01	9223	11.1	.0737	
Third-stage mass flow rate (MFR3)	.018	10235	22.7	.0700	
First-stage thrust misalinement - pitch (TMP1)	1.67 mrad	20084	99.5	.0572	
First-stage thrust misalinement - yaw (TMY1)	1.67 mrad	9277		.0438	.1919
Second-stage thrust misalinement - pitch (TMP2)	1.67 mrad	68251	129.5	.1923	
Second-stage thrust misalinement - yaw (TMY2)	1.67 mrad	3166			.2600
Third-stage thrust misalinement - pitch (TMP3)	.557 mrad	19620	32.6	.1525	
Third-stage thrust misalinement - yaw (TMY3)	.557 mrad				.0789
Fourth-stage coning rate - pitch (W4CP)	.03 rad/sec		10.8	.0650	.5645
Fourth-stage coning rate - yaw (W4CY)	.03 rad/sec	4000	12.3	.5781	.0603
II. AERODYNAMICS					
First-stage drag coefficient (CA01)	.01	8868		.0371	
First-stage normal force coefficients (CNAL)	.2	4432	10.7		
First-stage pitch moment coefficients (CM01)	.002	3112			
First-stage density variation (DRHO)	.0667	56598	28.3	.2220	
First-stage wind profile (FWN1)	-				.0842
First-stage moment due to roll axis shift of static margin (MSMR)	.1	3884	10.5		
First-stage jet vane drag coefficient (CDV1)	.1	6107		.0323	

TABLE 17 Concluded

NAME	1σ Error Mag.	3σ Dispersions			
	Fraction of nominal or as noted	Alt. (ft)	Vel. (ft/sec)	Flight Path Angle (deg)	Incl. (deg)
III. <u>GUIDANCE AND CONTROL</u>					
First-stage intervalometer and torquer scale factor (DKSG)	.0035	8128	22.9	.0794	
First-stage rate gyro bias - pitch (DPBE)	3.57 mrad/sec	5048	15.7		
First-stage timer error - first step (TIM1)	.078 sec	16677	50.5		
Second-stage dead band error - pitch (DBP2)	.1	8688	15.4	.0272	
Second-stage dead band error - yaw (DBY2)	.1				.0651

TABLE 19 Summary of statistical output of orbital elements with C_{M_0} as a bias error.

DISPERSED STATE (ORBITAL PLANE)

MEAN MAGNITUDE OF POSITION	=	2.0859461D 04
MEAN MAGNITUDE OF VELOCITY	=	1.7572246D 01
RST OF POSITION	=	6.5353609D 04
RST OF VELOCITY	=	2.0775510D 02

DISPERSED STATE(ECI)

MEAN MAGNITUDE OF POSITION	=	2.0859461D 04
MEAN MAGNITUDE OF VELOCITY	=	1.7572246D 01
RST OF POSITION	=	6.5353609D 04
RST OF VELOCITY	=	2.0775510D 02

DISPERSION OF THE SEMIMAJOR AXIS(FT.)

MEAN	=	-4.8762613D 02
STANDARD DEVIATION	=	2.0380975D 05
SMALLEST SAMPLE	=	-5.0747424E 05
2ND PERCENTILE SAMPLE	=	-3.6478100E 05
5TH PERCENTILE SAMPLE	=	-3.1977250E 05
95TH PERCENTILE SAMPLE	=	3.3091750E 05
98TH PERCENTILE SAMPLE	=	4.5070950E 05
LARGEST SAMPLE	=	8.5613425E 05

ECCENTRICITY DISPERSION

MEAN	=	-3.6613316D-04
STANDARD DEVIATION	=	6.6575543D-03
SMALLEST SAMPLE	=	-1.6740321E-02
2ND PERCENTILE SAMPLE	=	-1.3599855E-02
5TH PERCENTILE SAMPLE	=	-1.0568687E-02
95TH PERCENTILE SAMPLE	=	1.0327406E-02
98TH PERCENTILE SAMPLE	=	1.2805592E-02
LARGEST SAMPLE	=	2.6432975E-02

Table 19 continued

INCLINATION DISPERSION (DEGREES)

MEAN	=	7.4602757D-03
STANDARD DEVIATION	=	2.4414642D-01
SMALLEST SAMPLE	=	-9.4265270E-01
2ND PERCENTILE SAMPLE	=	-5.2470112E-01
5TH PERCENTILE SAMPLE	=	-4.1515160E-01
95TH PERCENTILE SAMPLE	=	3.7694168E-01
98TH PERCENTILE SAMPLE	=	4.5678234E-01
LARGEST SAMPLE	=	6.0951805E-01

LONG. OF ASCENDING NODE DISPERSION (DEGREES)

MEAN	=	4.1608137D-02
STANDARD DEVIATION	=	1.5617931D-01
SMALLEST SAMPLE	=	-3.7478828E-01
2ND PERCENTILE SAMPLE	=	-2.4051952E-01
5TH PERCENTILE SAMPLE	=	-2.0059013E-01
95TH PERCENTILE SAMPLE	=	3.2570267E-01
98TH PERCENTILE SAMPLE	=	3.8709164E-01
LARGEST SAMPLE	=	6.8717098E-01

ARGUMENT OF PERIGEE DISPERSION (DEGREES)

MEAN	=	-4.0251794D-01
STANDARD DEVIATION	=	3.7055724D 00
SMALLEST SAMPLE	=	-2.3311409E 01
2ND PERCENTILE SAMPLE	=	-7.4919395E 00
5TH PERCENTILE SAMPLE	=	-6.4229832E 00
95TH PERCENTILE SAMPLE	=	5.1720791E 00
98TH PERCENTILE SAMPLE	=	6.3734474E 00
LARGEST SAMPLE	=	1.1277952E 01

Table 19 continued

DISPERSION OF ARC LENGTH ALONG ORBIT (NM)

MEAN	=	1.1004333D 00
STANDARD DEVIATION	=	4.1714588D 00
SMALLEST SAMPLE	=	-1.2109131E 01
2ND PERCENTILE SAMPLE	=	-6.8486328E 00
5TH PERCENTILE SAMPLE	=	-5.4648438E 00
95TH PERCENTILE SAMPLE	=	7.8978271E 00
98TH PERCENTILE SAMPLE	=	9.0770264E 00
LARGEST SAMPLE	=	1.5031616E 01

RADIUS VECTOR DISPERSION (FT)

MEAN	=	1.0365741D 04
STANDARD DEVIATION	=	4.2014380D 04
SMALLEST SAMPLE	=	-1.0088150E 05
2ND PERCENTILE SAMPLE	=	-6.9783250E 04
5TH PERCENTILE SAMPLE	=	-5.7493750E 04
95TH PERCENTILE SAMPLE	=	7.7220750E 04
98TH PERCENTILE SAMPLE	=	9.1632999E 04
LARGEST SAMPLE	=	1.3408425E 05

INERTIAL VELOCITY DISPERSION (FPS)

MEAN	=	-1.1826802D 01
STANDARD DEVIATION	=	7.8614060D 01
SMALLEST SAMPLE	=	-2.3464258E 02
2ND PERCENTILE SAMPLE	=	-1.7335303E 02
5TH PERCENTILE SAMPLE	=	-1.3658008E 02
95TH PERCENTILE SAMPLE	=	1.1574487E 02
98TH PERCENTILE SAMPLE	=	1.3792505E 02
LARGEST SAMPLE	=	2.6832544E 02

Table 19 continued

AIRSPEED DISPERSION (FPS)

MEAN	=	-1.1537245D 01
STANDARD DEVIATION	=	7.8357581D 01
SMALLEST SAMPLE	=	-2.3115893E 02
2ND PERCENTILE SAMPLE	=	-1.7182788E 02
5TH PERCENTILE SAMPLE	=	-1.3384985E 02
95TH PERCENTILE SAMPLE	=	1.1970581E 02
98TH PERCENTILE SAMPLE	=	1.3338672E 02
LARGEST SAMPLE	=	2.6639087E 02

INERTIAL FLIGHT PATH ANGLE DISPERSION (DEGREES)

MEAN	=	-4.5231049D-02
STANDARD DEVIATION	=	3.2265029D-01
SMALLEST SAMPLE	=	-1.9914151E 00
2ND PERCENTILE SAMPLE	=	-6.7957932E-01
5TH PERCENTILE SAMPLE	=	-5.7303174E-01
95TH PERCENTILE SAMPLE	=	4.3431635E-01
98TH PERCENTILE SAMPLE	=	5.5918872E-01
LARGEST SAMPLE	=	9.1101593E-01

ATMOSPHERIC FLIGHT PATH ANGLE DISPERSION (DEGREES)

MEAN	=	-4.5149490D-02
STANDARD DEVIATION	=	3.2197091D-01
SMALLEST SAMPLE	=	-1.9866246E 00
2ND PERCENTILE SAMPLE	=	-6.7828038E-01
5TH PERCENTILE SAMPLE	=	-5.7188807E-01
95TH PERCENTILE SAMPLE	=	4.3357767E-01
98TH PERCENTILE SAMPLE	=	5.5781459E-01
LARGEST SAMPLE	=	9.0920863E-01

Table 19 continued

APOGEE DISPERSION (NM)

MEAN	=	-1.3857752D 00
STANDARD DEVIATION	=	6.3852778D 01
SMALLEST SAMPLE	=	-1.5806720E 02
2ND PERCENTILE SAMPLE	=	-1.2230279E 02
5TH PERCENTILE SAMPLE	=	-1.0079007E 02
95TH PERCENTILE SAMPLE	=	1.0418860E 02
98TH PERCENTILE SAMPLE	=	1.3761914E 02
LARGEST SAMPLE	=	2.6763898E 02

PERIGEE DISPERSION (NM)

MEAN	=	1.2253039D 00
STANDARD DEVIATION	=	7.8988785D 00
SMALLEST SAMPLE	=	-2.2613830E 01
2ND PERCENTILE SAMPLE	=	-1.4490021E 01
5TH PERCENTILE SAMPLE	=	-1.2023407E 01
95TH PERCENTILE SAMPLE	=	1.3627869E 01
98TH PERCENTILE SAMPLE	=	1.6005768E 01
LARGEST SAMPLE	=	1.9137604E 01

PERIOD DISPERSION (SEC)

MEAN	=	-2.9879091D-02
STANDARD DEVIATION	=	8.1185989D 01
SMALLEST SAMPLE	=	-2.0098926E 02
2ND PERCENTILE SAMPLE	=	-1.4468195E 02
5TH PERCENTILE SAMPLE	=	-1.2638763E 02
95TH PERCENTILE SAMPLE	=	1.3216333E 02
98TH PERCENTILE SAMPLE	=	1.8021918E 02
LARGEST SAMPLE	=	3.4369488E 02

Table 19 concluded

LONGITUDE DISPERSION (DEGREES)

MEAN	=	4.3836542D-02
STANDARD DEVIATION	=	1.1048907D-01
SMALLEST SAMPLE	=	-2.3559761E-01
2ND PERCENTILE SAMPLE	=	-1.5987110E-01
5TH PERCENTILE SAMPLE	=	-1.2136269E-01
95TH PERCENTILE SAMPLE	=	2.3862931E-01
98TH PERCENTILE SAMPLE	=	2.9681206E-01
LARGEST SAMPLE	=	4.7219753E-01

LATITUDE DISPERSION (DEGREES)

MEAN	=	-1.8473236D-02
STANDARD DEVIATION	=	6.9379439D-02
SMALLEST SAMPLE	=	-2.5030637E-01
2ND PERCENTILE SAMPLE	=	-1.5134001E-01
5TH PERCENTILE SAMPLE	=	-1.3144374E-01
95TH PERCENTILE SAMPLE	=	9.0687275E-02
98TH PERCENTILE SAMPLE	=	1.1377645E-01
LARGEST SAMPLE	=	2.0133686E-01

ALTITUDE DISPERSION (NM)

MEAN	=	1.7059655D 00
STANDARD DEVIATION	=	6.9146663D 00
SMALLEST SAMPLE	=	-1.6603000E 01
2ND PERCENTILE SAMPLE	=	-1.1484802E 01
5TH PERCENTILE SAMPLE	=	-9.4622116E 00
95TH PERCENTILE SAMPLE	=	1.2708900E 01
98TH PERCENTILE SAMPLE	=	1.5080936E 01
LARGEST SAMPLE	=	2.2067390E 01

TABLE 20

3-Sigma Cross Term Dispersions

Error Source Combination		Z	X	Y	$\dot{Z}$	$\dot{X}$	$\dot{Y}$
TMY 2	KRY 2	-.456 E4	-.137 E4	-.842 E5	-.107 E2	-.221 E1	-.152 E3
ROE 2	TYM 2	-.390 E4	-.284 E4	-.902 E5	-.901 E1	-.521 E1	-.163 E3
DBP 2	TMP 2	-.764 E5	.789 E5	.858 E4	-.190 E3	.143 E3	.144 E2
TMP 2	KRP 2	-.677 E5	.676 E5	.132 E4	-.167 E3	.127 E3	.261 E1
ROE 2	TMP 2	-.689 E5	.685 E5	-.709 E4	-.168 E3	.130 E3	-.139 E2
DBY 3	TMY 3	.139 E4	-.137 E4	-.360 E5	.334 E1	-.227 E1	-.802 E2
TMY 3	KRY 3	-.810 E3	-.819 E3	-.220 E5	-.199 E1	-.165 E1	-.450 E2
ROE 3	TMY 3	.803 E3	-.899 E3	-.239 E5	.199 E1	-.166 E1	-.499 E2
DBP 3	TMP 3	.319 E5	.251 E5	.200 E2	.854 E2	.529 E2	.718 E-1
TMP 3	KRP 3	-.192 E5	.153 E5	.105 E2	-.502 E2	.322 E2	.398 E-1
ROE 3	TMP 3	.197 E5	.157 E5	-.187 E4	.525 E2	.328 E2	-.387 E1
DBY 2	TMY 2	-.380 E4	-.324 E4	.105 E6	-.866 E1	-.555 E1	-.180 E3

X - Down Range Direction

Y - Out of Plane Direction

Z - Radial Direction

FIGURE A-10

ALGOL II JET VANE DRAG
BASED ON GROUND LEVEL STATIC TESTS
(ONE JET VANE)

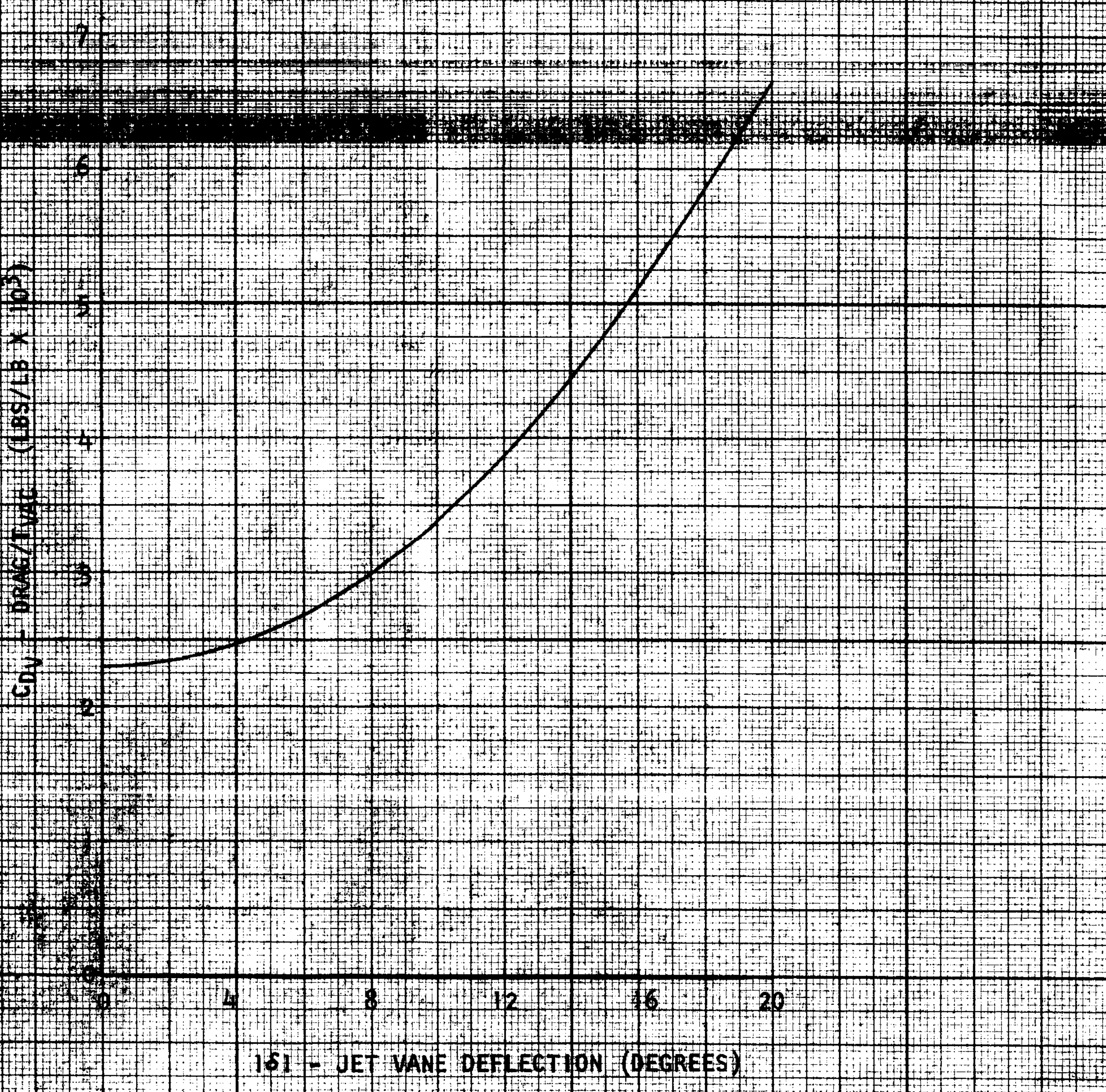

EUGENE DIETZGEN CO. MADE IN U.S.A.
NO. 340R-M DIETZGEN GRAPH PAPER MILLIMETER

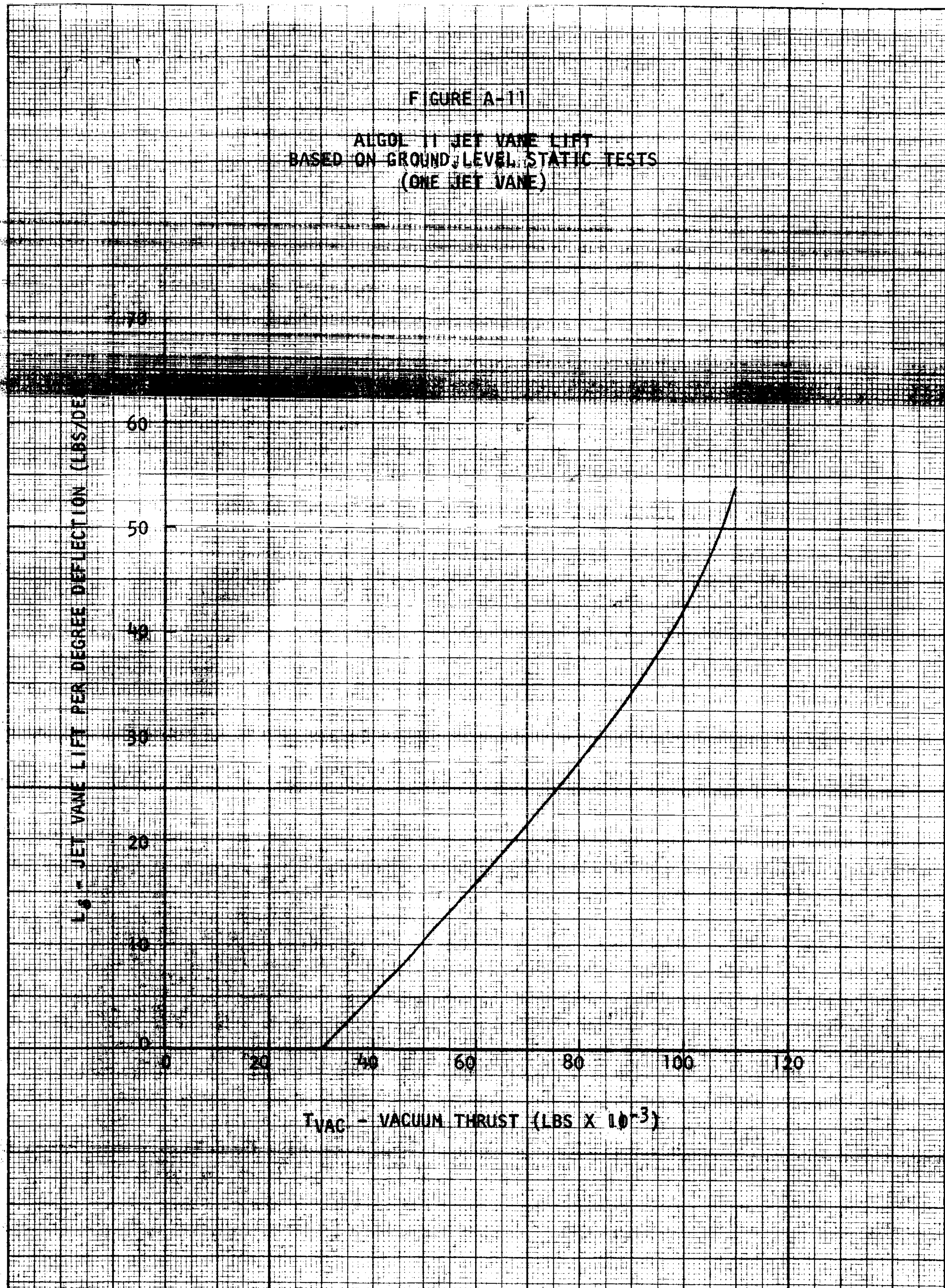

NO. 340R-M DIETZGEN GRAPH PAPER
MILLIMETER
EUGENE DIETZGEN CO.
MADE IN U.S.A.

TABLE 17 SIGNIFICANT ERROR SOURCES AND THEIR 3-SIGMA DISPERSIONS

NAME	1σ Error Mag. Fraction of nominal or as noted	3σ Dispersions Alt. (ft)	Vel. (ft/sec)	Flight Path Angle (deg)	Incl (deg)
I. MOTORS AND STRUCTURES					
First-stage inert weight (SIW1)	.0083	11689		.0496	
Second-stage inert weight (SIW2)	.0041	3854			
First-stage specific impulse (ISP1)	.0018	21360		.1129	
Second-stage specific impulse (ISP2)	.00094	8502	10.5	.0596	
Third-stage specific impulse (ISP3)	.0014	11472	22.7	.0929	
Fourth-stage specific impulse (ISP4)	.006		18.3		
First-stage mass flow rate (MFR1)	.014	24630		.1132	
Second-stage mass flow rate (MFR2)	.01	9223	11.1	.0737	
Third-stage mass flow rate (MFR3)	.018	10235	22.7	.0700	
First-stage thrust misalinement - pitch (TMP1)	1.67 mrad	20084	99.5	.0572	
First-stage thrust misalinement - yaw (TMY1)	1.67 mrad	9277		.0438	.1919
Second-stage thrust misalinement - pitch (TMP2)	1.67 mrad	68251	129.5	.1923	
Second-stage thrust misalinement - yaw (TMY2)	1.67 mrad	3166			.2600
Third-stage thrust misalinement - pitch (TMP3)	.557 mrad	19620	32.6	.1525	
Third-stage thrust misalinement - yaw (TMY3)	.557 mrad				.0789
Fourth-stage coning rate - pitch (W4CP)	.03 rad/sec		10.8	.0650	.5645
Fourth-stage coning rate - yaw (W4CY)	.03 rad/sec	4000	12.3	.5781	.0603
II. AERODYNAMICS					
First-stage drag coefficient (CA01)	.01	8868		.0371	
First-stage normal force coefficients (CNAL)	.2	4432	10.7		
First-stage pitch moment coefficients (CM01)	.002	3112			
First-stage density variation (DRHO)	.0667	56598	28.3	.2220	
First-stage wind profile (FWN1)	-				.0842
First-stage moment due to roll axis shift of static margin (MSMR)	.1	3884	10.5		
First-stage jet vane drag coefficient (CDV1)	.1	6107		.0323	